

# The Bengal Fan on different temporal and spatial scales

—

**Integrating seismoacoustic and IODP Expedition 354 data  
to examine internal and external controls on  
depositional processes**

Dissertation  
Zur Erlangung des Doktorgrades der Naturwissenschaften  
Am Fachbereich Geowissenschaften  
Der Universität Bremen

vorgelegt von:  
Fenna Bergmann

Bremen, September 2018

Gutachter:

Prof. Dr. Volkhard Spieß

Prof. Dr. Christian Hübscher



---

# Contents

Contents .....	i
List of Figures .....	iv
List of Tables.....	v
Thesis Abstract.....	1
Zusammenfassung.....	3
<b>1 Introduction.....</b>	<b>7</b>
1.1 Motivation and Objectives .....	7
1.2 Submarine channel-levee systems .....	12
1.2.1 Evolution and architecture of channel-levee systems.....	13
1.2.2 Modeling of channel-levee evolution.....	15
1.3 Regional Setting .....	16
1.3.1 Formation of the Bengal Fan.....	18
1.3.2 Sedimentation history of the Bengal Fan .....	19
1.3.3 Recent developments.....	22
1.4 Thesis Outline and declaration of co-author contributions .....	24
<b>2 Data and Methods.....</b>	<b>27</b>
2.1 Data Acquisition.....	28
2.1.1 SO93 .....	28
2.1.2 SO125 .....	28
2.1.3 SO188 .....	29
2.2 Multichannel seismic data processing.....	29
2.2.1 Pre-processing and geometry set-up.....	30
2.2.2 Trace editing.....	31
2.2.3 Velocity analysis and NMO correction .....	31
2.2.4 Pre-Stack noise attenuation .....	32
2.2.5 CMP-stacking and post-stack noise attenuation .....	33
2.2.6 Time migration.....	33
2.2.7 Reprocessing SO125 data .....	35
2.2.8 Watergun Processing.....	36
2.3 Parasound Echosounder Data .....	36
2.4 Swath Bathymetry Data.....	37
2.5 Integration of IODP 354 cores and seismic data.....	38
<b>3 Sinuosity-controlled deposition along a channel-levee system at the lower Bengal Fan.....</b>	<b>39</b>
Abstract.....	39
3.1 Introduction.....	40
3.1.1 Regional background - The Bengal Fan .....	41
3.1.2 Channel-Levee systems.....	42
3.2 Material and Methods .....	43
3.2.1 Seismoacoustic data - acquisition and processing .....	43
3.2.2 Relative volume and flux calculations .....	44
3.2.3 IODP Expedition 354 Site U1454.....	45

3.2.4	Radiocarbon ages.....	45
3.3	Results .....	45
3.3.1	Seafloor morphology.....	45
3.3.2	Overall channel-levee architecture .....	46
3.3.3	Levee units by Parasound– lithology integration .....	48
3.3.4	Other structural features .....	51
3.3.5	Stratigraphic framework.....	52
3.4	Discussion.....	54
3.4.1	Evolution of the Active Channel-Levee System.....	54
3.4.2	Overspill sedimentation as a function of the channel geometry .....	57
3.5	Conclusion .....	61
3.6	Acknowledgments.....	62
<b>4</b>	<b>Middle to Late Pleistocene architecture and stratigraphy of the lower Bengal Fan – Integrating multichannel seismic data and IODP Expedition 354 results.....</b>	<b>63</b>
	Abstract .....	63
4.1	Introduction .....	64
4.1.1	Regional Background .....	64
1.1.1	Previous work .....	66
1.1.2	IODP Expedition 354 .....	66
4.2	Data and Methods.....	68
4.2.1	Data acquisition and processing.....	68
4.2.2	Core-seismic integration .....	70
4.3	Results .....	70
4.3.1	Seismic facies definition and their link to drilling results.....	70
4.3.2	Regional deposition of hemipelagic sediments .....	71
4.3.3	Channel-levee systems .....	74
4.3.4	Unchannelized turbiditic sediments .....	75
4.4	Discussion.....	75
4.4.1	Regional depocenter migration.....	75
4.4.2	Sand deposition .....	82
4.5	Summary and Conclusions .....	84
4.6	Acknowledgments.....	84
<b>5</b>	<b>Increased sediment flux to the lower Bengal Fan during the Middle Pleistocene – Internal and external controls .....</b>	<b>85</b>
	Abstract .....	85
5.1	Introduction .....	85
5.1.1	The Bengal Fan – Regional setting .....	87
5.1.2	The Bengal Fan - Chrono- and Seismic Stratigraphy.....	88
5.2	Data and Methods.....	90
5.2.1	Multichannel seismic data.....	90
5.2.2	Integration of datasets .....	90
5.2.3	Sedimentation/accumulation rates.....	90
5.3	Results .....	91
5.3.1	Subfan C (~0.68-0.25 Ma).....	91
5.3.2	Accumulation rates .....	96
5.3.3	Migration and recurrence of channel-levee systems .....	97
5.4	Discussion.....	98
5.4.1	Sea-level independent deposition of hemipelagic sediments at 8°N? .....	98

---

5.4.2	Monsoon-related increase in Pleistocene sediment flux? .....	100
5.5	Conclusion .....	102
5.6	Acknowledgments .....	103
<b>6</b>	<b>Conclusion and future perspectives .....</b>	<b>105</b>
	<b>Acknowledgements .....</b>	<b>111</b>
	<b>References .....</b>	<b>113</b>
 <b>Appendix 1: Middle to Late Pleistocene Evolution of the Bengal Fan at 8° North:</b>		
	<b>Integrating Core and Seismic Observations for IODP Expedition 354 Transect</b>	
	<b>Chronostratigraphic Modeling.....</b>	<b>I</b>

---

## List of Figures

Figure 1.1: The source-to-sink concept .....	7
Figure 1.2: Size-comparison of the Bengal Fan and other large submarine fans .....	8
Figure 1.3: Overview map of the working area and the utilized seismic dataset .....	11
Figure 1.4: 3D-bathymetry map of a channel-levee system .....	12
Figure 1.5: Relationship of the channel-equilibrium profile to the actual channel slope.....	13
Figure 1.6: The three main types of overspilling .....	14
Figure 1.7: Downslope evolution of the sand-mud ratio within a channel-levee system .....	14
Figure 1.8: Physical model of a channel bend and overspill deposition .....	15
Figure 1.9: Overview map of the Himalaya-Bengal Fan source-to-sink system.....	16
Figure 1.10: Overview map of the Bengal Fan area and its surface channels .....	17
Figure 1.11: Paleogeographic reconstruction of the Indian plate at 65 Ma and 50 Ma .....	18
Figure 1.12: Interpreted seismic profile across the lower Bengal Fan.....	20
Figure 1.13: Upper Bengal Fan subfan maps .....	20
Figure 1.14: Lithostratigraphic summary of IODP Expedition 354.....	23
Figure 2.1: Map of the lower Bengal Fan including all processed seismoacoustic data .....	27
Figure 2.2: Standard processing flow applied to both multichannel seismic datasets.....	30
Figure 2.3: Scheme for channel switching during processing .....	31
Figure 2.4: The concept of common midpoint (CMP) binning .....	31
Figure 2.5: A CMP gather prior and post the normal moveout correction .....	32
Figure 2.6: Illustration of the effect of noise suppression and time migration.....	34
Figure 2.7: Comparison of SO125 multichannel seismic data before and after reprocessing .....	35
Figure 2.8: Vertical resolution differences of echosounder, watergun, and airgun seismic data ..	37
Figure 3.1: Overview of the Active Channel at the lower Bengal Fan .....	41
Figure 3.2: Different modes of overspill .....	43
Figure 3.3: Parasound profiles GeoB97-020, -023, and -025 crossing the Active Channel.....	46
Figure 3.4: Integration of Parasound data and Site U1454 core lithology .....	47
Figure 3.5: Parasound profile across a buried cut-off loop east of the Active Channel.....	49
Figure 3.6: Thickness maps of individual levee units .....	50
Figure 3.7: Age model for the Active Channel .....	53
Figure 3.8: Evolutionary model of the Active Channel.....	56
Figure 3.9: Reconstruction of local depocenter migration in the vicinity of Site U1454 .....	58
Figure 3.10: Illustration of the shift of overspill direction with increasing channel sinuosity .....	59
Figure 4.1: Overview map of the Bengal fan and its surface channels .....	65
Figure 4.2: Lithostratigraphic summary of IODP Expedition 354.....	67
Figure 4.3: Bathymetry map of the working area highlighting the used seismic dataset.....	68
Figure 4.4: Main acoustic features of channel-levee systems; core-seismic integration.....	69

Figure 4.5: Multichannel seismic Profile GeoB97-020 highlighting age marker, channel-levee systems and their relative stacking pattern .....	72
Figure 4.6: Thickness map of the Middle Pleistocene Hemipelagic Layer.....	74
Figure 4.7: Subfan sequence .....	77
Figure 4.8: Maps and cross sections of the three subfans B, C, and D .....	79
Figure 5.1: Bengal Fan and Subfan C overview map.....	86
Figure 5.2: Lithostratigraphic summary of IODP Expedition 354 drilling transect.....	89
Figure 5.3: Uninterpreted and interpreted multichannel seismic Profile GeoB97-020 .....	92
Figure 5.4: Subfan C and its subunits imaged by multichannel seismic Profile GeoB97-020 .....	93
Figure 5.5: Sum age-probability distribution of BAR1-3 .....	94
Figure 5.6: Lateral thickness and accumulation-rate variations of the Subfan C subunits .....	97
Figure 5.7: Absolute channel-levee ages vs. their lateral position .....	98
Figure 5.8: Bar plot illustrating volume, mass accumulation, and duration of Subfan C subunits	100

## List of Tables

Table 2.1: Summary of all seismic sources and their configuration.....	28
Table 2.2: Site Summary of IODP Expedition 354 sites.....	38
Table 3.1: Acoustic, lithological, and stratigraphic summary of levee units .....	48
Table 3.2: Calculated 2D-cross-sections and mass accumulation rates for turbiditic units .....	60
Table 4.1: Summary of the specifications of the utilized multichannel seismic datasets .....	69
Table 5.1: BAR correlation with IODP Expedition 354 drill sites and mean BAR-layer ages.....	95
Table 5.2: Acoustic and stratigraphic summary of the four subunits of Subfan C .....	96



## Thesis Abstract

Submarine fans are a common feature along continental margins and represent one of the main sinks for continentally derived sediments. Hence, they are regarded as excellent archives for long- and short-term climate variations as well as the continental uplift and erosion history. The Bengal Fan has attracted particular scientific attention as is it the primary sink of Himalayan material and, thus, recorder of one of the key areas in the global climate system. The fan deposition was initiated in the Early Eocene as a direct response to the India/Asia collision and the consequent uplift of the Himalayan Mountain Range. Since the Middle Miocene, channel-levee systems have been among the main conduits for sediment dispersal to the Bengal Fan. Frequent channel avulsion leads to lateral migration of deposition along and across the fan and, hence, the (spatial and temporal) accumulation pattern is very irregular. Thus, a comprehensive understanding of the fan's complex depositional dynamics is an essential prerequisite to ultimately connect changes in the sedimentary sink with changes in the source.

The here presented thesis examines the depositional dynamics of the Bengal Fan in order to contribute to the overall understanding of key aspects such as the tectonic/climate interaction and the Indian Monsoon evolution at the Himalayan Mountain range. A unique, integrated dataset of echosounder and multichannel seismic data extending for over 400 km across the lower Bengal Fan (8°N), results from the seven-site IODP Expedition 354 drilling transect at 8°N, and a novel, IODP 354 system-specific age-depth model enables an overarching study of the architecture, stratigraphy, and depositional processes of the Bengal Fan and channel-levee systems at various scales.

High-resolution Parasound data linked with levee lithology and radiocarbon ages derived from IODP Site U1454 were used to assess the spatial and temporal changes in deposition along the youngest channel of the Bengal Fan, the so-called *Active Channel*. Our analysis showed that the Active Channel started to develop approximately 27 kyrs ago, 10 kyrs earlier than previously proposed. Since ~10 ka, no terrestrial sediment has reached the overbank area anymore, while it has been shown in earlier studies that the Active Channel still receives overspill sediments in the Middle Bengal Fan area (16.5°N). Moreover, overspilling has been interrupted for a period of ~14 kyrs during the Last Glacial Maximum and the deglacial sea-level rise. Both times of interrupted overspill were associated with a decrease in turbidity current height. Mass accumulation rates during times of active overspill remained relatively constant, demonstrating a steady sediment flux to the lower Bengal Fan unaffected by sea-level variations. Spatial mapping of individual levee units was carried out to shed light on the relationship between channel sinuosity and overspill depositional pattern along the actively meandering channel on a sub-levee scale. Our results show that channel sinuosity has a strong influence on the overspilling deposition, resulting in a patchy deposition. However, the patchy deposition is equalized over time as a response to the dynamic channel geometry. Thus, when

transferring levee accumulation to sediment flux, it should be averaged over the entire lifetime of one channel-levee system in order to minimize statistical errors generated by short-term fluctuations.

The architecture and stratigraphy of the lower Bengal Fan since the Middle Pleistocene were studied utilizing a 420-km long multichannel seismic profile across all seven IODP Expedition 354 drill sites, emphasizing the dynamic character of the Bengal Fan. On millennial time-scales, deposition is focused along the active channel-levee system at any given time. With an average recurrence rate of 15 kyrs, the position of the active channel migrates across the fan, thereby often exceeding a lateral distance of 100 km between two successive systems. Moreover, sedimentation is organized in subfans whose location is controlled by the availability of accommodation space created by the uplift of the 85°E and Ninetyeast ridge and the location of the feeder canyon. While a subfan governs parts of the Bengal Fan, the adjacent areas are draped by hemipelagic deposition. In the study area, we identified three individual subfan phases since the Middle Pleistocene: Subfan B (1.24-0.68 Ma) constrained to the western fan while in the study area the Middle Pleistocene Hemipelagic Layer is deposited; Subfan C (0.68-0.25 Ma) constrained to the eastern fan; and Subfan D (0.25 Ma – recent) again constrained to the western fan, while the Late Pleistocene Hemipelagic Layer is deposited in the eastern fan area.

More than 60% of the terrestrial sediments deposited at the lower Bengal Fan is composed of sand and coarse silt deposited out of unchannelized turbidity currents, while muddy sediments, transported and deposited within channel-levee systems, only account for <40%. This highlights the key role of sand deposition for the fan construction and implies a hitherto underestimation of the sand content in large submarine fans.

Combining the seismic stratigraphy with a cores-seismic integrated age model data revealed constantly increasing accumulation rates and overall sediment load throughout the lifetime of Subfan C (Middle Pleistocene). The increasing input seems to reflect denudation rate changes in the source area, potentially linked to Middle Pleistocene climate variations. Subfan C fan sedimentation is interrupted thrice by decimeter-scale, regionally extending hemipelagic deposition. Their deposition does not appear to be systematically linked to sea-level variations but may be driven autocyclic. This observation also applies to the hemipelagic layers found in the levees of the Active Channel. This finding not only suggests that the Bengal Fan behaves contradictory to most other large submarine fans, which are starved during times of sea-level highstand, it also hints towards a relatively constant sediment delivery to the fan, at least since the Middle Pleistocene.

The outcome of this thesis provides new insights into the architectural and stratigraphic evolution of the lower Bengal Fan and marks a significant advancement towards an extensive understanding of the sedimentary archive in its full complexity. The relative seismic stratigraphy



developed in the scope of this thesis is an important step for the refinement of the IODP Expedition 354 chronostratigraphy. Moreover, it has been implemented into a core-seismic integrated age model specially designed for the IODP Expedition 354 drilling transect, thereby allowing novel insights into variations in sedimentation rate during the Middle Pleistocene and their potential linkage to sea-level and climate variability.

## Zusammenfassung

Submarine Fächer stellen eine der Hauptsinken für kontinentales Sediment dar und treten weit verbreitet entlang vieler Kontinentalhänge auf. Sie gelten daher als exzellentes Archiv für lang- und kurzfristige Klimaveränderungen sowie von kontinentaler Hebung und Erosion. Der Bengalfächer ist von besonderer wissenschaftlicher Relevanz da, er die primäre Senke für erodiertes Material aus dem Himalaya darstellt und somit die Entwicklung einer der Schlüsselregionen im globalen Klimasystem aufzeichnet.

Die Fächersedimentation im Bengalfächer begann im frühen Eozän als direkte Folge der Kollision der Indischen mit der Eurasischen Kontinentalplatte und der anschließenden Hebung des Himalayas. Seit dem mittleren Miozän sind sogenannte *channel-levee* Systeme einer der Haupttransportwege für Sediment innerhalb Bengalfächer. Regelmäßige Kanaldurchbrüche führen zu einer lateralen Migration der Ablagerung entlang und auch quer zum Fächer und sorgen für sowohl räumlich, als auch zeitlich sehr unregelmäßige Ablagerung. Ein umfassendes Verständnis der komplexen Ablagerungsstruktur des Fächers ist daher eine grundlegende Voraussetzung um Variationen in der Senke mit Veränderungen in der Quelle zu verknüpfen. Die hier präsentierte Arbeit strebt die genaue Untersuchung der Ablagerungsdynamik des Bengalfächers an, um zum allgemeinen Verständnis einiger Kernpunkte, insbesondere die Interaktion von Tektonik und Klima und die Entwicklung des Indischen Monsuns im Himalaya, beizutragen. Die Arbeit basiert auf einem ganzheitlicher Datensatz, bestehend aus Sediment-Echolot Daten und Mehrkanalseismik die sich über 400 km quer über den unteren Bengalfächer (8°N) erstrecken, sowie die Ergebnisse von den sieben Bohrkernen der IODP Expedition 354, durchgeführt bei 8°N, und einem neuartigen Alters-Tiefenmodell, entwickelt speziell für die Kerne von IODP 354. Dieser einmalige Datensatz ermöglicht eine übergreifende Studie der Fächerarchitektur, Stratigraphie und Ablagerungsprozesse auf verschiedenen Skalen. Hochauflösende Echolotdaten in Kombination mit lithologischen Informationen und Radiokarbondatierungen von IODP Kern U1454 wurden untersucht um die räumliche sowie zeitliche Variabilität von Sedimentablagerung entlang des jüngsten Kanals des Bengalfächers, des *Aktiven Kanals*, zu evaluieren. Unsere Analysen ergaben, dass der Aktive Kanal vor ca. 27.000 Jahren entstand, ungefähr 10.000 Jahre früher als bei früheren Studien vorgeschlagen. Seit

fast 10.000 Jahren erreicht die Levees des unteren Fächers kein kontinentales Sediment mehr, wohingegen frühere Studien vom mittleren Bengalfächer (16.5°N) gezeigt haben, dass dort auch rezent noch Sedimente aus dem Aktiven Kanal auf die Levees transportiert wird. Während des letzten glazialen Maximums und dem anschließenden Meeresspiegelanstieg gab es eine weitere, 14.000 Jahre andauernde Phase in der kein Material aus dem Kanal den Levee erreicht hat. Beide Zeiträume ohne terrestrische Sedimentation auf dem Levee werden mit einer Verringerung der Höhe der Trübestrome assoziiert. Allerdings bleiben die Massenakkumulationsraten in Zeiten aktiven Transports von Sediment aus dem Kanal auf die Levees relativ gleichmäßig, was einen beständigen Sedimenteintrag in den unteren Bengalfächer zeigt. Um den Zusammenhang von Kanalkrümmung zu Sedimentation entlang eines aktiv mäandrierenden Kanals zu beleuchten wurden individuelle Untereinheiten innerhalb des Levees kartiert. Unsere Ergebnisse zeigen, dass die Kanalkrümmung einen starken Einfluss auf die Ablagerung hat und dass sich daraus unregelmäßig verteilte Ablagerungszentren ergeben. Allerdings wird die unregelmäßige Ablagerung mit der Zeit durch den sich dynamisch verändernden Kanal ausgeglichen. Das bedeutet, wo aus Akkumulationsmessungen Sedimenteintragsmengen bestimmt werden sollen, empfiehlt es sich über die gesamte Lebenszeit eines channel-levee Systems zu mitteln um statistische Fehler, die durch die kurzzeitigen Veränderungen der Sedimentation entstehen, zu minimieren.

Die Architektur und Stratigraphie des unteren Bengalfächers seit dem mittleren Pleistozän wurden mit Hilfe eines 420 km langen mehrkanalseismischen Profils untersucht, welches alle sieben IODP Expedition 354 Bohrlokationen kreuzt. Diese Untersuchungen heben den dynamischen Charakter des Bengalfächers hervor. Auf Zeitskalen von tausend Jahren wird die Ablagerung entlang des jeweils aktiven Kanals fokussiert. Diese Kanäle haben eine durchschnittliche Lebensdauer von 15.000 Jahren und ihre Position migriert über den Fächer. Zwischen zwei aufeinanderfolgenden channel-levee Systemen liegen dabei oft laterale Distanzen von mehr als 100 km. Zusätzlich ist die Sedimentation in sogenannten Subfächern organisiert. Die Position eines Subfächers wird durch den zur Verfügung stehenden Ablagerungsraum, geschaffen durch die Hebung des 85°E und des *Ninetyeast* Rückens, sowie die Position des sedimentliefernden Canyons kontrolliert. Da ein Subfächer nur Teile des Bengalfächers bedeckt, findet in den angrenzenden Bereichen hemipelagische Sedimentation statt. In unserem Arbeitsgebiet konnten wir drei individuelle Subfächer-Phasen (seit dem mittleren Pleistozän) identifizieren: Subfächer B (1.24-0.68 Ma), beschränkt auf den westlichen Bengalfächer während im Arbeitsgebiet der *Middle Pleistocene Hemipelagic Layer* abgelagert wird; Subfächer C (0.68-0.25 Ma), beschränkt sich auf den östlichen Bengalfächer; und Subfächer D (seit 0.25 Ma), wiederum beschränkt auf den westlichen Bengalfächer, während der östlichen Fächer vom *Late Pleistocene Hemipelagic Layer* bedeckt wird.

Mehr als 60% der terrestrischen Sedimente im unteren Bengalfächer bestehen aus Sand und grobem Silt, die aus nicht-kanalisierten Trübestromen abgelagert werden. Hingegen machen

die feineren Sedimente, transportiert und abgelagert in channel-levee Systemen nur 40% der Sedimente aus. Diese Zusammensetzung unterstreicht die Schlüsselrolle von Sand für die Fächerarchitektur und deutet darauf hin, dass der Sandgehalt von großen submarinen Fächern bisher unterschätzt sein könnte.

Die Kombination der seismischen Stratigraphie mit einem Kern-Seismik-integrierten Altersmodell offenbart, dass Akkumulationsraten sowie die gesamte Sedimentfracht während der Aktivität von Subfächer C konstant ansteigen. Dieser ansteigende Eintrag scheint Variationen in den Denudationsraten im Quellgebiet zu reflektieren, welche wiederum mit Pleistozänen Klimavariationen verbunden sein könnten. Der Subfächer C wird außerdem von drei dezimetermächtigen, sich regional erstreckenden hemipelagischen Lagen unterbrochen. Deren Ablagerung zeigt keine systematische Verbindung mit Meeresspiegelschwankungen auf, sondern scheint autozyklisch gesteuert zu sein. Diese Beobachtungen gelten auch für die hemipelagischen Lagen, die in den Levees des Aktiven Kanals gefunden wurden. Diese Beobachtungen deuten nicht nur darauf hin, dass der Bengalfächer sich gegensätzlich zu den meisten anderen großen submarinen Fächern verhält, sondern auch auf eine seit dem mittleren Pleistozän konstante Sedimentzufuhr zum Fächer.

Die Ergebnisse dieser Arbeit liefern neue Erkenntnisse über die Architektur und Stratigraphie des unteren Bengalfächers und sind ein signifikanter Fortschritt für ein vollständiges Verständnis des Sedimentarchives in seiner vollen Komplexität. Die relative seismische Stratigraphie, die im Rahmen dieser Arbeit entwickelt wurde, ist ein wichtiger Schritt für die Verfeinerung der Chronostratigraphie entlang des IODP Expedition 354 Bohrtransekts. Zusätzlich wurde die seismische Stratigraphie in ein Kern-Seismik-integriertes Altersmodell, das speziell für den IODP Expedition 354 Transekt entwickelt wurde, implementiert. Dadurch werden ein erweitertes Verständnis der Variationen von Akkumulationsraten und ihre potentielle Verbindung zu Meeresspiegel- sowie Klimavariationen ermöglicht.



# Chapter 1

## 1 Introduction

### 1.1 Motivation and Objectives

Submarine fans are amongst the largest submarine sedimentary systems in the deep sea and a common feature at continental margins. They store continental sediments transported via rivers to margin and shelf and further into the deep sea, and thereby act as a fundamental archive for the continental tectonic and erosion history as well as long- and short-term climate variations (Fig. 1.1). The largest submarine fans found on Earth include the Bengal Fan (Curry *et al.*, 2003), the Indus Fan (Cliff *et al.*, 2002), the Amazon Fan (Flood *et al.*, 1997), the Congo Fan (Babonneau *et al.*, 2002), the Mississippi Fan (Twichell *et al.*, 1991), and the Monterey Fan (Fildani and Normark, 2004; Klaucke *et al.*, 2004) (Fig. 1.2).

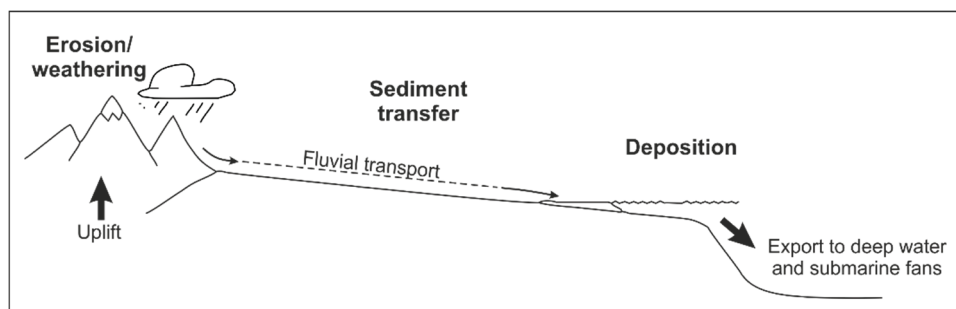


Figure 1.1: Source-to-sink concept illustrating the connection of the onshore sediment production area and the deposition of sediments in the deep sea, mainly in submarine fans, thereby forming important archives of the climate and erosion history of the source area. Modified after Blum and Hattier-Womack, 2009.

The Bengal Fan is of particular scientific importance as it is not only the largest submarine fan on Earth (Fig. 1.2) but also the primary record for one of the key areas in the global climate system – the Himalayan Mountains and the Asian Monsoon. The Asian monsoon is one of the largest climate systems and directly affects billions of people. It is driven by the land-ocean thermal contrast and its intensity concurrently is a first-order control on the Himalayan erosion rates (Galy and France-Lanord, 2001; Mohtadi *et al.*, 2016; Tada *et al.*, 2016; Wang *et al.*, 2017). Moreover, the monsoon's evolution and variability are suspected to be directly linked to the emergence and uplift of the Himalayan Mountain range and the Tibetan Plateau (Cliff *et al.*, 2008; Molnar *et al.*, 2010; Chatterjee *et al.*, 2013; Tada *et al.*, 2016). Additionally, Himalayan erosion seems to be an important driver of carbon burial, thereby playing an important role in the global carbon cycle (France-Lanord and Derry, 1997; Galy *et al.*, 2007).

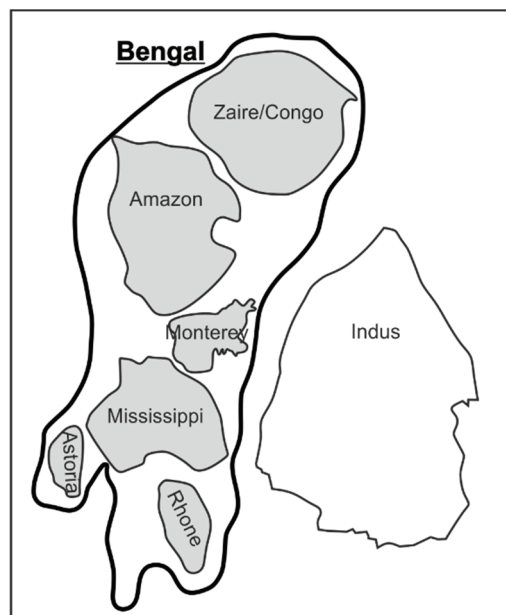


Figure 1.2: Size-comparison of the Bengal Fan, the largest submarine fan system on Earth, with some other large submarine fan systems (e.g. the Indus Fan, the second largest fan on Earth). Modified after Barnes and Normark 1985, Babonneau et al., 2002, Mulder, 2011.

About 80% of the material eroded in the Himalaya has been deposited in the Bay of Bengal, which makes the Bengal Fan the most complete record of the Himalayan erosion and weathering history. This sedimentary record provides a unique opportunity to study the Himalayan erosion history, thereby allowing to gain new insights into (i) the system's potential impact on the global carbon cycle; (ii) the timing and nature of the Indian/Asian collision; as well as (iii) the still debated linkage of the Himalayan Mountains/Tibetan Plateau uplift and the evolution of the Asian Monsoon. In that context, the Bengal Fan has been the target of two deep drilling campaigns in the last decades (DSDP Expedition 22; ODP Expedition 116; *Von der Borch et al., 1974; Cochran, 1990*) (Fig. 1.9). The sedimentary record derived during these expeditions has, amongst others, revealed changes in lithology, accumulation rates, grain sizes, and chemical composition and has been used to reconstruct Himalayan erosion rates, vegetation, and carbon burial (e.g. *Stow et al., 1990; France-Lanord et al., 1993; 2016; France-Lanord and Derry, 1994, 1997; Galy et al., 2007*).

Most of the Bengal Fan sediment is distributed along and stored within channel-levee systems. Previous studies have shown that these channel-levee systems are one of the main architectural elements of the fan (e.g. *Schwenk and Spieß, 2009*). However, frequent channel avulsions result in the lateral migration of the main depocenter (*Curry et al., 2003; Schwenk et al., 2003*). Thus, it lies within the nature of the fan that deposition is highly discontinuous at any one site. In order to overcome the challenges generated by the temporal and lateral depocenter migration, the Bengal Fan has been revisited by IODP expedition 354 in 2015 (*France-Lanord et al., 2016*). During this expedition, seven sites aligned along a west-east transect at 8°N were

drilled (*Figs. 1.3, 1.8 and 1.9*). Drilling locations for this expedition were designed based on an extensive seismoacoustic dataset acquired during three RV Sonne expeditions to the Bengal Fan (SO93 in 1994, SO125 in 1997, and SO188 in 2006) (*Fig. 1.3*). The 8°N transect at the lower Bengal Fan represents an ideal location to investigate the Bengal Fan's depositional history in high resolution while covering a large time span reaching back to the Early Miocene. Thus we utilized an integrated dataset combining the high-resolution seismoacoustic data with IODP Expedition 354 drilling results. This novel dataset enables us to examine the lateral and temporal succession of terrestrial input along the entire transect, thereby refining the stratigraphy of the drilling transect. On this basis, further insights into the tectonic/climate interaction of the source area and the Indian Monsoon evolution can be gained. Moreover, the unique dataset of high-resolution seismic lines and IODP drill sites allows for the first time a complete and detailed study of Bengal Fan's transport mechanisms and depositional processes. Their understanding is an essential prerequisite to ultimately connect changes in the sedimentary sink with changes in the sedimentary source.

Within this cumulative thesis, three standalone research manuscripts are presented. The three studies aim towards answering the below-outlined research question, defined based on the general considerations relevant for research of the sedimentary system Bengal Fan.

What is the variability of levee deposition in an actively meandering channel and how does it affect the interpretation of levee sediment cores?

Channel-levee systems are one of the main sediment distributors across and along submarine fans. Understanding their depositional behavior is an essential prerequisite to link the signal recorded in the sink with changes in the source area. The influence of channel-sinuosity on overspill deposition has been intensively studied by numerical and sandbox models (e.g. *Peakall et al., 2000; Straub et al., 2008, Huang et al., 2012*). However, most of these models have to use simplified boundary conditions, such as static sinuosity, downsizing or non-erosive channels. The integration of high-resolution Parasound data of the latest active channel of the Bengal Fan with lithological and chronostratigraphic information from the levee core provides the excellent opportunity to conduct a detailed study on the depositional behavior of an actively meandering channel-levee system in a natural setting in high resolution. This dataset furthermore provides essential information on the short-term impact of overspilling from a sinuous channel on levee accumulation rates and how this affects the interpretation of cores taken within a levee. (*Chapter 3*)

When was the *Active Channel* initiated and are there any indicators for intermittent channel-levee evolution?

The Bengal Fan differs from most other large submarine fans because it is considered as an active fan even throughout the Holocene sea-level rise. The Holocene transport pathway is the so-called *Active Channel* extending from the Swatch of No Ground shelf canyon south to the equator (*Fig. 1.10*). Sediment cores taken from the levees of the Active Channel at 16.5°N revealed active overspilling from at least 17.4 ka to 0.19 ka BP (*Weber et al., 1997; Hein et al., 2017*). However, high-resolution Parasound data show that the cores taken at 16.5°N do not reach the levee base and, thus, do not cover the entire lifetime of the Active Channel (*Hein et al., 2017*). Moreover, understanding the along-fan variations in channel evolution and sediment deposition is crucial to eventually be able to comprehend the variability of such a large sediment archive. We integrate a grid of high-resolution seismoacoustic data across the Active Channel at the lower Bengal Fan with IODP Expedition 354 drilling results (Site U1454). This comprehensive approach will allow to assess the onset of sediment transport in the Active Channel as well as to investigate whether Holocene activity also proceeded at the lower Bengal Fan. (*Chapter 3*)

What are the temporal and spatial dynamics of sediment pathway migrations across the Bengal Fan on local (channel) and regional (subfan) scales?

Previous studies show that the Bengal Fan sedimentation is highly discontinuous at a given location (e.g. *Curray et al., 2003; Schwenk et al., 2003; Schwenk and Spieß, 2009*). The area of active deposition migrates laterally across and along the Bengal Fan on the scale of channel-levee systems. Moreover, it has been suggested that channel-levee systems are organized in subfans which change deposition location as well. However, neither the temporal nor the spatial dynamics of depocenter migration are known. The integration of seismoacoustic data with IODP Expedition 354 drilling results allows conducting a comprehensive analysis of the overall style and variability of deposition. This includes the assessment of temporal and lateral depocenter migration, thereby advancing our comprehension of the overall fan dynamics and the transect's chronostratigraphy. (*Chapter 4*)

Which lithology is dominating the lower Bengal Fan?

The Bengal Fan is classified as a mud-rich fan and channel-levee systems seem to dominate fan construction since the Late Miocene (*Richards et al., 1998; Schwenk and Spieß, 2009*). Surprisingly, the cores recovered during IODP Expedition 354 contained significant amounts of sand (*Fig. 1.14*). Unraveling whether sand deposition may have a more important part in fan construction than in general expected will be vital for the assessment of spatial dynamics of fan deposition. If so, the general understanding of large submarine fans may have to be reassessed.



### What controls widespread hemipelagic deposition on the lower Bengal Fan?

IODP Expedition 354 revealed the existence of two several meters thick hemipelagic layers from Middle and Late Pleistocene times as well as numerous decimeter-scale hemipelagic layer. In general, hemipelagic deposition on submarine fans is associated with sea-level highstands when sediment is sequestered to the shelf and the fan is starved. One well-studied example showing such a cyclic recurrence of hemipelagic deposition is the Amazon Fan (Maslin *et al.*, 2006). However, research on the Active Channel showed that sediment delivery to the Bengal Fan proceeded throughout the Holocene highstand (Weber *et al.*, 1997; Hein *et al.*, 2017). A similar constant river-fan connection in earlier times would imply that the Bengal Fan behaves contradictory to other large submarine fans. Then, hemipelagic deposition would be either autocyclic controlled or reflect variations in continental erosion. (Chapter 3, 4 and 5)

### How variable are sediment accumulation rates on the lower Bengal Fan since the Middle Pleistocene? And what can be said about their controlling factors?

The depositional characteristics of the Bengal Fan result in discontinuous records at a given location. The west-east transect drilled during IODP Expedition 354 provides a nearly continuous sedimentary record of the Pleistocene (France-Lanord *et al.*, 2016). Nonetheless, it remains challenging to provide a high-resolution chronostratigraphy of the predominantly terrestrial material. The seismic stratigraphy developed in the scope of this thesis (Chapter 4) can be implemented into a core-seismic integrated age model specially designed for the IODP Expedition 354 drilling transect (Reilly *et al. (in prep.)*<sup>1</sup>). This allows for an important advancement in the transect's chronostratigraphy and provides novel insights into the regional deposition of hemipelagic sediments and the variations in sedimentation rate during the Middle Pleistocene and their potential linkage to sea-level and climate variability.

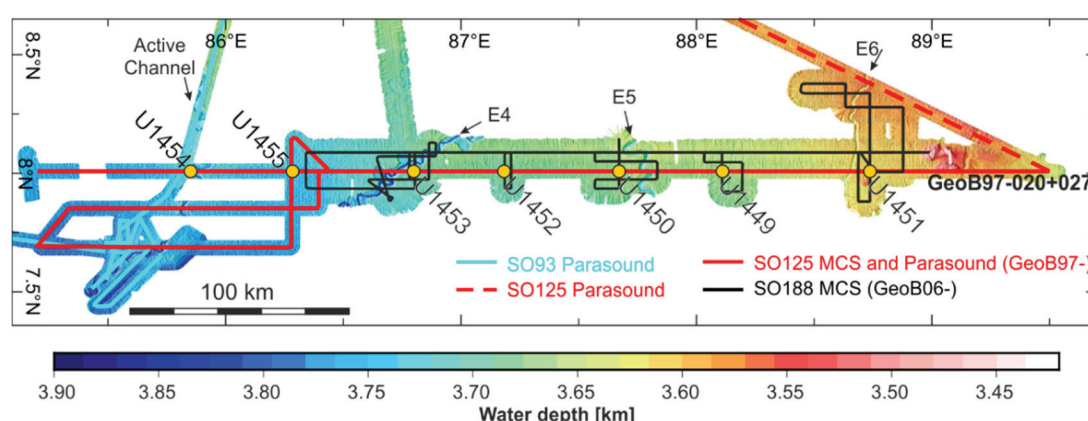


Figure 1.3: Overview map of the working area at the lower Bengal fan (around 8°N), the acquired seismoacoustic dataset utilized in this thesis, and IODP Expedition 354 drill sites (U1449-U1455). MCS: Multichannel seismic data. Blue lines: SO93 data; red lines: SO125 data (GeoB97-); black lines: SO188 data (GeoB06-). Surface channels (Active Channel, E4-E6) after Curray *et al.*, 2003.

<sup>1</sup> The here referenced manuscript in preparation refers to the manuscript presented in Appendix 1.

## 1.2 Submarine channel-levee systems

Submarine channel-levee systems, initiated and formed by downslope flowing turbidity currents, play an important role as conduits for the transport of terrestrial material over hundreds or thousands of kilometers into the deep sea and along the abyssal plains (Richards *et al.*, 1998; Stow and Mayall, 2000; Wynn *et al.*, 2007; Peakall and Sumner, 2015). They are a common feature on the Bengal Fan (Emmel and Curray, 1983; Hübscher *et al.*, 1997; Curray *et al.*, 2003; Schwenk *et al.*, 2005) as well as on other submarine fans such as the Indus (Clift *et al.*, 2002; Geadicke *et al.*, 2002), the Amazon (Flood *et al.*, 1997; Lopez 2001; Pirmez and Imran, 2003), and the Congo Fan (Babonneau *et al.*, 2002, 2010; Savoye *et al.*, 2009;).

Submarine channels tend to meander and are often highly sinuous with sinuosity changing as a function of slope and latitude (Wynn *et al.*, 2007; Peakall and Sumner, 2015 and references therein). Submarine channels evolve with every flow they experience and form complex 3D-depositional systems characterized by thalweg and meander migration, erosion and cut bank development, point bar deposition, channel avulsion, the formation of cut-off loops and/or terraces, and overbank deposition (Fig. 1.3) (e.g. Peakall *et al.*, 2000; Schwenk *et al.*, 2005; Kolla *et al.*, 2007; Wynn *et al.*, 2007).

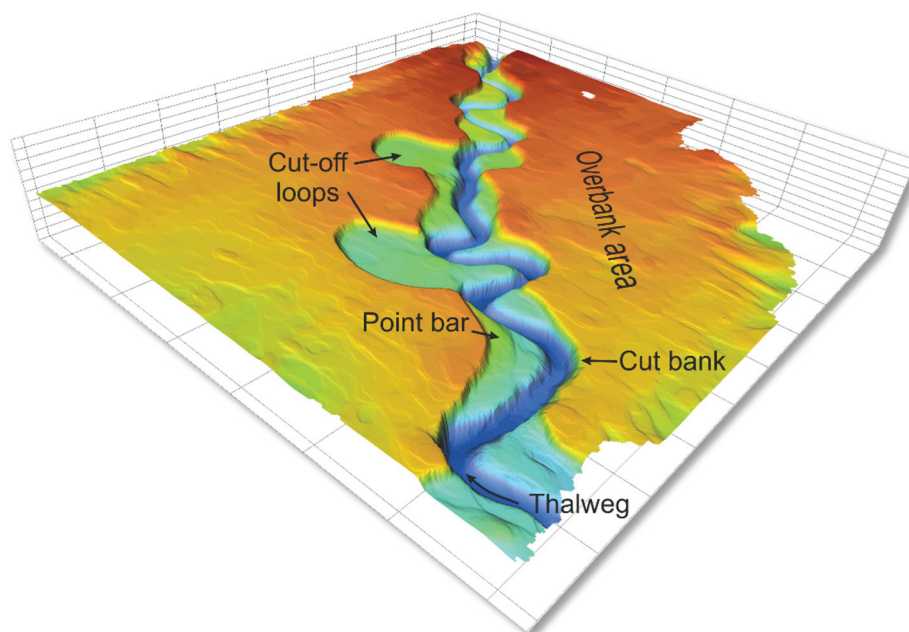


Figure 1.4: 3D-view of a surface channel-levee system of the Bengal Fan highlighting the complex interaction of lateral channel migration, channel avulsions, the formation of cut-off loops and terraces, erosion at cut banks and the formation of point bars.

### 1.2.1 Evolution and architecture of channel-levee systems

The formation of submarine channels is initiated by sediment-laden, self-channelizing turbidity currents (Imran *et al.*, 1998). In many submarine fans, the turbidity currents are initiated in canyons incised into the shelf or slope conveying the river-derived sediments from the river mouth further to the deep sea (Richards *et al.*, 1998; Wynn *et al.*, 2007).

The interplay between flow properties of the turbidity current (flow density, flow thickness or height, grain size of the suspended sediment) with the actual slope determines if a channel is aggradational or erosional (Kneller, 2003). The relation of the equilibrium profile, determined by the flow properties, to the actual slope controls where accommodation or erosion occur (Fig. 1.5). A reduction in flow size or density or an increase in grain size steepens the equilibrium profile and generates accommodation space. An increase in flow size or density increase or a decrease in grain size, however, can decrease the rate of accommodation or even result in an erosional channel (Fig. 1.5) (Kneller, 2003). A single channel can experience several changes in its equilibrium gradient and go through more than one incision, migration and aggradation cycles, thereby forming complex subsurface geometries (Sylvester *et al.*, 2011).

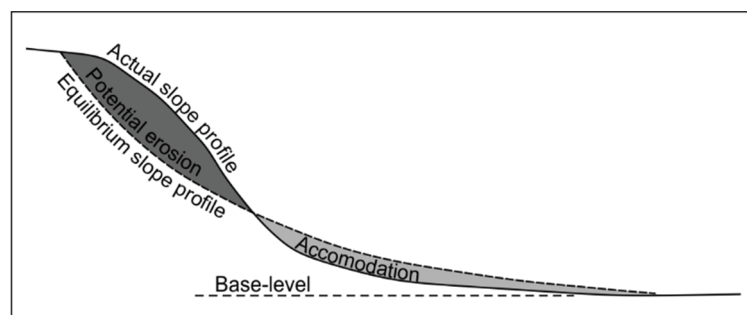
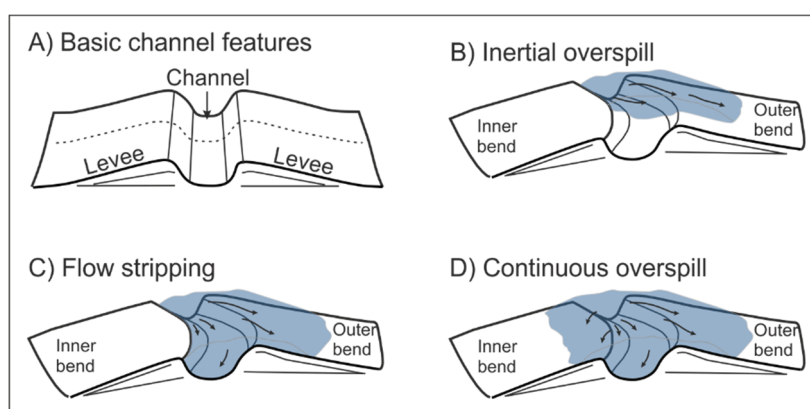


Figure 1.5: Schematic sketch of the relation of the equilibrium profile of a channel to the actual slope profile generating areas of potential erosion or accommodation of a channel. Modified after Kneller, 2003.

Submarine channels are often associated with levees, wedge-shaped sediment deposits flanking the channel (Fig. 1.6). Levees can be tens to hundredth meters in height and extend for tens of kilometers away from the channel axis (Wynn *et al.*, 2007). Levees are deposited where turbidity currents overspill onto the overbank areas, either because they exceed the channel relief or because the momentum of the current drives them out of the channel confinement. The sudden loss in confinement decelerates the current and leads to deposition of the transported material (Fig. 1.6). Commonly it is differentiated between three overspilling end-members: (1) the inertial overspill; (2) flow stripping; and (3) the continuous overspill on both sides of the channel. (Piper and Normark, 1983; Peakall *et al.*, 2000; Hansen *et al.*, 2015). Complete inertial overspills refers to the scenario of the entire flow exiting the channel at a channel bend (Fig. 1.6). Complete inertial overspill is a rare, extreme case of overspilling and requires the kinetic energy of the flow to exceed the potential energy related to the channel relief (Straub

*et al.*, 2011). During flow stripping, or partial inertial overspill, the upper, lower density, part of the current leaves the channel confinement, while the lower, high-density part remains within the channel (*Piper and Normark, 1983; Peakall et al., 2000*) (*Fig. 1.6*). Like the complete inertial overspill, flow stripping occurs mainly at channel bends. Continuous overspill to both sides of the channel (*Fig. 1.6*) is the volumetrically most important overspill type and occurs where current height exceeds the channel relief (*Peakall et al., 2000*).

Levees are characterized by an upward and laterally fining trend in grain size due to the vertical stratification within the mixed-loaded turbidity currents (*Pirmez and Imran, 2003; Meiburg and Kneller, 2010; Peakall and Sumner, 2015 and references therein*). Most channel-levee systems are underlain by lobes (*Posamentier and Kolla, 2003; Wynn et al., 2007; Savoye et al., 2009; Picot et al., 2016*).



*Figure 1.6: A: Schematic sketch of a submarine channel flanked by wedge-shaped levees deposited via overspill. B: Complete inertial overspill: The whole current escapes the channel confinement at channel bends. C: Flow stripping (or partial inertial overspill): The upper, less dense, part of the flow spills over at channel bends. D: Complete overspill: Overspill at both channel sides where the turbidity current height exceeds the channel relief. Modified after Hansen et al., 2015.*

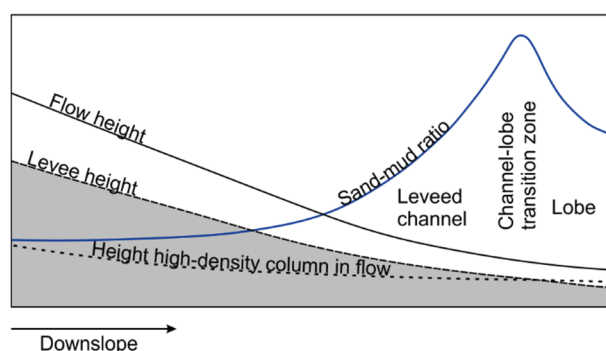
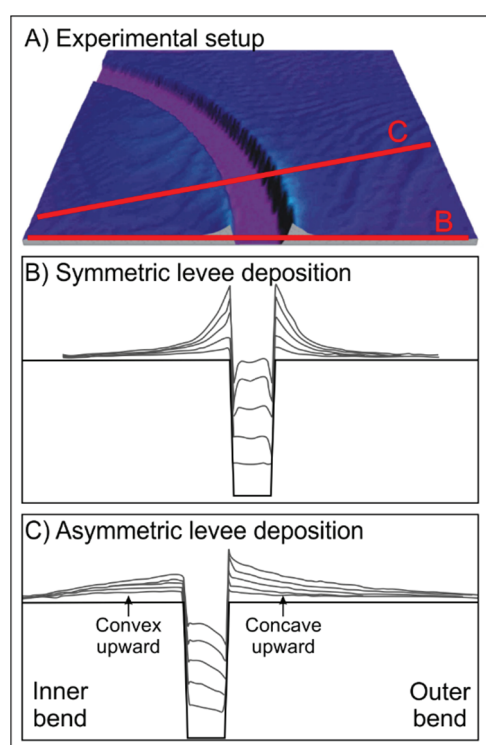


*Figure 1.7: Schematic sketch of the downslope evolution of the sand-mud ratio. The turbidity current traversing the channel is vertically stratified with the coarse fraction transported at the base of the flow. With every overspill event of the upper, more dilute part of the flow, the relative amount of sand increases. Where levee height and height of the high-density part of the flow are alike (channel-lobe transition zone) sand can overspill and lobes are deposited. Modified after Posamentier and Kolla, 2003 and Hansen et al., 2015.*

Lobes are deposited at the channel termination where the levee height is not sufficient anymore to further constrain the flow. Due to either continuous or sporadic overspill of the fine-grained part of the turbidity current during its downslope progradation, the sand/mud ratio of the flow increases downslope (Fig. 1.7) (Posamentier and Kolla, 2003). This results in lobes consisting of the coarse-grained, often sandy material transported as bed load confined within the channel (Pirmez et al., 1997; Lopez, 2001; Klaucke et al., 2004; Jegou et al., 2008).

### 1.2.2 Modeling of channel-levee evolution

Due to the infrequent nature of currents flowing through submarine channels and because most systems are inactive since the Holocene sea-level rise, obtaining direct measurements of flows traversing submarine channels is extremely difficult. Therefore, laboratory experiments and numerical modelling play an important role in studies investigating submarine channel processes (e.g. Imran et al., 1998; Peakall et al., 2000, 2007; Kane et al., 2008, 2010; Straub et al., 2008, 2011; Amos et al., 2010; Sylvester et al., 2011; Huang et al., 2012; Ezz et al., 2013; Peakall and Sumner, 2015). Several of these studies deal with depositional dynamics of turbidity currents in submarine channels, the interaction of channel sinuosity and flow properties, as well as the evolution and architecture of submarine levees. Laboratory experiments on the evolution of sinuous channels (Fig. 1.8) revealed a strong cross-channel asymmetry at



channel bends (Straub et al., 2008, 2011; Kane et al., 2010; Huang et al., 2012). Levees deposited at the overbank area of the outer channel bends (cut bank) are thicker, made up of coarser grains and have steeper flanks than the levees deposited at the inner bend overbank area (point bar) (Fig. 1.8). Kane et al. (2010) present a physical model of a sinuous channel bend undergoing 25 flow events. Already after 5 flow events the levee on the outer bend is significantly thicker than the levee on the inner bend (Fig. 1.8). The increased thickness on outer bends seems to be accompanied by coarser grain sizes (Amos et al., 2010; Huang et al., 2012). Moreover, there seems to be a relation between channel sinuosity and the shape of the levee. Levees on the inner

Figure 1.8: Physical model of a sinuous channel bend (Kane et al., 2010). A: 3D-view of the channel bend after 5 flow events. B and C: Transects (see A for location) through the channel and overbank deposits after 5 flow events. B: Proximal transect at a straight channel section. Both, levees and channel fill are approximately symmetric. C: Transect at sinuous channel section. Asymmetric levees with the taller levee at the outer bend side. Modified after Kane et al., 2010.



bend side are convex upward shaped whereas levees on the outer bend side are concave upward shaped (Huang *et al.*, 2012). Overall, total overspill seems to increase with increasing channel sinuosity and in general follows the pre-bend direction (Huang *et al.*, 2012; Ezz *et al.*, 2013). Where channels are (almost) straight, however, the levees on both sides of the channel develop relatively symmetrically (Straub *et al.*, 2008; Kane *et al.*, 2010; Huang *et al.*, 2012).

### 1.3 Regional Setting

The submarine Bengal Fan, drilled during IODP Expedition 354 (Figs. 1.9-1.11) is situated in the northeastern Indian Ocean bordered by India and Sri Lanka in the west, Bangladesh and Myanmar in the north and the Andaman-Nicobar Ridge and Sumatra in the east (Fig. 1.9). The fan evolved as a direct response of the Indian/Asian collision and today extends over 3000 km from the shelf off Bangladesh southwards to 7°S (Curry *et al.*, 2003). The Bengal Fan is underlain by two aseismic ridges emplaced during the northwards journey of the Indian Plate (Figs. 1.9 and 1.10) (Gopala Rao *et al.*, 1997; Krishna *et al.*, 2001a; Curry *et al.*, 2003).

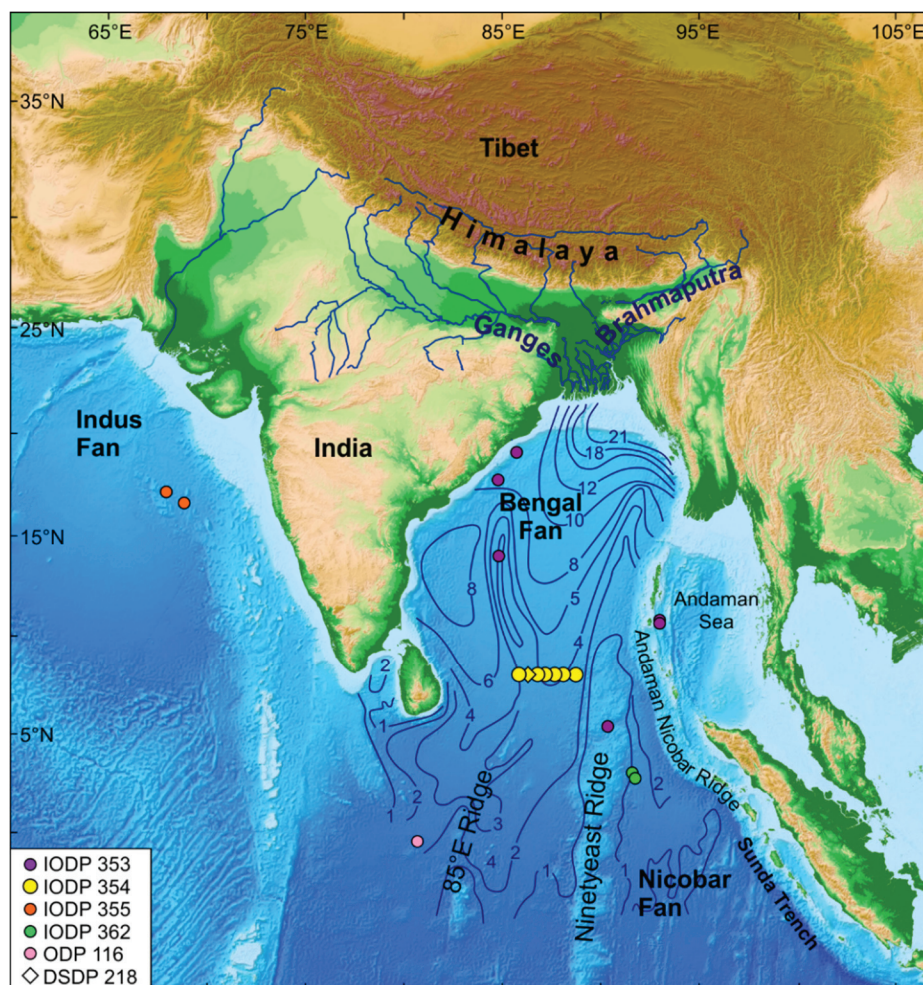


Figure 1.9: Overview map of the Bengal Fan in the northern Indian Ocean and the major onshore sediment delivering rivers, the Ganges and Brahmaputra. Blue isolines indicate the total sediment thickness in kilometers from sea floor to the oceanic second layer (redrawn after Curry, 1994).

One of them is the 85°E Ridge, which began to form ~85 Ma ago (Gopala Rao et al., 1997; Ismaiel et al., 2017) and which consist of N-S trending morphological highs (Bastia et al., 2010a). The ridge roughly follows the 85° meridian between ~5°S and 15°N and further continuous below the Mahanadi shelf in northeast India (Bastia et al., 2010a). The second aseismic ridge is the Ninetyeast Ridge, which was formed by the Kerguelen hot spot between ~95-38 Myrs (Gopala Rao et al., 1997; Krishna et al., 2001a, Krishna et al., 2012) and which strikes along the 90th meridian. Since the Middle Paleocene, the Ninetyeast Ridge separates the Bengal Fan from its second lobe, the Nicobar Fan, which is today situated in the Andaman Sea (Figs. 1.9 and 1.10) (McNeill et al., 2017a). Both ridges are partly exposed at the seafloor in the southern Indian Ocean and buried under Bengal Fan sediments in the northern Indian Ocean (Gopala Rao et al., 1997, Krishna et al., 2001a; Bastia et al., 2010a). Indications for Pliocene/Pleistocene uplift of both ridges are present as faults reaching into Pleistocene sediments and by an increased variance in sedimentation rates above versus between the ridges

in the Plio- and Pleistocene (Schwenk and Spieß, 2009). In the modern situation, the Ganga and Brahmaputra Rivers and their distributaries drain the northern and southern flank of the Himalaya and transport the eroded material to the delta. From there the sediment reaches the Swatch of No Ground (SoNG), a canyon deeply incised into the shelf (Figs. 1.9 and 1.10) (Kuehl et al., 1989; Kottke et al., 2003; Michels et al., 2003). From the SoNG sediment is episodically released to the fan. Sediment provenance proxy analyses of DSDP Site 218 reveal a major contribution of sediments from the northern mountain range area since ~12 Ma (Galy et al., 2010). This implies the existence of a connection similar to today between the Tibetan Plateau and the Bengal Fan for at least the last ~12 Ma (France-Lanord et al., 1993; Galy et al., 2010).

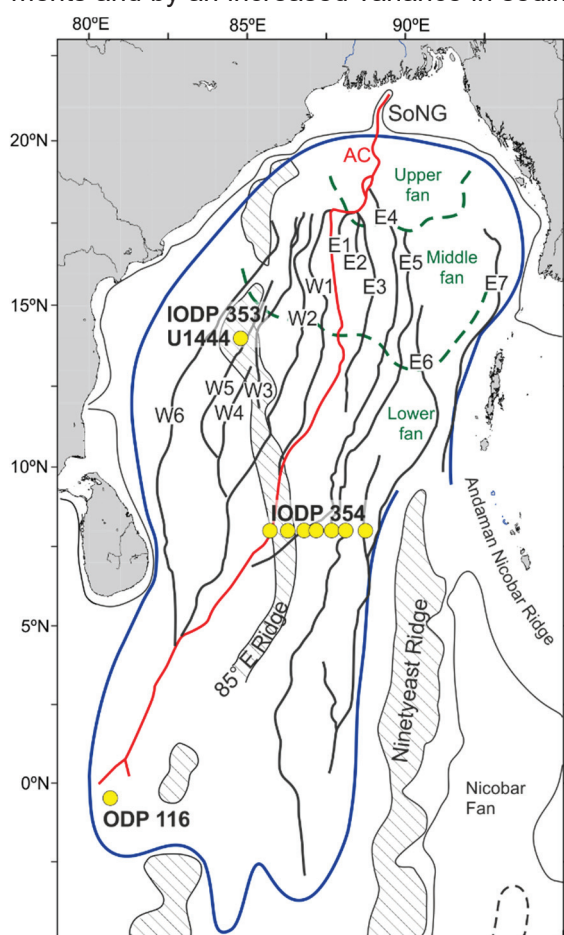


Figure 1.10: Overview map of the Bengal Fan (outline indicated by blue line). The Bengal Fan is underlain by the 85°E ridge and Ninetyeast Ridge (vertically striped features). The surface channels (solid black and red lines, W1-W6, AC (Active Channel), and E1-E7) highlight the characteristic tributary pattern of the Bengal Fan. Green stippled lines: Subdivision of the fan into upper, middle and lower fan based on the fan slope. SoNG=Swatch of No Ground. Fan outlines, surface channels, fan subdivision, and tectonic features redrawn after Curray et al., 2003, Bastia et al., 2010a, b; Choudhuri et al., 2014; McNeill et al., 2017a.

The recent fan surface is gently inclined southwards and dissected by several surface channels (Fig. 1.10). Based on downfan changes in gradient the fan is separated into three individual fan segments: The upper fan with an average slope of  $0.33^\circ$ ; the middle fan with an average slope angle of  $\sim 0.1^\circ$ ; and the lower fan with an average slope angle of  $0.05^\circ$  (Fig. 1.9) (Curry *et al.*, 2003). Like the Amazon or the Congo Fan, the Bengal Fan is classified as a mud-rich fan, which per definition contain less than 30% sand (Richards *et al.*, 1998).

### 1.3.1 Formation of the Bengal Fan

The formation of the Bengal Fan commenced in the in the Early Eocene as a direct response of the collision of the Indian Plate with the Eurasian continent (Curry *et al.*, 2003). The Indian plate separated from Gondwana in the Lower Cretaceous and began to move northwards (Gopala Rao *et al.*, 1997; Chatterjee *et al.*, 2013; Gibbons *et al.*, 2015). Around  $\sim 65$ -45 Ma the northern rim of the Indian Plate began to collide with the Eurasian continent. However, the exact timing and nature (e.g. multi-stage or one-stage collision) of the collision and the emergence of the Himalaya as a mountain range are still under debate (e.g. Alam *et al.*, 2003; Aitchison *et al.*, 2007; Dupont-Nivet *et al.*, 2010; van Hinsbergen *et al.*, 2012; Gibbons *et al.*, 2015; Hu *et al.*, 2016). Chatterjee *et al.* (2013) reviewed the evolution of the Indian Plate and the climatic evolution of India using a dynamic climate model. Following their summary, the Indian/Eurasian collision was initiated around  $\sim 85$  Ma ago with the collision of the Indian plate with the Kohistan-Ladakh Arc (KLA) along the Indus Suture (Fig. 1.11). The KLA, today located in the Nanga Parbat Syntaxis of the Himalaya, was subsequently accreted to the Indian Plate. Between  $\sim 65$ -52 Ma the Indian Plate accelerated until it eventually collided with Asia at  $\sim 52$  Ma (Fig. 1.11). As a consequence, the Tethys Ocean was closed and the uplift of Himalaya and Tibetan Plateau was initiated (Chatterjee *et al.*, 2013).

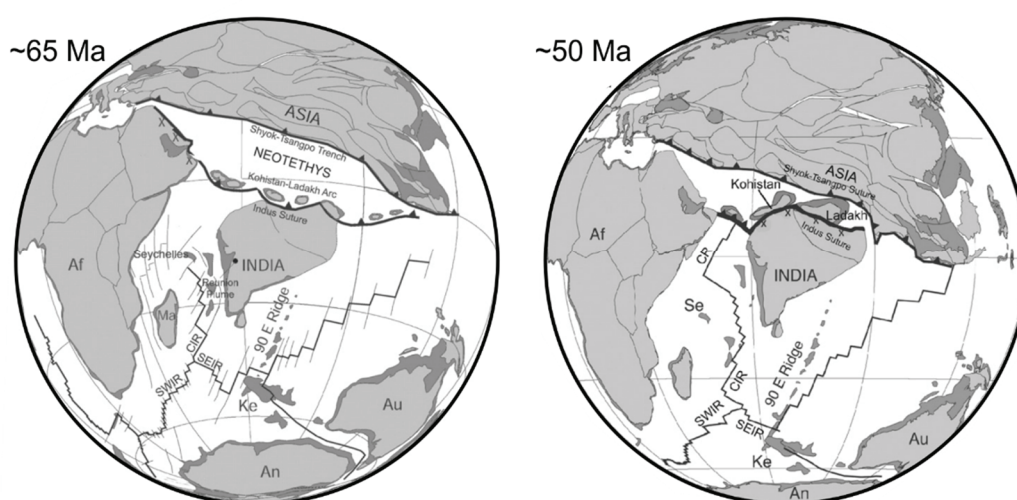


Figure 1.11: Paleogeographic reconstruction presented by Chatterjee *et al.*, 2013 illustrating the plate tectonic situation at  $\sim 65$  Ma after the collision of the Indian Plate with the Kohistan-Ladakh arc in the Late Cretaceous ( $\sim 80$  Ma) (left) and the initial collision of India and Asia in the Early Eocene ( $\sim 50$  Ma). Modified after Chatterjee *et al.*, 2013.



A more recent study (*Gibbons et al., 2015*) designed a regional plate tectonic model incorporating geological and geophysical datasets from numerous regions and studies. They propose that the collision between India and the KLA was diffuse and occurred between 61-50 Ma. Subsequently, seafloor spreading slowed down significantly at ~52-43 Ma. Finally, the collision between the Indian and the Eurasian plate occurred in two stages; the initial (soft) continent-continent collision occurred ~44±2 Ma ago and was followed by the complete (hard) continent-continent collision at ~38-35 Ma (*Gibbons et al., 2015*). Regardless of the controversy on the exact timing of collision events, the uplift of the Himalayan Mountain range and the Tibetan Plateau initiated by the continent-continent collision marks a drastic change in the regional topography. The uplift of the Himalaya/Tibetan Plateau is suspected to have a strong link to the formation and evolution of the Asian Monsoon, even though until now this link cannot be directly proven (*Zhisheng et al., 2001; Clift et al., 2008; Molnar et al., 2010; van Hinsbergen et al., 2012; Chatterjee et al., 2013; Tada et al., 2016*).

### 1.3.2 Sedimentation history of the Bengal Fan

Sedimentation in the Bay of Bengal was initiated in the Middle to Late Eocene after the collision of India with Asia and the formation of the Bay of Bengal (*Curry et al., 2003*). The post-collision sedimentary sequence of the Bengal Fan reaches thicknesses of up to 16.5 km with maximum deposition near the continental shelf (*Fig. 1.9*) (*Curry, 1994; Curry et al., 2003*). Over time the fan gradually prograded southwards, thereby generating a base hiatus of increasing duration downfan (Oligocene to Miocene) (*Curry, 1994; Curry et al., 2003*). Sediments deposited from fan onset until the Late Miocene consist of predominantly sheeted turbidites, while since the Late Miocene the sheeted turbidites are frequently intercalated with channel-levee systems (CLSs) (*Curry et al., 2003; Schwenk and Spieß, 2009, Krishna et al., 2016*) (*Fig. 1.12*). The onset of channel-levee formation occurred nearly synchronously along large parts of the fan and has been associated with a decrease in grain size observed in the distal fan (ODP Leg 116 sites), which in turn seems to be connected to an increase in Himalayan weathering at ~7 Ma (*Cochran, 1990, Stow et al., 1990; Derry and France-Lanord, 1996; Schwenk and Spieß, 2009*). This time is also marked by the expansion of C4 plants in the Himalayan basin and has been suspected to mark a time of major readjustments of the Asian monsoon system (*France-Lanord and Derry, 1994; Zhisheng et al., 2001*). The majority of the channel-levee systems are filled and buried except for the most recent ones that are still visible as bathymetric features at the seafloor (*Fig. 1.10 and 1.12*) (*Curry et al., 2003; Schenk and Spieß, 2009*). These surface channels decrease in number downfan due to the reoccupation of old channel pathways, thereby creating the tributary channel pattern that is characteristic for the Bengal Fan (*Fig. 1.10*) (*Emmel and Curry, 1983; Curry et al., 2003*). The frequent avulsion and lateral migration of CLSs as documented by seismic investigations of the subsurface

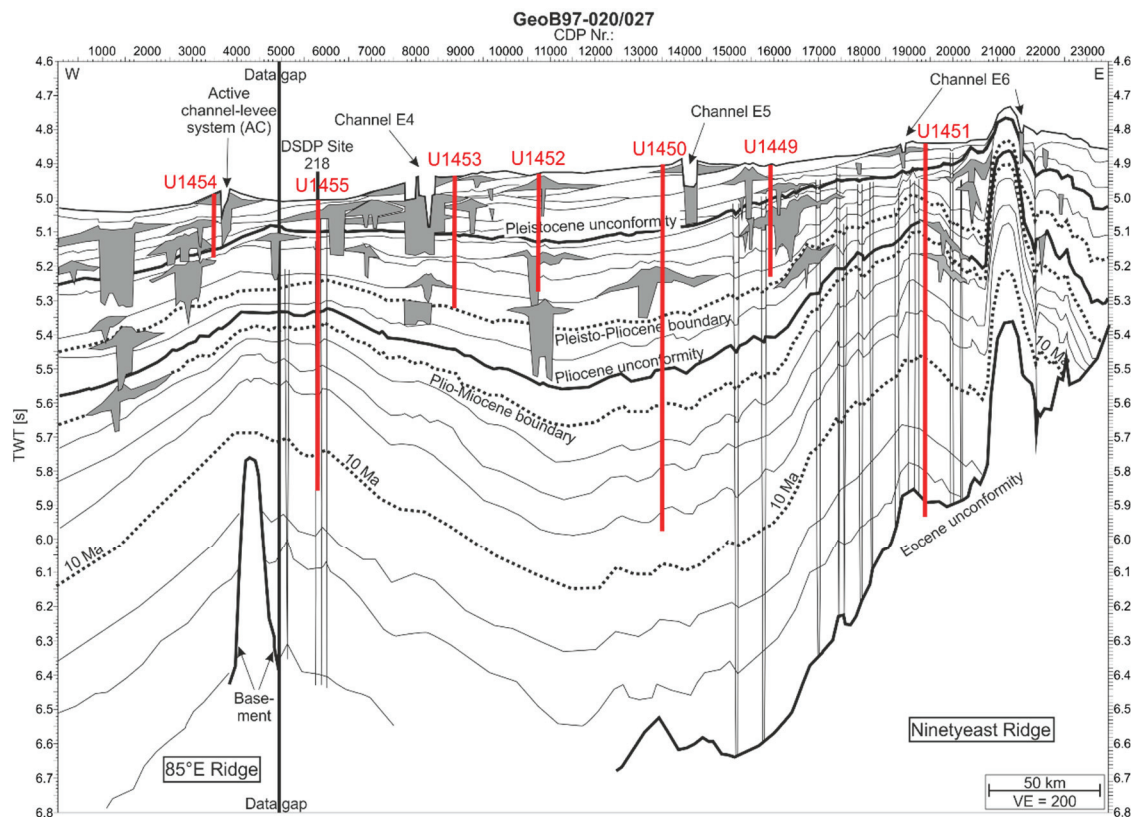


Figure 1.12: Interpreted line drawing of multichannel seismic Profile GeoB97-020+27 (Schwenk and Spieß, 2009) crossing all seven IODP Expedition 354 drill sites (indicated in red). Gray: Channel-levee systems. Age assignments from Schwenk and Spieß, 2009, based on DSDP Site 218. Modified after Schwenk and Spieß, 2009.

(e.g. Schwenk et al., 2005; Schwenk and Spieß, 2009) results in the formation of a complex depositional system characterized by highly discontinuous accumulation at a given location (Fig. 1.12). Moreover, deposition migrates on the scale of subfans, restricted areas of the fan receiving turbiditic sediments, while the adjacent area is cut off from fan sedimentation (Curry et al., 2003). Within the Pleistocene sediments of the upper Bengal Fan Curry et al., 2003 discerned the four subfans A, B, C, and D separated by distinct unconformities (Fig. 1.13). Following Curry et al., 2003, these subfans were active from 1.9-0.96 Ma (A), 0.96-0.465 Ma (B), 0.465-0.125 Ma (C), and 0.125 Ma to present (D).

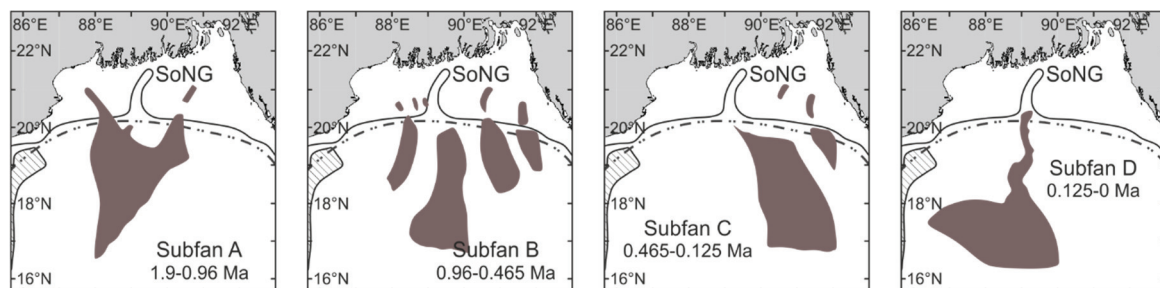


Figure 1.13: The concept of subfan formation on the upper Bengal Fan in the Quaternary introduced by Curry et al., 2003. The migration from one subfan to another represents major depocenter migration. Maps are based on a net of seismoacoustic data. Modified after Curry et al., 2003.

However, more recent seismic investigations corrected the onset of the most recent Subfan D to 0.3 Ma (*Weber et al., 2003; Schwenk and Spieß, 2009*). Subfan location migrates laterally from west to east thus covering different areas of the Bengal Fan (*Fig. 1.13*). *Curray et al., 2003* suggest that subfan location is strongly controlled by the position of the supplying canyon system. Their data further suggest that the subfans A, B, and C were supplied by more than one shelf canyon, either simultaneously or successively (*Fig. 1.13*), and that the SoNG has been one of these sediment-supplying canyons at least since the active Phase of Subfan C.

The sedimentary section of the Bengal Fan displays several regional unconformities identified in seismic data (*Cochran, 1990; Krishna et al., 2001b; Schwenk and Spieß, 2009*). In the central Indian Ocean an unconformity of Miocene age is well visibly (*Cochran, 1990; Krishna et al., 2001a*), while two unconformities of earliest Pliocene and Late Pleistocene age were also detected in the northern Indian Ocean (*Krishna et al., 2001b; Schwenk and Spieß, 2009*). These unconformities have been interpreted as results of intraplate folding events, and potentially linked to lithological changes observed at ODP Leg 116 Sites (*Cochran, 1990; Stow et al., 1990*). However, this interpretation has to be revised given the recent developments on the Bengal Fan sedimentation history (Chapter 1.3.3) (*France-Lanord et al., 2016*).

The Bengal Fan differs significantly from other large submarine fans, such as the Amazon, Indus, or Mississippi Fan, as it remained active also during the Holocene highstand despite the disconnection of river and fan (*Hübscher et al., 1997; Weber et al., 1997, 2003; Goodbred and Kuehl, 2000; Curray et al., 2003; Hein et al., 2017*). This constant supply has been preserved due to sediment bypassing along the shelf into the shelf canyon SoNG (*Kuehl et al., 1989; Michels et al., 2003, Palamenghi et al., 2011*). After being trapped temporarily in the SoNG, sediment is released episodically towards the fan via turbidity currents (*Kuehl et al., 1998; Michels et al., 1998; Rogers et al., 2015*)

The current average suspension load carried by the Ganges and Brahmaputra is estimated to ~1.06 Gt/a (*Bangladesh Water Development Board, 1972; Delft Hydraulics and Danish Hydraulics Institute, 1996; Milliman and Farnsworth, 2011*) while the overall sediment flux of both rivers, integrated over several hundred to thousands of years, ranges between 1.2-2.2 Gt/a (*Lupker et al., 2012, 2017*). Since the Middle Holocene, about 75% of the sediment load transported by the supplying rivers Ganges and Brahmaputra is deposited in the floodplains and the subaqueous delta while the remaining 25% is further transferred to the shelf SoNG and the Bengal Fan (*Goodbred and Kuehl, 1999*). Sediment distribution remains very similar in recent times with ~70% of the sediment load sequestered in floodplain and shelf and ~30% reaching SoNG and fan (*Kuehl et al., 1997; Goodbred and Kuehl, 1998; Michels et al., 1998*). A high-resolution study of the subaqueous delta revealed a decrease in mean annual storage rates in the foreset in the last ~300 years from ~22% to 13.5% of the present total suspension load

supply to the delta (~1 Gt/a) (*Palamenghi et al., 2011*). Holocene sediment dispersal along the Bengal Fan is realized via the Active Channel (AC) (*Fig. 1.10*) (*Hübscher et al., 1997; Weber et al., 1997, 2003; Hein et al., 2017*). The AC extends from the shelf more than 2500 km southwards to the equator (*Fig. 1.10*) and has experienced active overspilling at 16.5°N at least since 17.4 kyrs BP until 190 yrs BP (*Hein et al., 2017*).

### 1.3.3 Recent developments

In the last three years the Indus Fan, the Bengal Fan and the Nicobar Fan have been revisited by four International Ocean Discovery Program (IODP) Expeditions (IODP 353, Indian Monsoon Rainfall; IODP 354, Bengal Fan, IODP 355, Arabian Sea Monsoon, IODP 365, Sumatra Subduction Zone; *Clemens et al., 2016; France-Lanord et al., 2016; Pandey et al., 2016; McNeill et al., 2017b*) (*Figs. 1.3 and 1.9*). Of special interest for this study is IODP Expedition 354 'Neogene and late Paleogene record of Himalayan orogeny and climate: A transect across the Middle Bengal Fan' which took place in February/March 2015. During the Expedition seven sites along a 320 km long W-E transect on the lower Bengal Fan (8°N) were drilled. Three deep-penetrating (900-1200 mbsf, U1450, U1451, U1455) and 4 shallow sites (200-300 mbsf, U1449, U1452, U1453, U1454) were completed in order to address the major research questions of (i) the emergence of the Himalaya and the onset of fan deposition, (ii) the fan evolution in Miocene and Pliocene times and the monsoonal impact on sediment supply and flux throughout this time, (iii) the role of the Himalaya-Bengal Fan source-to-sink system in the global carbon cycle and climate and (iv) the spatial depocenter variability and its control on the fan architecture (*France-Lanord et al., 2001; 2016*). The expedition chose to drill along a W-E transect in order to overcome the issue of lateral migrating deposition induced by channel avulsion and subfan migration. Coring locations were placed along the multichannel seismic Profile GeoB97-020+27 (*Fig. 1.12*) (*Schwenk and Spieß, 2009*). The drilling recovered predominantly terrestrial sediments composed of clay, silt, and sand deposited within channel-levee systems and unconfined turbidites (*Fig. 1.14*). The terrestrial sediments are intermittently intercalated by more nannofossil rich sediments which were described as calcareous clay (*Fig. 1.14*) and most likely have a hemipelagic origin (*France-Lanord et al., 2016*). Especially remarkable was the recovery of two thick calcareous clay layers, one at the very top of sites U1449-1453 and U1455, and one in a depth of ~80-180 mbsf recovered at all seven sites (*Fig. 1.14*), both most likely of hemipelagic origin. Based on the identification of several stratigraphic markers (Toba Tephra, magnetic reversals) these two layers were tentatively dated to the Late Pleistocene (Late Pleistocene Hemipelagic Layer, LPHL) and Middle Pleistocene (Middle Pleistocene Hemipelagic Layer, MPHL) age (*Fig. 1.14*). More detailed studies on both layers have provided further insight into their nature and timing (*Weber et al., 2018; Weber and Reilly, 2018*).



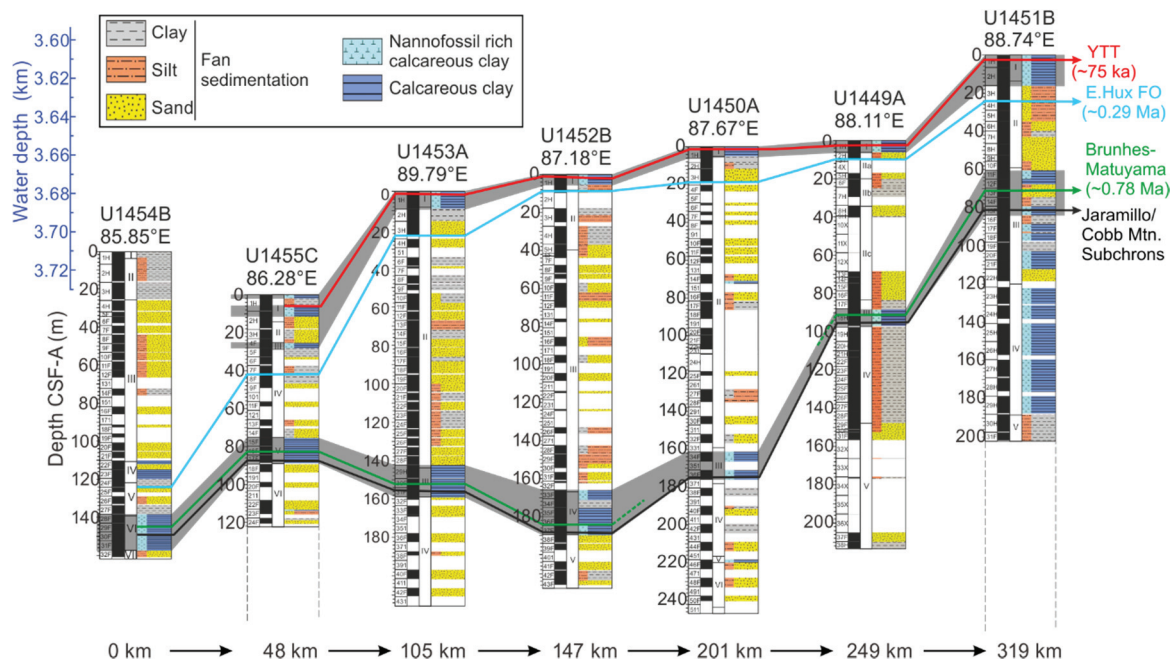


Figure 1.14: Lithostratigraphic summary of IODP Expedition 354 (the upper 250 m) showing lithologies that constitute >10% of the core (modified after France-Lanord et al., 2016). YTT=Youngest Toba Tephra, age after Gasparotto et al., 2000. E. Hux FO= First Occurrence *Emiliana huxleyi*. Ages of E. Hux FO and Brunhes-Matuyama boundary after Gradstein et al., 2012. Gray shaded areas highlight the two long-lasting hemipelagic sequences. Upper: Late Pleistocene Hemipelagic Layer (250 ka till recent; Weber et al., 2018). Lower: Middle Pleistocene Hemipelagic Layer (1.24-0.68; Weber and Reilly, 2018).

The MPHL seems to have had its onset at  $\sim 1.24$  Ma and its deposition ceased roughly at  $\sim 0.68$  Ma (Weber and Reilly, 2018). However, the uppermost boundary of the MPHL appears to be asynchronous. Based on physical properties the Middle Pleistocene layer has been separated into a more or less pure hemipelagic part lasting from  $\sim$ MIS37 through MIS25 and a mixed hemipelagic/turbiditic part lasting from  $\sim$ MIS25-MIS17 (Weber and Reilly, 2018). A multi-proxy study using magnetic and physical properties, stable isotopes, geochemistry, and grain sizes dates the LPHL to  $\sim 0.25$ - $0.2$  Ma until present with an average sedimentation rate of 2.3 cm/ka (Weber et al., 2018, Weber and Reilly, 2018). The MPHL is located in the same depth in which Schwenk and Spieß, 2009 identified and traced an unconformity of Pleistocene age (Chapter 1.3.2) (Figs. 1.12 and 1.14). The correlation of the MPHL with an unconformity in the seismic data shows, that the unconformity is related to the shift from hemipelagic to turbiditic deposition and not to intraplate folding (Chapter 1.3.2) (France-Lanord et al., 2016). Detrital zircon U-Pb provenance records sampled along the IODP Expedition 354 drilling transect confirm that sediments from  $8^{\circ}$ N represent Himalayan sources (Blum et al., 2018). Moreover, part of the zircon record represents the unmixed Ganges and Brahmaputra end members, indicating the temporary split of the Ganges and Brahmaputra rivers and the separated delivery of material to the fan along two pathways (Blum et al., 2018).

## 1.4 Thesis Outline and declaration of co-author contributions

This cumulative thesis comprises an introductory chapter (Chapter 1), a methods chapter (Chapter 2) and three joint-authorship manuscripts that will be submitted to peer-reviewed international journals. Chapter 1 provides a general introduction to the scientific background and research question of this thesis and summarizes the geological background of the working area. Chapter 2 summarized the methods of single and multichannel seismic data acquisition and processing applied during this study. The chapters 3 to 5 consist of three joint-authorship, standalone manuscripts which are outlined below. They were developed in close cooperation with the co-authors. Information on the individual contribution of each co-author is as well outlined below. In Chapter 6 the outcome of the three main chapters is summarized in an overarching conclusion. Finally, in the appendix an additional joint-authorship manuscript (main author B. Reilly) is provided, presenting an innovative age-depth modeling for the IODP Expedition 354 drill sites. This age-depth model incorporates the relative seismic stratigraphy and channel-levee stacking pattern presented in Chapter 4. Moreover, it introduces three additional stratigraphic markers identified and defined based on the seismic analysis conducted in the scope of this thesis.

### **Chapter 3:**

#### *Sinuosity-controlled deposition along a channel-levee system at the lower Bengal Fan*

**Authors:** Fenna Bergmann, Tilmann Schwenk, Volkhard Spiess, Hendrik Lantzsch, Petra Dekens, Valier Galy, and Christian France-Lanord  
To be submitted to *Marine and Petroleum Geology*

This chapter focusses on an integrated study of high-resolution sediment echosounder (Parasound) profiles, multichannel seismic data, and IODP Expedition 354 drilling results. The study investigates the active channel-levee system at the lower Bengal Fan (8°N) with a focus on the assessment of spatial and temporal changes in deposition along the channel and the relationship between channel sinuosity and overspill deposition on a sub-levee scale. The echosounder, multichannel seismic (MCS; GeoB97), and swath-bathymetry data used in this study were acquired during the two RV Sonne research cruises SO93 in 1994 and SO125 in 1997. Co-author V. Spiess was responsible for the acoustic data acquisition during SO93 and chief scientist during SO125. MCS profiles GeoB97-020-23 and GeoB97-25-26 were processed by co-author T. Schwenk and two master students (F. Gernhardt and M. Höhne). The bathymetry data were pre-processed by T. Schwenk in 1997 and revised by master student F. Warnke in 2018. H. Lantzsch provided the core description of IODP Site U1454 and the corresponding paragraph in the methods chapter. P. Dekens and V. Galy provided radiocarbon ages and the corresponding paragraph in the methods chapter.

---

I confirm that I processed all utilized echosounder data and MCS Profile GeoB97-024, carried out the interpretation of all utilized data, created all figures/tables and wrote, except from two short paragraphs of the methods chapter (see above), all sections of the manuscript. The development of the scientific concept benefited greatly from regular discussions with T. Schwenk, V. Spiess, H. Lantzsch and C. France-Lanord. Draft Versions were reviewed by T. Schwenk, H. Lantzsch, and C. France-Lanord. (*Personal contribution: 85%*)

#### **Chapter 4:**

##### *Middle to Late Pleistocene architecture and stratigraphy of the lower Bengal Fan – Integrating multichannel seismic data and IODP Expedition 354 results*

**Authors:** Fenna Bergmann, Tilmann Schwenk, Volkhard Spiess, and Christian France-Lanord  
To be submitted to *Basin research*

This chapter discusses the Middle to Late Pleistocene architecture and stratigraphy of the lower Bengal Fan at 8°N utilizing an integrated dataset of high-resolution multichannel seismic data and IODP Expedition 354 drilling results. It addresses the relative stacking of channel-levee systems, the organization of deposition in locally restricted subfans and gives new evidence for the key role of sand deposition to the fan architecture.

The MCS (GeoB97, GeoB06) and the swath-bathymetry dataset was acquired during the two research cruises RV Sonne SO125 in 1997 and SO188 in 2006. Both cruises were carried out in cooperation of the University of Bremen and the BGR Hannover under V. Spiess as chief scientist. The seismic dataset GeoB97 (except for Profile GeoB97-024) has been processed by co-author T. Schwenk with the assistance of two master students (F. Gernhardt and M. Höhne). The bathymetry data was also provided by T. Schwenk. I confirm that I processed all MCS data of dataset GeoB06 as well as Profile GeoB97-024, carried out the interpretation of all utilized data, developed the scientific concept in close communication with my co-authors, created all figures/tables and wrote all sections of the manuscript. Draft versions were reviewed by T. Schwenk and C. France-Lanord. (*Personal contribution: 90%*)

#### **Chapter 5:**

##### *Increased sediment flux to the lower Bengal Fan during the Middle Pleistocene – Internal and external controls*

**Authors:** Fenna Bergmann, Brendan Reilly, Tilmann Schwenk, Volkhard Spiess, and Christian France-Lanord  
To be submitted to *Basin Research*

This chapter synthesizes the seismic stratigraphy developed in Chapter 4 with a core-seismic integrated age model (manuscript presented in the appendix). It discusses regional deposition of hemipelagic sediments in the lower Bengal Fan, the refinement of the IODP drilling transect stratigraphy on a 100 ka timescale and Middle Pleistocene variations in sedimentation rates. This study focuses on the multichannel seismic Profile GeoB97-020+27 which has been acquired during RV Sonne cruise SO125 and processed by co-author T. Schwenk. Ages for channel-levee systems, which are presented in this study, as well as ages for three hemipelagic layers, which are an important part of the study's stratigraphy, were provided by co-author B. Reilly. I confirm that I interpreted all utilized data, developed the scientific concept in close cooperation with B. Reilly and during regular discussions with the remaining co-authors, created all figures and tables and wrote all sections of the manuscript. Draft versions were reviewed by T. Schwenk and B. Reilly. (*Personal contribution: 85%*)



## Chapter 2

### 2 Data and Methods

The acoustic dataset used in this study was acquired during the three research cruises SO93, SO125 and SO188 carried out with the RV Sonne as a cooperation between the University Bremen and the BGR Hannover in 1994, 1997 and 2006, respectively (*Kudrass et al., 1994; Spieß et al., 1998, 2006*). The acquired dataset comprises high-resolution sediment echosounding data (Parasound (SO93, SO125)), swath bathymetry data (Hydrosweep (SO93, SO125) and Simrad EM120 (SO188)) as well as multichannel seismic (MCS) data (SO125 and SO188) (*Fig. 2.1*). MCS data acquisition was conducted with different seismic set-ups by using a multichannel seismic streamer and different sized GI guns, resulting in datasets with differing subbottom penetration/resolution ratios (*Tbl. 2.1*).

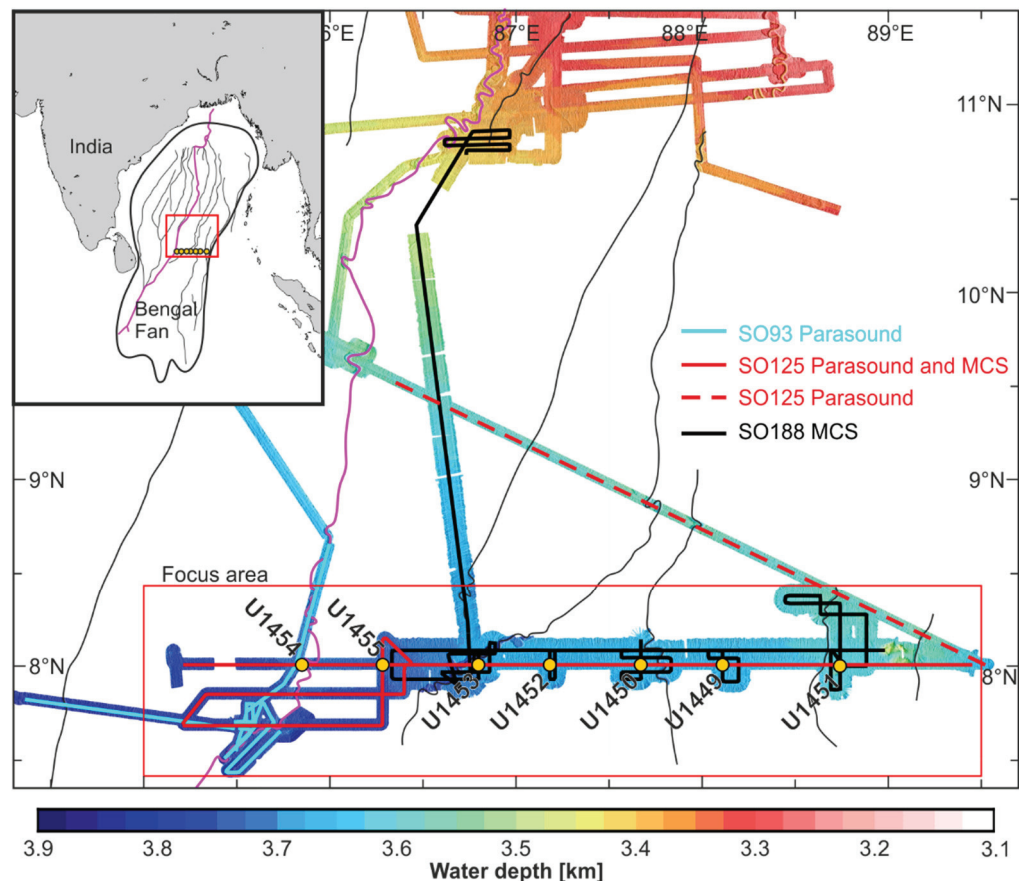


Figure 2.1: Overview map of the working area on the lower Bengal Fan and the acquired sediment echosounder (Parasound), bathymetry, and multichannel seismic (MCS) datasets utilized in this study. A: Bengal Fan outline and surface channels (after Curray et al., 2003). Pink channel: Active Channel. Red square shows the location of B. B: Surface channels (after Curray et al., 2003), bathymetry, and tracks of the processed and interpreted (profiles located in the focus area) acoustic data. Light blue: SO93 Parasound data; red: SO125 Parasound and MCS data; black: SO188 MCS.

The combination of decimeter-scale resolution sediment echosounder data for shallow sub-seafloor investigations and GI-gun data for deeper penetration at m-scale resolution allows a detailed seismo-stratigraphic analysis. Processing was carried out following the standard processing steps after *Yilmaz, 2001* using the custom-made software WinGeoApp (*H. Keil, University Bremen*) and the commercial seismic processing software Vista<sup>2014</sup> (*Schlumberger*). Data interpretation was done with all dataset integrated into the IHS Kingdom 2016.1 software package. The Kingdom software supports the integration of drilling and seismic data, spatial mapping of reflectors, gridding of predefined horizons, and calculation of thickness maps. Data interpretation and acoustic unit definitions were carried out following the principles of seismic stratigraphy presented by *Mitchum et al., 1977*.

*Table 2.1: Summary of all seismic sources and their configuration processed and interpreted in this study.*

	Source Volume	Source frequency range [Hz]	No. of recording channels	Channel Spacing [m]	Vertical Resolution [m]	Bin Size [m]
<b>SO125 airgun</b>	2x 0.41 l	~100-500	48	12.5	~5	12
<b>SO125 watergun</b>	0.16 l	~100-300 ~500-800	48	12.5	~7 ~2	12
<b>SO188 airgun</b>	4.1 l Generator 1.7 l Injector,	~25-200	96	6.25	~15	8
<b>Echo-sounder</b>	-	~4000	1	-	~0.2	-

## 2.1 Data Acquisition

### 2.1.1 SO93

The research cruise SO93 took place in January/February 1994 and has been divided into three individual Legs. During Leg 1 ~425 km of high-resolution echosounding data have been recorded in the lower Bengal Fan in the region of 7.5-8.5°N/84-86°E (*Fig. 2.1*) (*Spieß et al., 1998*). Parasound data recorded during this cruise provided a high-resolution dataset of the Active Channel (*Chapter 3*).

### 2.1.2 SO125

During the research cruise SO125, taking place in October and November 1997, 8 Parasound and MCS profiles (GeoB97-020-027) with a total length of ~780 km have been acquired in the vicinity of DSDP Site 218 (*Van der Borch et al., 1974*) in preparation for the recently drilled IODP holes U1449U1455 on the lower Bengal Fan (*Fig. 2.1*) (*France-Lanord et al., 2016*). During the recording of these profiles, two seismic source types were deployed and shot alternating: A Sercel Generator-Injector (GI) Airgun with a chamber volume of 2x0.41 l; and two simultaneously triggered Sercel S15 waterguns with a chamber volume of 0.16 l. Both sources were operated with an air pressure of ~145 bar and a shot rate of 13 s (between the two

sources). Data were recorded with a 48-channel SYNTRON seismic streamer consisting of a tow lead, two 50 m stretch sections and six active sections, each 100 m long and each subdivided into 16 hydrophone groups. Every second hydrophone group was used during recording resulting in a channel spacing of 12.5 m. The data were recorded with the BISON Spectra recording unit (University Bremen) with airgun and watergun data stored in alternating seismograms. The recording length was set to 4000 ms with a recording delay adjusted according to the water depth (mostly 4500 ms). The sample rate was constantly set to 0.125 ms and the raw seismic data were stored in the standard format SegY.

### 2.1.3 SO188

The research cruise SO188 took place in June and July 2006 and acquired MCS, swath bathymetry and echosounder data between the Bengal shelf and 8°N in the lower Bengal Fan (*Spieß et al., 2006*). Data acquisition on the lower Bengal Fan (close to 8°N, profiles GeoB06-221-264) was dedicated as the pre-site survey for IODP Expedition 354 (*France-Lanord et al., 2001, 2016*) (*Fig. 2.1*). During the recording of the profiles processed in the framework of this thesis (GeoB06-221–276; *Fig. 2.1*) two seismic sources were deployed: (1) A Sercel GI-Airgun with chamber volumes of 4.1 l (Generator) and 1.7 l (Injector); and (2) a Sercel watergun with a chamber volume of 0.16 l. The two sources were triggered with a delay of 2 s in a time interval of 10 s. The GI-Gun was towed approximately 16 m behind the ship in a water depth of ~6-8 m. Both guns were operated with an air pressure of ~130 bar. For recording a multichannel seismic streamer (SYNTRON) with a 50 m long stretch section and 12 active sections of 50 m length each was used. The active sections were subdivided into several subgroups resulting in 96 channels with a channel spacing of approximately 6.25 m. Data recording was conducted with the custom-made acquisition system MaMuCS (*Marine Multichannel Seismics; H. Keil, University Bremen*). The data were recorded with a sampling rate of 0.125 ms and a recording delay of 4-4.5 s. The shots of airgun and watergun were recorded in the same seismogram. Raw data were stored in SegY format.

## 2.2 Multichannel seismic data processing

The overall aim of seismic data processing is to enhance the image quality of the geological subsurface structures in order to allow a reliable data interpretation. To obtain a reliable and high-quality image, noise has to be removed and seismic events have to be migrated to their true subsurface position. Multichannel-seismic data provide the advantage of multiple coverages of every point on the seafloor. This allows the sorting of all seismic traces representing the same point on the seafloor into Common-Midpoint (CMP) gathers. Subsequent stacking of all traces within one CMP-gather suppresses random noise and thereby significantly enhances the signal to noise (S/N) ratio. Other processing steps applied to the data include geo-referencing, interactive velocity analysis, normal move out (NMO) correction, pre-

and post-stack noise suppression, and time migration (*Fig. 2.2*). The sequence of processing steps applied and the boundary conditions set during processing were adjusted according to the requirements for each dataset and each profile. Within the scope of this thesis in total 57 MCS (GeoB97-024 and GeoB06-221-276) profiles have been processed. The MCS profiles GeoB97-020-23 and 25-27 have been reprocessed just prior to IODP Expedition 354 by T. Schwenk and have been provided in the reprocessed version for this thesis. Profiles GeoB06-265-276 have been processed but after all not been included in this thesis as they lie out of the focus area.

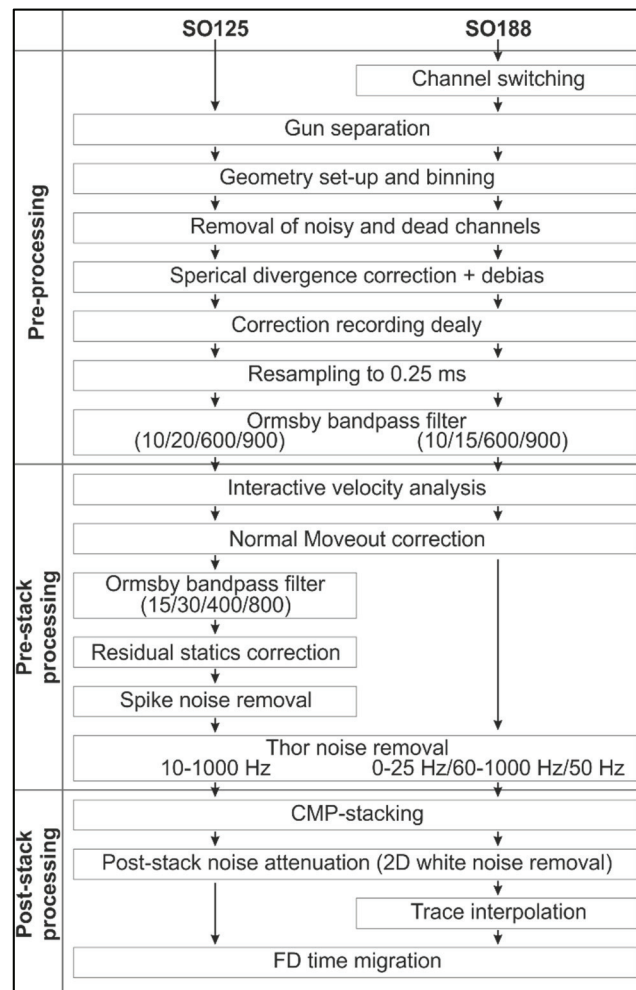


Figure 2.2: Standard processing flow applied to the SO125 and SO188 MCS data.

## 2.2.1 Pre-processing and geometry set-up

The very first pre-processing step, applied only to SO188 data, was the switching of the two middle channels of each hydrophone group, which were incorrectly connected during data recording. (*Fig. 2.3*). In a next step the two guns, recorded for each profile in the same raw-data file, had to be separated. The SO125 data had to be split horizontally (watergun and airgun data in alternating seismograms) while the SO188 data had to be split vertically (both guns with a delay of 2 seconds in one seismogram). Afterward, absolute source and receiver loca-

tions for each shot were determined using trigger times, the ship's GPS position and the relative distances between GPS and source and receiver (geometry set-up). This allows the data sorting in CMP gather and in a later processing step the CMP-stacking to enhance the S/N ratio. Under the assumption of a flat seafloor topography, a CMP-gather combines source-receiver pairs with variable offsets imaging the same area on the sea floor (bin) (Fig. 2.4). Bin size has to be chosen to enable a high lateral resolution (small bin size) while also support a sufficient noise suppression (large bin size). For the data of this study bin sizes of 12 m (SO125) and 8 m (SO188) have been chosen.

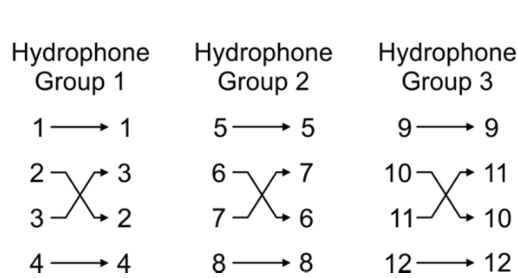


Figure 2.3: Scheme after which the central two channels of each hydrophone group (SO188 data) were switched in order to maintain the correct channel order.

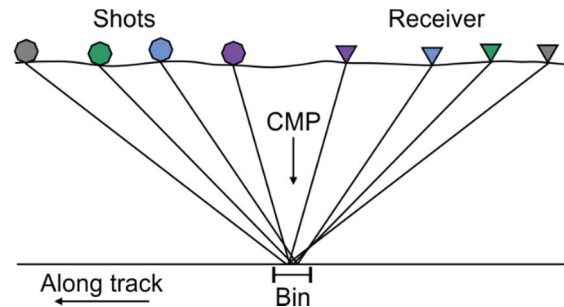


Figure 2.4: Common Midpoint (CMP) binning: Shot-receiver pairs of various offsets sharing the same (common) midpoint in a pre-defined area on the seafloor (bin) are gathered for subsequent velocity analysis, normal moveout correction and CMP stacking.

### 2.2.2 Trace editing

Noisy and dead channels were removed from the data set in order to improve the S/N ratio and stacking quality. Channel quality varied during data acquisition. Therefore, removal of channels has been adjusted during processing for each profile accordingly. In the same processing step the data were debiased to center the amplitudes of each trace at zero and the recording delay was corrected to shift the data in the correct water depth. Moreover, a spherical divergence correction has been applied to correct for the effect of amplitude loss due to the spherical spreading of the source signal. Finally, all data were resampled to 0.25 ms in order to decrease data volume and calculation times of subsequent processing steps.

### 2.2.3 Velocity analysis and NMO correction

The normal-moveout (NMO) is generated by the offset variance (source-receiver distance) of the traces and describes the travel time difference between a seismic event at zero offset and the offset of the individual traces (Fig. 2.5). The NMO results in hyperbolic shaped seismic events in CMP-gathers and has to be corrected prior to CMP-stacking. The shape of the hyperbola depends on the water depth, velocity and reflector geometry. For the NMO correction, the seismic velocity field of the subbottom has to be known. A velocity field can be determined

via interactive velocity analysis based on travel times and source-receiver offsets. For a reliable velocity analysis, large source-receiver offset are required. Here, the velocity analysis was beneficial to the imaging quality due to the vertically and horizontally highly variable subbottom properties of the seismic data set (channel-levee systems; sand vs. clay), despite the technically short offsets (streamer length  $\sim 650$  m; water depth  $>3500$  m).

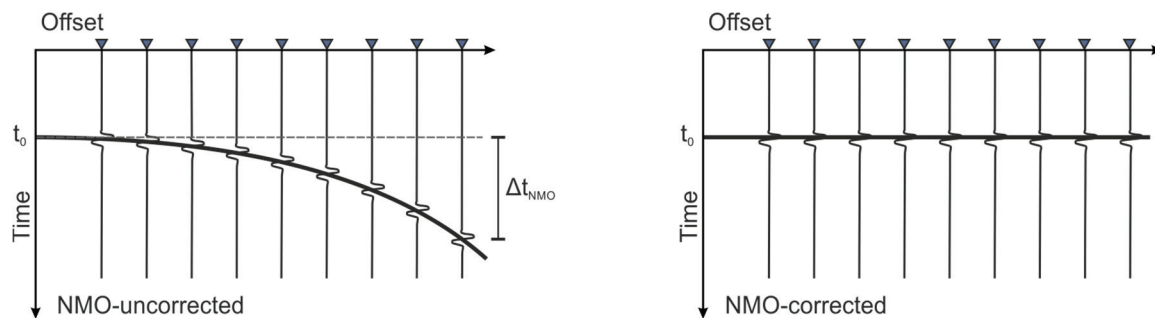


Figure 2.5: Left: CMP gather prior to the normal moveout (NMO) correction. The hyperbolic arrangement of the seismic events due to the with offset increasing travel time ( $\Delta t_{NMO}$ ). Right: CMP gather after NMO correction.

Vista<sup>2014</sup> provides a tool for interactive velocity analysis where the velocity model is picked at selected CMP control points along the profile. The basis for velocity picking is the NMO velocities along the hyperbolic seismic events, the stacking quality produced with a certain seismic velocity, and the semblance of stacks produced with a certain velocity.

Depending on profile length and subbottom properties, control points were chosen for every profile individually. Control point spacing was irregular with denser placing in areas with lateral variations of the subbottom properties, for instance in areas with channel-levee systems. Where possible control points were placed in areas with more or less horizontal reflectors in order to avoid false velocities created by inclined reflectors.

In the case of the SO188 dataset, some profiles showed unexpected high velocity at the seafloor reflector (1600-1650 m/s). The discrepancy between these high velocities and the expected  $\sim 1500$  m/s (water velocity) may be caused by an incorrect geometry set-up or delay correction. However, the occurrence of the too high travel velocities was unsystematic and their exact source could not be determined. For processing purposes, the affected profiles were manually shifted to a water depth resulting in a seafloor velocity similar to the unaffected profiles ( $\sim 1500$  m/s). The necessary shift varied from profile to profile and lay between 200 and 600 ms. After the velocity analysis and NMO-correction, data were shifted back into their actual water depth.

## 2.2.4 Pre-Stack noise attenuation

Various noises sources may affect signal quality during data acquisition. Common sources of noise are produced by the ships engine and/or waves (low-frequency noise) and electrical



noise (coherent noise peak at 50 Hz and its harmonics). Therefore, all data were filtered with an Ormsby-bandpass filter (SO125: filter flanks 10/20/600/900 pre-NMO-correction; 15/30/400/800 post-NMO-correction; SO188: filter flanks 10/15/600/900 pre-NMO-correction) in order to suppress low and high-frequency noise. Especially the SO188 data were still noisy after bandpass filtering, mostly due to a very strong 50 Hz peak overlapping with the main frequency range of the data (25 – 200 Hz). Thus, all data have additionally been treated by THOR-noise suppression. THOR is a nonlinear process using threshold median replacement in the frequency domain (*Butler, 2012*). It requires NMO-corrected input data, detects noise based on its incoherence and can be designed to just treat noise in predefined frequencies. For the SO125 data, THOR has been applied once on the frequency range of 10-1000 Hz. The SO188 have been treated with THOR thrice successively, each time treating a different frequency range (first run 0 – 25 Hz; second run 60 - 10000 Hz; third run 50 Hz). THOR was especially efficient in removing the strong 50 Hz peak from the SO188 data without having to bandpass filter this frequency range (*Fig. 2.6*).

The NMO-corrected SO125 data were furthermore corrected for residual statics using the Vista tool MCorrel and for spike noise via despiking. The residual static correction compensates for vertical movement of source and receiver due to waves and thereby improves stacking quality. Despiking removes spike noises by comparison of amplitudes along a trace within a pre-defined time window with the ambient background amplitudes.

### **2.2.5 CMP-stacking and post-stack noise attenuation**

After pre-stack noise attenuation data were CMP-stacked by averaging all traces within one CMP gather and thereby enhancing the signal/noise ratio.

The 4D-DEC algorithm provided by Vista<sup>2014</sup> is a tool to remove white noise from stacked traces. It uses cross-correlation of energy peaks with adjacent traces in small, predefined time and space windows. Energy peaks which do not correspond to a continuous reflector in the neighboring traces are removed. In order to allow for dipping reflectors, the maximum expected dip can be manually adjusted. 4D-DEC greatly improved the signal/noise ratio and image quality of all data and has been applied as the last processing step before time migration (*Fig. 2.6*).

### **2.2.6 Time migration**

Migration is a processing step applied to seismic data in order to move dipping reflectors into their true subsurface position. Moreover, migration removes so-called bowties originating from synclines and anticlines, and it collapses diffraction hyperbola originating from point- or disrupted reflectors (e.g. boulders or faults). After migration, the stacked section resembles the actual geology and allows for accurate interpretation. Before final migration, empty CMPs were filled by trace padding. Afterward a Finite Differences (FD) Time Migration was applied using the velocity field determined during the interactive velocity analysis (*Fig. 2.6*). The FD Time

Migration is robust for lateral velocity variations and therefore well suited for the data in this study characterized by frequent lateral variations in lithology (sand vs. clay).

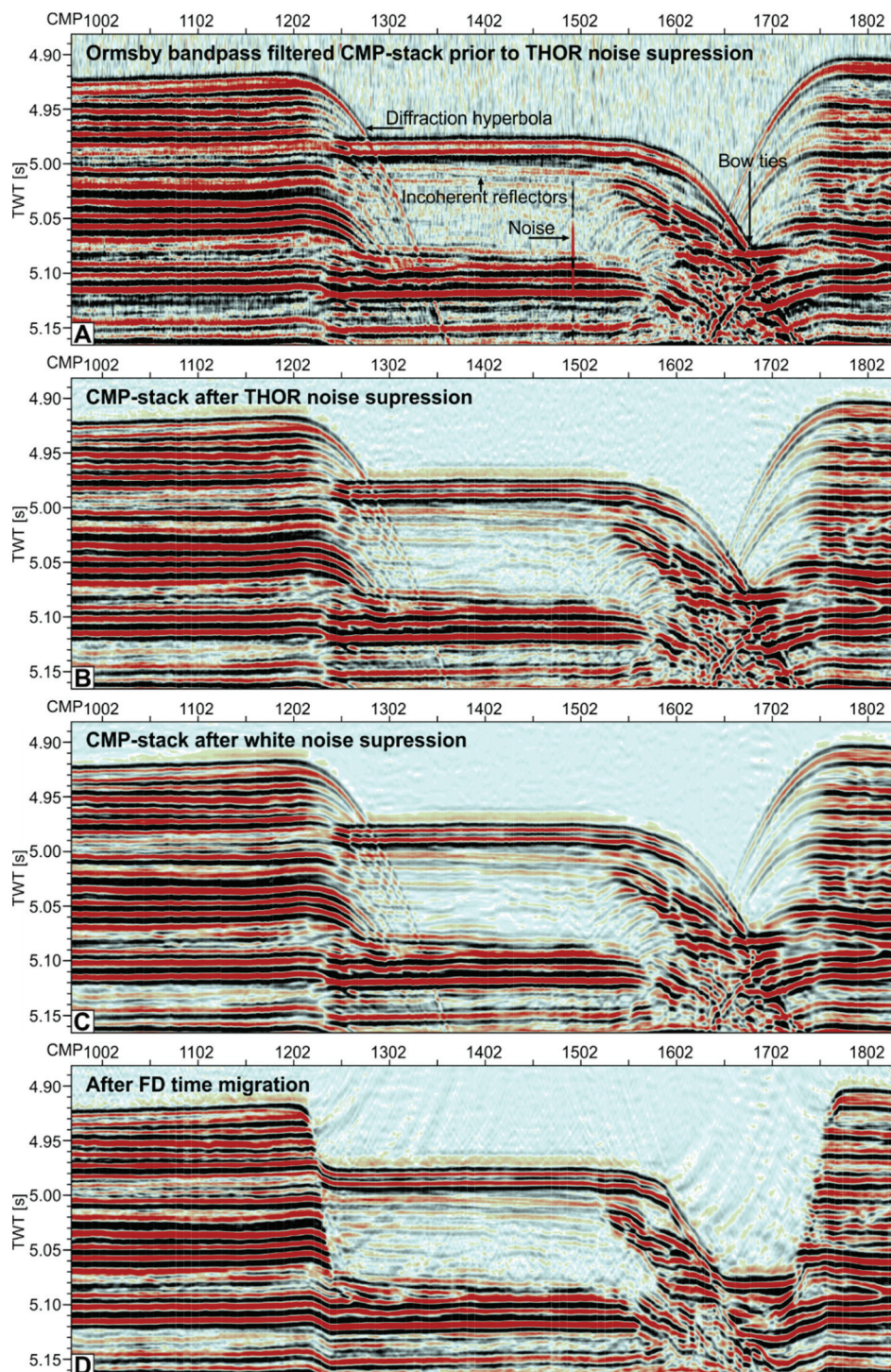


Figure 2.6: CMP stack of Profile GeoB06-253 illustrating the effect of noise attenuation using the Vista2014 THOR and 4D-Dec modules and the effect of time migration. A: Ormsby bandpass filtered CMP stack prior to THOR and 4D-Dec noise attenuation. B: CMP stack after applying the THOR noise suppression shows significantly enhanced S/N ratio and reflector coherency. C: CMP stack after applying 4D-Dec, further improvement of reflector coherency. D: Time-migrated CMP stack. Diffraction hyperbola and bow ties are removed and dipping reflectors are moved to their true subsurface position.



### 2.2.7 Reprocessing SO125 data

Multichannel seismic profiles GeoB97-020 to -027 were already processed and published in the years 2003 and 2009 (Schwenk, 2003 (*dissertation*); Schwenk and Spieß, 2009). Just prior to IODP Expedition 354 the data have been revised and reprocessed. New processing techniques and the progress in software developments enabled a considerably improved noise suppression and allowed for a smaller binning (20 m vs. 12 m), thereby increasing the horizontal resolution. Moreover, the new processing enhanced the reflector coherency (Fig. 2.7), the contrast between levee sediments and non-levee sediments, and significantly improved the imaging of deeper structures, in particular, the Bengal Fan base-reflector (Fig. 2.7, B and C).

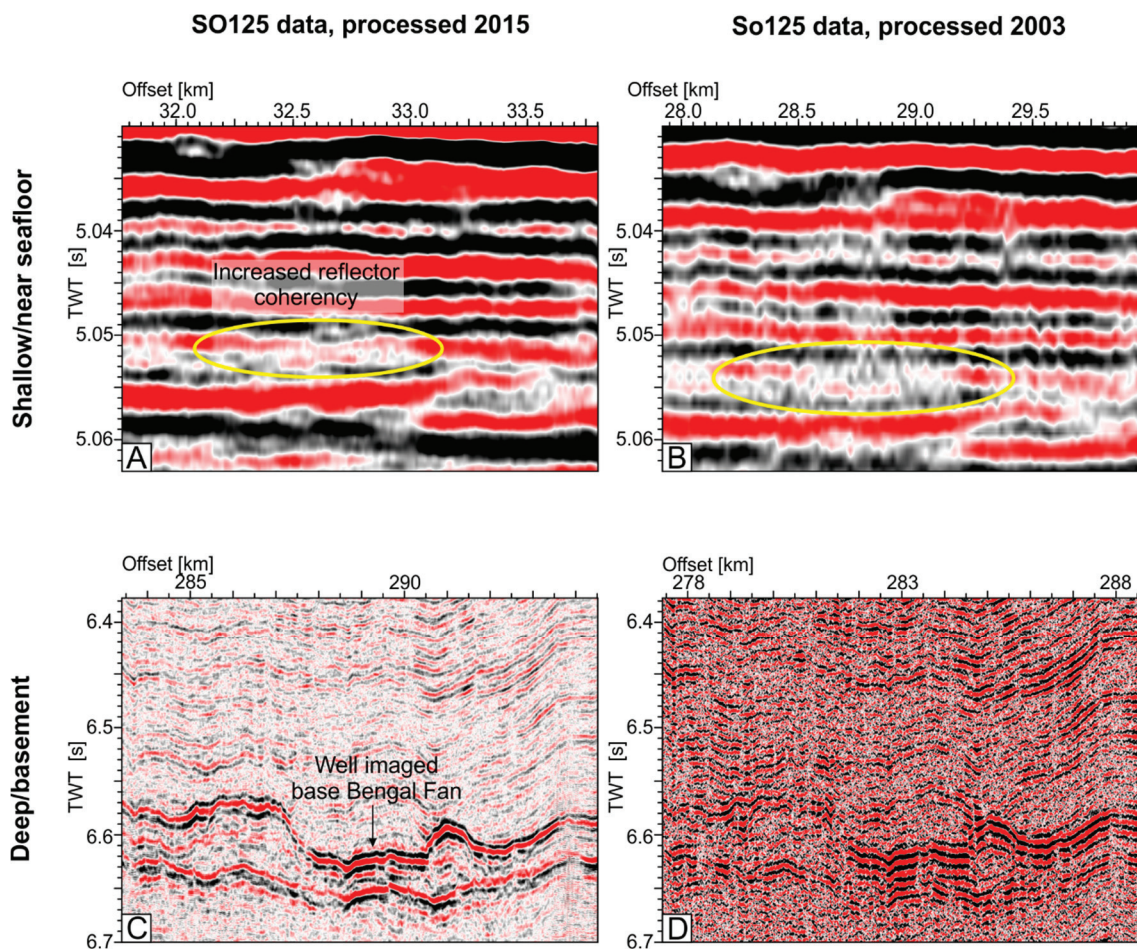


Figure 2.7: Comparison of processed SO125 used in this study (A and C) and processed So125 published by Schwenk, 2003 and Schwenk and Spieß, 2009 (B and D). The use of a smaller bin size and more sophisticated noise suppression applied during the reprocessing of the data enhanced reflector coherency, vertical resolution and the imaging of deeper lying structure. Please note that A and B and C and D show the same close-up but that the offset is slightly different due to technical reasons.

### 2.2.8 Watergun Processing

The seismic signal emitted by the Sercel watergun (0.16 l chamber volume) has a frequency range of ~100-800 Hz, resulting in a higher vertical resolution than the GI-airgun seismic data (*Tbl. 2.1*). Simultaneously, the frequency range covered by the watergun should penetrate deeper into the subbottom than the echosounder data. To test the potential advantages of the watergun seismic data compared to the GI-airgun and echosounder data, watergun profile GeoB97-020 has been processed. The processing results have shown that the watergun data indeed have a higher resolution than the GI-airgun data in the upper 100-150 ms (TWT) (*Fig. 2.8, B and C*). However, signal attenuation of the high-frequency signal (vertical resolution ~2 m) in the upper ~100 ms TWT is so strong that only the low-frequency part (vertical resolution ~5-7 m) penetrates below that. This means that the high-frequency part is only preserved in a depth range which is also covered by the very-high-resolution Parasound data (*Fig. 2.8, A and B*). At the same time, the watergun data are strongly disturbed by a precursor generated during signal emission (*Fig. 2.8 B*). Additionally, due to its short wavelength, the high-frequency part of the signal is very prone to streamer-internal depth variations created by wave action. This results in vertical shifts of the seismic signal, often exceeding wavelength and therefore being difficult to fully correct. In summary, the watergun data did not prove advantageous and as a consequence has not been included in this thesis.

### 2.3 Parasound Echosounder Data

The RV Sonne is equipped with the hull-mounted sediment echosounder Parasound capable of sediment and water column imaging. The Parasound makes use of the parametric effect by simultaneously emitting two high-energy signals of similar frequencies (e.g. 18 and 22 kHz). By nonlinear-acoustic interaction, it generates a secondary frequency (difference frequency, e.g. 4 kHz). The secondary frequency is restricted to the transmission beam of the high-frequency primary signals leading to a very narrow transmission angle (4°) and a footprint of only 7% of the water depth (*Grant and Schreiber, 1990*).

Parasound data used in this study were acquired, configured to achieve a secondary frequency of 4 kHz, thereby enabling a subbottom signal penetration between 10-200 m (depending on the sediment type) and a vertical resolution on a decimeter scale. The data were digitally recorded with the data acquisition system ParaDIGMA (*Spieß, 1993*).

Raw data were converted into SegY-format using the custom-made software PS32SegY (*H., Keil, University Bremen*). All Parasound profiles were additionally bandpass-filtered and converted via Hilbert transformation to an envelope to enhance reflector coherency.



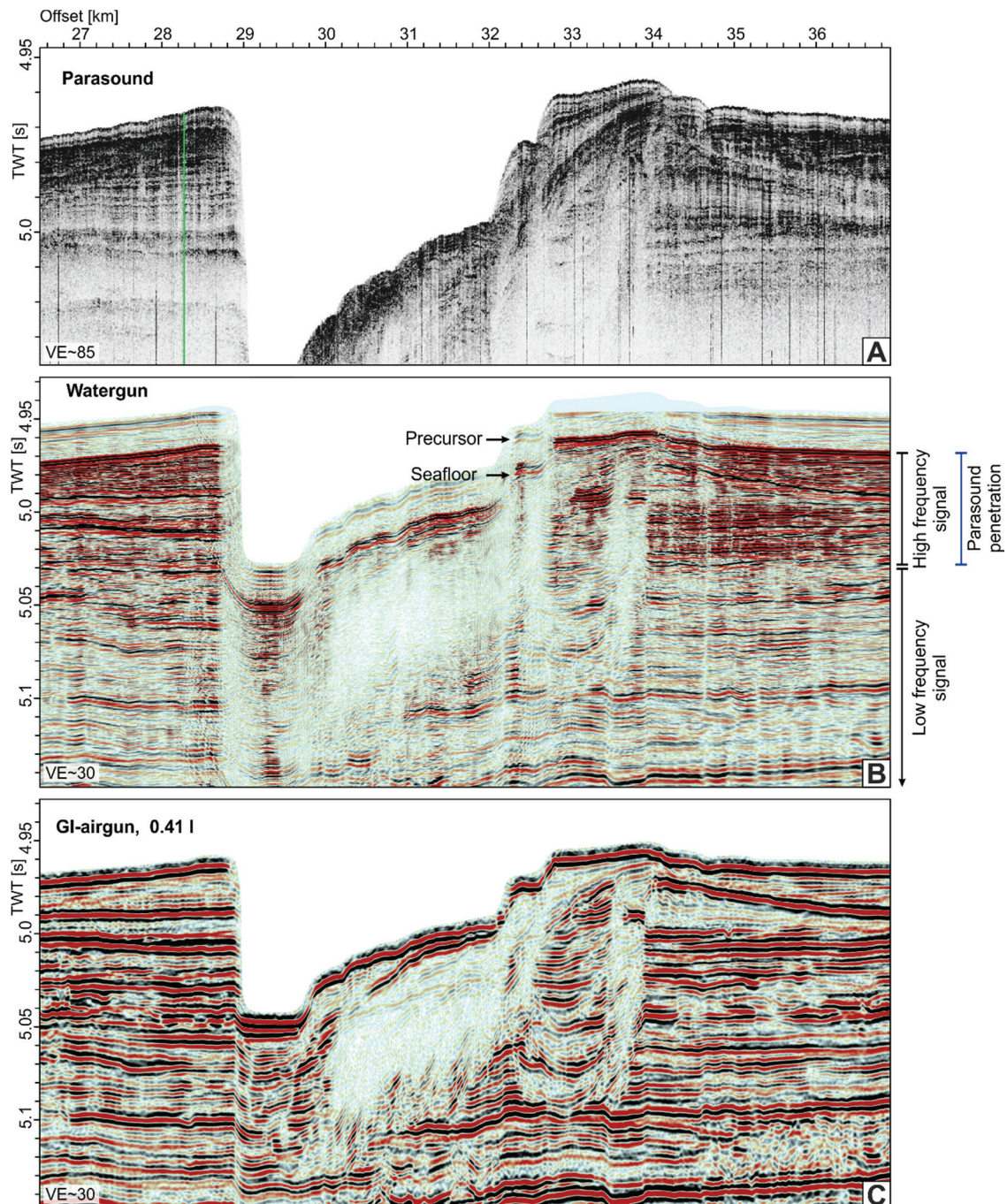


Figure 2.8: Comparison of Parasound echosounder (a), watergun (B), and GI-airgun (C) data showing that the high-frequency part of the watergun signal (vertical resolution  $\sim 2$  m) covers the upper  $\sim 100$ - $120$  ms TWT, the same depth range which is penetrated by the very-high-resolution Parasound data. Only the low-frequency watergun signal (vertical resolution  $\sim 5$ - $7$  m) penetrates deeper with a resolution likewise the GI-airgun data.

## 2.4 Swath Bathymetry Data

The Hydrosweep swath bathymetry sounder (used during SO93 and SO125) is a hull-mounted system permanently installed on RV Sonne. The Hydrosweep is a 59-beam swath sounder

which provides a swath width of up to twice the water depth. The sonar frequency of the Hydrosweep is 15.5 kHz and the aperture angle of every beam is 2.3°.

The Simrad EM120 was used for bathymetry mapping during SO188. The system consists of two linear transducer arrays in a Mills Cross configuration, with separate units for transmitting and receiving. It works with a sonar frequency of 12 kHz, an emission beam angle of 150° (across-track) versus 1° (along-track), and 191 beams per ping (beam dimension 1° by 2°). The achievable swath width on a flat bottom can be up to 6 times the water depth, dependent on the roughness of the seafloor.

Multibeam bathymetry data shown in this study were provided in a processed version. Processing was conducted using the software 'QPS Fledermaus' and the open source software MB-systems (Caress and Chayes, 2017).

## 2.5 Integration of IODP 354 cores and seismic data

Seven sites, aligned on a west-east transect, were drilled during IODP Expedition 354 (Fig. 1.14 and 2.1 and Tbl. 2.2). All cores are crossed by MCS Profile GeoB97-020+27. Because no continuous downhole logging was conducted during IODP Expedition 354, the relevant sections of the seven cores (upper 100-200 m, down to the Middle Pleistocene Hemipelagic Layer) were integrated into the seismic data using a constant velocity individually chosen for each site (Tbl 2.2). The velocities were based on the best achievable fit between prominent reflectors and significant changes in core lithology and physical properties such as magnetic susceptibility (MS) and natural gamma radiation (NGR). Prominent hemipelagic layers can well be distinguished from the surrounding sediments due to their low magnetic susceptibility (MS), low natural gamma radiation (NGR) and a strong impedance contrast. Moreover, the velocities were cross-checked with the P-wave velocities measured on the cores directly showing a good agreement between the measured average velocities and the once used for core-seismic integration.

Table 2.2: Site Summary of IODP Expedition 354 sites used in this study and the velocities used to integrate the cores with the multichannel-seismic data.

Site	Latitude (N)	Longitude (E)	Water Depth [m]	Total Penetration [m]	Core recovery [%]	Seismic velocity used for seismic integration [m/s]
U1449A	8.01	88.11	3652.7	213.5	61	1640
U1450A	8.01	87.67	3655.3	687.4	64	1680
U1451A	8.01	88.74	3607.3	582.1	86	1650
U1452B	8.01	87.18	3670.3	217.7	79	1680
U1453A	8.01	86.79	3679.5	215.7	88	1650
U1454B	8.01	85.85	3710.3	161.8	88	1640
U1455C	8.01	86.28	3732.5	949.0	56	1640

## Chapter 3

### 3 Sinuosity-controlled deposition along a channel-levee system at the lower Bengal Fan

Fenna Bergmann<sup>1</sup>, Tilmann Schwenk<sup>1</sup>, Volkhard Spiess<sup>1</sup>, Hendrik Lantzsch<sup>1</sup>, Petra Dekens<sup>2</sup>, Valier Galy<sup>3</sup>, Christian France-Lanord<sup>4</sup>

<sup>1</sup> Faculty of Geosciences, University of Bremen, Klagenfurter Strasse 2-4, D-28359 Bremen, Germany

<sup>2</sup> Department of Earth & Climate Sciences, San Francisco State University, 1600 Holloway Avenue, San Francisco CA 94131, USA

<sup>3</sup> Department of Marine Chemistry and Geochemistry, Woods Hole Oceanographic Institution, 266 Woods Hole Rd., Woods Hole, MA 02543, USA

<sup>4</sup> Centre de Recherches Pétrographiques et Géochimiques, CNRS Université de Lorraine, BP 20, 54501 Vandoeuvre les Nancy, France

#### Abstract

Channel-levee systems are one of the main controllers of sediment distribution and deposition in sedimentary systems worldwide. One of these systems is the Bengal Fan, the most complete record of the tectonic and climatic history of the Himalayan area. Understanding the evolution and the depositional behavior of the channel-levee systems distributing material along and across the Bengal Fan is a prerequisite when working with this sedimentary archive.

Here, we present results from an integrated study of high-resolution sediment echosounder (Parasound) profiles, multichannel seismic data and IODP Expedition 354 drilling results, investigating the active channel-levee system at the lower Bengal Fan (8°N). We focus on the assessment of spatial and temporal changes in deposition along the Active Channel and the relationship between channel sinuosity and overflow depositional patterns in a natural setting. Further, we investigate mass accumulation rates and sedimentary fluxes to the Bengal Fan. Using radiocarbon dating, we develop an age model for the Active Channel. The onset of overflow deposition at 8°N occurred around ~26.8 ka BP. Active overflow lasted for only 3.2 ka, interrupted twice by times of hemipelagic deposition at ~25.5-11.5 ka BP and 9.6 ka BP – recent. Our results suggest that both times of interruption were triggered by a decrease in turbidity-current height and that no general link between hemipelagic deposition at 8°N and sea level exists.

Spatial mapping of individual levee units revealed a strong influence of channel sinuosity on the overflowing deposition resulting in a patchy deposition. This highlights that, on short terms,

sedimentation rate cannot be directly transferred to flux. Mass accumulation rates during the investigated time intervals, however, stay relatively constant despite the locally uneven deposition, demonstrating a constant sediment flux unaffected by sea-level variations. On longer terms, the patchy deposition is equalized in response to the dynamic channel geometry. Thus, we suggest to average sedimentary budgets over the entire lifetime of one-channel-levee system in order to minimize statistical errors generated by short-term fluctuations.

### 3.1 Introduction

The Himalaya Mountains – Bengal Fan source-to-sink system is one of the largest sedimentary systems in the world. The majority of sediment eroded in the Himalayan Mountains is stored in the Bengal Fan, thereby providing the most complete sedimentary record of the erosional, tectonic, and climate history of the area since fan initiation in the Early Eocene (*Curray et al., 2003*). Channel-levee systems (CLSs) are the main controller of sediment distribution and deposition along and across the Bengal Fan (*Curray et al., 2003; Schwenk and Spieß, 2009*). Understanding the depositional/erosional behavior and evolution of CLSs is an essential prerequisite to ultimately draw inferences from the sink (here the Bengal Fan) to changes in the source (here the Himalaya, Tibetan Plateau). Thus, the evolution of turbidity-current induced CLSs and the depositional behavior within a channel and on its levees has been a long-term research subject (*e.g. Komar, 1969; Imran et al., 1998; Peakall et al., 2000; Kneller 2003; Straub et al., 2008; Peakall and Sumner, 2015*). However, most recent studies are primarily based on indirect observations. Numerical or sandbox models illustrate the general behavior of overspill deposition and grain size sorting in sinuous channel-levee systems (*e.g. Peakall et al., 2000; Straub et al., 2008, Huang et al., 2012*), using simplified boundary conditions such as a static sinuosity, downsizing or non-erosive channels.

In this study, we investigate depositional processes along the most recent active channel of the Bengal Fan (Active Channel, AC) by integration of high-resolution seismoacoustic data and IODP Expedition 354 drilling results from 8°N (*Fig. 3.1*). The dataset provides the rare opportunity to conduct a high-resolution study on the depositional behavior of a meandering channel-levee system in a natural setting and provides further insides into the evolution of channel-levee systems at the Bengal Fan, in particular of the Active Channel.

The study aims to investigate (1) the depositional style and facies succession of the AC as well as its evolution in space and time, (2) the relationship between channel sinuosity and overspill depositional patterns in a natural setting, and (3) mass accumulation rates and volumes of individual levee units in order to provide constraints for the quantification of sedimentary fluxes onto the Bengal Fan.



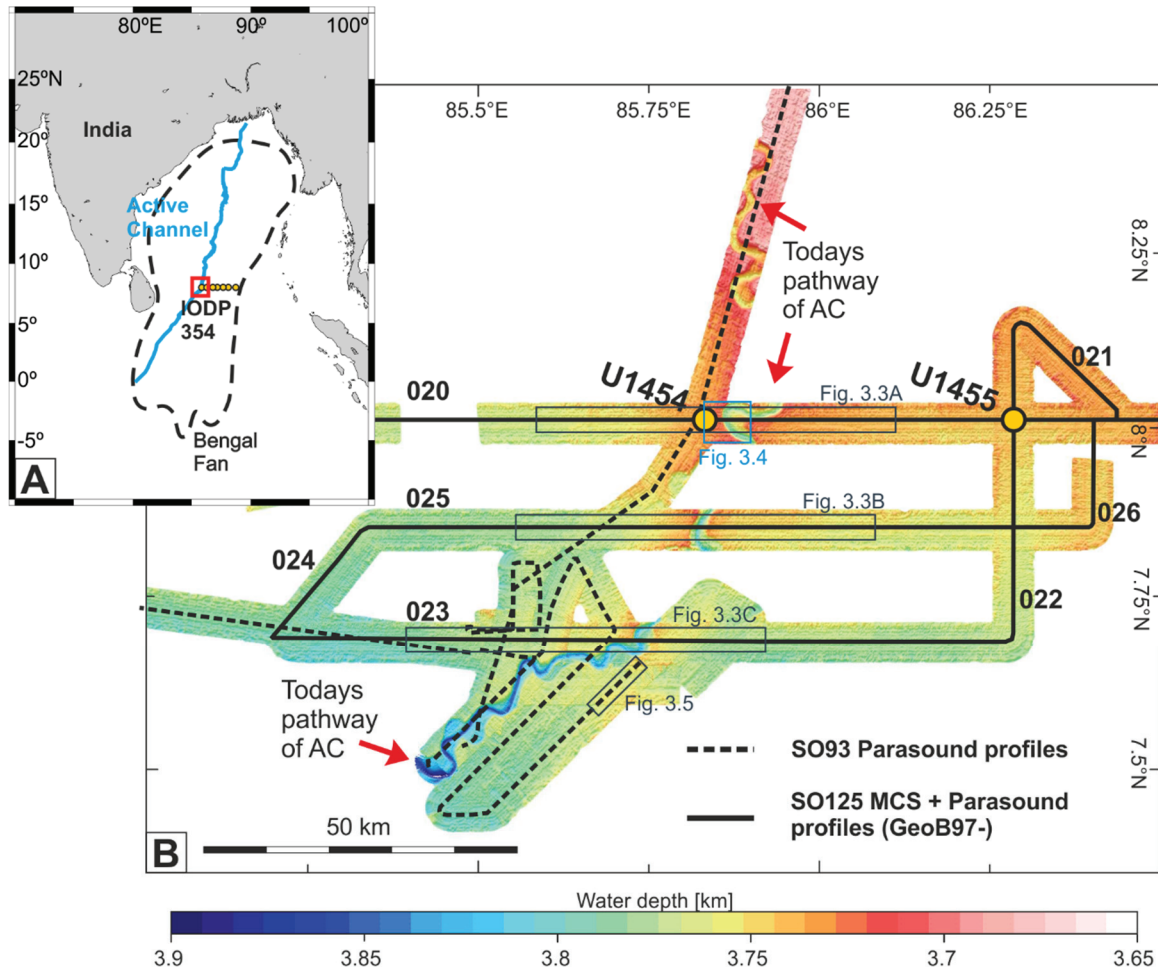


Figure 3.1: A: Overview map of the Bengal Fan (outline of the fan marked by a dashed line, after Curray *et al.*, 2003); the pathway of the Active Channel (AC) is indicated in blue. IODP Expedition 354 sites at 8°N are marked by yellow dots. B: Bathymetric map of the study area at 8°N (red square in A) illustrating the AC pathway, IODP 354 Sites U1454 and U1455 as well as the acoustic dataset used in this study. MCS: Multichannel seismic.

### 3.1.1 Regional background - The Bengal Fan

The submarine Bengal Fan covers large areas of the Indian Ocean and is bordered by India and Sri Lanka in the West, Bangladesh, and Myanmar in the North and the Andaman-Nicobar ridge and Sumatra in the East. It extends over 3000 km southwards and receives Himalayan sediments since its initiation in the Early Eocene (Curray *et al.*, 2003).

Since the Late Miocene, sediment transport along the fan has been dominated by CLSs, initiated and further shaped by episodically occurring turbidity currents (Curray *et al.*, 2003; Schwenk and Spieß, 2009). Frequent channel avulsions on the upper fan have resulted in the abandonment of old channels and the formation of new channel-levee systems, occasional channel-reoccupations and the subsequently developing tributary channel pattern (Curray *et al.*, 2003). This has led to the development of a complex erosional/depositional system with lateral depocenter migration over the entire fan (Curray *et al.*, 2003; Schwenk and Spieß,

2009). Today, the Ganges and Brahmaputra rivers are the main sediment source for the Bengal Shelf and Fan. Merging a number of smaller tributaries, they drain the northern as well as the southern flank of the Himalayan range. In the course of the Holocene sea-level rise, the Ganges-Brahmaputra delta development was initiated at ~11 ka, trapping large amounts of the river discharge (*Goodbred and Kuehl, 2000a, b*). Although the direct connection between river/delta and fan is interrupted since 9-6.5 ka ago, sediment is still transported to the fan via the deep incised shelf canyon Swatch of No Ground (SoNG) and along the fan via the Active Channel (AC; *Fig. 3.1*) (*Kuehl et al., 1989; Curray et al., 2003; Kottke et al., 2003*). The activity of the AC during the Holocene highstand has been reported by several studies working on this system at 16.5°N (*Hübscher et al., 1997; Weber et al., 1997, 2003; Hein et al., 2017*). Just recently, the study by *Hein et al., (2017)* showed active overspill deposition since at least 17.4 kyrs BP lasting until 190 yrs BP. Additionally, a sample of wood debris of ~10.5 ka in age, found within the AC at 4.2°N, proves Holocene activity of the AC even south of our study area (*Weber et al., 2003*).

### 3.1.2 Channel-Levee systems

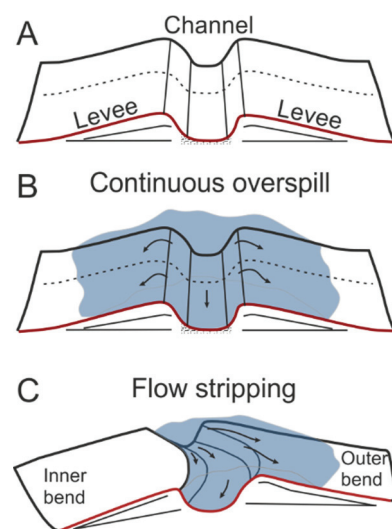
Channel-levee systems (CLSs) are known as major architectural elements within the Bengal Fan (*Hübscher et al., 1997; Curray et al., 2003; Schwenk et al., 2005; Schwenk and Spieß, 2009*) and also within other submarine fan systems such as the Congo or the Amazon Fan (e.g. *Lopez 2001; Pirmez and Imran, 2003; Jegou et al., 2008; Savoye et al., 2009; Babonneau et al., 2010; Picot et al., 2016*). They are initiated and further shaped by self-channelizing turbidity currents and subsequently act as conduits for further flow events (*Imran et al., 1998*). Levees are wedge-shaped sedimentary deposits flanking submarine channels (*Fig. 3.2*) formed wherever the height of the turbidity flow exceeds the channel relief and grow with every overspilling turbidity current. They are characterized by an upward-fining trend of grain sizes due to a vertical separation within mix-loaded turbidity currents (*Pirmez and Imran, 2003*). A distinction is made between two end-member modes of overspilling, the continuous overspill, and the overspill via flow stripping when the flow is unable to completely follow a channel bend and splits up (*Fig. 3.2*) (*Piper and Normark, 1983; Peakall et al., 2000*).

At the distal end of channels as well as below the levees bases, terminal lobes are a common feature formed during the downfan progradation of the CLSs (*Posamentier and Kolla, 2003; Picot et al., 2016; Savoye et al., 2009*). The lobes are composed of coarse, sandy material and often connected to small distributary channels acting as sediment conduit (*Pirmez et al., 1997; Jegou et al., 2008; Savoye et al., 2009; Picot et al., 2016*).

The evolution of channel-levee systems and their depositional behavior have been a long-term research subject of outcrop and 2D/3D seismic survey studies (e.g. *Peakall et al., 2000, Hansen et al., 2015*), as well as physical (e.g. *Peakall et al., 2007; Straub et al., 2008, 2011; Kane et al., 2008, 2010; Ezz et al., 2013*) and numerical models (e.g. *Imran et al., 1998; Amos et al.,*



2010; Huang *et al.*, 2012). Several recent studies focused on the influence of channel sinuosity on depositional mechanics (e.g. Straub *et al.*, 2008, 2011) or the external geometry of levees (e.g. Kane *et al.*, 2010; Huang *et al.*, 2012; Nakajima and Kneller, 2013) proving that deposition on levees is strongly influenced by the sinuosity of the associated channel. Sandbox and numerical models of sinuous channel bends reveal a strong cross-channel asymmetry of the levees at bent channel sections induced by flow stripping of the turbidity currents (Peakall *et al.*, 2000, 2007; Straub *et al.*, 2008; Kane *et al.*, 2010; Huang *et al.*, 2012). Levees deposited at the overbank area of the outer side of a channel bend (cut bank side) are thicker and of slightly coarser grain size than the levees deposited on the inner side of a channel bend (point bar side) (Straub *et al.*, 2008; Amos *et al.*, 2010; Kane *et al.*, 2010; Huang *et al.*, 2012). Furthermore, there seems to be a relation between levee shape and channel sinuosity: Outer bend levees show a more concave upward shape whereas inner bend levees are shaped convex upward (Huang *et al.*, 2012). On the contrary, deposition on the levees along (nearly) straight channel sections and at meander inflection points is nearly symmetrical (Straub *et al.*, 2008; Kane *et al.*, 2010; Huang *et al.*, 2012). The amount of total overspill and the grain size increase



with increasing sinuosity (Amos *et al.*, 2010; Huang *et al.*, 2012). Aside from modeling, several high-resolution studies, such as the work presented by Schwenk *et al.*, 2003 or Babonneau *et al.*, 2010, investigated the variability of actively meandering channels and the formation of intra-channel deposits such as point bars or inner-levee terraces. However, to our knowledge there is no study so far that shows how deposition on levees is influenced by an actively meandering channel on a sub-levee scale.

Figure 3.2: Sketch of a channel-levee system (A) illustrating its general geometry and the two major modes of deposition: Continuous overspill (B) and overspill via flow stripping (C). Modified after Hansen *et al.*, 2015.

## 3.2 Material and Methods

In this study, we use an integrated dataset of seismoacoustic data from the vicinity of the AC at 8°N and the results of IODP Site U1454B, drilled during IODP Expedition 354 into the western levee of the AC (Fig. 3.1).

### 3.2.1 Seismoacoustic data - acquisition and processing

The seismoacoustic dataset is compiled of swath-bathymetry, very-high-resolution parametric sediment echosounder (Parasound), and high-resolution multichannel seismic (MCS) data acquired during the two research cruises SO93 in 1994 and SO125 in 1997, both carried out in

cooperation of the University of Bremen and the BGR Hannover (*Fig. 3.1*). The dataset consist of three W-E trending cross-sections through the AC (GeoB97-020, GeoB97-023, and GeoB97-025; Parasound as well as MCS data), one long channel-parallel Parasound profile and two additional N-S trending profiles (Parasound + MCS) connecting these three cross sections and several short profiles recorded in the southern part of the study area (Parasound) (*Fig. 3.1*). In total, ~750 km of very high-resolution Parasound data were utilized for this study. During recording the secondary frequency was set to ~4 kHz to achieve a decimeter-scale vertical resolution while imaging the upper 50 – 100 m of the sediment column. All Parasound profiles are bandpass-filtered and converted via Hilbert transformation to an envelope to enhance reflector coherency. MCS data were acquired (only during SO125) using a 2x0.41 I Sercel GI-Airgun as source emitting in a frequency range of ~50-300 Hz with a main frequency of ~150 Hz resulting in a vertical resolution of ~5m and a sub-seafloor penetration of ~1 km. As receiver a 48-channel analog streamer with a channel spacing of 12.5 m was used. All MCS data underwent a full multichannel seismic data processing including CMP-Binning, filtering, stacking and time-migration.

Processing and interpretation of Parasound and MCS datasets was conducted with the software 'Vista 14; Seismic Data Processing' and 'IHS Kingdom 2016'. Bathymetry data were processed with the software 'QPS Fledermaus' and the open source software MB-systems (*Carrass and Chayes, 2017*).

Conversions of two-way-traveltime (TWT) to depth was done using a constant velocity of 1500 m/s. Grids were calculated with a flex gridding algorithm, 3 km extrapolation from control points and a grid cell spacing of 100 m (*Fig. 3.6*).

### 3.2.2 Relative volume and flux calculations

Sediment volumes and fluxes were calculated for the three Parasound profiles GeoB97-020, GeoB97-023 and GeoB97-025 providing a full cross-section of the levee, in order to investigate temporal variations throughout the levee evolution. In a first step, the 2D-cross sections of individual levee units (for each of the three profiles) were determined. In a next step, these 2D-cross sections were extrapolated for an along-channel distance of 1 km since the N-S profile shows no significant changes along this distance. The resulting volumes are necessary for the calculation of sediment fluxes. Subsequently, the calculated volumes were summed up for each unit and along each profile. Hence, volumes listed in *Table 3.2* in total represent a distance of 3 km along the channel. Mass accumulation rates (MAR) were then calculated based on equation (1) with  $V$  representing the volume of the corresponding unit,  $t$  the duration of its deposition and  $DBD$  the dry bulk density measured during IODP Expedition 354 (*France-Lanord et al., 2016*).

$$(1) \quad MAR = \frac{V \cdot DBD}{t}$$

### 3.2.3 IODP Expedition 354 Site U1454

IODP Site U1454 is located at 08°0.39'N, 85°51.00'E in a water depth of about 3721 m. It is the westernmost site drilled during IODP Expedition 354 and situated 800 m west of the thalweg of the AC (Figs . 3.1 and 3.3). Hole U1454B was drilled down to a depth of 161.8 m with a recovery of 129.51 m of sediment including the silty and clayey levee sediments of the levee and an underlying sand-rich section (France-Lanord *et al.*, 2016). On-board visual description and smear slides were performed for each sediment section. Lithologies for siliciclastic components are based on the relative proportions of sand-, silt-, and clay-sized particles. The term clay is used to describe particles <4 µm in diameter. The term calcareous clay is used for a mixture of clay particles and 10-75% of calcareous components and represents sediments predominantly deposited hemipelagically.

### 3.2.4 Radiocarbon ages

The radiocarbon age of planktonic foraminifera was measured at the National Ocean Science Mass Spectrometry Facility (NOSAMS, Woods Hole, USA) following acid hydrolysis with H<sub>3</sub>PO<sub>4</sub>, catalytic conversion of the evolved CO<sub>2</sub> to graphite and AMS analysis. Radiocarbon ages were corrected for a constant surface reservoir age of 400 14C years and calibrated using IntCal13.

The radiocarbon age of wood debris was measured at NOSAMS following Acid-Base-Acid treatment, closed tube combustion, and AMS analysis. Radiocarbon ages were calibrated using IntCal13.

## 3.3 Results

### 3.3.1 Seafloor morphology

The bathymetric map of the study area (Fig. 3.1) shows a ~140 km long section of the AC between 8.5°N and 7.4°N in a water depth of 3650-3900 m. Here, the AC runs southwards until 7°45' N where it turns towards the southwest. In the study area, the AC shows 19 meanders with an average sinuosity of ~1.33 (peak values up to 2.6). Seafloor and channel thalweg are gently sloping southwestwards with slope angles between 0.05° and 0.1°. The channel relief (levee crest to recent thalweg) increases from north to south from 60-65 m to 90-95 m.

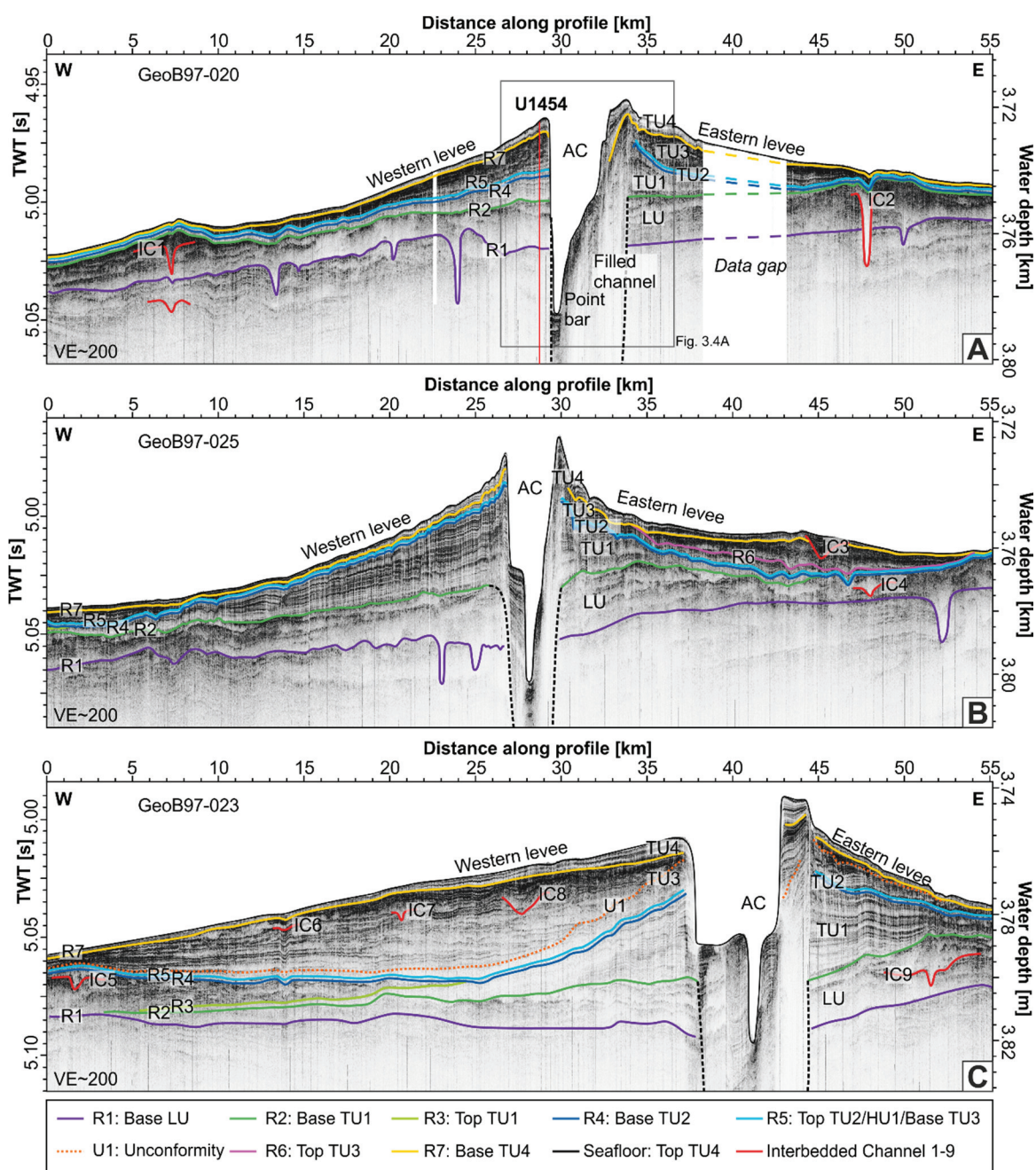


Figure 3.3: Central part of Parasound Profiles GeoB97-020 (A), GeoB97-025 (B) and GeoB97-023 (C) showing the Active Channel (AC) and corresponding levees as well as IODP Site U1454. For location see Fig. 3.1. Note that the profiles are strongly vertically exaggerated.

### 3.3.2 Overall channel-levee architecture

The west-east trending, 120 km long Parasound Profile GeoB97-020 (Figs. 3.1 and 3.3) crosses Site U1454 and the AC roughly orthogonally to a meander bend apex. Here, the channel is 65 m deep and asymmetric with a steeper slope in the west and a point bar in the east. The channel is flanked by typical, wedge-shaped levees with bases marked by a distinct acoustic reflector (Fig. 3.3; R2).



A north-south comparison of the three Parasound profiles GeoB97-020, GeoB97-025, and GeoB97-023 (Fig. 3.3) shows a change of the internal levee structures from well-layered reflections in the northern and central cross-section to a more irregular pattern with internal channels and acoustically transparent sections in the southern cross-section.

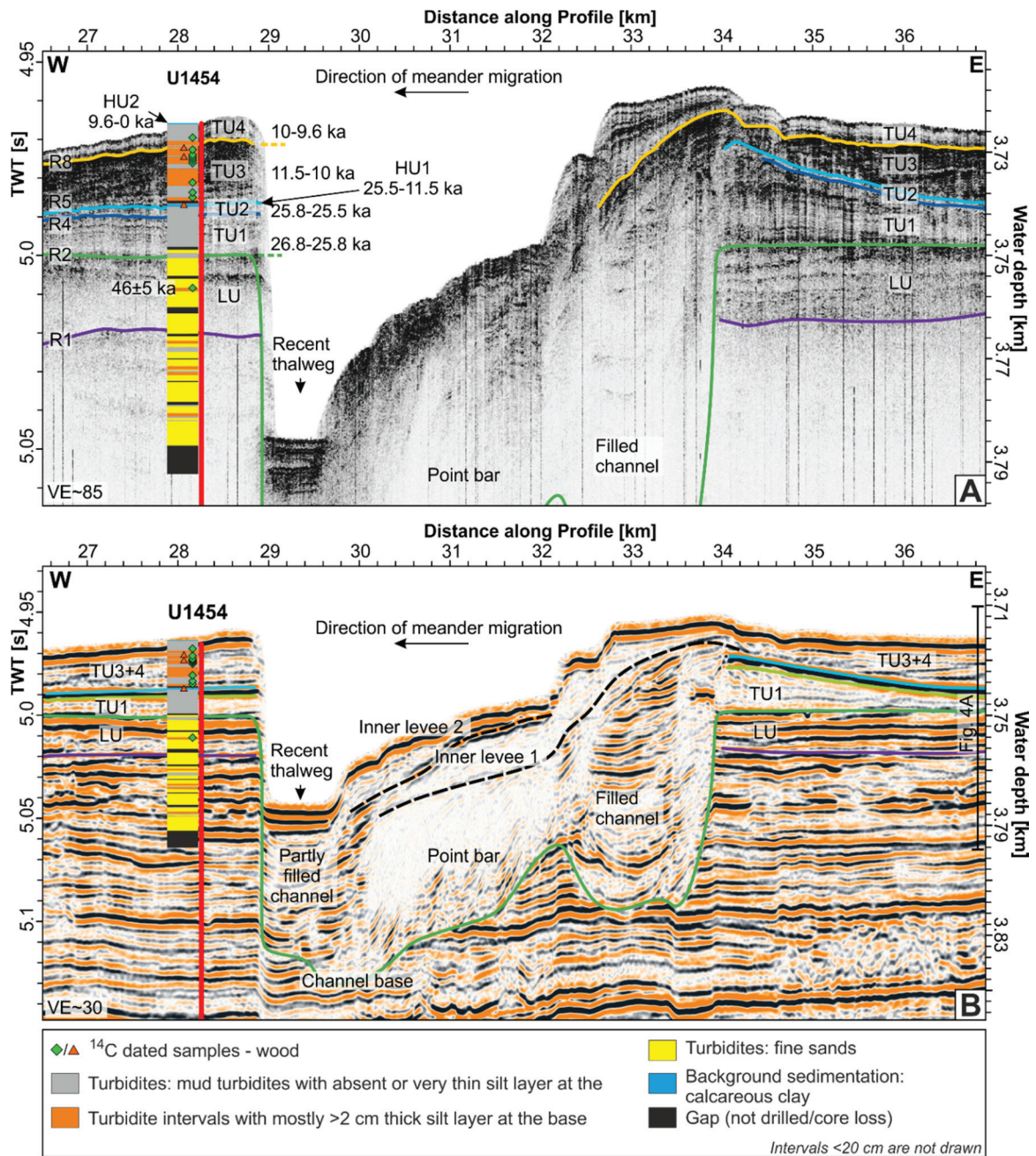


Figure 3.4: A: Integration of Parasound data and Site U1454 lithology with resulting levee units. B: MCS data illustrating internal channel architecture. For location see Fig. 3.1. Note that A and B show the same along-profile section but have different vertical exaggeration.

### 3.3.3 Levee units by Parasound– lithology integration

Seven main acoustic units (Lobe Unit (LU), Turbiditic Units (TU) 1-4, Hemipelagic Units (HU) 1 and 2) were determined by integrating the seismo-stratigraphic analysis (Fig. 3.3) and lithological properties (Fig. 3.4). A summary of all units is shown in Table 3.1.

Table 3.1: Summary of levee units including their acoustic properties, external geometry, lithology, depositional process, and age ranges determined based on the age model presented in Fig. 3.7.

Unit	Amplitudes	Reflector configuration	Main Lithology	Thickness at Site U1454B [m]	Depositional Process	Sedimentation rate [m/ka]	Age range [ka BP]
HU2	-	-	Yellow calcareous mud	0.22	Hemipelagic	0.023	9.6-recent
TU4	Moderate	Parallel, divergent	Light gray mud	3.51	Overspill	8.7	10-9.6
TU3	Moderate to high	Parallel, divergent	Gray clay interbedded with gray silt	12.98	Overspill + crevasse splay	8.7	11.5-10
HU1	-	-	Nannofossil rich calcareous clay	0.46	Hemipelagic	0.033	25.5 - 11.5
TU2	Reflection-free	-	Gray to dark gray clay, very fine grained	1.91	Overspill	8.7	25.8-25.5
TU1	Moderate	Divergent	Gray to dark gray mud	8.85	Overspill	8.7	26.8-25.8
LU	Reflection-free	-	Sand	15.55	Unconfined turbidites	--	younger than 46 ± 5

#### Acoustic Unit LU

The lowermost Unit LU is characterized by acoustically transparent patches and prolonged reflections of moderate to high amplitude, both incorporating few small channels (Figs. 3.3 and 3.4). The discordant base of LU (R1) reflects a smooth, southwards inclined surface (Fig. 3.6A) incised by several small channels of varying depth (4-25 m) (Fig. 3.3). The number of channels is decreasing southwards from 4 (at GeoB97-020) to none (at GeoB97-023). LU has a discordant upper boundary (R2) to the overlying unit. Lithologically, LU is defined by dark gray to gray sand (Fig. 3.4) containing several centimeter-sized wood fragments (France-Lanord et al., 2016). The lack of internal structures and layering in the cores could be a result of high drilling disturbance (France-Lanord et al., 2016) and does not necessarily reflect in situ conditions.

#### Unit TU1

TU1 is the lowermost levee unit discernible by its well-layered, low to medium amplitude divergent reflection pattern downlapping onto its base (R2, Fig. 3.3). The unit is enclosed by the discordant reflections R2 and R3. The base of TU1 (R2) is smooth and southwest-wards dipping (Fig. 3.6B). Overall, TU1 is wedge-shaped but shows variable thicknesses in both directions, across the channel and from north to south. In the northern cross-section, TU1 is convex



upward shaped west of the channel while it is concave upward east of the channel (*Figs. 3.3 and 3.6B*). In the central and southern profile, the external geometry of TU1 is more symmetric with respect to the channel. The thickness of TU1 increases southwards where it reaches a maximum of ~34 m (*Fig. 3.6B*). More local depositional maxima can be observed in channel proximity. The volume of TU1 calculated for 3 km along the channel is 1.44 km<sup>3</sup> (*Tbl. 3.2*). The lithology of TU1 is dominated by gray to dark gray mud turbidites with absent or very thin (<2 cm) silt layers at the base (*Fig. 3.4*).

### Unit TU2

The acoustically transparent unit TU2 lies on top of TU1 and is draping the underlying topography (*Fig. 3.3*). It is enclosed by the reflections R4 (bottom) and R5 (top). TU2 extends throughout the entire study area. The Thickness of TU2 is ~1.9 m proximal to the channel and decreases slightly in more distal parts. TU2 consist of homogenous gray clay (*Fig. 3.4; Tbl. 3.1*).

### Unit HU1

Unit HU1 is defined based on the visual core description and is too thin to be resolved in the Parasound data. It directly overlies TU2 (*Fig. 3.4; Tbl. 3.1*), is ~0.46 m thick and consists of homogenous gray clay enriched in nannofossils and foraminifera. In the Parasound images, reflector R5 (the top of TU2) is considered to also represent HU1.

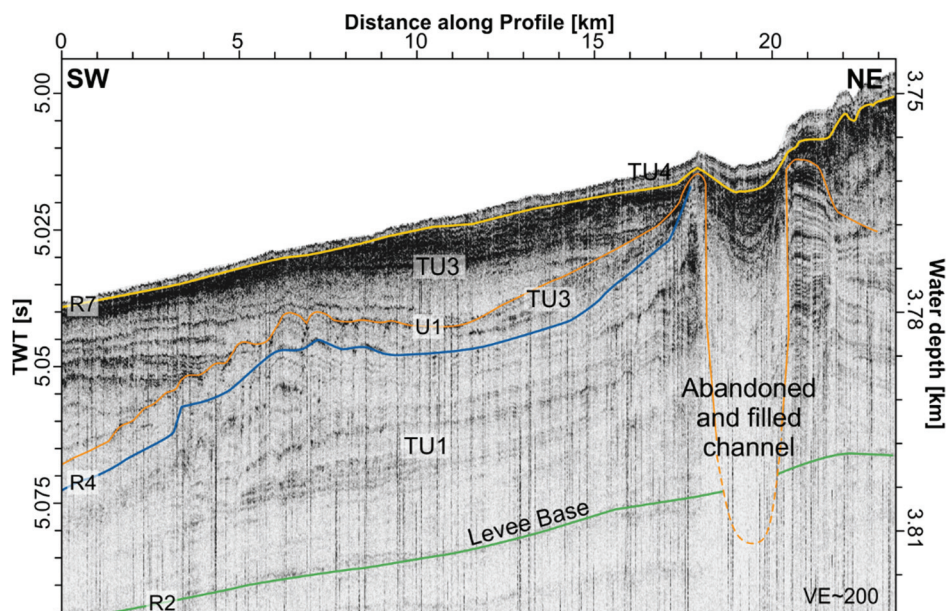


Figure 3.5: Parasound profile running parallel to the AC in the southern study area crossing an abandoned and filled channel segment. For location see Figure 3.1.

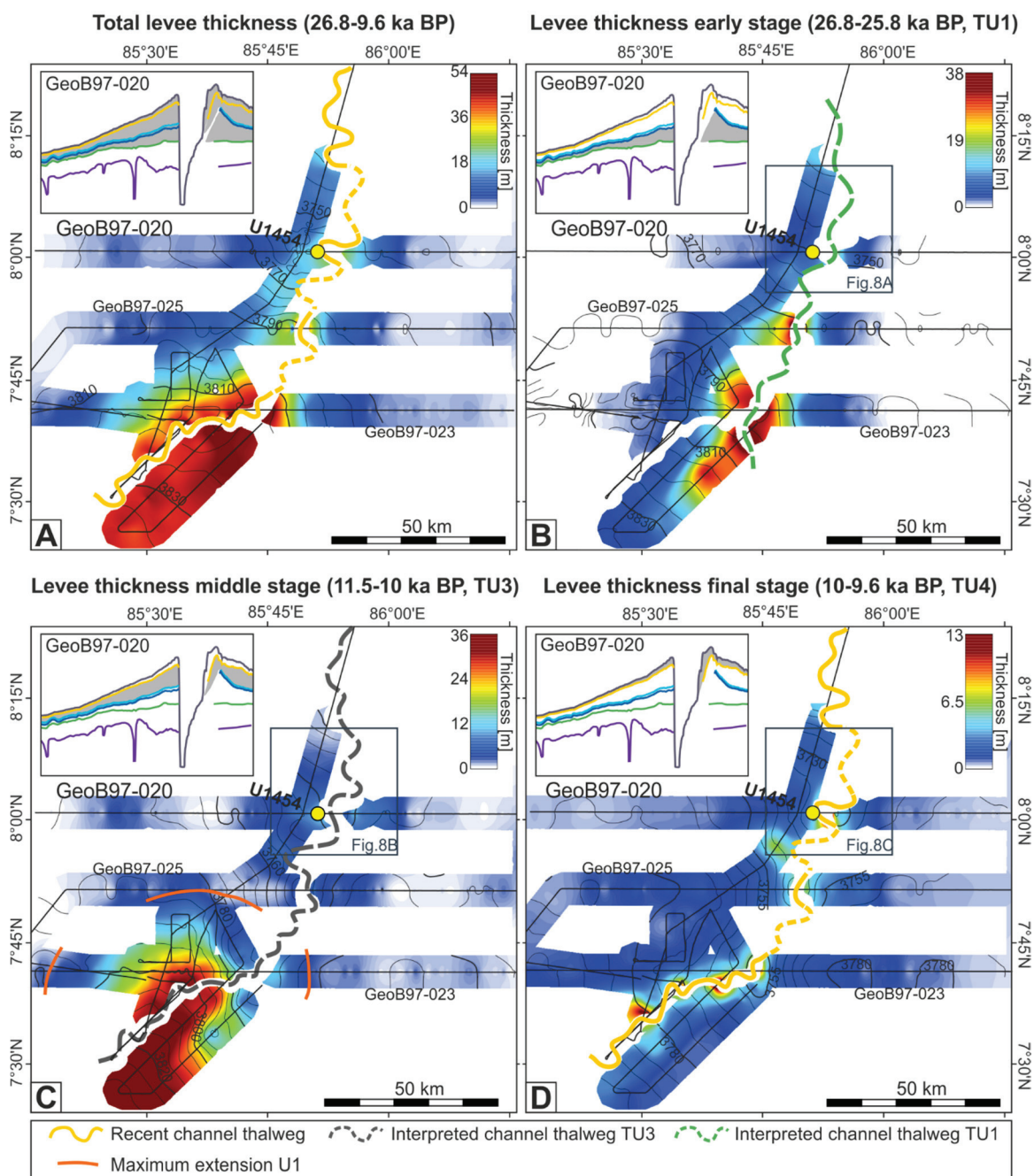


Figure 3.6: Thickness maps based on Parasound data showing (A) the entire levee, (B) the lowermost turbiditic Unit TU1, (C) Unit TU3, and (D) the uppermost turbiditic Unit TU4. Contour lines represent the underlying topography.

### Unit TU3

Unit TU3 can be found on top of TU2 and HU1. TU3 is characterized by well-layered and divergent reflections downlapping onto its base (R5, Fig. 3.3). South of Profile GeoB97-025 reflections are less parallel and partly disrupted by small, erosive channels and acoustically transparent bodies (Figs. 3.3 and 3.5). The base of TU3 (R5, Fig. 3.6C) is dipping more steeply to the southwest in the southern half of the study area than in the northern half. The thickness of TU3 decreases, as typical for a levee, with distance to the channel. However, unit thickness

also varies in N-S direction by showing a prominent area of increased deposition south of Profile GeoB97-025 and smaller-scale patches of increased deposition proximal to the channel thalweg (*Fig. 3.6C*). Unit TU3 encloses a volume of 1.54 km<sup>3</sup> along 3 km of the channel (*Tbl. 3.2*). In the southern part, within the area of increased deposition, an internal unconformity (U1) is separating TU3 into an upper and a lower part. (*Figs. 3.3 and 3.6C*). Overlying reflections onlap onto U1. The above-mentioned disturbed reflectors and erosive channels exclusively exist in this part of the study area, above U1. TU3 consists of turbidites of dark gray to gray clay interbedded with dark silt (*Fig. 3.4*) found at the base of the turbidites in layers partly <2 cm thick but dominantly >2 cm thick.

#### Unit TU4

Unit TU4, overlying TU3, shows well layered, divergent reflections of medium amplitude. The unit is enclosed by the discordant reflections R7 and the seafloor. The base of TU4 is inclined southwards and slightly elevated proximal to the channel (*Fig. 3.6D*).

TU4 is wedge-shaped (maximum thickness 12 m) with patchy, local accumulation maxima in channel proximity (*Fig. 3.6D*). The volume of Unit TU4 is 0.50 km<sup>3</sup> along 3 km of the channel (*Tbl. 3.2*). TU4 consists of turbidites of light-gray clay, again with absent or very thin (<2 cm) silt layers at the base (*Fig. 3.4*).

#### Unit HU2

HU2 is the uppermost unit defined based on the visual core description (*Fig. 3.4, Tbl. 3.1*). At the top of Site U1454B, a ~22 cm thick layer of yellow calcareous clay has been identified. Its color and composition clearly separate it from the underlying TU4. The unit is too thin to be resolved in the Parasound data but is assumed to be present throughout the study area and not only at Site U1454.

### **3.3.4 Other structural features**

#### Buried channels

*Figure 3.5* shows a ~2.3 km wide, abandoned and filled channel located in the south of the study area. The top of this buried channel and its adjacent levees is marked by U1, which separates TU3 vertically. The buried channel is overlain by onlapping reflectors of the upper TU3 and TU4. The channel base exceeds signal penetration. The channel fill is acoustically transparent in the lower part and shows high amplitude, wavy reflections in the upper part. This buried channel must have been the active thalweg of the AC until the early stage of TU3. After its abandonment, the new channel path developed in close proximity. From there, overspilling turbidity currents rapidly filled the abandoned channel and deposited onlapping on U1. Several

other and significantly smaller channels are interbedded into the sediments of LU (*Fig. 3.3A-C*) and between the levee units TU1, 3, and 4 (*Fig. 3.3B and C*). These channels build up small deposits of several meters in heights.

### Channel thalweg

The MCS Profile GeoB97-020 (*Fig. 3.4B*) shows, that the AC had been eroded significantly below the recent level of the thalweg. The deepest channel thalweg was 100 m beneath the levee base, about 62 m deeper than at present. The channel filling is characterized by two packages of medium amplitude, parallel to subparallel reflections, a ~2.5 km wide section of transparent to intermediate amplitude, chaotic reflections in between, and a smaller unit of similar appearance to the east (*Fig. 3.4B*). The first described unit represents a former, filled channel branch and the filling of the recent thalweg, whereas the latter units are interpreted as point bars deposited during the lateral migration of the channel (*Schwenk et al., 2005; Babonneau et al., 2010*). The middle and eastern parts of the channel fill are overlain by sub-horizontal, low amplitude reflections (*Fig. 3.4B*; inner levee 1+2) resembling the seismic appearance of the levees.

### **3.3.5 Stratigraphic framework**

The oldest radiocarbon age of  $46 \pm 5$  ka was measured on a piece of wood debris sampled from 34.5 m CSF-A (*Fig. 3.4*, Unit LU). Due to its unknown onshore storage time, this age does not necessarily represent the age of deposition. However, it constrains the maximum possible age of the onset of levee formation at 8°N to not being older than  $46 \pm 5$  ka BP. Ages measured within the Units TU3 and 4 range from 22.15 ka to 11.2 ka BP (*Fig. 3.7*). Ages (both, measured on wood debris and foraminifera) decrease downcore indicating reworking of upfan material. Still, the youngest age within TU3 (11.2 ka BP in 14.5 m CSF-A) provides a maximum age for all sediments deposited above. The sample taken within HU1 at 17.09 m CSF-A dates to 23.12 ka BP. Owing to the fact that this sample has been taken within a calcareous clay-dominated, hence hemipelagic, sequence it is considered as representing depositional age.

Following *Weber et al. (2018)* and their work on the hemipelagic drape at IODP Site U1452, we assigned a sedimentation rate of 2.3 cm/ka to HU2. For the other units, sedimentation rates (at Site U1454) are based on the integration of reliable radiocarbon ages and the maximum age constraints provided by the reworked radiocarbon samples under consideration of their depositional processes (for discussion on depositional processes see Chapter 4.1.1). Linear interpolation between the calculated age of the base of HU2 and the youngest sample measured within TU3 (11.2 ka) provides a minimum turbiditic sedimentation rate of 8.7 m/ka. Linear interpolation between the calculated age of the base of TU3 and the age marker within HU1 gives a sedimentation rate of ~3.3 cm/ka for HU1. Assuming the sedimentation rate of 8.7 m/ka for all turbiditic sediments at 8°N (TU1-4) the following stratigraphy for the AC at 8°N has been





## 3.4 Discussion

### 3.4.1 Evolution of the Active Channel-Levee System

#### Depositional processes

Unit LU corresponds to 15 m of massive sands (*Figs. 3.4 and 3.8A*) and is interpreted as terminal lobe deposited during the initiation phase of the channel. The incisions at the base of the lobe resemble features found by previous studies on other fans (*Jegou et al., 2008; Picot et al., 2016*) and are interpreted as small-scale channels feeding the lobe (*Fig. 3.8A*).

Overspill-driven sedimentation is represented by the units TU1, TU3 and TU4 building up classical, wedge-shaped levees with reflections diverging towards the channel (*Figs. 3.3 and 3.8B, D, E*). The onset of overspill deposition is marked by a sharp upward change from a sand-dominated (LU) to a clay- and silt-dominated lithology (TU1) at the transition from LU to TU1. The filled channel in the south of the study area is the remnant of an avulsion event occurring during the deposition of TU3 and a subsequent westward 'jump' of the active channel pathway (*Figs. 3.5 and 3.6*). This avulsion event initiated a phase of reorganization and readjustment in the southern study area resulting in crevasse splays (often associated with levee breaching; *Posamentier and Kolla, 2003*) forming small channels intercalating the overspill sediments of the upper TU3 and initiation of small-scale mass wasting deposits (*Figs. 3.4 and 3.5*). Based on its lithological properties TU2 is interpreted as a turbiditic unit as well. The difference in acoustic properties of TU2 versus TU1, 3 and 4 (reflection free versus parallel layered; *Tbl. 3.1*) is the result of the homogeneity of TU2 and the absence of silty layers at the turbidite bases.

On the contrary to the four overspill dominated units, the homogeneous units HU1 and HU2 do not reveal turbidite beds or other indicators of overspill deposition. The nannofossils and foraminifera integrated into HU1 require a calm depositional regime and indicate a shut off of overspill deposition. A similar absence of overspill can be assumed for the deposition of HU2. Consequently, HU1 and HU2 are considered to represent hemipelagic sedimentation (*Fig. 3.8C, F*).

In conclusion, the formation of the Active Channel at 8°N is a succession of an initial lobe phase (LU) followed by the buildup of channel and levees (TU1-4); interrupted by hemipelagic sedimentation during times of absent overspilling (HU1 and HU2) (*Figs. 3.4 and 3.8*). Such an on-off behavior has not yet been described for other submarine fans. Both Amazon and Congo Fan did reveal hemipelagic sequences interrupting channel-levee complexes but levee-internal equivalents are missing (*Piper et al., 1997; Lopez 2001; Savoye et al., 2009; Babonneau et al., 2010*)

#### Stratigraphic context and sedimentation rates

The levee buildup can be separated into 5 main phases with: (1) the lobe formation prior to ~26.8 ka BP but not before  $46 \pm 5$  ka BP; (2) active overspill for 1 kyr (TU1 and 2) between



26.8-25.8 ka BP; (3) a phase without overspill lasting 14 kyrs (HU1); (4) the restart of overspill deposition at 11.5 ka BP for another ~1.9 kyrs (TU3 and 4) from 11.5-9.6 ka BP; and (5) hemipelagic deposition (HU2) since 9.6 ka BP (*Fig. 3.8*).

This age model provides a solid framework for the evolution of the levee even though it is based on a limited number of constraints. The main potential error source is the episodic deposition of turbidites. This may result in temporal variations in sedimentation rates which we cannot account for. This is, in particular, relevant for TU2, which dominantly comprises very fine turbiditic sediment deposited out of suspension. Thus, a lower sedimentation rate can be expected for this unit. An additional source for uncertainties exists in the sedimentation rate used to determine the duration of HU2 (0.023 m/ka after *Weber et al., 2018*). Slight over- or underestimations of this sedimentation rate would result in a significant change in turbiditic sedimentation rate.

With 8.7 m/ka the turbiditic sedimentation rate at 8°N is in the range of findings from 16.5°N (<50 to >500 cm/kyr; *Hein et al., 2017*) and other fans, such as the Amazon Fan (5-25 m/ka; *Lopez, 2001*). At 16.5°N sedimentation rate peaks between 12.8-13.6 ka and at ~10 ka (*Hein et al., 2017*). During the first peak at 16.5°N turbiditic sediments were absent at the levee at 8°N while the latter peak concurs with the deposition of TU3 and 4.

The here proposed onset of the AC levee deposition predates the onset presented by earlier studies (that were conducted upfan at 16.5°N) by 14 kyrs (*Weber et al., 1997*) and 9 kyrs (*Hein et al., 2017*). However, our findings are still in agreement with these studies, as the sampled gravity cores from 16.5°N did not reach the levee base. The total lifetime of the channel is estimated to 26.8 kyrs and therefore longer than the average lifetime of channel-levee systems at the Quaternary Amazon Fan (2-8 kyrs) or the Northern and Axial Congo Fan (~10.4 and ~5.5 kyrs, respectively), but similar to lifetimes of channel-levee systems during the deposition of the Southern Congo Fan (~17.4 kyrs) (*Piper et al., 1997; Lopez, 2001; Droz et al. 2003; Maslin et al., 2006; Savoye et al. 2009*). However, it is very important to notice that the veritable active formation of the levees by overspilling lasted only ~3.2 kyrs (TU1-4), which is significantly shorter than the total lifetime.

### Periods of reduced overspill

Three possible scenarios explain the deposition of the hemipelagic sediments of HU1 (25.5-11.5 ka) and HU2 (9.6 ka -recent): (1) An inactive Bengal Fan not receiving any sediment; (2) reduced sediment input to the fan resulting either in the termination of turbidity currents upfan of 8°N, or a decrease in turbidity current heights hindering overspill onto the levee; and (3) the termination of turbidity currents upfan of 8°N caused by an avulsion. Scenario 1, the complete shut-off of the Bengal Fan, is ruled out for both hemipelagic sequences as constant sediment supply to the levee has been observed at 16.5°N, at least since 17.4 kyrs BP until 0.19 kyrs

BP (Hein *et al.*, 2017). Scenario 2, more precisely a decrease in turbidity current heights, is favored for both HUs.

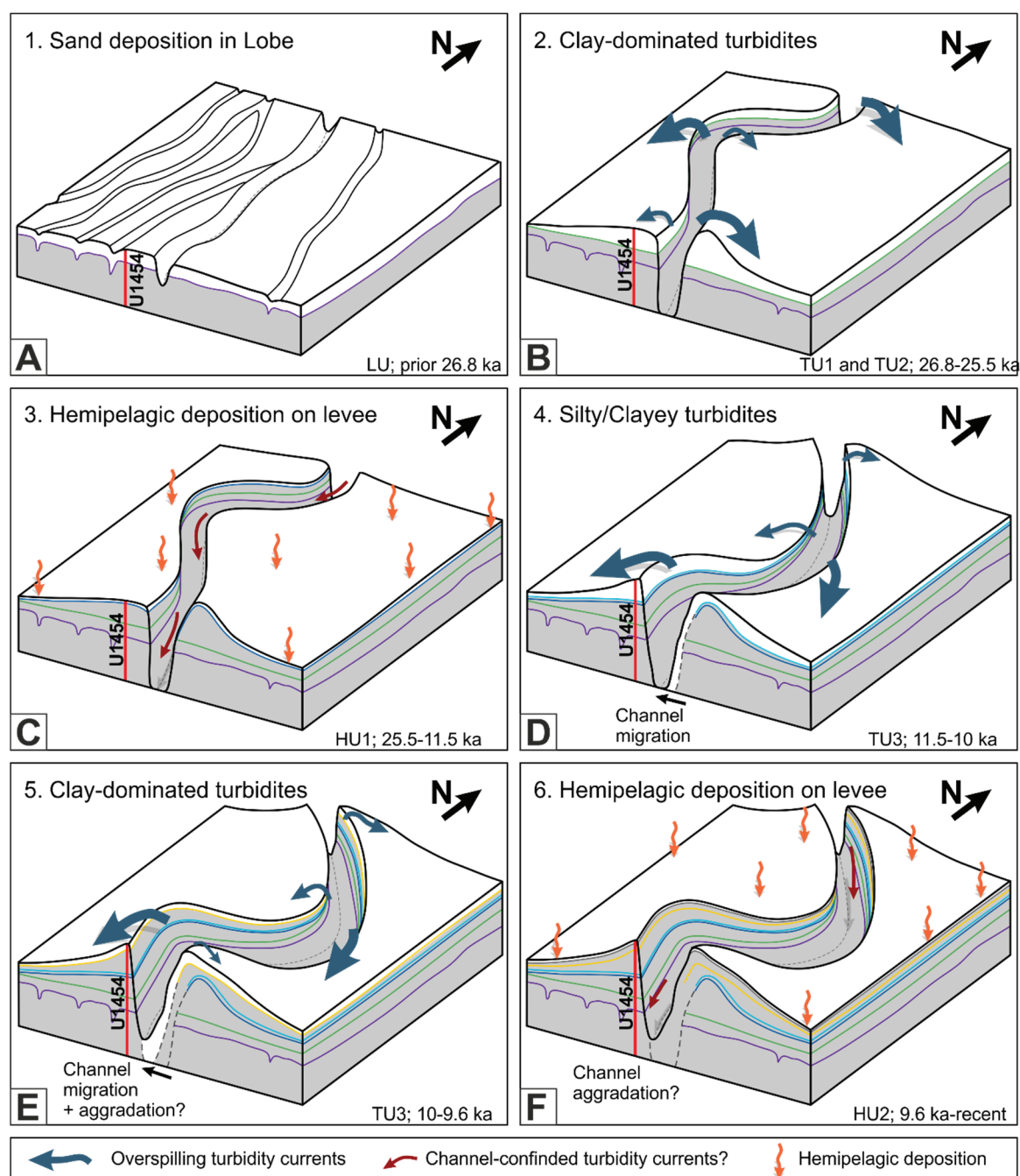


Figure 3.8: Schematic sketch of the evolution of the Active Channel-levee system in the vicinity of Site U1454 and the relationship between channel sinuosity and overspill deposition. The front view corresponds to Profile GeoB97-020. Blue arrows represent overspill deposition. Thick blue arrows furthermore represent the direction of maximum overspill. Orange arrows indicate hemipelagic deposition. A: Channel initiation and lobe deposition; B: Deposition of the first two levee units; C: Interruption of levee growth, hemipelagic deposition on the levee, only channel-confined turbidity currents. D and E: Reactivation of levee growth simultaneously with the westward migration of the channel thalweg. F: Again interruption of levee growth, hemipelagic deposition on the levee, turbidity currents are confined to the channel.

The sedimentation rate of HU1 is slightly higher than the sedimentation rate of the hemipelagic drape (HU2; Chapter 3.3.5) implying that minor overspill is still ongoing. Moreover, at 16.5°N sedimentation on a topographically lower terrace close to the channel thalweg (Core 118KL) is relatively constant until at least ~190 ka, implying that overspill during the deposition of HU2 is continuous at 16.5°N. However, at the same time (~10 ka) sedimentation rates drop on both the western and eastern levee at 16.5°N (cores 117KL and 120 KL) (*Hein et al., 2017*), suggesting a reduction in turbidity current heights. Another explanation for the deposition of HU2 may be a, so far unmapped, upfan avulsion. However, we observed a thalweg aggradation of 62 m (*Fig. 3.4B*) in the MCS data, which must have occurred during the latest stages of channel development. Reduction in flow size, along with a reduced density or an increase in grain size, is one of the major triggers for a CLS to become aggradational (*Kneller, 2003*) supporting our interpretation of a decrease in current height resulting in the deposition HU2. If both hemipelagic layers are connected to a reduction in flow size, they may have been deposited during times of decreased sediment supply to the fan. However, both layers formed during two different times within the sea-level cycle, namely the sea-level lowstand during the Last Glacial Maximum (LGM) (HU1) and the Holocene sea-level rise and highstand (HU2) (*Fig. 3.7*). Thus, deposition of hemipelagic sediments on the levee is not necessarily linked to sea-level highstands as proposed in general sequence stratigraphy models. The deposition of HU2 correlates with the initiation of the Ganges-Brahmaputra delta at 11 ka, trapping large amounts of the river output (*Goodbred and Kuehl, 2000a, b*). The deposition of HU1 proceeds throughout sea-level fall, lowstand and rise giving no hint to a connection to onshore or on-the-shelf trapping of sediments.

### 3.4.2 Overspill sedimentation as a function of the channel geometry

#### Depocenter shifts through time and space

Since **TU4** is the youngest overspill unit, we assume that the channel pathway must have been deeper than today (or at least similar) during its deposition, allowing for the direct connection of the mapped depocenters to the channel geometry. TU4 is characterized by discrete depositional maxima close to almost all displayed meander bends (*Figs. 3.3 and 3.6D*) as proposed by analog and numeric models (e.g. *Straub et al., 2008; Kane et al., 2010*). This clear link between channel curvature and deposition was utilized to reconstruct the position of the thalweg during the deposition of TU1 and TU3.

**TU1** has been deposited on the relatively horizontal surface of the underlying lobe (*Fig. 3.6*). Therefore, overspill itself is the main factor controlling its thickness distribution. The thicker and concave upward shaped eastern levee at Profile GeoB97-020 (*Fig. 3.3*) indicates a meander bend mirrored to the recent situation. A similar assumption can be made for Profile GeoB97-023 (*Figs. 3.3 and 3.6*). In Profile GeoB97-025 TU1 appears to be symmetrical on both sides

of the levee, pointing to a straighter channel segment in that area (Figs. 3.3 and 3.6). Additionally, the channel pathway was located further to the east in the southern study area prior to the channel avulsion that occurred at the beginning of TU3. Therefore, the main deposition of TU1 was concentrated to the east of today's channel pathway (Fig. 3.6).

Unit **TU3** is characterized by thick deposits in the southern study area (Fig. 3.6C). This area of increased deposition must have been the result of the channel avulsion that occurred shortly after the onset of TU3. The necessary accommodation space is given by the presence of a topographic low (Fig. 3.6C). Besides this accommodation-space controlled depositional maxima, the thickness distribution of TU3 reveals smaller scale thickness maxima (Figs. 3.6C-D) associated with outer channel bends.

Grain sizes at Site U1454 change from mud dominated turbidites (TU1 and 2) to turbidites with larger silt contents at the base (TU3) back to mud dominated turbidites (TU4) (Fig. 3.4). The higher silt contents of TU3 results in higher reflection amplitudes in all Parasound profiles on both sides of the channel independent from channel geometry. This widespread distribution of the increased grain sizes implies that this is not an effect of the influence of channel sinuosity on overspilling grain sizes as implied by some models (Amos *et al.*, 2010, Huang *et al.*, 2012) but rather caused by a change in the delivered material.

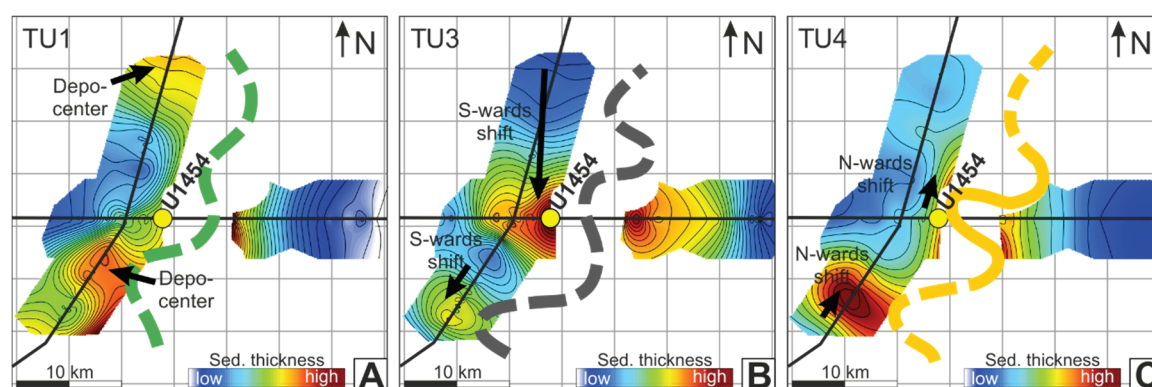


Figure 3.9: Local depocenter migration and channel pathway (green, gray and yellow line) reconstruction in the vicinity of Site U1454 of the three levee units (from old to young) TU1 (A), TU3 (B) and TU4 (C); Colors indicate sediment thickness of the corresponding unit. Please note that the colorscale for the three units represent different absolute values. Black arrows highlight the up- and downfan migration of the main depocenter through time. Contour lines represent 0.5 s TWT.

The spatial mapping of individual levee units demonstrates that meander of submarine channel-levee systems migrate not only laterally but also down- and upfan. The area of focused deposition south of Site U1454 (Fig. 3.9A) shifted ~6 km southwards (Fig. 3.9B) and subsequently northwards for ~2-4 km (Fig. 3.9C) due to change of the channel sinuosity. This observation is an add-on to models working with a static channel sinuosity (e.g., Peakall *et al.*, 2000, 2007; Straub *et al.*, 2008; Kane *et al.*, 2010; Huang *et al.*, 2012), which imply that main deposition would be focused on the same spot, creating a localized depositional maximum. As a

consequence, the increasing sinuosity due to meander growth causes a movement of the over-  
spill depocenter across the position of IODP Site U1454 (Fig. 3.10) finally leading to significant  
changes in sedimentation rates. These findings illustrate that spatial and temporal variations  
in levee deposition might often be misinterpreted as a source-to-sink signal when results from  
sediment cores are not framed by a robust seismo-acoustic dataset.

It is worthwhile to test if a similar behavior may be one of the factors driving sedimentation rate  
changes in the Congo or Amazon Fan, which have so far been linked to channel relief (Savoie  
*et al.*, 2009) and the glacial/interglacial on-off behavior of the fan and general proximity to the  
overspilling channel (Mikkelsen *et al.*, 1997), respectively.

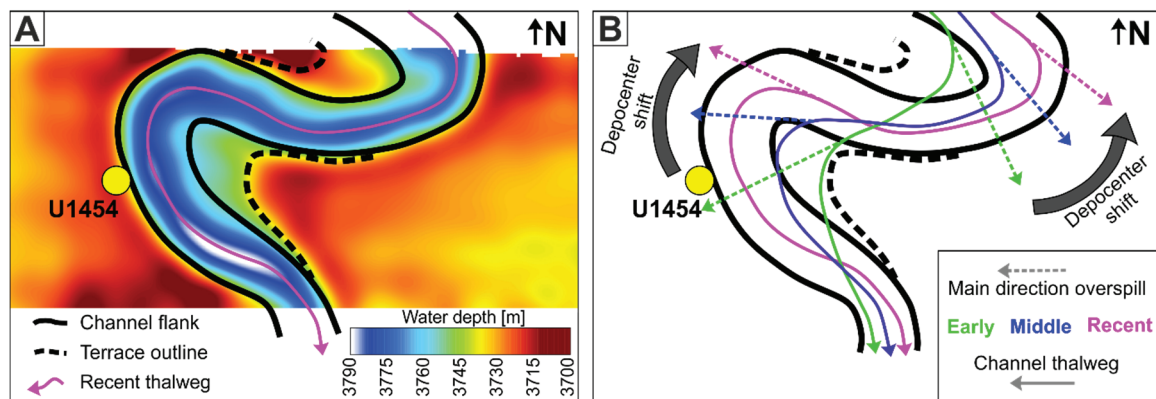


Figure 3.10: Top view on the meander bend next to Site U1454. A: Bathymetric map showing the recent channel thalweg (pink line), the recent channel flanks (black, solid line) and the outline of terraces formed during the migration of the meander (black stippled lines). B: Schematic sketch of the shift of the overspill direction due to increasing meander sinuosity and the subsequent shift of the main depocenter.

### Sediment fluxes

The overall turbiditic deposition within the entire levee is more or less laterally equalized over time as shown by the evenly distributed thickness (Fig. 3.6A). An exception is a depositional maximum in the south where deposition was controlled by accommodation space after channel avulsion (TU3). Based on the volume of each turbidite unit (Tbl. 3.2) it is possible to calculate mass accumulation rates (MAR) to investigate variations in sediment flux to our study area. The MARs of the three turbidite units TU1, 3 and 4 are almost constant (1.3-1.6 Mt/ka; Tbl. 3.2), denoting a uniform sedimentary flux. This reveals three very important findings: 1) Local changes in sedimentation rate are caused by the relative position to the channel, but do not represent changes in incoming flux; 2) the constant turbiditic flux to the levee is unaffected by sea-level variations. TU1 was deposited prior to the LGM when sea level was -120 m and still falling (Fig. 3.7). In contrast, TU3 and 4 were deposited while sea level was at -55-45 m; and 3) the uniform flux implies that, when using a long-time average on the scale of a systems lifetime, it can be used to assess and evaluate sedimentary fluxes and budgets from IODP sites drilled through levees.



Table 3.2: Calculated 2D-cross-sections and mass accumulation rates for the three turbiditic units TU1, 3 and 4.

	TU1	TU3	TU4	Total
Average Dry Bulk Density [kg/m <sup>3</sup> ]*	1140	1370	1040	-
2D-Cross Section (GeoB97-020+023+025) [km <sup>2</sup> ]**	1.44	1.54	0.50	3.48
Volume (GeoB97-020+023+025) [km <sup>3</sup> ]**	1.44	1.54	0.50	3.48
Duration [ka]	1	1.5	0.4	2.9
MAR [Mt/ka]**	1.3	1.4	1.6	-

\* After France-Lanord *et al.*, 2016

\*\*representing the sum of deposition at the three cross sections GeoB97-020+023 and 025; each of them extrapolated for 1 km along the channel.

To put our data into a more regional context, we used the MARs of the turbiditic units TU1, 3 and 4 and calculated a 'total' sedimentary flux to the Bengal Fan of 1.45 Gt/a (TU1), ~1.25 Gt/a (TU3), and ~1.16 Gt/a (TU4), respectively, as a first order estimation. These calculations are based on the assumption of a total channel length of 2650 km (after the surface map of *Curray et al.*, 2003) and are valid for the times of active overspill deposition at 8°N.

The recent average suspension load of the Ganges and Brahmaputra rivers is approximately 1.06 Gt/a (*Bangladesh Water Development Board, 1972; Delft Hydraulics and Danish Hydraulics Institute, 1996; Milliman and Farnsworth, 2011*), while the overall flux of Ganges and Brahmaputra, integrated over the last several hundred years, ranges between 1.2-2.2 Gt/a (*Lupker et al.*, 2012, 2017). The suspension load flux does not account for the sediment transported as bed load. However, bed load grain sizes measured in the Ganges and Brahmaputra rivers are between 2.1 to 2.5  $\Phi$  (~180-200  $\mu\text{m}$ ) (*Garzanti et al.*, 2010) which is larger than the grain sizes of the turbidites forming the levee at 8°N. Thus, bed load seems to play no major role in the sediment flux to the levee. Moreover, direct measurements of the Ganges bed load (measured at Harding Bridge) estimate bed load to represent less than 2% of the suspension load (*Lupker et al.*, 2011).

The sediment flux to the fan during levee deposition at 8°N (TU1 and TU3-4; 26.8-25.8 and 11.5-9.6 ka; *Tbl. 3.1*) has been slightly higher than the recent suspension load of 1.06 Gt/a (*Milliman and Farnsworth, 2011*). This may imply that the overall sediment load in the Ganges and Brahmaputra rivers has been higher, as it is also implied by the overall flux integrated over the last several hundred years (1.2-2.2 Gt/a; *Lupker et al.*, 2012; 2017). Particularly interesting is the constant flux during 11.5-9.6 ka (TU3 and 4), contradicting the idea that most of the supplied sediments were trapped in the floodplain and Bengal shelf during the rising sea level between 11 – 7 ka (*Goodbred, 2003; Hinderer, 2012*).

Our simplified calculations contain some uncertainties, such as the limited data coverage (3 cross sections). They furthermore do not account for downfan decreasing sediment load in turbidity currents (*Pirmez and Imran, 2003*), levee erosion during lateral meander migration, or



upfan terminating turbidity currents. However, the first-order flux estimates at the levee of the AC suggest that sediment load of the rivers and transport to the fan has been higher than 1 Gt/a and that a constant flux can be sustained independently from sea level, at least for the times of active overspill at 8°N.

### 3.5 Conclusion

Utilizing an integrated dataset of very-high-resolution Parasound data as well as IODP Site U1454 results, we investigated the evolution of the active channel-levee system of the Bengal Fan at 8°N, overspill deposition next to an actively meandering channel, and provided estimations for sedimentary fluxes to the Bengal Fan.

Our study shows that the AC started to develop at 26.8 ka which is significantly earlier than discussed in earlier studies (12.8 ka, *Weber et al., 1997*). The AC underwent a phase without overspilling (25.5-11.5 ka, Unit HU1) during the LGM and the deglacial sea-level rise, and does not receive overspilling sediments anymore since ~9.6 ka (Unit HU2). We interpret both phases of hemipelagic deposition on the levee to be caused by a reduction in turbidity current thickness. However, their deposition during different stages of sea level shows that deposition of hemipelagic sediments on the levee is not necessarily linked to sea-level highstands as proposed in general sequence stratigraphy models. The deposition of HU2 may have been triggered by on-shore sediment trapping due to the development of the Ganges-Brahmaputra delta, while the deposition of HU1 proceeds throughout sea-level fall, lowstand and rise, giving no hint to a sea level connection.

We present the first investigation of short-term variations in deposition along an actively meandering channel on a sub-levee scale while also incorporating field data. Unit heights across the channel can vary up to a threefold, where high accumulation can be clearly linked to channel bends. The investigation of the three individual time slices particularly deciphers the up/downfan shift of the main depocenter associated with the movement of channel bends and the consequently patchy depositional pattern. Finally, it highlights that sedimentation (rates) from a levee location (as here Site U1454) cannot be transferred to sediment fluxes directly. However, these short-term variations are equalized over the lifetime of the channel in response to the dynamic channel geometry and the topographically controlled accommodation space. We show that mass accumulation rates on the levee are almost constant throughout the lifetime of the AC, implying a constant sediment flux to the study area, unaffected by sea level variations. As a consequence, we suggest that, where no multiple coverage of a channel-levee system is available, budgets should be averaged over the entire lifetime of one channel-levee system in order to minimize statistical errors generated by short-term fluctuations.

### **3.6 Acknowledgments**

This work was funded by the German Research Foundation (DFG) within the IODP Priority program (Grant No. SCHW1551/7-1/2). Collection of seismoacoustic data was funded by BMFT Project 03 G 0093 A (So93) and BMBF Grant no, 03 G 0125A (SO125). We would also like to thank captain, crew and scientific party of RV Sonne cruises SO93, SO125, and of IODP Expedition 354.

## Chapter 4

### 4 Middle to Late Pleistocene architecture and stratigraphy of the lower Bengal Fan – Integrating multichannel seismic data and IODP Expedition 354 results

Fenna Bergmann<sup>1</sup>, Tilmann Schwenk<sup>1</sup>, Volkhard Spiess<sup>1</sup>, Christian France-Lanord<sup>2</sup>

<sup>1</sup>Faculty of Geosciences, University of Bremen, Klagenfurter Strasse 2-4, D-28359 Bremen, Germany

<sup>2</sup>Centre de Recherches Pétrographiques et Géochimiques, CNRS Université de Lorraine, BP 20, 54501 Vandœuvre les Nancy, France

#### Abstract

The Bengal Fan records the tectonic and climate history of the Himalayas since its initiation during the Eocene. Eroded material from the mountain range is transported along and across the Bengal Fan via frequently avulsing channel-levee systems resulting in a complex, laterally migrating depositional pattern. We utilize an integrated dataset of high-resolution multichannel seismic data and IODP Expedition 354 drilling results in order to decipher the Middle to Late Pleistocene architecture and stratigraphy of the lower Bengal Fan at 8°N. Channel-levee systems have average lifetimes of 15 kyrs and migrate laterally over >100 km. Detailed mapping allowed the development of a relative succession of channel-levee systems to improve the transect chronostratigraphy. Moreover, it showed the organization of fan sediments in subfans locally restricted to parts of the Bengal Fan while the adjacent area undergoes hemipelagic deposition. We image three deposition phases since the Middle Pleistocene: Subfan B (1.24-0.68 Ma) deposited in the western fan simultaneously with the Mid-Pleistocene Hemipelagic Layer in the eastern fan, Subfan C (0.68-0.25 Ma) deposited in the eastern fan, and Subfan D (0.25 Ma – recent) again located in the western fan and deposited simultaneously with the Late Pleistocene Hemipelagic Layer in the eastern fan. Subfan location and switch are partly controlled by accommodation space created by the uplift of the 85°E Ridge and Ninetyeast Ridge during Pleistocene times. More than 60% of the sediments reaching 8°N are composed of sands deposited out of unchanneled turbidity currents. This not only suggests that sand content in large (mud-rich) submarine fans may be significantly underestimated until now. It further demonstrates the importance of sand deposition for the overall fan architecture.

## 4.1 Introduction

The Bengal Fan is the largest submarine fan on Earth and the primary sink of sediments eroded in the Himalayan Mountains. Thus, the Bengal Fan is well-suited to investigate the climate/tectonic link of the Indian/Asian collision and the Himalayan uplift, as well as the role of the mountain range and its weathering/erosion in the global carbon cycle (*Emmel and Curray, 1983; Derry and France-Lanord, 1997; Curray et al., 2003; Galy et al., 2007; France-Lanord et al., 2016*). In this context, the Bengal Fan was the target of IODP Expedition 354 drilling 7 sites at 8°N (*France-Lanord et al., 2016*). Since the Late Miocene deposition on the Bengal Fan was dominated by channel-levee systems (CLSs) which are initiated and further shaped by downslope flowing turbidity currents (*Schwenk and Spieß, 2009*). Frequent channel avulsions and reoccupation of older pathways formed a depositional system with lateral depocenter migration over the entire fan (*Curray et al., 2003, Schwenk and Spieß, 2009*). Thus, a west-east oriented drilling transect was chosen for IODP Expedition 354. However, the thorough understanding of processes influencing the material during its transport across and along the fan is a prerequisite to draw inferences from the sink (here the Bengal Fan) to the evolution of the source (here the Himalayan Mountains/Tibetan Plateau). Therefore, we investigate deposition mechanisms at the lower Bengal Fan on regional and local scales by integrating high-resolution multichannel seismic (MCS) data with the IODP Expedition 354 drilling results. The data allow the correlation of stratigraphic time markers in between drill sites while also accounting for phases of sedimentation not covered by the drilling. This study further investigates the fan architecture, the stacking of subfans, the succession of individual Pleistocene CLSs and the importance of sediments deposited via unconfined turbidity currents.

### 4.1.1 Regional Background

The Bengal Fan is bordered by India and Sri Lanka in the West, Bangladesh, and Myanmar in the North, and the Andaman-Nicobar Ridge and Sumatra in the East (*Fig. 4.1*). It extends over 3000 km southwards from the shelf edge to 7°S and covers almost the entire Bay of Bengal (*Fig. 4.1*) (*Emmel and Curray, 1983; Curray et al., 2003*). The Bengal Fan was initiated subsequent to the collision of India with Asia in the Middle Paleocene to Early Eocene and the uplift of the Himalayan mountain range and Tibetan Plateau (*Curray et al., 2003; Gibbons et al., 2015; Tada et al., 2016*). The fan is underlain by the two aseismic ridges 85°E Ridge and Ninetyeast Ridge emplaced during the northward movement of the Indian plate (*Figs. 4.1 and 4.8*) (*Gopala Rao et al., 1997; Krishna et al., 2001a; Bastia et al., 2010a*). The ridges are buried under sediments in the northern Indian Ocean and partly exposed in the Central Indian Ocean. The Eocene to Early Miocene sediment section of the Bengal Fan is composed of sheeted turbidites, while since the Late Miocene sediment supply via CLSs dominates (*Curray et al., 2003; Schwenk and Spieß, 2009*).

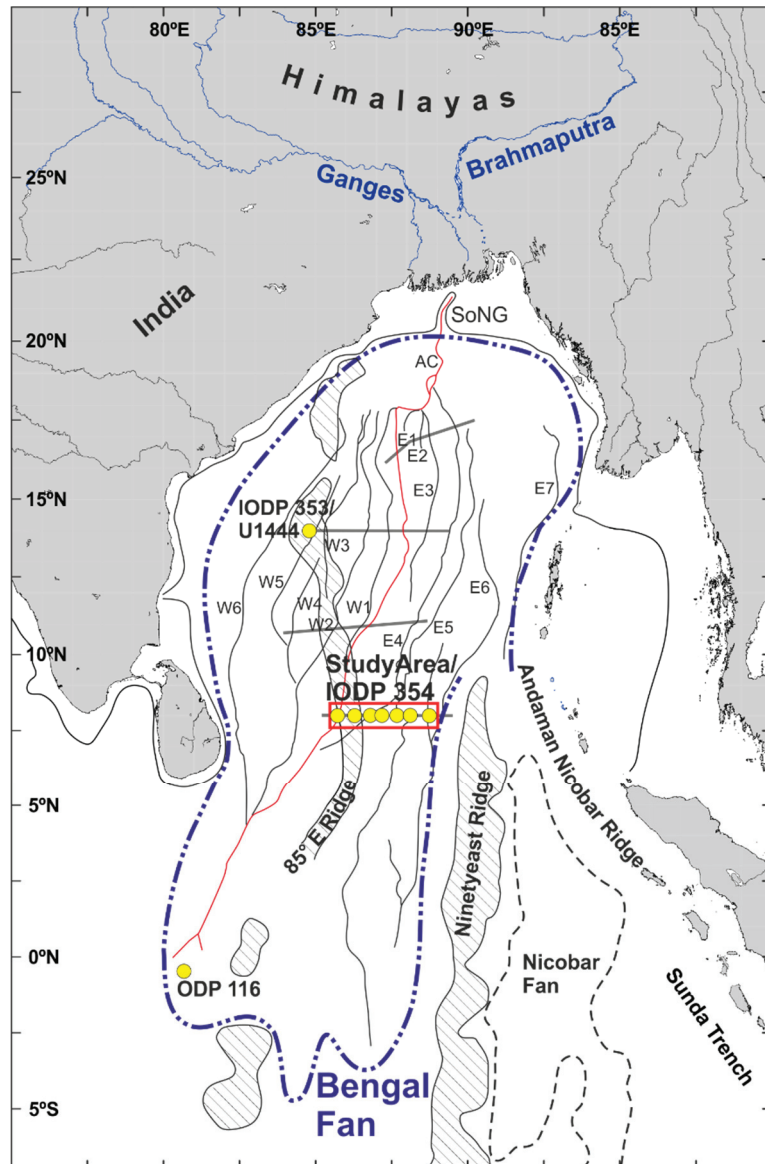


Figure 4.1: Overview map of the Bengal Fan. Black and red lines: Surface channels after Curray et al., 2003; Grey lines: Multichannel seismic profiles as shown in Figure 4.8; Red square: Study area. SoNG=Swatch of No Ground. Tectonic features and fan outlines redrawn after Curray et al., 2003; Bastia et al., 2010a, b; Choudhuri et al., 2014; McNeill et al., 2017a.

The CLSs act as the main sediment distributor forming a complex depositional system including frequent channel avulsion, reoccupation of older pathways, and lateral depocenter migration (Curray et al., 2003; Schwenk and Spieß, 2009). Like the Amazon or the Congo Fan, the Bengal Fan is classified as a fine-grained or mud-rich fan, which per definition contains less than 30% sand (Richards et al., 1998, Bouma, 2000, 2001). In the modern situation, sediment is transported from the Himalayan area to the shelf mainly via the Ganges and Brahmaputra rivers. The material is temporarily stored in the deep incised shelf canyon Swatch of No Ground (SoNG) before it is episodically released to the fan (Kuehl et al., 1989; Kottke et al., 2003; Michels et al., 2003).



### 1.1.1 Previous work

Several previous seismic studies have been conducted on the Bengal Fan investigating the fan evolution and architecture (e.g. *Gopala Rao et al., 1997; Weber et al., 1997, 2003; Curray et al., 2003; Schwenk et al., 2003, 2005; Schwenk and Spieß, 2009 or Krishna et al., 2016*). *Curray et al., 2003* mapped surface CLSs including abandoned channels (E7-E1 and W6-W1) as well as the youngest system, the Active Channel (AC), which also received sediments in Holocene times (*Weber et al., 1997; Hein et al., 2017*). Some of these channels (E4, E5, E6, and AC) reach our study area, while the other channels are located further west or terminate upfan (*Fig. 4.1*). Based on the mapping of surface and buried CLSs, *Curray et al., 2003* introduced the concept of subfans which govern only parts of the Bengal Fan while other areas received no or almost no fan sedimentation during the same time period. For the upper Bengal Fan, the four subfans A (1-9-0.96 Ma), B (0.96-0.465 Ma), C (0.465-0.125 Ma), and D (0.125 Ma to present) have been mapped and dated by correlation to DSDP Site 218 (*Curray et al., 2003*). Subfans, also called channel-levee complexes, are common for large submarine fans and have also been described for the Amazon Fan (e.g. *Flood and Piper 1997; Piper et al., 1997; Lopez, 2001*), the Congo Fan (e.g. *Savoye et al., 2009*), or the Mississippi Fan (e.g. *Bouma et al., 1989*).

The investigation of 4 (almost) W-E trending MCS profiles by *Schwenk and Spieß, 2009* revealed numerous other CLSs filled and buried by younger sediments. Their dataset includes the MCS Profile GeoB907-020+027, along which the IODP 354 drill sites have been planned and drilled. A reprocessed version of this profile has been used in this study. *Schwenk and Spieß, 2009* identified two regional unconformities tentatively dated by correlation to DSDP Site 218 as of Pliocene (~4.8 Ma) and Pleistocene (~0.645 Ma) age. Following *Schwenk and Spieß, 2009*, both unconformities correlate with intraplate folding events found in the central Indian Ocean (*Krishna et al., 2001b*) and/or with lithological changes at ODP Leg 116 sites (*Cochran, 1990; Stow et al., 1990*). However, IODP Exp. 354 drilling showed that at least the Pleistocene unconformity correlates with the boundary between a regional extending sequence of hemipelagic sediments (Mid-Pleistocene Hemipelagic layer, MPHLL; see chapter below) and overlying turbiditic sediments (*France-Lanord et al., 2016*).

### 1.1.2 IODP Expedition 354

IODP Expedition 354 '*Bengal Fan*' took place in February/March 2015 and drilled 7 sites along a W-E transect at 8°N (Sites U1449-U1455; for location see *Figs. 4.1 and 4.3*). At all seven sites, a record spanning the last 1-2 Mys has been recovered. The overall lithology of the cores is dominated by siliciclastic sediments composed of sand, silt, and clay turbidites (*Fig. 4.2; France-Lanord et al., 2016*). The turbiditic sediments alternate with intervals of calcareous clay and nannofossil-rich calcareous clay layers of predominantly hemipelagic origin.

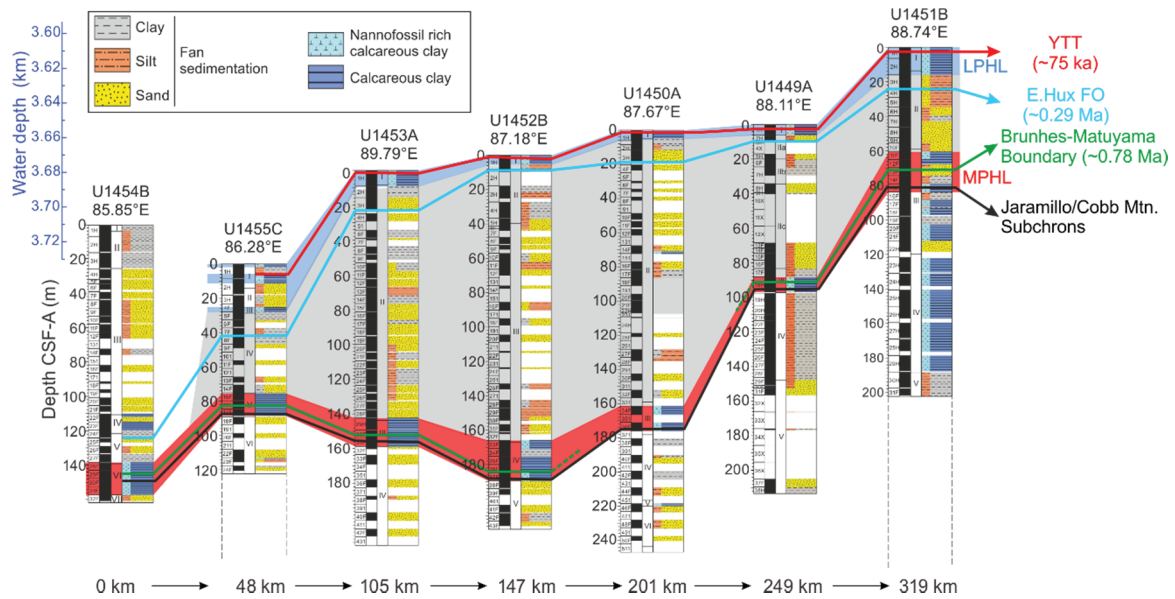


Figure 4.2: Lithostratigraphic summary of Expedition 354 showing lithologies that constitute >10% of the core (modified after France-Lanord et al., 2016). YTT=Youngest Toba Tuff, age after Gasparotto et al., 2000. LPHL= Late Pleistocene Hemipelagic layer. E. Hux FO= First Occurrence *Emiliana huxleyi*. MPHL=Mid Pleistocene Hemipelagic layer. Ages of E. Hux FO and Brunhes-Matuyama boundary after Gradstein et al., 2012. Gray shading highlight sediments of Subfan C. Not shaded areas mark sediments of Subfan D. For locations of cores see Figures 4.1 and 4.3.

At each of the seven sites, two prominent regional extending calcareous clay layers, several meters thick, have been recovered, namely the Mid-Pleistocene Hemipelagic layer (MPHL) and the Late Pleistocene Hemipelagic layer (LPHL) (Fig. 4.2). The MPHL comprises the Matuyama-Brunhes Boundary (0.778 Ma), the Jaramillo Subchron (1.072-0.988 Ma), and/or the Cobb Mountain Subchron (1.186-1.072 Ma) (Gradstein et al., 2012; France-Lanord et al., 2016). Weber and Reilly, 2018 showed that the MPHL is composed of a pure hemipelagic part (their Unit 2a) lasting from ~MIS37-MIS25 (~1.24-0.93 Ma) overlain by a mixed hemipelagic/turbiditic part (their Unit 2b) lasting from ~MIS25-MIS17 (~0.93-0.68 Ma). Where the MPHL is purely hemipelagic, sedimentation rates are 2-2.5 cm/ka. Weber and Reilly, 2018 further suggest that the top of the MPHL is asynchronous. However, the poor age constraints complicate the accurate dating of the Top of the MPHL at all seven IODP sites. The LPHL marks another phase of long-lasting and regional extending hemipelagic deposition draping the sediments at sites U1449-U1453, the eastern part of the Expedition 354 drilling transect (Fig. 4.2). At Site U1455 the hemipelagic sediments of the LPHL are intermixed with turbiditic material (France-Lanord et al., 2016) while at Site U1454 only a ~ 22-centimeter thick hemipelagic drape has been recovered representing the last ~10 ka (Chapter 3). One stratigraphic marker within the LPHL is the Youngest Toba Tephra (YTT, ~0.75 Ma; Gasparotto et al., 2000) which has been recovered at the 6 eastern IODP 354 sites. The LPHL has an average sedimentation rate of ~2.3 cm/ka and its onset has been dated to ~0.25 Ma (Weber et al., 2018; Weber and Reilly, 2018). The stratigraphy of the drilling transect is further constrained by the

first occurrence (FO) of *Emiliana huxleyi* (~0.29 Ma; age after *Gradstein et al., 2012*) identified in all seven drill sites between the LPHL and the MPHL (*Fig. 4.2*). The remaining sediments contain several thin hemipelagic layers and seismic data is required to correlate these undated layers between drill sites.

## 4.2 Data and Methods

In this study, we present high-resolution multichannel seismic (MCS) data of the Bengal Fan in integration with drilling results from the IODP Expedition 354 carried out in February/March 2015 (*Figs. 4.2 and 4.3*).

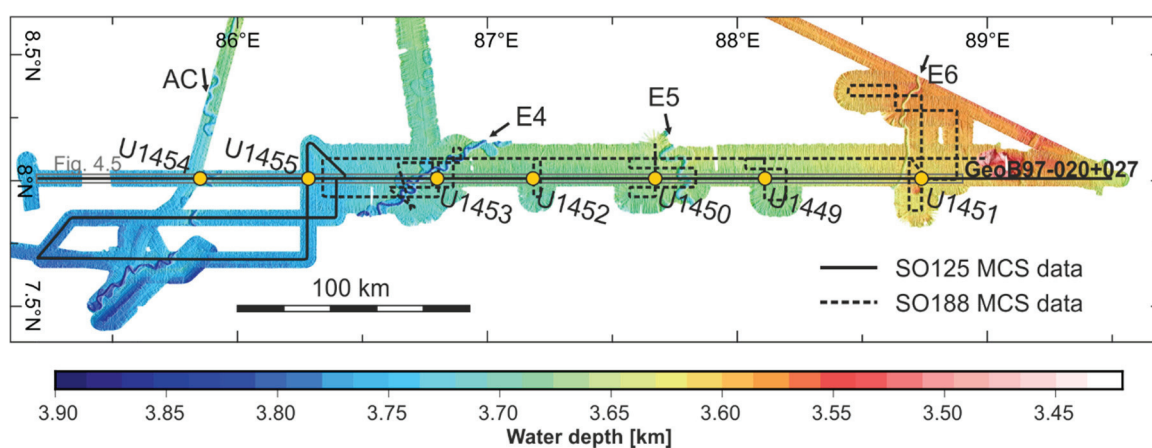


*Figure 4.3: Bathymetric map of the study area at 8°N. Black and red lines: Multichannel seismic profiles used in this study. Yellow dots: IODP Expedition 354 drill sites. AC, E4, E5, and E6: Surface channels after *Curry et al., 2003*.*

### 4.2.1 Data acquisition and processing

The MCS dataset used in this study was acquired during the two research cruises SO125 in 1997 and SO188 in 2006, in cooperation of the University of Bremen and the BGR Hannover (*Spieß et al., 1998, 2006*). The dataset consists of 52 profiles with a total length of ~1500 km (*Fig. 4.3*).

The MCS data were recorded with two differently sized seismic sources (both GI-guns) and different recording units resulting in two datasets with different vertical and horizontal resolution as well as a different subseafloor penetration. An overview of the configurations for both datasets is given in Table 4.1. All data underwent full multichannel-seismic data processing including CMP-Binning, velocity analysis, normal-moveout correction, stacking, noise reduction, static corrections, and time migration. Processing and interpretation of the MCS data were conducted with the software 'Vista 14; Seismic Data Processing' and 'IHS Kingdom 2016'. Bathymetry data shown in *Figure 4.3* were processed onboard with the software 'QPS Fledermaus' and the open source software MB-systems (*Caress and Chayes, 2017*). Time-depth conversion shown on figures were conducted with a velocity of 1500 m/s for the water column



and a seismic velocity of 1650 m/s for the sub-seafloor. The thickness of the MPHL (Chapter 3.1.1) has been converted from two-way travel time (TWT) to meters using the average P-wave velocity of calcareous clay measured during IODP Expedition 354 (1530 m/s) (France-Lanord et al., 2016).

Table 4.1: Summary of the specifications of the utilized multichannel seismic datasets.

	Seismic Source Volume	No. of Channels	Channel Spacing [m]	Frequency range [Hz]	Vertical Resolution [m]	Bin Size [m]
SO188	4.1   Generator 1.7   Injector,	96	6.25	25-200	~15	8
SO125	2x 0.41	48	12.5	100-500	~5	12

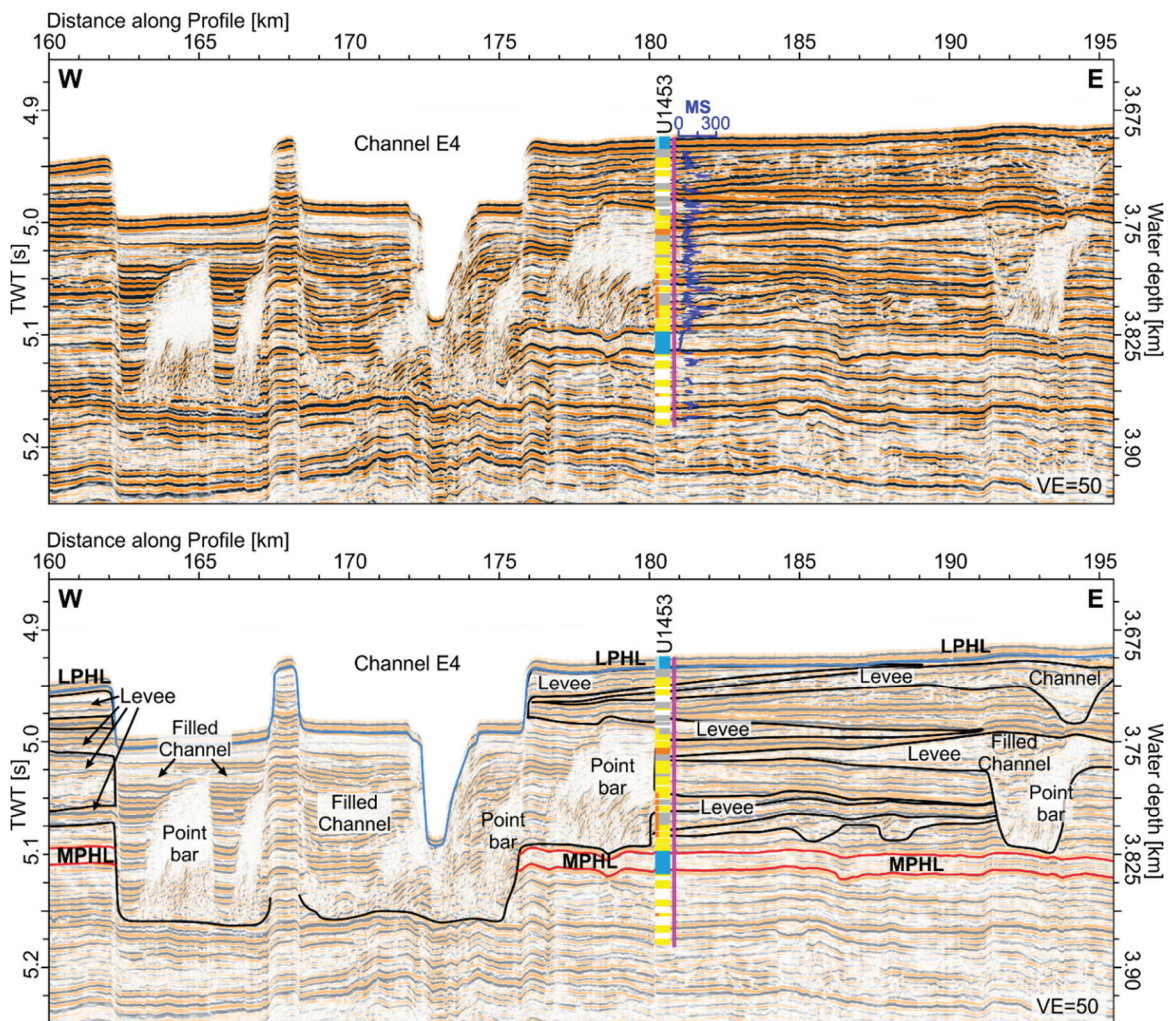


Figure 4.4: Top: Uninterpreted multichannel seismic data near Site U1453 and channel E4. MS=Magnetic Susceptibility, onboard measured, SI-units (France-Lanord et al., 2016). Bottom: Interpreted multichannel seismic data near Site U1453 and channel E4 including the main architectural elements of channel-levee systems (channel fill, point bars, levees) intercalated by HAPRs (high amplitude reflection packages) and Hemipelagic Layers. LPHL=Late Pleistocene Hemipelagic layer. MPHL=Mid-Pleistocene Hemipelagic layer. For location see Fig. 4.5.

### 4.2.2 Core-seismic integration

Because of borehole instability, downhole logging was conducted only at Site U1453 and velocity measurements exist only for the section between ~70-220 mbsf. Therefore, core-seismic integration down to the MPHL was done using an individual constant velocity for every drill site determined based on the best fit of prominent seismic reflections with core lithology and physical properties (Fig. 4.4). Additionally, velocities were cross-checked with onboard measured p-wave velocities (France-Lanord et al., 2016). Hemipelagic lithologies are characterized by low magnetic susceptibility (MS) and low natural gamma radiation (NGR) (France-Lanord et al., 2016). Due to their impedance contrast to the surrounding turbiditic sediments, these can be very well correlated to high amplitude reflections in the seismic data (Fig. 4.4). The best fit between the MCS data and IODP 354 drilling results was achieved with a constant velocity of ~1640 m/s for sites U1449, U1454, and U1455, ~1650 m/s for sites U1451 and U1453, and ~1680 m/s for sites U1450 and U1452.

## 4.3 Results

The 420 km long, west-east oriented MCS Profile GeoB97-020+027 crosses all IODP Expedition 354 drill sites and the 85°E Ridge and the Ninetyeast Ridge (Fig. 4.5). The seafloor along the profile is declining westwards from ~3.6 km to ~3.75 km water depth. It is presented in this study in order to illustrate the stratigraphic framework and the lateral and vertical evolution of the Bengal Fan at 8°N. We focus on the upper part of the profile including the MPHL and the section above. All available age markers found within this section (MPHL, LPHL, E. Huxleyi FO, YTT) as well as all reflectors, which are considered as representing isochrones (CLS base reflectors, hemipelagic layer), have been traced along the MCS data and correlated with the drill sites. The seismic facies definition is based on the lithological information obtained during IODP Expedition 354 integrated with the work of Schwenk et al., 2005 and Schwenk and Spieß, 2009.

### 4.3.1 Seismic facies definition and their link to drilling results

Schwenk et al., 2005 (based on work on the Amazon Fan, e.g. Flood et al., 1997; Lopez, 2001) defined the 4 seismic facies *Levee Deposits*, *HARPS* (*high amplitude reflection packages*), *Channel Fill* and *CHARS* (*chaotic high amplitude reflection packages*) as typical seismic facies for the Bengal Fan CLSs. We additionally introduce the seismic facies *Hemipelagic Layer*.

The *Levee Deposits* are wedge-shaped units of diverging, low to moderate amplitude reflections interpreted as levees deposited from channelized turbidity currents (Figs. 4.4 and 4.5). IODP Expedition 354 shows that they consist of dominantly clay/silt turbidites but also contain sandy sediments (France-Lanord et al., 2016). The levees onlap the underlying strata and usually occur together with associated channels (Figs. 4.4 and 4.5). The fill of buried channels



is characterized by parallel, distinct reflections of low to moderate amplitude with sharp lateral boundaries to the surrounding strata (*Figs. 4.4 and 4.5*). Transparent or low amplitude blocks adjacent to open and filled channels represent point bars – indicators of lateral channel migration (*Fig. 4.4*). CHARS at the base of surface and buried channels are interpreted as aggradation channel fill (*Lopez, 2001; Schwenk et al., 2005*) deposited from the coarse sediment fraction confined with the channel (*Pirmez and Imran, 2003*). Neither point bars nor the fill of a channel or CHARS were recovered during IODP Exp. 354. HARPS are parallel to subparallel reflection packages intercalated between the CLSs. *Schwenk et al., 2005* interpreted them based on observations from the Amazon Fan as massive to graded sands deposited from unchannelized turbidity currents as channel lobes or intra-channel deposits (*Figs. 4 and 5*). IODP Exp. 354 drilling results confirm that the HARPS consist of sands, locally intercalated with silts and clays (*France-Lanord et al., 2016*). The HARPs (also referred to as unchannelized turbiditic sediments) are of variable amplitude and reflector configuration. Where HARPs are deposited in-between CLSs, they are characterized by rather continuous reflections of medium to high amplitude. HARPS located directly below CLSs are less continuous and represent terminal lobes deposited during the downward migration of the CLS (*Picot et al., 2016*). Hemipelagic Layers appear as single, well-confined and consistent high amplitude reflections or, where layer thickness exceeds vertical seismic resolution, as two consistent, high amplitude reflection confining lower amplitude internal reflectors. The Hemipelagic Layers are continuous and distributed regionally where not eroded by CLSs. They are often associated with overlying reflections onlapping and composed of dominantly calcareous clay and nannofossil rich calcareous clay (*Figs. 4.4 and 4.5*).

### 4.3.2 Regional deposition of hemipelagic sediments

#### The Mid-Pleistocene Hemipelagic layer

The Mid-Pleistocene Hemipelagic layer (MPHL) is an almost continuous layer throughout the whole study area, acoustically represented by two high-amplitude reflections (MPHL-T at top and MPHL-B at bottom) confining parallel, lower amplitude internal reflections (*Fig. 4.4*). Along Profile GeoB97-020+027 the MPHL exists between km 35 - 420. The depth of the MPHL varies from west to east with ~180 ms (~148 m) below the seafloor west of Site U1454, 80 ms (~66 m) below the seafloor above the 85°E ridge, 200-210 ms (~173 m) below the seafloor in the center of Profile GeoB97-020+27 and only ~30 ms (~25 m) below the seafloor in the east (*Fig. 4.5*). The layer has two thickness maxima. The first one around Site U1451 (*Fig. 4.7*), where drilling shows that it consists of 3 individual hemipelagic layers enclosing two layers of terrestrial sands, silts and minor amounts of clay (*Fig. 4.2*). The second thickness maximum lies between sites U1452 and U1450 (*Figs. 4.2 and 4.7*). The latter thickness increase is accompanied by a decreased amplitude of MPHL-T and intercalation of turbiditic sediments into the upper part of the MPHL at Sites U1452 and U1450 (*France-Lanord et al., 2016*).

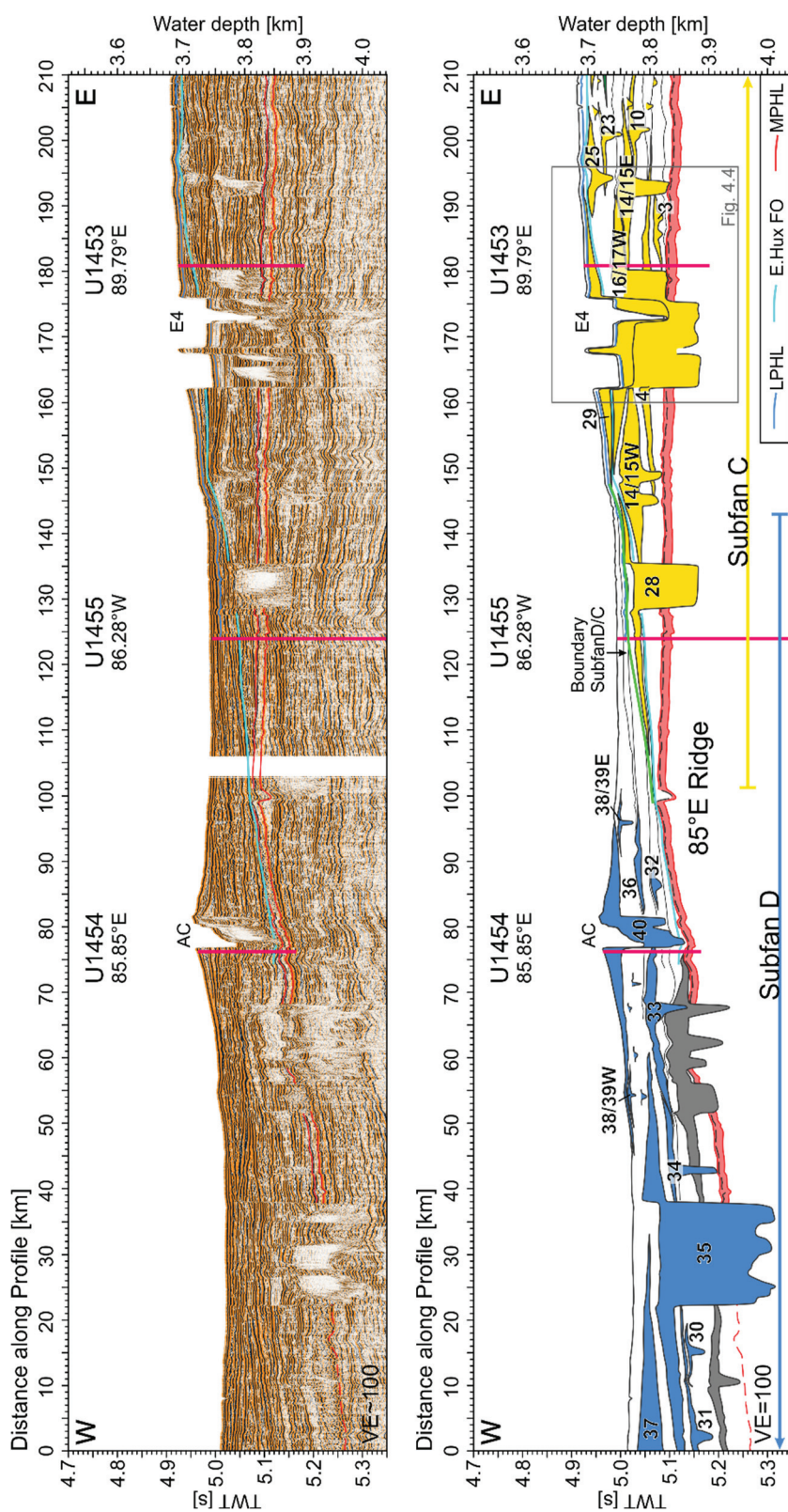


Figure 4.5-Part1: Top: Uninterpreted multichannel seismic Profile GeoB97-020+27 and IODP Expedition 354 drill sites. Bottom: Interpreted line drawing of Profile GeoB97-020+027 indicating channel-levee systems (CLSs) and their succession (numbered upsection). Yellow CLSs=Subfan C, blue CLSs=Subfan D. LPHL= Late Pleistocene Hemipelagic layer. E. Hux FO= First Occurrence *Emiliana huxleyi*. MPHL=Mid Pleistocene Hemipelagic layer. For location see Fig. 4.1, 4.3

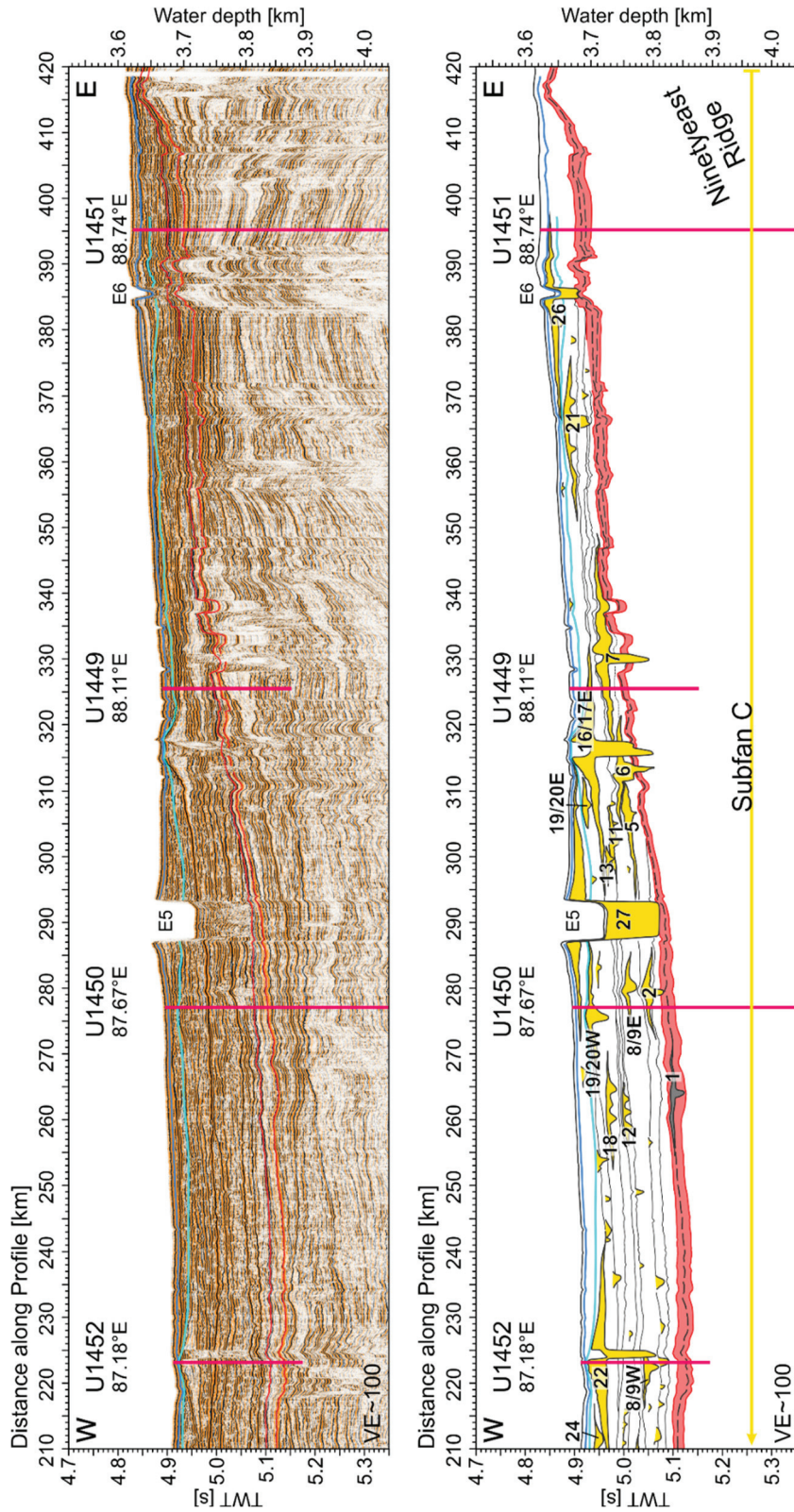


Figure 4.5-Part 2: Top: Uninterpreted multichannel seismic Profile GeoB97-020+27 and IODP Expedition 354 drill sites. Bottom: Interpreted line drawing of Profile GeoB97-020+027 indicating channel-levee systems (CLSs) and their succession (numbered upsection). Yellow CLSs=Subfan C, blue CLSs=Subfan D. For location see Fig. 4.1, 4.3; for legend see Fig. 4.5-Part 1.



### The Late Pleistocene Hemipelagic layer

The Late Pleistocene Hemipelagic layer (LPHL) is, like the MPHL, a continuous layer east of 86°E. It is seismically represented by a double reflector of high amplitude draping the sediments (*Fig. 4.5*). In the vicinity of Site U1449 and Site U1452, the top of the LPHL is intersected by small channels indicating recent turbiditic activity. The thickness of the LPHL increases in the vicinity of Site U1455 due to the intercalation of turbiditic sediments. The LPHL submerges west of Site U1455 and fades out between Site U1455 and U1454 (*Fig. 4.5*).

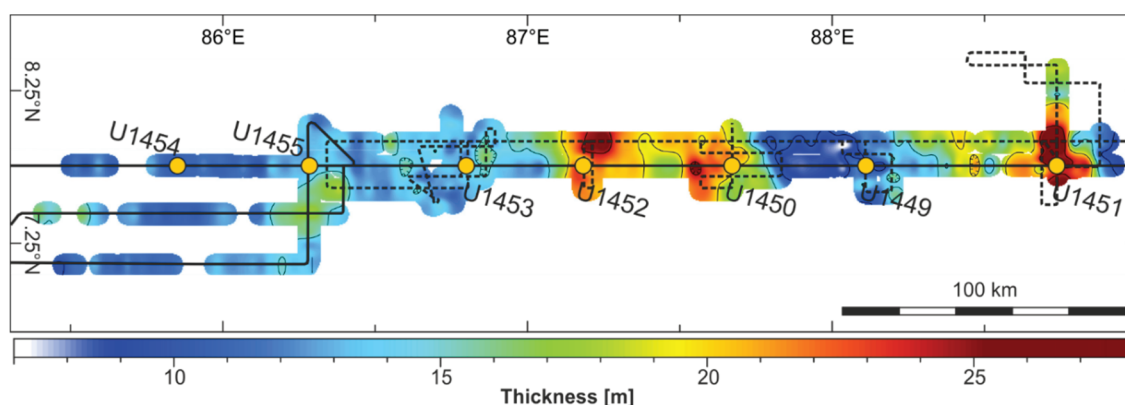


Figure 4.6: Thickness map of the Mid-Pleistocene Hemipelagic layer (MPHL). Conversion of two-way travel time into meters has been conducted with a velocity of 1530 m/s.

### 4.3.3 Channel-levee systems

Based on the above described seismic facies interpretation, 42 CLSs have been identified above the MPHL and another CLS has been found incorporated into the MPHL. Based on the tracing of levee base reflectors of all CLSs, a relative stacking pattern has been developed from the oldest (#1) to the youngest (#40) (*Fig. 4.5*). For systems 8 and 9, 14 and 15, 16 and 17, 19 and 20, and 38 and 39, respectively, base reflectors were not clearly separable. Hence, these systems are numbered as a/b-W or a/b-E according to their relative lateral position on Profile GeoB97-020+027. In addition to these 42 well-developed CLSs, several small channels without levees were identified but not considered for the stacking pattern.

4 CLSs represent the surface channels AC (No. 40), E4 (29), E5 (No. 27), and E6 (No. 26). The system E4 shows three separable levees (*Fig. 4.4*, see also *Schwenk and Spieß, 2009* and their *Fig. 3*), each of which is counted as an individual system (No. 4, 14/15W, and 29).

The width of the levees ranges from a few kilometers to 40 km (e.g. the Active Channel). The maximum levee thickness is likewise variable, ranging from a few meters up to ~40 m. The eroded channel relief (base of the levee to depth of maximum erosion) exceeds the levee heights in almost all CLSs. The maximum channel relief of ~163 m is reached at system No. 35. The CLSs cluster at three locations, namely west of the 85°E Ridge (km 0-80 in *Fig. 4.5*), east of the 85°E Ridge (km 130-230) and between Site U1450 and U1449 (km 270-340). Between

these areas of channel-levee development, the sub-seafloor is dominated by HARPS and small, unleveed channels (*Fig. 4.5*).

The CLSs have been grouped into two subfans. The older subfan includes the systems 02-29. CLS No. 1 (km 265) marks the reappearance of CLS formation in the study area after the deposition of the MPHL (*Figs. 4.5 and 4.6*). The lateral position of two subsequent systems within this subfan back and forth between site U1455 and U1451 (*Fig. 4.5*). The distance between two successive systems ranges from <10 km up to >150 km. The older subfan includes the development of the surface channels E4, E5, and E6, each draped by the LPHL, and is constrained by the 85°E Ridge and the Ninetyeast Ridge.

The youngest subfan includes the CLSs 30-40, which are all located west of the 85°E Ridge (*Fig. 4.5*). The distance between two successive systems in this subfan ranges from ~10-100 km. The younger subfan is less constrained by IODP Exp. 354 drill sites. The MCS data covers only the eastern levee of CLS No. 37 and it is unknown how many additional CLSs are located outside of our data range. The two unlabeled CLSs at km 10 and 60, respectively, cannot conclusively be assigned to any subfan (*Fig. 4.5*). The depth of the biostratigraphic datum *E. Huxleyi* FO at the sites U1455 and U1454 indicates that both CLSs are most likely older than system No. 28, but reflections between these CLSs are ambiguous.

#### 4.3.4 Unchannelized turbiditic sediments

Besides the numerous CLSs, large parts of the sediments are composed of unchannelized sediments (HARPs; *Fig. 4.5*). When omitting the hemipelagic parts, the remaining unchannelized sediments represent ~63% of the total amount of sediments deposited along Profile GeoB97-020+027 (above the MPHL), while the CLSs represent the remaining 37%. The unchannelized sediments spread laterally for tens to hundreds of kilometers, a lot further than the levees do, while maintaining a relatively flat surface by onlapping the underlying CLSs.

## 4.4 Discussion

### 4.4.1 Regional depocenter migration

#### Hemipelagic vs. turbiditic deposition

The Mid- and Late Pleistocene Hemipelagic layers (MPHL and LPHL) mark two phases of hemipelagic deposition at 8°N and hence, the absence of turbiditic fan deposition along the IODP drilling transect during these times.

As described above, the MPHL is thickening in the center of the study area due to the intercalation of thin turbidites with hemipelagic sediments (*Figs. 4.2 and 4.6*). The existence of a mixed hemipelagic/turbiditic layer has also been discussed by *Weber and Reilly, 2018* (their Unit 2b) and marks the transition from a hemipelagic dominated regime to the subsequent



turbiditic dominated regime. The onlapping reflectors overlying the MPHL imply that the turbiditic sedimentation first reappeared proximal to Site U1452 and from there spread gradually west and eastwards, underlining the asynchronous character of the upper boundary of the MPHL.

The top of the MPHL appears as distinct unconformity in the seismic data due to its acoustic properties and the onlap of the overlying turbiditic sediments. *Schwenk and Spieß, 2009* mapped this 'unconformity' of Pleistocene age along Profile GeoB97-020+27 and correlated its formation with intraplate tectonics active in the Central Indian Ocean (*Krishna et al., 2001b*). However, IODP Expedition 354 showed that their Pleistocene unconformity is identical with the MPHL caused by the turbiditic sediments onlapping the hemipelagic sediments. At ODP Leg 116 sites at  $\sim 1^{\circ}\text{S}$ , they observed an unconformity (Unconformity B) of similar age ( $\sim 0.8$  Ma) associated with an increase in sedimentation rate and grain size (*Cochran, 1990*). The occurrence of this unconformity has been linked with the intensification of Pliocene-Pleistocene glaciation (*Cochran, 1990*). *Schwenk and Spieß, 2009* identified other unconformities of Pliocene and Miocene age at  $8^{\circ}\text{N}$  and a set of undated unconformities at  $11^{\circ}\text{N}$ ,  $14^{\circ}\text{N}$ , and  $16.5^{\circ}\text{N}$  (Ua-Ug, *Fig. 4.8*). However, based on our new findings after the integration of MCS with IODP Expedition 354 results, we propose that all these unconformities are actually hemipelagic sediments linked to the absence of fan deposition in this area, rather than tectonic activity. In the case of Unconformity B, it may even represent the same time as the MPHL does.

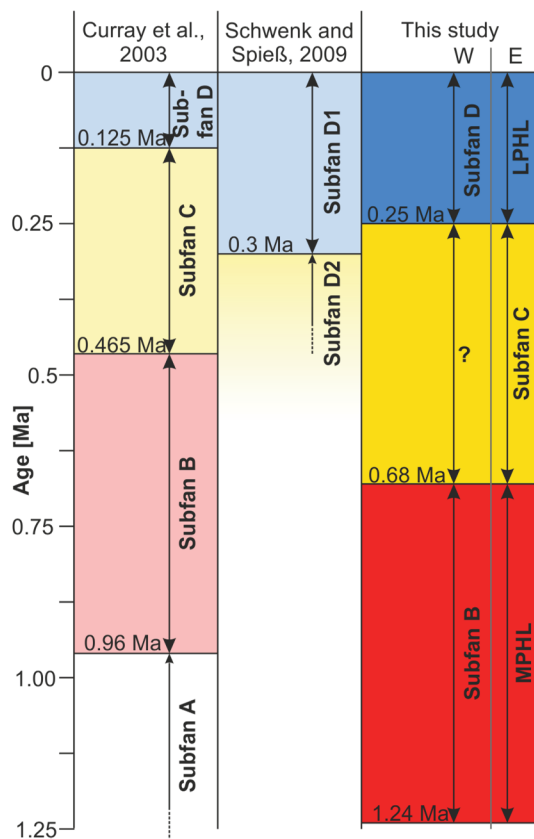
One important question is how the deposition of such regional, long lasting, hemipelagic deposition is triggered. Looking at the LPHL the CLS succession clearly shows that it has been deposited simultaneously with the younger subfan observed in our seismic data (*Fig. 4.5*). The simultaneous occurrence of hemipelagic and fan sediments can be explained with the concept of subfans introduced for the upper Bengal Fan by *Curray et al., 2003*, and which govern only parts of the Bengal Fan for a given period while other areas receive (almost) no fan sedimentation. This horizontal succession of fan and non-fan sediments we observe implies, that there is no generally valid link between hemipelagic deposition on the Bengal Fan and a fan shut-off but that hemipelagic deposition can be connected only to the deflection of terrestrial material into other regions. Consequently, the MPHL also represents a timespan with fan deposition not reaching  $8^{\circ}\text{N}$  and/or being deflected to the west of our study area.

### Timing of subfans

Since the onset of the MPHL, three individual phases of deposition can be distinguished at  $8^{\circ}\text{N}$ . The oldest is the MPHL itself ( $\sim 1.24$ - $0.68$  Ma; *Weber and Reilly, 2018*), deposited in our study area while at the same time fan deposition must have occurred elsewhere. The MPHL is followed by the two subfans identified in the seismic data ( $\sim 0.68$ - $0.25$  Ma and  $\sim 0.25$  Ma – recent, respectively) and the deposition of the LPHL simultaneously with the younger subfan. With our new data we are able to extend the subfans, first introduced by *Curray et al., 2003*,

as far south as 8°N and get an improved control over their timing. In order to correlate our findings on subfan deposition with the findings from earlier studies (*Curry et al., 2003*; *Schwenk and Spieß, 2009*), we combine subfan location (discussed in Chapter 4.1.3, *Fig. 4.8*) and timing (this chapter, *Fig. 4.7*).

*Curry et al., 2003* separate the Middle and Upper Pleistocene into the four subfans A, B, C, and D (1.9-0.96 Ma, 0.96-0.465 Ma, 0.465-0.125 Ma, and 0.125-0 Ma, respectively). Ages of these subfans were determined by correlation of their base reflectors from the upper fan to



DSDP Site 218 (*Curry et al., 2003*). However, recovery and age constraints at DSDP Site 218 were poor as it has been only spot-cored (*Von der Borch, 1974*), resulting in large uncertainties. The uncertainties in dating individual hemipelagic layers are further increased because their tops seem to be laterally asynchronous depending on where subsequent turbiditic deposition reappeared.

*Figure 4.7: Subfan sequences as interpreted by Curry et al., 2003, Schwenk and Spieß, 2009 and this study and simultaneously deposited hemipelagic layer (this study). Naming of subfans in this study after naming from Curry et al., 2003. Dating of subfans in this study based on Weber et al., 2018 and Weber and Reilly (in review). LPHL=Late Pleistocene Hemipelagic Layer; MPHIL=Mid-Pleistocene Hemipelagic Layer.*

Evidently, the most recent Subfan D and our younger subfan represent the same depositional unit, including, amongst others, the Active Channel. Profile GeoB97-020+027 covers the easternmost part of Subfan D plus the hemipelagic equivalent, the LPHL. *Weber et al., 2003* and *Schwenk and Spieß, 2009* suggested Subfan D started to develop around ~300 ka ago, earlier than suggested by *Curry et al., 2003*. Assuming that the onset of the LPHL also makes the onset of Subfan D we are able to limit its initiation to having occurred after ~0.29 ka (E. Hux FO) but before ~0.25-0.2 ka (age of LPHL base after *Weber et al., 2018* and *Weber and Reilly, 2018*) (*Fig. 4.7*).

*Curry et al., 2003* discuss that their second oldest Subfan C is restricted to the eastern part of the Bengal Fan and does not reach DSDP Site 218. However, we do observe fan deposition at 8°N directly prior to the deposition of Subfan D. We are confident that this older subfan observed at 8°N and Subfan C are the same, but propose an earlier onset of Subfan C (~0.68 Ma, *Weber and Reilly, 2018*) than *Curry et al., 2003* did (0.465 Ma) (*Fig. 4.7*).

The MPHL is the third oldest depositional unit identified in our data and represents a time during which no fan sediments reached our study area. Following the concept of subfans, fan sedimentation must have occurred elsewhere during this time. The third oldest unit 3 identified by *Curray et al., 2003* is Subfan B. Thus, we propose that the MPHL is the hemipelagic equivalent to Subfan B, such as the LPHL is the hemipelagic equivalent to Subfan D. The results from IODP Exp. 354 (*France-Lanord et al., 2016*) and the work from *Weber and Reilly, 2018*, imply that Subfan B had its onset and termination earlier than proposed by *Curray et al., 2003* (Fig. 4.7).

### Regional extension of subfans

In Figure 4.8 we present a model of subfan location for large parts of the Bengal Fan, connecting our new findings from 8°N with the early work from *Curray et al., 2003*. For this model, we additionally utilized the MCS profiles GeoB97-028, 041, and 059/069 published by *Schwenk and Spieß, 2009* and IODP Expedition 353 Site U1444 located at ~14°N directly above the 85°E Ridge (*Clemens et al., 2016*). Findings and assumptions behind our model of subfan location are: 1) the subfan synchronously deposited with the MPHL is not covered by the IODP Expedition 354 and our MCS data. However, the subfan location can only be west of the 85°E since east of our study area lies the Nicobar Fan, which is disconnected from the Bengal Fan since ~2 Ma ago (*McNeill et al., 2017a*). 2) No turbiditic sedimentation reached Site U1444 between ~3.5 and 0.45 Ma ago (Unit 2, 169-95 m CSF-A; *Clemens et al., 2016*). However, gravity anomaly maps (e.g. *Bastia et al., 2010a*) and MCS lines (*Schwenk and Spieß, 2009*) show that Site U1444 is located above a very high elevated section of the 85°E Ridge marking this long-lasting hemipelagic phase as a local phenomenon. 3) Top and bottom of Unit 2, Site U1444, correlate with the unconformities U<sub>c</sub> and U<sub>d</sub> at 14°N identified by *Schwenk and Spieß, 2009*. These two unconformities split up just east of Site U1444 where they are intercalated by turbiditic sediments. 4) Tentative northwards tracing of the MPHL (along preliminary processed MCS profiles) correlates it with Unconformity U<sub>b</sub> at 11°N (*Schwenk and Spieß, 2009*). 5) Combining our findings with the studies of *Curray et al., 2003* and *Schwenk and Spieß, 2009* we assigned the surface channels E2-E7 to Subfan C and the surface channels W1-W6, the AC and E1 to Subfan D. 6) The unconformities U<sub>e</sub> and U<sub>f</sub> (16.5°N; *Schwenk and Spieß, 2009*) enclose Subfan C. 7) The elevation of the 85°E Ridge varies from north to south and thus allows turbidity currents to overflow this ridge at some places while others act as topographic barrier (*Bastia et al., 2010a; Radhakrishna et al., 2012*).

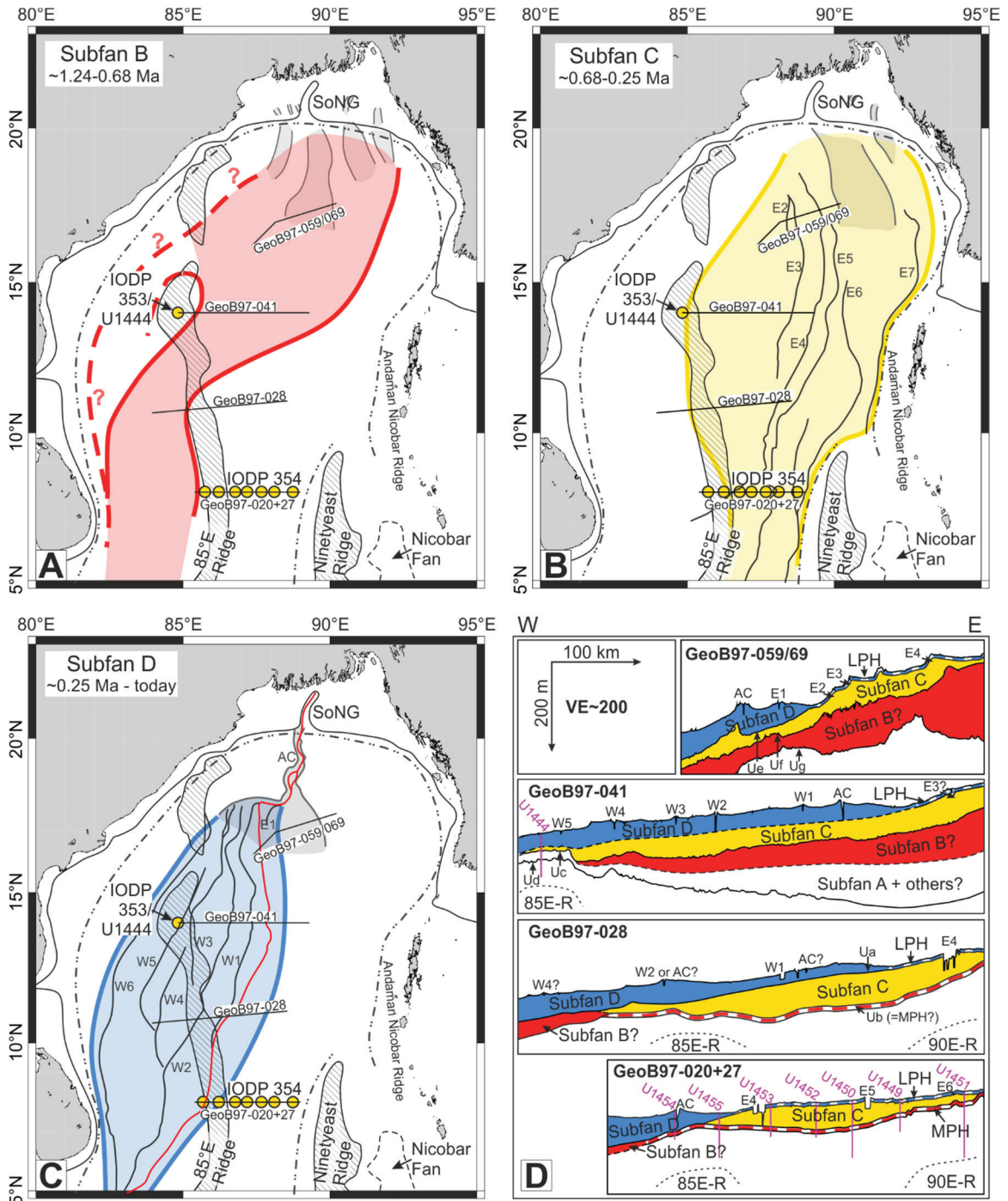


Figure 4.8: A-C: Interpreted map of subfans B (red), C (yellow) and D (blue) based on IODP Exp. 354, IODP Exp. 353 Site U1444, Multichannel seismic profiles GeoB97-059/69, 041, 028 and 020+27 (Schwenk and Spieß, 2009 and this study). Surface channels and the position of subfans on the upper Bengal Fan (thin colored lines) after Curray et al., 2003. D: Sketch of the subfans B, C and D in cross section along the multichannel seismic profiles GeoB97-059/69, 041, 028 and 020+27 (Schwenk and Spieß, 2009 and this study). Ua-Ug=Unconformities after Schwenk and Spieß, 2009. W1-W5, AC, E3-E6=Surface channels after Curray et al., 2003 and Schwenk and Spieß, 2009.

The deposition of the hemipelagic MPH at both MCS profiles at 8°N and 11°N proves the absence of the simultaneously deposited Subfan B there. However, at the MCS profile at 8°N



(GeoB97-020+27), the acoustic character of the unconformity associated with the MPHL is different in the very west compared to the remaining profile (*Fig. 4.5*). The distinct set of high amplitude reflections enclosing a lower amplitude package characterizing the MPHL disappear west of CLS No. 35 (*Fig. 4.5*). This may be connected to the presence of the actual fan sediments of Subfan B and the absence of the MPHL. A similar, although not that distinct, change in acoustic appearance is observed for Ub in the west of Profile GeoB97-028. The long-lasting hemipelagic deposition at IODP Site U1444 proves the absence of Subfan B at this location. However, turbiditic sediments deposited west of Site U1444, between the unconformities Uc and Ud (14°N) cover the timespan from ~0.45-3.5 Ma, including the time of deposition of Subfan B. Thus, we interpret the upper part of turbiditic sediments enclosed by Uc and Ud as Subfan B. Furthermore, based on the sequence of subfans, we interpret the sediments enclosed by the unconformities Ug and Uf at 16.5°N (*Fig. 4.8*) as Subfan B. Unfortunately, except for the Active Channel, no absolute age constrain consist at 16.5°N making this interpretation uncertain. Our data do not cover the Bengal Fan west of the 85°E Ridge. Nonetheless, in general sediments from the Bay of Bengal can also reach this part of the Bengal Fan (e.g. *Bastia et al., 2010a; Krishna et al., 2016*). Therefore and due to the disconnection of Nicobar and Bengal Fan prior the formation of Subfan B (see discussion above), we consider the western Bengal fan as the most likely location of Subfan B.

Subfan C is well constrained in the eastern Bengal Fan by the surface channels E2-E7 and its deposition at 8°N. Unconformities traced on the profiles at 16, 14 and 11°N indicate that Subfan C is partly underlying Subfan D in large parts of the Bengal Fan, while at 8°N the two subfans lie side by side. At IODP 353 Site U1444 turbiditic sedimentation (onset Unit 1, *Clemens et al., 2016*) commences at ~0.44 Ma after the basin east of the site has been filled.

Subfan D is very well constrained by surface channels and the clear evidence of turbiditic sedimentation at Site U1444 and Sites U1454 and U1455 during its formation. We proposed a Subfan D which spans less eastwards than suggested by *Curry et al., 2003*. This is best seen in Profile GeoB97-059/69 (*Schwenk and Spieß, 2009*) where Subfan D clearly onlaps Subfan C.

### Control on subfan migration

The three subfans B, C, and D investigated in this study all span over several glacial-interglacial cycles. It seems that at least for the two subfans C and D fan sediments have been deposited rather constantly. This is in contrast to the Amazon Fan where subfans, also called channel-levee complexes, are deposited during sea-level low stands only and channel-levee complex switching is triggered by the subsequent low stand. During highstands, however, hemipelagic sediments are deposited in thin layers over the entire fan separating the channel-levee complexes (*Piper et al., 1997; Lopez, 2001, Maslin et al., 2006*). On the Congo Fan, the location and switch between channel-levee complexes are mainly controlled by accommodation



space (Savoie *et al.*, 2009). The resulting depositional pattern is very similar to the Bengal Fan with thicker hemipelagic sequences deposited simultaneously with fan sediments in the adjacent area. This suggests that also the controlling mechanism for subfan switching on both fans is alike.

The resemblance of Bengal and Congo Fan is also expressed in the lifetimes of the channel-levee complexes. Subfan C and D last about 453 and 250 kyrs, respectively, while the three channel-levee complexes on the Congo Fan have lifetimes of ~210-330 kyrs (Savoie *et al.*, 2009). Channel-levee complexes on the Amazon Fan, on the other hand, last only for individual glacial-interglacial cycles (~10-50 ka, Piper *et al.*, 1997; Lopez 2001). The Congo Fan differs significantly from other large submarine fans due to its constant connection to the feeding river (e.g. Babonneau *et al.*, 2010). For the Bengal Fan a similar behavior is known for Holocene times with sediments bypassing along the shelf to the feeder canyon and further to the Fan (Kuehl *et al.*, 1989; Hein *et al.*, 2017). It is likely that sediment bypassing also maintained a constant sediment supply to the Bengal Fan during earlier highstand explaining the analogy of Congo and Bengal Fan.

Following Curray *et al.*, 2003, the initial position of the subfans on the upper Bengal Fan is controlled by the changing location of the feeder canyon. Our results show that in the middle and lower fan accommodation space becomes a more and more dominant factor. The accommodation space was mainly controlled by the uplift of the 85°E Ridge and the Ninetyeast Ridge creating distinct basins. In the case of Subfan C and D uplift at 8°N must have occurred synchronous or immediately after the deposition of the MPHL, in order to create (and maintain) the accommodation space for Subfan C. Uplift might have continued during the deposition of Subfan C but must have ceased eventually allowing the accommodation space to be filled up and the subfan to migrate westwards. At 14°N (IODP Site U1444) where a thick hemipelagic layer covers the time from ~5.5-0.44 Ma, the 85°E ridge must have been uplifted significantly earlier in order to create the basin filled up by Subfan B and even older sediments (Clemens *et al.*, 2016) (Fig. 4.8).

While the formation and architecture of the 85°E Ridge and the Ninetyeast Ridge during the northwards movement of the Indian Plate have been intensively studied (e.g. Krishna *et al.*, 2009; Bastia *et al.*, 2010a; Ismaiel *et al.*, 2017) little is known about the more recent tectonic activity. However, several faults above both ridges are visible in the seismic data reaching into the Pleistocene sediments. Furthermore, Schwenk and Spieß, 2009 found evidence for Pliocene and Pleistocene uplift of both ridges at 8°N by showing that sedimentation rates above both ridges are lower compared to the basin in between and that the variance is lower in Miocene times and higher during the Pliocene and Pleistocene. They connected the uplift events with the events of intraplate deformation in the Central Indian Ocean (Krishna *et al.* 2001b).

### Local depocenter shifting

Our data provide nearly full coverage of the evolution of Subfan C at 8°N during which in total 28 CLSs reached 8°N (CLS 02-29, *Figs. 4.5 and 4.6*). Using the total duration of Subfan C the average lifetime for CLSs is calculated to ~15 kyrs. These calculations do not include the at least 30 small and unleveed channels visible in the MCS data (*Fig. 4.5*), which are believed to develop during the downfan migration of a CLS as feeder channel within the terminal lobe (*Jegou et al., 2008, Picot et al., 2016*). Considering that these small channels represent CLS terminating further upfan the average lifetime of the CLSs must be shorter. The fact that 20-30 meter high levees can be built up in a very short time has previously been shown by work on the Active Channel revealing sedimentation rates of ~8.7 m/ka (*Chapter 3*).

Again, the Bengal Fan resembles the Congo Fan where CLSs have lifetimes of 5-17 kyrs and avulsion is suspected to be controlled by an interplay of internal and external forcing (*Savoie et al., 2009; Picot et al., 2016*). On the Amazon Fan CL-lifetimes are shorter (3-8 kyrs) and channel avulsion is associated with small-scale sea level variations within the glacial-interglacial cycle (*Piper et al., 1997; Maslin et al., 2006, Jegou et al., 2008*). The variable size of CLSs on the Bengal Fan implies unequally long lifetimes rather than a regular succession. This suggests autocyclic processes such as upfan avulsions as main control on the CLS lifetimes and not cyclic trigger such as sea-level variations. However, to fully understand if small-scale sea-level changes might have been an influence on channel avulsions, more accurate control on CLS ages is required.

One of the striking findings on Profile GeoB97-020+27 is a prominent segment of 50-60 km width lacking CLSs (*Fig. 4.5*, between Site U1452 and U1450). This CLS-gap has also been observed at the SO188 MCS profiles located 10 km upfan (*Fig. 4.3*) but not at the MCS profiles at 11, 14 and 16.5°N (*Schwenk and Spieß, 2009*), implying the lack of CLS being a local phenomenon. Curiously enough this gap coincides with the today topographically lowest part of the MPHL where turbiditic deposition restarted after the MPHL (*Fig. 4.5*, km ~210-280). CLS tend to fill such topographic lows, but this accommodation space has been filled by unchanneled turbiditic sediments only. Therefore it is suggested that during the deposition of Subfan C CLSs located in its center did not prograde down to 8°N. Instead, they must have terminated upfan and only their depositional lobes reached the drilling transect. Since progradation downfan is a matter of time, such timespans might be characterized by more frequent avulsion events leading to shorter lifetimes of CLSs.

### **4.4.2 Sand deposition**

As described in Chapter 3.3, about 63% of the sediments reaching 8°N (along Profile GeoB97-020+027) are deposited by unchanneled turbidites (HARPs) as indicated by their onlapping nature and preservation of a nearly flat surface/seafloor.

Where successfully recovered by the IODP 354 drilling, the HARPs are composed of dominantly fine sands to coarse silts (*France-Lanord et al., 2016; Adhikari et al., in press*). The reflection pattern of the HARPs is consistent throughout the MCS data while the IODP 354 sites exhibit numerous drilling gaps. Thus, drilling gaps within the HARPs most likely represent the loss of sand during drilling implying that the HARPs can be, similar to the Amazon Fan (*Lopez, 2001*), considered as sand to coarse silt dominated facies. In turn, this implies that about 63% of the material accumulated at 8°N (at least since the MPHL) is composed of coarse silt to fine sand. Moreover, the amount of sand might be even underestimated because the sediments deposited on the channel floors and within abandoned channels, can contain significant amounts of sand.

In general, the sand/mud ratio of turbidity currents increases downfan due to the loss of the smaller grain sizes via overspill, resulting in a net increase of sands towards the fan base (*Bouma, 2001; Posamentier and Kolla, 2003*). Thus, the sand quantity at 8°N may not be fully representative for the entire Bengal Fan. Still, the amount of sand deposited at 8°N is significantly higher than the threshold of 30% separating mud-rich from mixed sand-mud systems (*Richards et al., 1998*). Besides, not all channels developing at the Bengal Fan reach as far south as 8°N. This has been demonstrated by the mapping of surface channels (*Curray et al., 2003*) and by the high amount of unleveed distributary channels visible in the seismic data (Chapter 3.2). Moreover, lobes develop not only at the final termination of a channel but also via successive bifurcations during its downfan progradation (*Picot et al., 2016; Dennielou et al., 2017*).

Our findings of a significant contribution of sand to the Bengal Fan is further supported by the sediments recovered at IODP Site U1444 at 14°N. There the turbiditic dominated part of the Pleistocene is composed of clayey, silty and sandy turbidites and a sand content of about 50% (*Clemens et al., 2016*). Likewise, other 'mud-rich' submarine fans seem to contain more sand than expected. *Pirmez et al., 1997* discuss the existence of massive sand packages on middle and lower Amazon Fan (30 m and >100 m thickness, respectively).

The sand within Subfan C has an average deposition rate of ~35 cm/ka (max. thickness (150 m)/duration Subfan C (~430 ka)) and seems to be delivered almost constantly to 8°N during the subfan's active phase of more than 400 ka. In general, the sand recovered in the IODP Expedition 354 is characterized by the same grain size range than the sediment transported today as suspended load in the basal water of the Ganges and Brahmaputra rivers and in their bedload (*Lupker et al., 2011; Garzanti et al., 2010*).

All in all, our observations not only demonstrate the dominance of unconfined sedimentation to the Bengal Fan architecture but further suggest that the sand content in large (mud-rich) submarine fans might be significantly higher than published in generalized models. Moreover, it empathizes the key role of understanding the sand deposition in order to link sedimentary fluxes to the Bengal Fan with tectonic or climate events from the source area.

## 4.5 Summary and Conclusions

This study utilized multichannel seismic data from the lower Bengal Fan in integration with IODP Expedition 354 drilling results in order to investigate the relative stratigraphy and deposition along the drilling transect at 8°N. Sedimentation in the study area is characterized by turbiditic fan sedimentation via CLSs and unchannelized turbidity currents and regional hemipelagic deposition. Turbiditic deposition governs parts of the Bengal Fan forming so-called subfans while hemipelagic deposition dominates simultaneously in the remaining fan area creating layer up to >20 m thickness. Since the Middle Pleistocene the three subfans B (1.24-0.68 Ma), C (0.68-0.25 Ma), and D (0.25 Ma-recent) and two hemipelagic layers (Mid Pleistocene Hemipelagic Layer (MPHL, 1.24-0.68 Ma; *Weber and Reilly, 2018*) and Late Pleistocene Hemipelagic Layer (LPHL, 0.25 Ma- recent; *Weber et al., 2018*) have been formed in the Bengal Fan. The location of the subfans alternates between the western and the eastern fan filling up available accommodation space, potentially created by the uplift of the 85°E Ridge and Nintyeast Ridge during Pleistocene times. The LPHL and the MPHL represent the hemipelagic equivalents to the subfans B and D, respectively. The transition from one subfan to another does not correlate with glacial-interglacial cycles but is controlled by available accommodation space and/or changes in the supplying canyon as suggested by *Curray et al., 2003*.

Above the MPHL the sediments in the study area are constructed of 42 CLSs and numerous unleveed channels composing 37% of the total sediments deposited. The average lifetime of CLSs during the deposition of subfan C was ~15 ka. However, the variable size of CLSs in the study area indicates a random distribution of the maturity of individual systems which in turn suggests autocyclic processes such as upfan avulsions as main control on the CLS lifetimes. The CLSs are intercalated by sediments (HARPs) composed of sands with minor amounts of silts and clays deposited from unchannelized turbidity currents. The unchannelized turbiditic sediments compose ~63% of the total sediment volume. This demonstrates the dominance of unchannelized sedimentation to the fan architecture and further shows that the sand content in large submarine fans might be higher than expected. The channel-levee stacking pattern developed and presented in this study enables the comparison and correlation of the seven IODP Expedition 354 drill sites on a relative stratigraphy.

## 4.6 Acknowledgments

This study was funded through the German Research Foundation (DFG) within the IODP Priority program (Grant No. SCHW1551/7-1/2). We would like to thank captain, crew and scientific party of RV Sonne cruises SO93, SO125, and SO188, and IODP Expedition 354. Funding for the collection of seismic data was provided by BMFT Project 03 G 0093 A (So93), BMBF Grant no, 03 G 0125A (SO125), and BMBF Grant No. 03 G 0188A (SO188).

## Chapter 5

### 5 Increased sediment flux to the lower Bengal Fan during the Middle Pleistocene – Internal and external controls

Fenna Bergmann<sup>1</sup>, Brendan Reilly<sup>2</sup>, Tilmann Schwenk<sup>1</sup>, Volkhard Spiess<sup>1</sup>, Christian France-Lanord<sup>3</sup>

<sup>1</sup>Faculty of Geosciences, University of Bremen, Klagenfurter Strasse 2-4, D-28359 Bremen, Germany

<sup>2</sup>College of Earth, Ocean and Atmospheric Sciences, Oregon State University, Corvallis OR 97331, USA

<sup>3</sup>Centre de Recherches Pétrographiques et Géochimiques, CNRS Université de Lorraine, BP 20, 54501 Vandoeuvre les Nancy, France

#### Abstract

The Bengal Fan records the erosion of the central Himalaya and Tibetan Plateau since its initiation in the Early Eocene. High-resolution multichannel seismic data were correlated with IODP Expedition 354 drilling results and integrated with a system-specific age-depth model. This allows an important advance in the transects stratigraphy and provides novel insights into the regional deposition of hemipelagic sediments and the variations in accumulation rates since the Middle Pleistocene. Accumulation rates and overall sediment load increase constantly in the time interval from ~0.68-0.25 Ma, independently from sea level variations. Instead, the increasing input seems to reflect denudation rate changes in the source area, which may be linked to climate variability. Fan sedimentation (in the time between 0.68-0.25 Ma) was interrupted three times by the deposition of regionally extending hemipelagic layers. Again, no systematic link to sea-level variations has been observed. This implies that the Bengal Fan behaves contradictory to the general understanding of submarine fans being starved in times of sea-level highstands. It further implies a constant sediment delivery to the fan since the Middle Pleistocene.

#### 5.1 Introduction

The Bengal Fan is the most complete sedimentary record of Himalayan uplift, erosion and weathering history. Over the last decades, the fan has been the target of numerous deep drilling campaigns (e.g. DSDP 22, *Von der Borch et al., 1974*; ODP 116, *Cochran, 1990*; IODP 353, *Clemens et al., 2016*; IODP 354, *France-Lanord et al., 2016*) and (multichannel) seismic



surveys (e.g. RV Sonne cruises SO93, 125, and 188; *Kudrass et al., 1994; Spieß et al., 1998, 2006*). The sedimentary and geophysical records acquired during these expeditions have been used in various studies to learn more about the source-to-sink system, including the climate-tectonic interactions of the source area and the Bengal Fan's role in the global carbon cycle (e.g. *Derry and France-Lanord, 1996, 1997; Galy et al., 2010; Hein et al., 2017*). However, working with data from the Bengal Fan is challenging due to its size and complexity. Sediment transported to the fan mainly via Ganges and Brahmaputra has to bypass the floodplains, the delta, and the continental shelf before reaching the Bengal Fan itself (*Fig. 5.1*). The Bengal Fan is characterized by lateral depocenter migration, often over distances exceeding 100 km (*Curry et al., 2003; Schwenk and Spieß, 2009; France-Lanord et al., 2016; Chapter 4*).

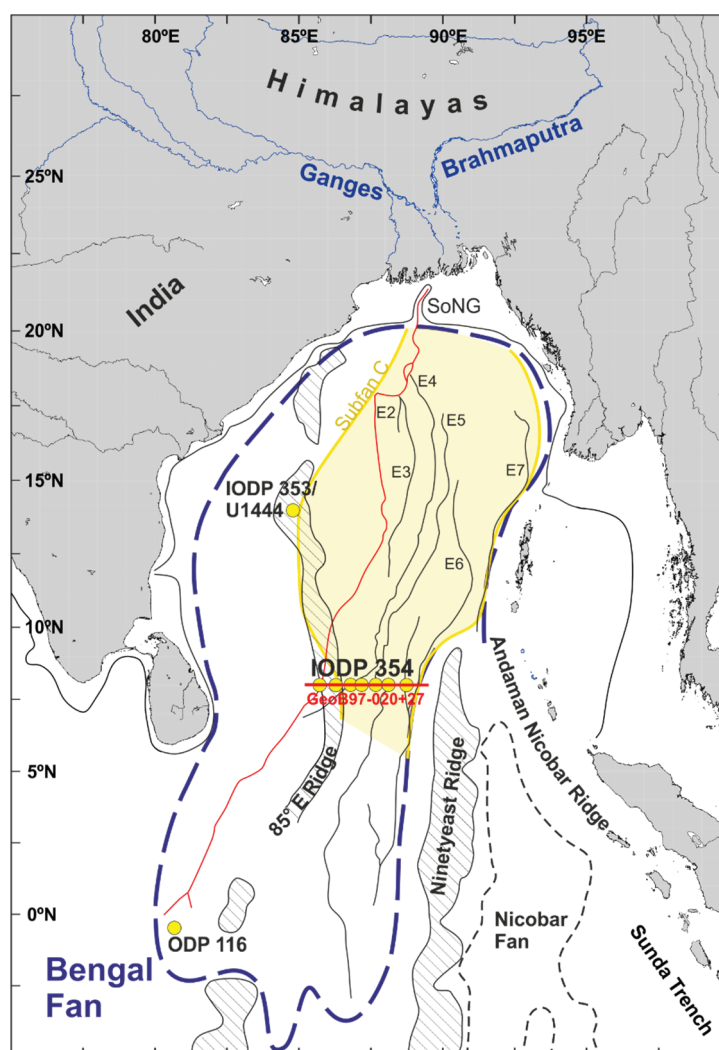


Figure 5.1: Overview map of the Bengal Fan (blue stippled line). Yellow shaded area: Subfan C deposition after Chapter 4. Black lines: Surface channels associated with Subfan C; red line: youngest channel-levee system (Active Channel), formed after the abandonment of Subfan C. Surface channels after *Curry et al., (2003)*. Multichannel seismic Profile GeoB97-020+27 at 8°N, crossing all IODP Expedition 354 drill sites, marked in red. Tectonic features and fan outline are redrawn after *Curry et al., 2003; Bastia et al., 2010a, b; Choudhuri et al., 2014; McNeill et al., 2017a*.

These depositional characteristics result in discontinuous records at a given location. Therefore, seven sites were drilled during IODP Expedition 354 in 2015, which were aligned on a west-east transect (*Figs. 5.1 and 5.2*) to provide a nearly continuous sedimentary record of Pleistocene times (*France-Lanord et al., 2016*). Determining a high-resolution chronostratigraphy of the predominantly terrestrial-sourced sediments remains challenging. Therefore, *Reilly et al. (in prep.)* developed a novel core-seismic integrated age-depth model factoring age constraints, lithology and seismic stratigraphy of the drilling transect.

In this study, we integrate the seismic stratigraphy and the age model to improve the chronostratigraphy along the drilling transect and to investigate recurrence rates of channel-levee systems. We further examine the regional deposition of hemipelagic sediments and the variations in accumulation and mass accumulation rates during the Middle Pleistocene and their potential linkage to sea level and climate variability. This work is based on the seismic stratigraphy along the IODP Expedition 354 drilling transect presented by *Chapter 4* and the core-seismic integrated age model designed by *Reilly et al. (in prep.)*.

### 5.1.1 The Bengal Fan – Regional setting

The Bengal Fan is situated in the Indian Ocean and extends for >3000 km from the shelf of India and Bangladesh southwards. The fan has received Himalayan sediment since its initiation in the Early Eocene after the collision of the Indian and Eurasian plate and the subsequent uplift of the Himalaya and Tibetan Plateau (*Curray et al., 2003; Gibbons et al., 2015*). Today, eroded Himalayan material is transported to the Bengal Shelf via the major rivers Ganges and Brahmaputra. After being released to the ocean, sediment bypasses the shelf and is temporarily stored in the *Swatch of No Ground* (SoNG), a canyon incised into the shelf ~100 km west of the Ganges-Brahmaputra delta. Sediment is episodically released out of the canyon to the fan via turbidity currents, thereby maintaining fan activity even during the Holocene Highstand along the Active Channel (*Fig. 5.1*) (*Kuehl et al., 1989; Weber et al., 1997, Michels et al., 2003; Hein et al., 2017*).

Sediments deposited in the Bengal Fan are dominantly turbiditic, transported by two main processes: Sediments deposited since fan initiation until the Miocene are characterized by sheeted turbidites (*Schwenk and Spieß, 2009; Krishna et al., 2016*). Since the Late Miocene, the sheeted turbidites are frequently intercalated with channel-levee systems (CLSs) (*Curray et al., 2003; Schwenk and Spieß, 2009*). The CLSs are characterized by clayey/silty levees and sands at the channel base while the sheeted turbidites contain mostly sand (*Schwenk et al., 2005; France-Lanord et al., 2016; Chapter 4*). Deposition on the Bengal Fan is further characterized by lateral migration on two different scales. On timescales of ~250-500 ka fan sedimentation was organized in subfans governing only parts of the Bengal Fan while the adjacent areas were draped by hemipelagic sediments (*Curray et al., 2003; Chapter 4*). Subfan

positions were controlled by the location of the feeding canyon on the shelf and the two aseismic ridges 85°E Ridge and Ninetyeast Ridge emplaced during the northwards journey of the Indian plate (*Gopala Rao et al., 1997; Krishna et al., 2001a; Curray et al., 2003; Bastia et al., 2010b; Chapter 4*). The two ridges acted as topographic barrier constraining fan sedimentation. Since the Middle Pleistocene, four individual subfans (subfans A, B, C, D) have been identified alternately occupying the western and eastern Bengal Fan (*Curray et al., 2003; Chapter 4*). On shorter time scales fan sedimentation migrated laterally via channel avulsion (*Curray et al., 2003; Schwenk and Spieß, 2009*). In our study area at 8°N channel avulsion occurred on average every 15 kyrs and the lateral distance between two CLSs can exceed 150 km (*Chapter 4*).

### 5.1.2 The Bengal Fan - Chrono- and Seismic Stratigraphy

#### IODP Expedition 354 stratigraphy

During IODP Expedition 354 a seven-site W-E transect at 8°N (Sites U1449-U1455) was drilled at the lower Bengal Fan. Sediments recovered at the seven sites are dominated by terrestrial sands and silts, irregularly intercalated with more hemipelagic dominated material (calcareous clay) (*Fig. 5.2; France-Lanord et al., 2016*). The drilling further revealed the existence of two thick hemipelagic layers, the Middle and Late Pleistocene Hemipelagic Layer (MPHL and LPHL) (*Fig. 5.2*). Overall, the MPHL lasted from about 1.24 Ma until 0.68 Ma (*Weber and Reilly, 2018*). However, the top of the MPHL is clearly asynchronous. It is oldest in the central drilling transect (sites U1450, U1452, U1453, approximately MIS 17/15) and youngest in the far east of the drilling transect (Site U1451, approximately MIS 10/9) (*Weber and Reilly, 2018*). The LPHL, its base likewise being asynchronous, had its onset around 0.25 Ma (*France-Lanord et al., 2016; Weber et al., 2018*). *Weber and Reilly, 2018* further discern the terrestrial sediment section between the MPHL and the LPHL into two temporally overlapping units: A mixed hemipelagic/turbiditic unit (~MIS17-13) and a turbiditic dominated unit (~MIS15-12 – ~MIS8-7).

#### Seismic stratigraphy

Prior to IODP Expedition 354 *Schwenk and Spieß (2009)* investigated the seismic stratigraphy along the drilling transect. They based their work on the multichannel seismic (MCS) line GeoB97-020+27 recorded in W-E direction at 8°N (*Fig. 5.1*). This MCS profile is ~420 km long and crosses all seven IODP Expedition 354 sites (U1449-U1455). Utilizing the new insights gained by IODP Exp. 354 drilling, In *Chapter 4* we revised the seismic stratigraphy of Profile GeoB97-020+27. On the basis of the work of *Curray et al. (2003)*, *Schwenk and Spieß (2009)*, and *Chapter 4*, the seismic stratigraphy at 8°N for the here relevant upper 200 m can be summarized as follows:

The Middle Pleistocene Hemipelagic Layer (MPHL) and Subfan C (0.68-0.25 Ma) extend over large parts of our study area (*Fig. 5.3*). Subfan D and the Late Pleistocene Hemipelagic Layer

(LPHL), deposited concurrently (0.25 Ma – recent), occur only in the western and eastern part of the profile, respectively (Figs. 5.3 and 5.4). The fan sediments of subfans C and D consist of ~60% sheeted turbidites, which are composed predominantly of sandy material. The remaining ~40% consists of 42 CLSs, composed of clayey, silty and sandy sediments. The MPHL and the LPHL represent regionally extending hemipelagic deposition at times when active fan sedimentation was focused on other fan areas.

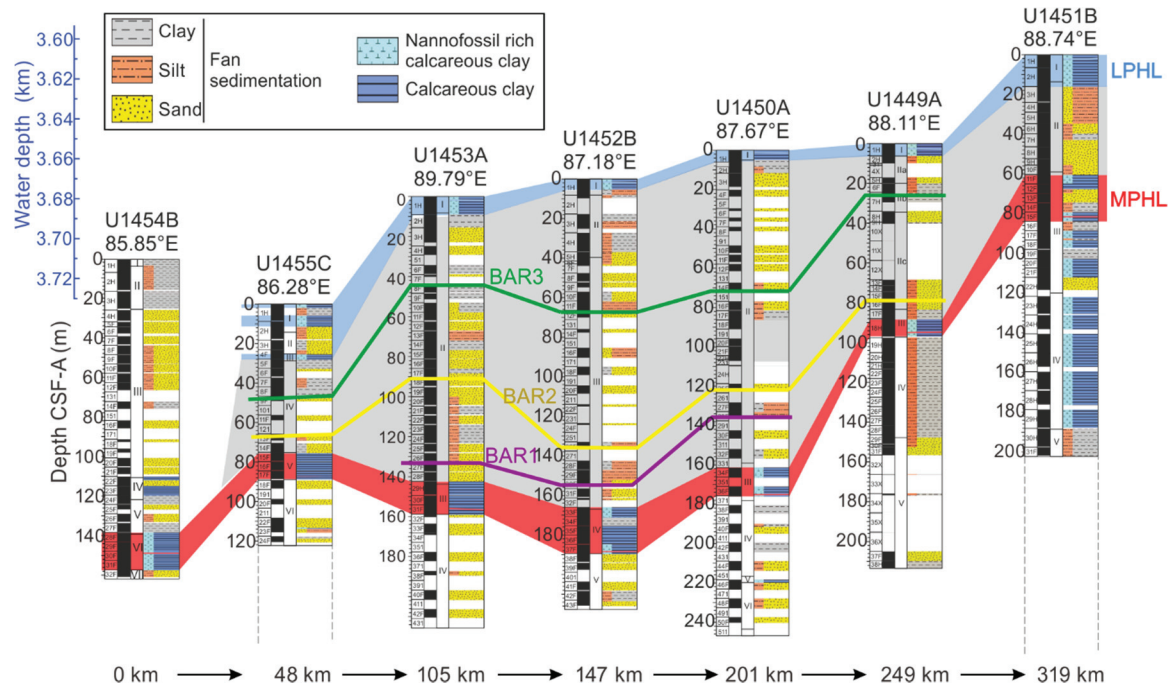


Figure 5.2: Lithostratigraphic summary of the upper 200 m of cores drilled during IODP Expedition 354. Only lithologies that constitute >10% of the core are included (modified after France-Lanord et al., 2016). LPHL= Late Pleistocene Hemipelagic Layer. MPHL=Middle Pleistocene Hemipelagic Layer. BAR1-3: Brunhes-aged Reflectors representing thin hemipelagic layers. Gray shaded area: Subfan C sediments. For locations of cores see Figs. 5.1, 5.3.

### Core-Seismic integrated age model

Reilly et al. (*in prep*) designed a system specific age-depth model for the seven IODP Expedition 354 drill sites using a Bayesian approach that respects the law of superposition. The model factors the known age constraints of ash layers (Youngest Toba Tephra (YTT), Oldest Toba Tephra (OTT), Mark et al., 2017), biostratigraphy (*Emiliana huxleyi* first occurrence, Gradstein et al., 2012), and magnetostratigraphy (Matuyama-Brunhes Magnetic Reversal, Jaramillo Subchron and Cobb Mountain Subchron, Channell et al., 2016). It further incorporates variable sedimentation rates for fan sedimentation and hemipelagic sedimentation. Moreover, it uses the seismic data in terms of relative stratigraphy of the channel-levee systems and regionally extending reflectors (Chapter 4).

The age model of Reilly et al. (*in prep*) outputs ages for the last 1.25 Ma (Middle Pleistocene-present) for all seven IODP Expedition 354 sites. It further proved that the three regionally

extending reflectors BAR1, BAR2, and BAR3, intercalated into the sediments of Subfan C, correlate with calcareous clay sediments (*France-Lanord et al., 2016; Reilly et al. (in prep.)*). Moreover, *Reilly et al. (in prep.)* measured magnetic susceptibility (MS) and scanning XRF Ca/Ti ratios to distinguish hemipelagic (low MS, high Ca/Ti,) and fan sediments (high MS, low Ca/Ti). Within hemipelagic sediments, sediment lightness ( $L^*$ ) can be used to identify orbital scale variations, with  $L^*$  highs generally corresponding to interglacial/interstadial times (*Weber et al., 2018; Weber and Reilly, 2018*). At Site U1452 BAR3 correlates with a ~80 cm thick calcareous clay layer. However, only the upper 47 cm of this layer are clearly of hemipelagic origin (rich in nanofossils, high Ca/Ti, low MS) and have been deposited during the transition from a glacial to an interglacial signal (low vs. high  $L^*$ ) (*Reilly et al. (in prep.)*).

## 5.2 Data and Methods

### 5.2.1 Multichannel seismic data

Profile GeoB97-020+27 has been acquired during the research cruise SO125 in 1997, carried out as a pre-site survey for IODP Expedition 354 in cooperation with the University of Bremen and the BGR Hannover (*Spieß et al., 1998*). For recording a 48-channel streamer (channel spacing 12.5 m) and a 2x0.41 l Generator-Injector (GI) gun were utilized. The main frequency of the MCS data ranges from 100-500 Hz resulting in a vertical resolution of ~5 m. The profile underwent a full multichannel-seismic processing including CMP-binning (12 m inline bin size), noise reduction, velocity analysis, NMO-correction, stacking, and time-migration.

Processing and interpretation of the MCS data were done using the software 'Vista 14; Seismic Data Processing' and 'IHS Kingdom 2016'.

### 5.2.2 Integration of datasets

IODP Expedition 354 cores and the age-model of *Reilly et al. (in prep.)* were linked with the MCS data using constant seismic velocities of ~1640 m/s (sites U1449, U1454, and U1455), ~1650 m/s (sites U1451 and U1453), and ~1680 m/s (sites U1450 and U1452).

CLS ages are either directly derived from the age-depth model or derived via linear interpolation between the two chronologically closet modeled ages. Error bars for the modeled ages represent the 97.5% confidence interval while error bars for the interpolated ages represent the maximum and minimum error from the chronologically closet modeled ages.

### 5.2.3 Sedimentation/accumulation rates

Accumulation rates were calculated along the seismic profile using the depths and ages of the three BAR layers (*Tbl. 5.1*) and of MPHL and LPHL after *Weber et al., 2018 and Weber and Reilly, 2018*. For the conversion of unit thickness from two-way-traveltime (TWT) into meter and then into accumulation rate (*Tbl. 5.2*) velocities from the core sites (Chapter 2.2) have



been linearly interpolated along the profile. Mean BAR ages were calculated based on the age-probability distribution of the three layers determined at IODP sites U1449, U1453 and U1452 by age-depth modeling (*Reilly et al. (in prep.)*, their *Fig. 9* and this study, *Fig. 5.5*). Limited recovery and fewer age-control points within the sediment recovered at Site U1450 result in larger age uncertainties at this site (for more detail see *France-Lanord et al., 2016* and *Reilly et al. (in prep.)*). Therefore, we excluded ages determined for Site U1450 from our investigation.

For the calculation of accumulation rates BAR layers have been linearly interpolated in places where they were eroded by channel-levee systems. Compaction of sediments has a minor influence in the upper 200 m of IODP Expedition 354 cores (*France-Lanord et al., 2016*). Therefore, accumulation rates have not been corrected for compaction. Accumulation rates have also not been corrected for the duration of the hemipelagic layers BAR1-3 (Chapter 5.3.2).

Mass accumulation rates for individual seismic units have been calculated using an average dry bulk density of 1.5 g/cm<sup>3</sup> (averaged for all dry bulk density measurements taken at sites U1449, U1452 and U1453 in the according depth interval, *France-Lanord et al., 2016*), the 2D-cross section of each unit extrapolated for 1 km along-fan, and the duration of each unit (*Tbl. 5.2*).

## 5.3 Results

In this section, we present results derived from Profile GeoB97-020+27, with a focus on the deposition of Subfan C in the Middle Pleistocene (~0.68-0.25 Ma, as defined in *Chapter 4*).

### 5.3.1 Subfan C (~0.68-0.25 Ma)

Subfan C covers the eastern ~300 km of Profile GeoB97-020+27 (*Figs. 5.3 and 5.4*). It is vertically bounded by the MPHL at the bottom and the LPHL at the top and contains 28 channel-levee systems (No. 2-29, *Fig. 5.3*), including the three surface channels E4, E5, and E6 (naming after *Curray et al., 2003*). CLSs are represented by low amplitude, diverging reflectors (levees) accompanied by nearly transparent areas and high-amplitude, parallel reflections within old channels, as shown by *Schwenk et al., 2005* and in *Chapter 4*. CLSs are intercalated by packages of medium to high amplitude, parallel to sub-parallel reflections, the so-called High Amplitudes Reflection Packages (HARPs, see *Schwenk et al., 2005; Chapter 4*). Subfan C is horizontally separated into four subunits C1-C4 by three regionally extending reflectors BAR1, BAR2 and BAR3 (Brunhes-Aged Reflectors) (*Fig. 5.4*; see also *Reilly et al. (in prep.)*).



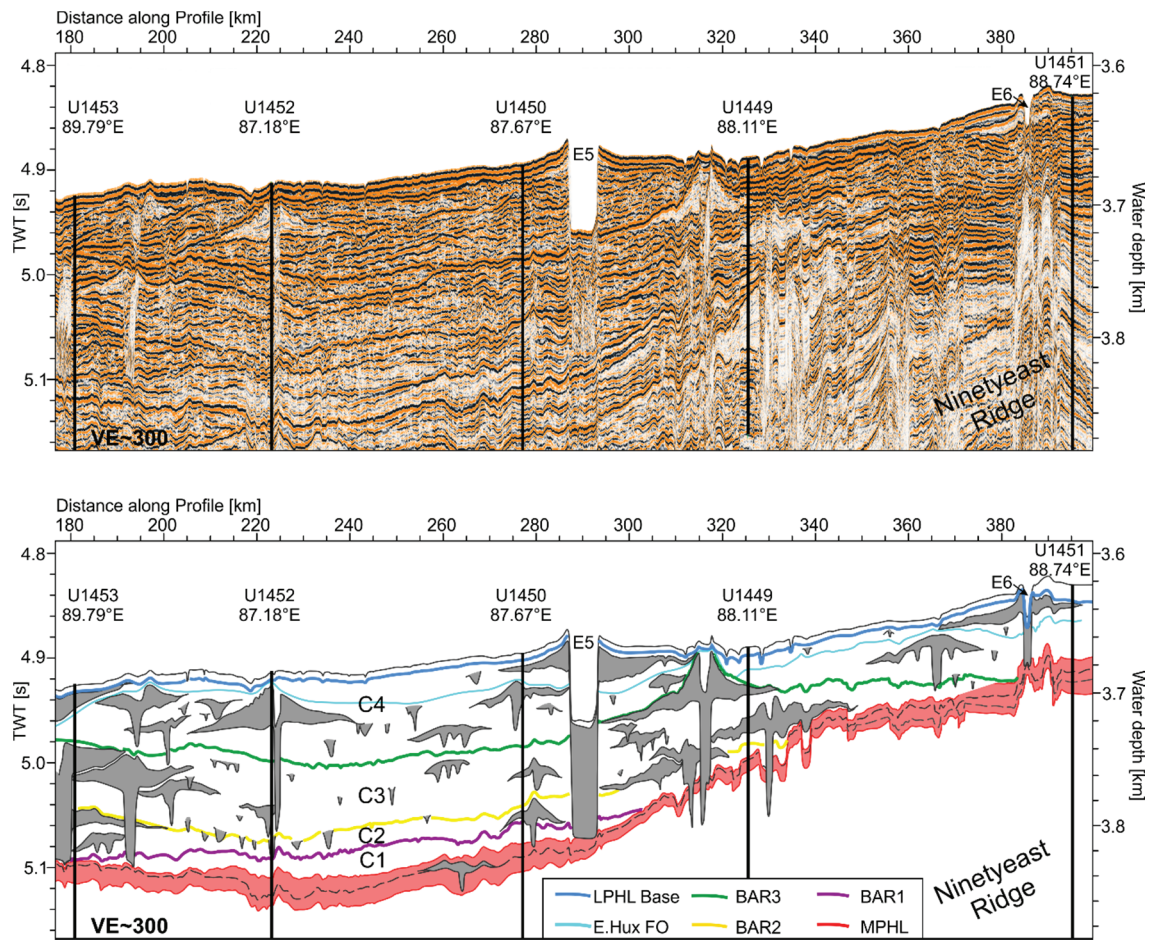


Figure 5.4: Top: Uninterpreted section of multichannel seismic Profile GeoB97-020+27 focusing on Subfan C deposits. Bottom: Interpreted line drawing indicating channel-levee systems (gray) and hemipelagic layer intercalated into Subfan C (BAR1-3). LPHL= Late Pleistocene Hemipelagic Layer. E.Hux FO= First Occurrence *Emiliana huxleyi*. MPHL=Middle Pleistocene Hemipelagic Layer. IODP Expedition 354 sites are marked by vertical black lines. For location see Fig. 5.1, 5.3.

### BAR1-3 – Regional Hemipelagic layer

The three BAR reflectors, first introduced by *Reilly et al. (in prep.)*, are of high amplitude and continuous throughout most parts of Subfan C. BAR1 overlies the MPHL in the proximity of Site U1453 in the west and in-between Site U1450 and U1449 in the east (approx. at km 305, Fig. 5.4). BAR2 terminates against the MPHL ~12 km west of Site U1455 and east of Site U1449 between approx. km 330-350 (Fig. 5.4). BAR3 overlies the MPHL between U1454 and U1455 and between km 380-390, just west of Site U1451 (Fig. 5.4). Where recovery was sufficient, the BAR layers correlate with layers of calcareous clay (~0.02-0.88 m thickness) (Tbl. 5.1) and are therefore considered as regionally deposited hemipelagic layers.

Following the age-depth model presented by *Reilly et al. (in prep.)* the mean ages of BAR1-3, calculated from the results of Sites U1449, U1552, and U1453, are 510 ka, 457 ka, and 330 ka, respectively (Tbl. 5.1). Comparison with the global sea level curve (Fig. 5.5) reveals that the age distribution of BAR1 peaks at sea level of -60 to -50 m during times of a relatively



stable sea level and has a good agreement at Sites U1452 and U1453. BAR2 peaks at a sea level of about -100 m during times of sea level fall (Fig. 5.5), largely defined by the results from Site U1453 with greater uncertainty at Sites U1449 and U1452. The age distribution of BAR3 peaks at a sea level of about -90 to -80, at times of rapidly rising sea level (Fig. 5.5), which is consistent with physical property observations from Site U1452 (Reilly *et al. (in prep.)*).

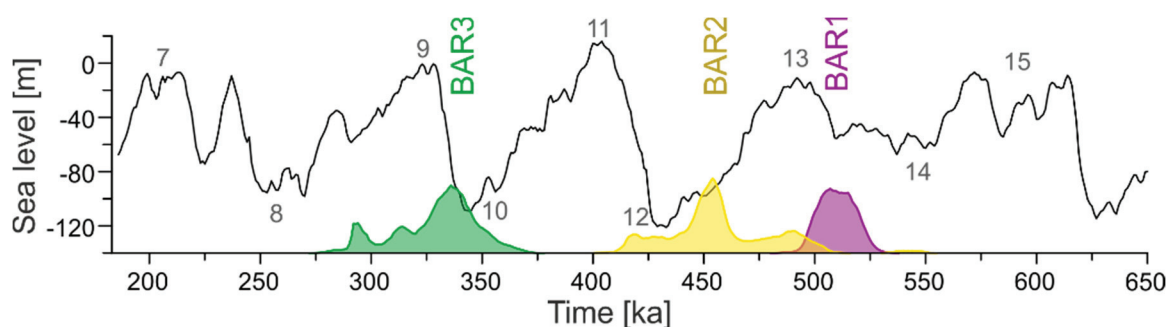


Figure 5.5: Sum age probability distribution of all observations of Brunhes Age Reflectors (BAR1 (pink), BAR2 (yellow), and BAR3 (green)), calculated from all ages in the interval between the uppermost and lowermost depth estimates based on seismic data (at IODP sites U1453, U1452 and U1449); after Reilly *et al. (in prep.)* The global sea level and marine isotope stage (MIS) numbers are included for comparison (Spratt and Lisiecki, 2016). Modified after Reilly *et al. (in prep.)*.

### Subfan C - Subunits

#### **C1 (~0.68-0.51 Ma)**

Seismic Unit C1 (Figs. 5.3 and 5.4) is the lowermost unit of Subfan C. It is vertically bounded by the MPHL (bottom) and BAR1 (top). The unit overlies the MPHL and terminates together with BAR1 west of Site U1453 and between sites U1550 and U1449, at approx. km 300 (Figs. 5.3 and 5.4). C1 is the only subunit of Subfan C without channel-levee systems incorporated. The unit lasted for ~170 ka from 0.68-0.51 Ma (Tbl. 5.2).

#### **C2 (~0.51-0.457 Ma)**

Seismic Unit C2 (Figs. 5.3 and 5.4) directly overlies Unit C1. It is vertically limited by BAR1 and the MPHL at the bottom and BAR2 at the top. The Unit stretches further east than C1 and terminates against the MPHL west of Site U1455 at km 110 and near Site U1449, approximately at km 334. It encloses the three CLSs No. 2, 3, and 4 and several small, unleveed channels (Figs. 5.3 and 5.4). The unit lasted for ~53 ka from 0.51-0.457 Ma (Tbl. 5.2).

#### **C3 (~0.46-0.33 Ma)**

Unit C3, overlying Unit C2, (Figs. 5.3 and 5.4) is confined by BAR2 and the MPHL (bottom) and BAR3 (top). The unit extends beyond C2 and terminates by overlapping onto the MPHL west of Site U1455, between km 105-110 and west of Site U1451, at km ~380 (Figs. 5.3 and 5.4).

C3 comprises 12 CLSs (No. 5-17) as well as several small, unleveed channels. The unit lasted for ~127 ka from 0.457-0.33 Ma. (*Tbl. 5.2*)

#### **C4 (~0.33-0.25 Ma)**

Unit C4 (*Fig. 5.4*) is the uppermost subunit of Subfan C and bounded by BAR3 and the MPHIL at the bottom and the LPHL at the top. In the west, C4 terminates against the MPHIL between sites U1454 and U1455 (near km 100; *Fig. 5.3*). The eastern termination is not imaged by Profile GeoB97-020+27. Nonetheless, the unit thins out significantly at the eastern end of the profile and is suspected to terminate against the Ninetyeast Ridge just east our study area. Unit C4 encloses numerous small channel without levees and 12 CLSs (No. 18-29). The unit lasted for ~80 ka from 0.33-0.25 Ma (*Tbl. 5.2*).

*Table 5.1: Summary of BAR correlation with calcareous clay layers (CCL) at IODP Expedition 354 drill sites (France-Lanord et al., 2016) and mean BAR-layer ages and the 97.5% confidence interval for all sites where the layer ages have been reliably modeled (ages after Reilly et al. (in prep.)). Note that age estimates for Site U1450 are excluded due to their large uncertainties.*

Layer	Site	Correlation to CCL in cores?	Age [ka]			Mean age [ka]
			2.5%	50%	97.5%	
BAR3	U1455	No correlation; sediment disturbed by lobe	-	-	-	330
	U1453	Drilling gap	286	327	365	
	U1452	Core 12F-1 (~0.47 m thick)	325	337	351	
	U1450	Core 14F3/4 (~0.6 m + ~0.4 m thick)	-	-	-	
	U1449	Core 7H-3 (~0.5 m thick)	291	325	355	
BAR2	U1455	Core 13F-1 (~0.48 m thick)	-	-	-	457
	U1453	Core 20F-1 (~0.02m thick)	444	453	464	
	U1452	Core 26F-2 (~0.88 m thick)	447	482	503	
	U1450	Drilling gap	-	-	-	
	U1449	No correlation; sediment disturbed by CLSs/lobe	413	436	541	
BAR1	U1453	Top MPHIL (Core 29H)	503	515	527	510
	U1452	Core 30F-1 (~0.4 m thick)	495	505	517	
	U1450	Drilling Gap	-	-	-	



### 5.3.2 Accumulation rates

Analysis of thickness and turbiditic accumulation rates of subunits C1-C4 along Profile GeoB97-020+27 show that unit thickness, accumulation rate and lateral spreading increase constantly from C1 to C4 (*Fig. 5.6, Tbl. 5.2*). C1 is the thinnest unit with the lowest accumulation rate (mean accumulation rate: 8 cm/ka, maximum accumulation rate: 15 cm/ka) restricted to the central basin between the 85°E Ridge and Ninetyeast Ridge. C2 has a mean accumulation rate of 35 cm/ka peaking with 86 cm/ka near km 180 (*Fig. 5.6*) due to the incorporated CLS No. 4 (*Figs. 5.4 and 5.6*). Likewise, C3 has a mean accumulation rate of 35 cm/ka and reaches a maximum accumulation rate of 63 cm/ka. Overall the highest maximum accumulation rates (102 cm/ka) and mean accumulation rates (54 cm/ka) rate, as well as maximum lateral spreading, is reached in C4.

All three BAR layers have been recovered at Site U1452. For this site, the age-depth model of *Reilly et al. (in prep.)* outputs a median hemipelagic accumulation rate of 6 cm/ka. Considering the thickness of each layer at Site U1452, their durations are estimated to 6 ka (BAR1), 15 ka (BAR2), and 8 ka (BAR3), respectively. The accumulation rates described in this chapter do not consider the deposition of BAR1-3 because these layers are too thin to be resolved with our MCS data. However, the duration of BAR1-3 is with 6-15 ka short compared to the overall duration of C1, C3, and C4. Thus, the impact of subtracting BAR deposition time from unit duration is minor and would only result in an increase in mean accumulation rate of less than 2.5 cm/ka. An exception is C2, which is more prone to uncertainties due to its shorter duration. When subtracting the maximum BAR-layer duration (15 ka) from the duration of C2, the mean accumulation rate of C2 would increase from 35 cm/ka to 49 cm/ka.

Mass accumulation rates for the four units C1-C4 (*Tbl. 5.2*), calculated for a volume extrapolated for 1 km along-fan are: C1: 0.015 Mt/ka; C2: 0.12 Mt/ka; C3: 0.15 Mt/ka; C4: 0.26 Mt/ka.

*Table 5.2: Summary of the four subunits of Subfan C including their bounding reflectors, ages, duration, mean accumulation rates, and mass accumulation rates (MAR). \*MARs are calculated for a volume extrapolated 1 km along-fan.*

Unit	Top		Bottom		Duration [ka]	Sed. Rate [cm/ka] Mean/Median/Max	Mass Accumulation [Mt/ka]*
	Reflector	Age [ka]	Reflector	Age [ka]			
C4	LPHL Base	250	BAR3	330	80	54/57/102	0.26
C3	BAR3	330	BAR2	457	127	35/40/63	0.15
C2	BAR2	457	BAR1	510	53	35/32/86	0.12
C1	BAR1	510	MPHL Top	680	170	8/8/15	0.015

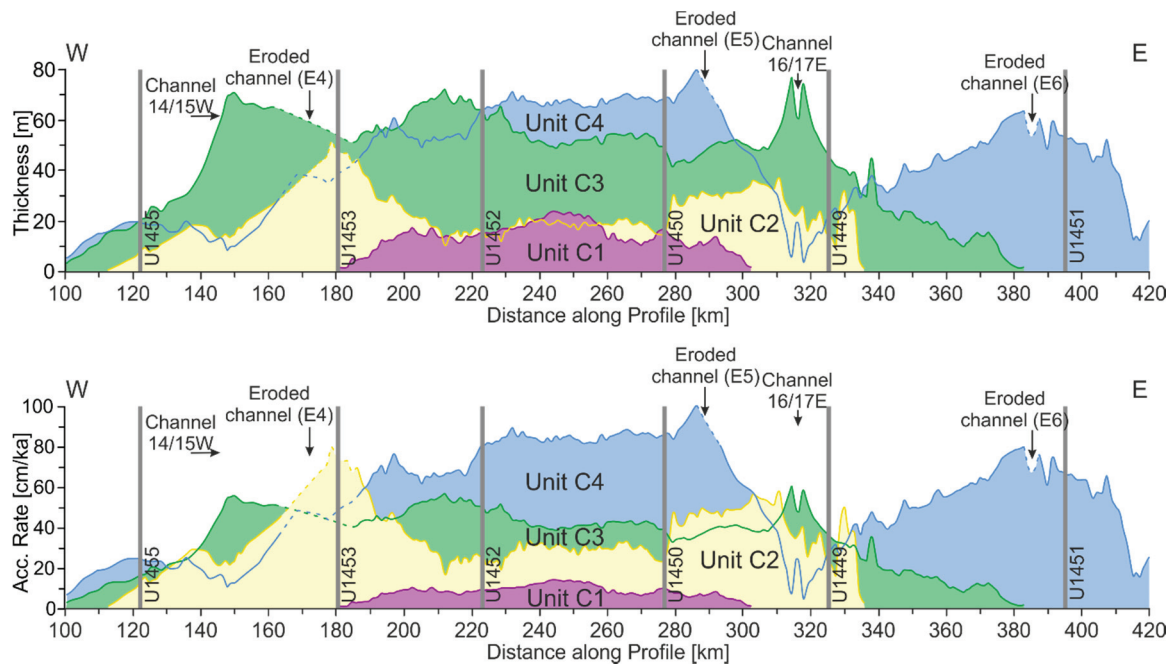


Figure 5.6: Top: Thicknesses of the four subunits C1-C4 along MCS Profile GeoB97-020+27. Bottom: Accumulation rates of the four subunits C1-C4 along MCS Profile GeoB97-020+27. Where lines are stippled seafloor has been eroded by channel-levee systems and BAR layers have been linearly interpolated.

### 5.3.3 Migration and recurrence of channel-levee systems

The age-depth model of *Reilly et al. (in prep)* used the relative succession of channel-levee systems (*Chapter 4*) as relative age constraints. The final model outputs absolute ages plus error range for the levee bases of all channel-levee systems drilled at the IODP Expedition 354 sites (*Figs. 5.3 and 5.7*).

Just after the reappearance of fan sedimentation along Profile GeoB97-020+27 (onset Subfan C, 0.68 ka) the recurrence rate of CLSs is low. The oldest four CLS are separated by ~50 ka without CL-formation. Channel recurrence rate increases after ~0.45 Ma (within Unit C3) and peaks between ~0.4-0.25 Ma (Unit C3 and C4) with a recurrence rate of 3-2 ka (average recurrence rate ~7 ka; 22 CLSs, No. 7-29, formed between 0.4-0.25 Ma). The CLSs developing after ~0.25-0.23 Ma recur less frequent. However, this time span is not representative as it is part of Subfan D which is not fully covered by our data.

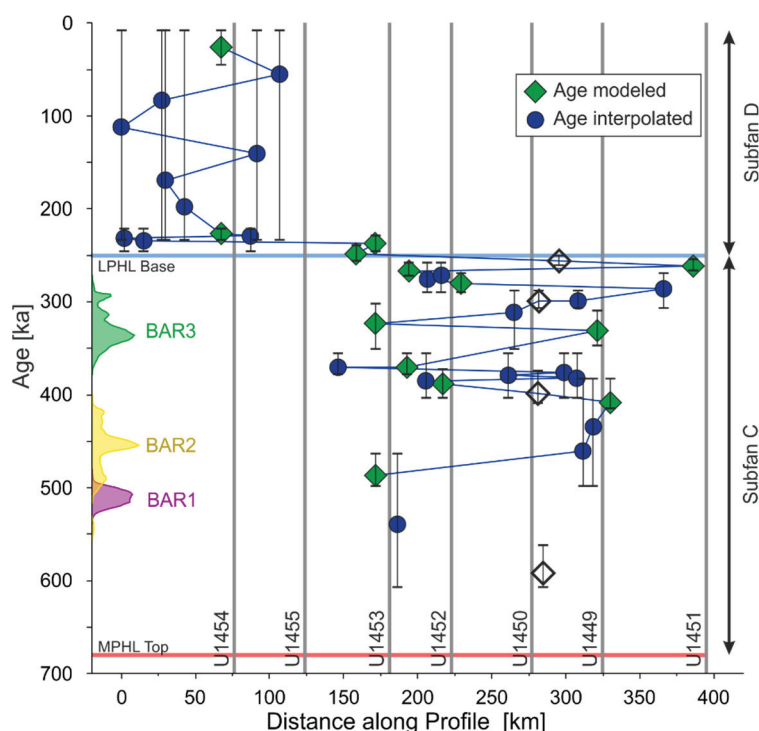


Figure 5.7: Absolute channel-levee ages vs. their lateral migration along MCS Profile GeoB97-020+27 (see Fig. 3). Green diamonds: Ages modeled, after Reilly et al. (in prep.). Error bars represent the 97.5% confidence interval. Blue circles: Interpolated ages. Unfilled symbols: Ages modeled at Site U1450 where age uncertainties are larger. Age distributions of BAR1-3 (see Fig. 5) are plotted for orientation. LPHL: Late Pleistocene Hemipelagic Layer. MPHL: Middle Pleistocene Hemipelagic Layer.

## 5.4 Discussion

### 5.4.1 Sea-level independent deposition of hemipelagic sediments at 8°N?

The three BAR layers are 3 additional stratigraphic markers significantly improving the chronostratigraphy of the drilling transect and the seismic data on a ~100 ka time scale. In the context of the seismic stratigraphy (Fig. 5.3), the age model provided by Reilly et al. (in prep), (Fig. 5.5) and the approximate age of the top of the MPHL after Weber and Reilly, 2018, the ages of the three BARS layers can be discussed as follows:

BAR1 is with a mean age of  $\sim 510 \pm 15$  ka the oldest of the three layers. The layer onlaps the MPHL near U1453 and U1449 where the MPHL lasted at least until MIS 15/16. This fits well with the age probability distribution of BAR1 (Fig. 5.5) peaking midway of MIS 13. A similar agreement between the three datasets exists for BAR2 and 1. The intermediate layer BAR2 onlaps the MPHL east of Site U1449 where the top of the MPHL has been dated to approximately MIS 15. This is consistent with the outcome of the age probability distribution peaking in the early MIS 12. BAR3 is best constrained. It onlaps the MPHL near Site U1451 where the top of the MPHL seems to be as young as MIS 9. The age probability distribution of BAR3

peaks at the transition of MIS 10 to 9, which is confirmed by its physical properties placing the layer at a glacial-interglacial transition (*Reilly et al. (in prep.)*).

One important question is what might have triggered the temporal absence of fan sedimentation and instead resulting in hemipelagic deposition at the lower Bengal Fan.

Relative sea-level variations are considered as one of the most common factors controlling sediment transfer to submarine fans: Fans receive most sediment during lowstands when river and fan are directly connected and are starved during highstands when the sediment is sequestered on the shelf (e.g. *Bouma, 2001; Mulder, 2011 and references therein, Einsele, 2013*). A prominent example of such a sea-level controlled fan is the Amazon Fan (e.g. *Maslin et al., 2006*).

If we consider the potential age range (including error range) for the three BAR layers in the context of global sea-level variations, they may all three have been deposited during times of sea-level highstands (*Fig. 5.5*). However, the age probability distribution peaks of the three layers imply three different stages within the glacial-interglacial cycle for the deposition of the three layers: BAR1 within an interglacial during times of a relatively higher sea level compared to the subsequent interglacials; BAR2 at times of falling sea level during an interglacial; and BAR3 during a glacial-interglacial transition at times when the sea level just started to rise. This suggests, that the deposition of the observed hemipelagic layers BAR1-3 may have been triggered independently from relative sea-level variations, which in turn means that the Bengal Fan behaves contradictory to general fan models. That such a sea-level independent behavior throughout the Middle Pleistocene is a reasonable scenario is corroborated since the Bengal Fan also remained active throughout the Holocene highstand period via sediment bypassing from the river mouth to the shelf-canyon SoNG and from there to the fan (*Weber et al., 1997, Michels et al., 2003; Hein et al., 2017*).

If not sea level drives the deposition of the hemipelagic BAR layers, their deposition must be triggered either by (1) a decrease in overall sediment input, potentially linked to a decrease in Himalayan denudation rates; (2) a complete fan shut-off; or (3) fan internal processes such as a northwards termination of the fan, the temporal (sub-) fan migration away from our study area, or the very local confinement of fan activity along a distinct CLS.

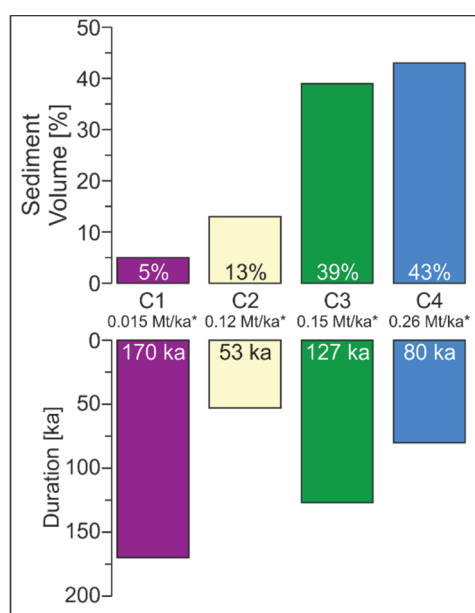
The Asian monsoon is one of the first order controls on Himalayan erosion rates (*Galy and France-Lanord, 2001*). Its intensity is controlled by different factors such as tectonics, orbital forcing or ocean circulations acting on orbital, millennial, and decadal to seasonal time-scales (*Zhisheng et al., 2015; Mohtadi et al., 2016*). The observed times of hemipelagic deposition on the lower Bengal Fan may correlate to times of a weakened Asian monsoon lasting for several thousands of years. However, this would require the very unlikely situation of the irregular, non-periodic recurrence of times with a weakened monsoon, which, at the same time, would have to have a stronger impact than orbitally forced monsoon variability.

A complete shut-off of the fan, if not caused by a decrease in erosion rates, may be linked to a delta reorganization as observed throughout Holocene times (e.g. *Goodbred and Kuehl, 2000b; Goodbred et al., 2014*). But again, we would expect delta reorganizations to be coupled with times of sea-level highstands. Accordingly, autocyclic controls seem to be the likeliest explanation for the deposition of BAR1-3. Even so, we can exclude confined sedimentation within a specific CLS to result in the deposition of the BARs. Otherwise, we would expect widespread hemipelagic deposition associated with all CLSs, or at least certain CLSs being remarkably different in their size/duration and geometry. But neither the seismic data nor the IODP Expedition 354 drilling supports this interpretation (*Figs. 5.2 and 5.3*). However, upfan avulsions and the lateral migration of active fan deposition are common processes on the Bengal Fan (*Curry et al., 2003; Schwenk and Spieß, 2009; Chapter 4*).

Unfortunately, our database does not allow to assess whether the BAR layers are a phenomenon restricted to certain parts of the fan or mark fan wide events. Nonetheless, the data imply, sea level variations cannot exclusively explain the regional hemipelagic deposition on the lower Bengal Fan. This sea-level independent deposition pattern further implies a long-term stable connection between river and fan existing at least since the Middle Pleistocene. This connection preserves a constant sediment supply to the fan. A similar behavior is observed on the Zaire/Congo Fan fed by a canyon extending across the continental shelf sustaining fan sedimentation through-out the Holocene until the present day (e.g. *Babonneau et al., 2002*).

#### 5.4.2 Monsoon-related increase in Pleistocene sediment flux?

The overall accumulation rates determined for Subfan C (8-101 cm/ka; *Tbl. 5.2*) are in the same range as the median accumulation rates (42-160 cm/ka) estimated at the IODP Expedition 354 drills sites by age-depth modeling (*Reilly et al. (in prep.)*). Moreover, the separation of Subfan C into the four subunits C1-C4 (*Fig. 5.4*) and the estimation of accumulation rates along



the drilling transect clearly reveals a strong increase in accumulation rates at 8°N from the oldest (C1, mean sed. Rate 8 cm/ka) to the youngest unit (C4, mean sed. Rate 54 cm/ka), accompanied by an increase in lateral extension (*Fig. 5.6*). We interpret C1, which lasted from ~0.68-0.51, to represent the mixed turbiditic-hemipelagic Unit 3 (0.68-0.48 Ma) defined by *Weber and Reilly, 2018*. Accumulation rates of C1 are with 8 cm/ka four times higher than accumulation

*Figure 5.8: Bar plot illustrating the volume percentage of the four subunits C1-C4 (top) together with their absolute duration (bottom). \*Mass accumulation rates calculated for a volume extrapolated for 1 km along-fan.*



rates of the underlying MPHL (2-2.5 cm/ka, *Weber and Reilly, 2018*) but in the same range of BAR deposition rates (~6 cm/ka) and rather low compared to the averaged accumulation rate of Subfan C (35 cm/ka, *Chapter 4*). We interpret the other three units C2-C4 (0.51-0.25 Ma) to represent the turbiditic dominated Unit 4 defined by *Weber and Reilly, 2018*.

Plotting the sediment volume together with the total duration of each unit underlines the drastic increase of sediment input over time (*Fig. 5.8*). About 43% of Subfan C's volume is supplied by C4, the unit with the second shortest duration, while C1, the longest lasting unit, supplies only 5% of the sediments to Subfan C (*Fig. 5.8*). An exception is the second oldest Unit C2 which lasted significantly shorter compared to the other units. This may be connected to the relatively large error range of BAR2, the reflector bounding the top of C2 (*Tbl. 5.1*).

The same picture is drawn when comparing the mass accumulation rates of the four units, estimated for a volume extrapolated to 1 km<sup>3</sup> in along-fan direction (*Tbl. 5.2*). The mass accumulation rate of C4 is more than 17 times higher than the mass accumulation rate of C1. Moreover, increase in mass accumulation, like the recurring deposition of hemipelagic layers, seems to act independently of relative sea level variations.

One might think that the increasing sediment accumulation is linked to the prograding nature of the fan as shown by *Curry et al., (2003)* for the times of fan initiation. If we apply this simplified model to our data, a similar scenario may explain the observed increase in deposition at 8°N since ~0.68 Ma. In the early stage of Subfan C (C1) sediments may have filled up accommodation space created prior to the onset of Subfan C, while fan deposition has been constrained to other parts of the Bengal Fan. Then, only some of the turbidity currents would have reached 8°N explaining the low accumulation rates observed for C1. Thus, the low accumulation rates of C1 may be autocyclic controlled by the geometry of the fan. However, if we would consider a constant sediment supply and fan progradation as the only process influencing the downfan dispersal of sediments, we would expect to observe a constant or even decreasing thickness at 8°N for the other three units C2-C4. Instead, we can clearly image that the amount of sediment, the unit thickness, the lateral extension of each unit and the rate of accumulation increase, hinting towards overall increasing flux to the Bengal Fan. Here the same observation as for the regional deposition of hemipelagic layers applies: A connection of increasing sediment input with sea level variations is not likely because sea level undergoes constant variations during the duration of Subfan C, while the sediment flux, averaged over the time-scale we can resolve, constantly rises. These observations lead us to hypothesize that the increased accumulation rates at 8°N are a source-driven signal, which may be connected to an intensified Himalayan denudation rate. This hypothesis is supported by the recurrence rate of Subfan C CLSs at 8°N (*Fig. 5.7*) increasing simultaneously with the overall increase in accumulation rate: Just after the reappearance of fan sedimentation to our study area, when accumulation rate is low (units C1 and C2), the time between two subsequent CLSs is 15-20

kyrs longer than at times with increased accumulation rate (units C3 and C4) (*Fig. 5.7*). This resemblance hints towards a correlation of overall sediment input and channel avulsion events on the fan. Meander growing and thalweg elevation of channel-levee systems, which finally leads to avulsions, develop with every turbidity current. Thus, the increasing number of avulsions points is linked to an increase in recurrence rate of turbidity currents during the construction of Subfan C.

A source-driven increase in sediment input as observed from our data may be linked to variations in Asian Monsoon intensity or changes in Himalayan Uplift. While the Himalaya and the Tibetan Plateau have undergone three major pulses of uplift at ~40-03 Ma (southern and central Tibetan Plateau), at ~25-20 Ma (northern Tibetan Plateau), and at ~15-10 Ma (northeastern to eastern Tibetan Plateau), no major uplift events occurred in the last 500 ka (*Tada et al., 2016*). Nonetheless, there is, albeit being controversial, evidence for variations in Asian Monsoon strength since the Pleistocene. A study from the South China Sea indicates Late Pliocene to Holocene intensification of the East Asian Monsoon (*Clift et al., 2008*), while at the same time erosion rates in the central Himalaya seem to increase (*Huntington et al., 2006*). Records from the Chinese Loess Plateau suggest a weakened East Asian summer monsoon and a stronger winter monsoon in the period of ~1.25-0.5 Ma, while since 0.5 Ma the amplitude of both, summer and winter monsoon variations, seems to have increased (*Sun et al., 2006*). On the other hand, *Zhisheng et al., (2001)* propose a weakening of Indian and East Asian summer monsoon simultaneously with a strengthening of the East Asian Winter Monsoon since 2.6 Ma.

Our data favor a source-driven control over a sea-level or autocyclic trigger for the increase in accumulation. Despite this preference, we are aware that our observations from the lower Bengal Fan reflect only a small part of the very large Fan system. Additional data from up- and downfan is needed to support this hypothesis to eventually contribute to the understanding of the Pleistocene climate variations.

## 5.5 Conclusion

The new interpretation of multichannel-seismic data from the lower Bengal Fan in integration with IODP Expedition 354 drilling results and the novel age-depth model of *Reilly et al. (in prep)* allow to significantly improve the chronostratigraphy along the IODP Expedition 354 drilling transect on a scale of ~100 ka for the time since the Middle Pleistocene, and provide new insights into the Middle Pleistocene sedimentation history. In the time from 0.68-0.25 fan sedimentation is restricted within Subfan C, located in the eastern Bengal Basin. Subfan C is bounded by the Middle Pleistocene Hemipelagic Layer (MPHL, 1.24-0.68 Ma; *Weber and Reilly, 2018*) at the bottom and the Late Pleistocene Hemipelagic Layer (LPHL, 0.25-recent; *Weber et al., 2018*) at the top. Three regional extending hemipelagic layers (BAR1-3) separate Subfan C into four individual units, namely C1-C4. The age probability distribution of the three

Bar layers, determined by *Reilly et al. (in prep)* reveals that their deposition most likely occurs independently from sea level variations, indicating that the Bengal Fan behaves contradictory to the general understanding of submarine fans being starved during times of sea-level high-stands. The depositional pattern of Subfan C further implies a long-term stable sediment supply to the fan at least since the Middle Pleistocene. In our study area, accumulation rates of Subfan C increase in the time from ~0.68-0.25 Ma from approximately 8 cm/ka to 57 cm/ka. The increase in accumulation is accompanied by increased unit thicknesses and lateral extension and corroborated by a simultaneous increase in channel recurrence rates. We hypothesize that the increase in sediment accumulation is not fan-internal or sea-level controlled but a source-driven signal. It may be the expression of changes in monsoon intensity during the Middle Pleistocene. However, further support by additional data from down- and upfan is needed to transfer our local observations to the entire Bengal Fan.

## 5.6 Acknowledgments

This study was funded by the German Research Foundation (DFG) within the IODP Priority program (Grant No. SCHW1551/7-1/2). Funding for the collection of seismic data during expedition SO125 was provided by BMBF Grant no, 03 G 0125A. We would also like to thank captain, crew and scientific party of RV Sonne cruise SO125 and IODP Expedition 354.



## Chapter 6

### 6 Conclusion and future perspectives

Within this thesis, hydroacoustic data, including echosounder and multichannel seismic datasets, were integrated with drilling results from the IODP Expedition 354 to investigate the architecture and evolution of the lower Bengal Fan at different scales. The Bengal Fan is the main sink for Himalayan sediments and, thus, represents the primary recorder of the Himalayan erosion as well as Asian Monsoon history. The current thesis examined the spatial and temporal variability of sediment delivery and depositional processes since the Middle Pleistocene at the lower Bengal Fan (8°N) in order to enhance our overall understanding of the fan evolution as well as to advance our knowledge on the link between source and sink. The three studies presented within this thesis focused on (i) the impact of an actively meandering channel on levee formation as well as the Late Quaternary to Holocene activity of the Bengal Fan (*Chapter 3*); (ii) the temporal and spatial dynamics of depocenter migration (*Chapter 4*); (iii) the interplay of different depositional processes (channelized and unchannelized turbidity currents vs. hemipelagic deposition) (*Chapter 4 and 5*); as well as (iv) accumulation-rate variability and their potential link to climate changes in the source area (*Chapter 5*). The outcomes highlight the importance of a comprehensive approach to be able to understand the Bengal Fan's complex depositional dynamics and to ultimately connect changes in the sedimentary sink with changes in the sedimentary source.

The main conclusions of our research, in regard to the main research questions outlined in Chapter 1.1, are synthesized in the following,

What is the variability of levee deposition in an actively meandering channel and how does it affect the interpretation of levee sediment cores?

The case study of the Active Channel (*Chapter 3*) provided an excellent opportunity to examine short-term variations in levee construction along an actively meandering channel. The combination of high-resolution Parasound data across this channel-levee system and sediment cores from the western levee enabled a sub-levee scale resolution and the investigation of the spatial variability throughout three individual time slices/levee units.

Highest levee-accumulation rates could clearly be linked to outer channels bends. This is in good agreement with physical and numerical models of channel-levee systems (e.g. *Kane et al., 2010; Huang et al., 2012*) and provides a strong tool to reconstruct former channel pathways. Spatial thickness maps revealed a threefold variation in levee height for one particular time slice across the channel. The movement of channel bends through time results in the up- and downfan shift of the main depocenter and, consequently, in a patchy depositional pattern. This highlights that sedimentation rates at any point on a levee are highly variable through



time. Nonetheless, the short-term depositional variations are equalized over time as a response to the dynamic channel geometry and topographically controlled accommodation space. Hence, sedimentation rates from a levee (here Site U1454) cannot directly be transferred to sediment fluxes. Instead, sediment fluxes and budgets should be averaged over a sufficiently long time-average in order to minimize statistical errors generated by channel-induced short-term fluctuations.

When was the *Active Channel* initiated and are there any indicators for intermittent channel-levee evolution?

The evolution of the *Active Channel* (*Chapter 3*) has been investigated based on the correlation of acoustic units, derived from a detailed analysis of Parasound data, and IODP core lithology. We developed an age model for the *Active Channel* at 8°N based on radiocarbon ages under consideration of depositional processes (turbiditic vs. hemipelagic). Overspilling sediments have an average deposition rate of 8.7m/ka. Mass accumulation rates of the individual levee units remain relatively constant indicating a steady sediment flux, at least during times of active overspilling.

Our study indicates that the *Active Channel* at 8°N has been initiated around 27 ka ago. This is considerably earlier than suggested by previous studies conducted at 16.5°N (*Weber et al., 1997; Hein et al., 2017*). Overspill sedimentation on the levees of the *Active Channel* has been interrupted during the LGM and the deglacial sea-level rise (25.5-11.5 ka, Unit HU1). During this time, a thin hemipelagic layer has been deposited, covering the levee. A second interruption of overspill started ~9.6 ka ago and, once again, led to the formation of a hemipelagic drape. Both phases of hemipelagic deposition were interpreted as being linked to a reduced turbidity-current height while the channel itself remained active. The decrease in turbidity current height is potentially caused by decreased sediment input, which, however, does not appear to be systematically linked to sea-level highstands.

What are the temporal and spatial dynamics of sediment pathway migrations across the Bengal Fan on local (channel) and regional (subfan) scales?

The evolution of the Bengal Fan since the Middle Pleistocene (*Chapter 4*) has been strongly controlled by significant changes in depocenter locations at different time- and spatial scales. On millennial time scales, deposition is constrained to channel-levee systems. The channel-levee systems on the lower Bengal Fan appear to be dominantly erosive and usually, the channel relief exceeds the levee height. Frequent channel avulsions result in an average channel-levee system lifetime of ~15 ka. The variable size of channel-levee systems indicates that channel avulsion must be dominantly autocyclic controlled. The lateral distance between two subsequent systems often exceeds 100 km and their relative succession emphasizes the dynamic character of the Bengal Fan deposition.

On longer time-scales, channel-levee systems are organized in subfans. Subfans focus terrestrial sedimentation to parts of the Bengal Fan, while in the remaining area hemipelagic deposition dominates. We merged our findings and earlier published data (*Curry et al., 2003; Schwenk and Spieß, 2009*) and developed a comprehensive model for the spatial and temporal evolution of the subfans maps expanding south to 8°N (*Fig. 4.8*). The Middle Pleistocene to Holocene sediment section can be differentiated into the three subfans B (1.24-0.68 Ma), C (0.68-0.25 Ma), and D (0.25 Ma-recent). The subfan location seems to be strongly controlled by accommodation space created by the uplift of the 85°E ridge and the Ninetyeast Ridge as well as the position of the sediment-supplying canyon but does not appear to be linked to glacial-interglacial cycles. Like the channel-levee systems, subfans migrate across the Bengal Fan and alternately occupy the western and the eastern fan. While Subfan C reaches our study area in its full extent, no terrestrial sediments of Subfan B and only the westernmost extension of Subfan D are imaged by our data. Instead, the Middle and Late Pleistocene Hemipelagic Layer, the hemipelagic equivalents to subfan B and D, respectively, were deposited in the working area. Hence, we concluded that the subfans B and D were located further westward. We provided a relative stratigraphy based on the thorough tracing of all channel-levee base reflectors and time markers. Moreover, the seismic stratigraphy has been implemented into a core-seismic integrated age model specially designed for the IODP Expedition 354 drilling transect (*Appendix 1; Reilly et al. (in prep.)*).

By revealing a striking spatial and temporal depocenter variability, the chapters' outcomes highlighted the importance of accounting for sediment dynamics when working with the Bengal Fan in particular but also other fan systems in general as sedimentary archives.

#### Which lithology is dominating the lower Bengal Fan?

Although the Bengal Fan is classified as a mud-rich fan, we could show that over 60% of the sediments at 8°N are composed of sandy material deposited out of unchannelized turbidity currents. A similarly high sand content has been recovered at IODP Expedition 353 Site U1444 close to 15°N. These observations highlight the dominance of unchannelized sedimentation for fan construction and imply a hitherto underestimation of the sand content in large submarine fans.

#### What controls widespread hemipelagic deposition on the lower Bengal Fan?

The lower Bengal Fan is constructed of terrestrial material intercalated with hemipelagic layers with meter to decimeter-scale thicknesses. The two prominent hemipelagic layers from Middle and Late Pleistocene times (MPHL, 1.24-0.68 Ma; LPHL, 0.25 Ma -recent) are considered as hemipelagic subfan equivalents (MPHL – Subfan B; LPHL – Subfan D). The deposition of both layers is autocyclic controlled and represent times of subfan migration away from our study area. Furthermore, a set of three decimeter-scale hemipelagic layers, namely BAR1-3, were

identified throughout large parts of Subfan C. Their deposition does not appear to be systematically linked to sea-level variations but may be driven autocyclic. The same observation applies to the hemipelagic layers within the levees of the Active Channel. Overall, this strongly suggests that the Bengal Fan behaves contradictory to other large submarine fans, which are starved during times of sea-level highstand. Moreover, it indicates constant sediment delivery to the lower Bengal Fan since the Middle Pleistocene.

How variable are sediment accumulation rates on the lower Bengal Fan (8°N) since the Middle Pleistocene? And what can be said about their controlling factors?

The linkage of the seismic stratigraphy with the novel age-depth model developed by *Reilly et al. (in prep)* allowed for an important advancement in the transect's chronostratigraphy and enabled us to refine it to a ~100 ka time scale. The three hemipelagic layers BAR1-3 separate Subfan C into four individual subunits (C1-C4). By applying the age model to the seismic data, a constant increase of sediment accumulation rates, unit thickness and lateral extension from the oldest (C1; mean acc. Rate 8 cm/ka) to the youngest (C4; mean acc. Rate 57 cm/ka) subunit was revealed. The increase in accumulation rate is accompanied by an increasing channel recurrence rates and seems to remain steady throughout several glacial-interglacial cycles. Such changes in accumulation rate may reflect a source-driven signal such as a variable monsoon intensity. To corroborate this hypothesis, additional data from up- and downfan is required to transfer these local observations to the source-to-sink system in general.

The findings presented in this thesis are a very important step towards a profound understanding of the source-to-sink system Himalayan Mountains – Bengal Fan. The established seismic stratigraphy was essential for the refinement of the chronostratigraphy and will continue to play an important role in the coherent interpretation of the findings from the IODP 354 sites.

This thesis gave rise to new questions, which may be addressed by future research.

The sedimentary section at 8°N dates back to the Early to Middle Miocene and the seismic data clearly show the unconformity at the base of the fan associated with the times of fan initiation. Extending the stratigraphic concept into greater depth will permit to investigate crucial aspects of the erosional history of the Himalaya and the relationship between erosion and climate fluctuations including (a) the exact onset of Himalayan erosion; (b) the divers discussed change in Himalayan weathering, climate, and lithology 7-8 Ma ago; (c) the impact of the onset of Northern Hemisphere Glaciation on erosion and sedimentation; and (d) the nature and trigger mechanism of the transition from only sheeted turbidites to the onset of channel-levee system formation in the Late Miocene.

In order to extend the stratigraphy into greater depth, it will be crucial to investigate the tectonic setting at 8°N. The available seismic data show that especially deeper-lying structures and sediments above the 85°E and Ninetyeast Ridge are disturbed by faults displacing individual layers by tenths of meters. Moreover, several faults appear to extend (almost) up to the sea-floor indicating recent activity. Moreover, a detailed study of these faults may shed light on the tectonic evolution of the 85°E and Ninetyeast Ridge.

Expanding the scientific investigations and the chronostratigraphy up- and downfan will allow testing, if the at 8°N observed fan characteristics and depositional events are fan-wide phenomena or locally restricted. Gaining a (more) complete picture of turbiditic sedimentation rates and hemipelagic dominated times/areas as well as their along-fan variability could be used to determine sediment budgets for different time slices, thereby enhance the general understanding of the source-to-sink link and the climate/tectonic interactions in the source area. During the research Expedition SO125, SO126 and SO188 extensive multichannel seismic surveys were acquired from the Bengal Shelf south to 8°N. Tentative tracing of the striking Middle Pleistocene Hemipelagic Layer proved its existence also at 11°N. In a similar manner, all distinctive reflections and age makers can be expanded to other fan areas. Extending the already available seismic dataset for this purpose by additional lines would be beneficial, especially in regards to the abundant channel-levee systems interrupting the strata.

Moreover, our results strongly suggest that the dynamics of the Bengal Fan do not follow the general understanding of large submarine fans. The fan seems to constantly receive sediments independently of glacial-interglacial cycles. Furthermore, sand deposition dominates the construction of the lower Bengal Fan, indicating that sand content in large submarine fans has hitherto been underestimated. Extending the observation up-and downfan as well as in greater depth will allow to test our hypothesis and also if these observations apply for the entire Bengal Fans and earlier times. If so, the general understanding of (large) submarine fans may have to be reassessed.

Finally, intensive work in numerous disciplines is currently conducted by the IODP Expedition 354 scientific party on the seven IODP 354 drill sites. Findings in terms of age modeling, biostratigraphy, geochemistry, sedimentology, and provenance studies, amongst others, are constantly updated and extended, opening up a wide range for interdisciplinary and integrated research.





## Acknowledgements

Firstly, I would like to thank my supervisor Volkhard Spieß for providing the great opportunity to conduct my Ph.D. within his working group and for his support throughout my Ph.D. project. Thank you for the great chance to become part of the Bengal Fan IODP community and to participate in exceptional research cruises and field trips. Moreover, I would like to express my sincere gratitude to Tilmann Schwenk for constant support and encouragement, his always open door, and for the sometimes vital, friendly reminder of my own strength. I could not have imagined having a better advisor for my Ph.D. time.

I would also like to thank Christian Hübscher for agreeing to be my second reviewer.

Besides my two supervisors, I would like to thank the rest of my thesis committee, Christian France-Lanord and Hendrik Lantzsch, for their insightful comments, encouragement, and support, and the fruitful discussions, not only during my thesis committee meetings. My sincere thanks also go to Brendan Reilly and Peter Selkin, who hosted me during my research stay at Oregon State University and the University of Washington, Tacoma. Thanks for the great and hopefully long-lasting cooperation.

This study was funded by the German Research Foundation (DFG) within the IODP Priority program (Grant No. SCHW1551/7-1/2). I would also like to express my gratitude to GLOMAR for providing funding support, thereby enabling my research stay and my attendance at the IMS 2017, as well as the IAS for their travel support to attend the ISC 2018.

A heartfelt thank you to my colleagues and friends and the Marine Technology/Environmental Research working group Noemi Fekete, Julia Haberkern, Hanno Keil, Florian Meier, Aisgo Oguro, Asli Özmaral, Carlos Ramos, Anna Reusch, Nora Schulze, Lena Steinmann, and Stefan Wenau for your technical and scientific support, your patience and advice, and, very importantly, for your friendship and all the fun we had in the last years during coffee breaks, 'seismic events', and in numerous other occasions.

Lena and Frida, thanks for all the walks taking my mind off work thoughts. Jette and Jule, thank you for your valuable suggestions given by running uncontrolled over my keyboard. Nora, our office wouldn't be our office, without you.

And of course, I owe my family and friends a great debt of gratitude. You are great, guys. I couldn't imagine my life without you.

Hessel, uit de grond van mijn hart, bedankt voor al je steun de afgelopen Jaren en het feit dat ik altijd op je kan vertrouwen.



---

## References

- Adhikari, S.K., Sakai, T., Yoshida, K., in press. Data report: Grain size analysis of Bengal Fan sediments at sites U1450 and U1451, IODP Expedition 354.
- Aitchison, J.C., Ali, J.R., Davis, A.M., 2007. When and where did India and Asia collide? *Journal of Geophysical Research: Solid Earth* (1978–2012) 112. <https://doi.org/10.1029/2006JB004706>
- Alam, M., Alam, M.M., Curray, J.R., Chowdhury, M.L.R., Gani, M.R., 2003. An overview of the sedimentary geology of the Bengal Basin in relation to the regional tectonic framework and basin-fill history. *Sedimentary Geology* 155, 179-208. [https://doi.org/10.1016/S0037-0738\(02\)00180-X](https://doi.org/10.1016/S0037-0738(02)00180-X)
- Amos, K.J., Peakall, J., Bradbury, P.W., Roberts, M., Keevil, G., Gupta, S., 2010. The influence of bend amplitude and planform morphology on flow and sedimentation in submarine channels. *Marine and Petroleum Geology* 27, 1431-1447. <https://doi.org/10.1016/j.marpetgeo.2010.05.004>
- Babonneau, N., Savoye, B., Cremer, M., Klein, B., 2002. Morphology and architecture of the present canyon and channel system of the Zaire deep-sea fan. *Marine and Petroleum Geology* 19, 445-467. [https://doi.org/10.1016/S0264-8172\(02\)00009-0](https://doi.org/10.1016/S0264-8172(02)00009-0)
- Babonneau, N., Savoye, B., Cremer, M., Bez, M., 2010. Sedimentary architecture in meanders of a submarine channel: detailed study of the present Congo turbidite channel (Zaiango project). *Journal of Sedimentary Research* 80, 852-866. <https://doi.org/10.2110/jsr.2010.078>
- Bangladesh Water Development Board (1972), Sediment investigations in main rivers of Bangladesh, Water Suppl. Pap. 359, Dhaka.
- Barnes, N.E., Normark, W.R., 1985. Diagnostic parameters for comparing modern submarine fans and ancient turbidite systems, *Submarine fans and related turbidite systems*. Springer, pp. 13-14. [https://doi.org/10.1007/978-1-4612-5114-9\\_3](https://doi.org/10.1007/978-1-4612-5114-9_3)
- Bastia, R., Radhakrishna, M., Das, S., Kale, A.S., Catuneanu, O., 2010a. Delineation of the 85°E ridge and its structure in the Mahanadi Offshore Basin, Eastern Continental Margin of India (ECMI), from seismic reflection imaging. *Marine and Petroleum Geology* 27, 1841-1848. <https://doi.org/10.1016/j.marpetgeo.2010.08.003>
- Bastia, R., Das, S., Radhakrishna, M., 2010b. Pre- and post-collisional depositional history in the upper and middle Bengal fan and evaluation of deepwater reservoir potential along the northeast Continental Margin of India. *Marine and Petroleum Geology* 27, 2051-2061. <https://doi.org/10.1016/j.marpetgeo.2010.04.007>
- Blum, M.D., and Hattier-Womack, J., 2009. Climate change, sea-level change, and fluvial sediment supply to deepwater depositional systems. *External Controls on Deep Water Depositional Systems: SEPM, Special Publication 92*, 15-39.
- Blum, M., Rogers, K., Gleason, J., Najman, Y., Cruz, J., Fox, L., 2018. Allogenic and Autogenic Signals in the Stratigraphic Record of the Deep-Sea Bengal Fan. *Scientific Reports* 8, 7973. [10.1038/s41598-018-25819-5](https://doi.org/10.1038/s41598-018-25819-5)
- Bouma, A.H., Coleman, J.M., Stelting, C.E., Kohl, B., 1989. Influence of relative sea level changes on the construction of the Mississippi Fan. *Geo-Marine Letters* 9, 161-170. <https://doi.org/10.1007/BF02431043>
- Bouma, A.H., 2000. Coarse-grained and fine-grained turbidite systems as end member models: applicability and dangers. *Marine and Petroleum Geology* 17, 137-143. [http://dx.doi.org/10.1016/S0264-8172\(99\)00020-3](http://dx.doi.org/10.1016/S0264-8172(99)00020-3)

- Bouma, A., 2001. Fine-grained submarine fans as possible recorders of long-and short-term climatic changes. *Global and Planetary Change* 28, 85-91. [https://doi.org/10.1016/S0921-8181\(00\)00066-7](https://doi.org/10.1016/S0921-8181(00)00066-7)
- Butler, P., 2012. Strong Noise–Removal and Replacement on Seismic Data, Geo-convention 2012: Vision. Canadian Society of Petroleum Geologists.
- Caress, D. W., and D. N. Chayes, MB-System: Mapping the Seafloor, <https://www.mbari.org/products/research-software/mb-system>, 2017
- Channell, J.E.T., Hodell, D.A., and Curtis, J.H., 2016, Relative paleointensity (RPI) and oxygen isotope stratigraphy at IODP Site U1308: North Atlantic RPI stack for 1.2–2.2 Ma (NARPI-2200) and age of the Olduvai Subchron: *Quaternary Science Reviews*, v. 131, p. 1–19, doi: 10.1016/j.quascirev.2015.10.011.
- Chatterjee, S., Goswami, A., Scotese, C.R., 2013. The longest voyage: Tectonic, magmatic, and paleoclimatic evolution of the Indian plate during its northward flight from Gondwana to Asia. *Gondwana Research* 23, 238-267. <http://dx.doi.org/10.1016/j.gr.2012.07.001>
- Choudhuri, M., Nemèok, M., Stuart, C., Welker, C., Sinha, S.T., Bird, D., 2014. 85° E Ridge, India—constraints on its development and architecture. *Journal of the Geological Society of India* 84, 513-530. <https://doi.org/10.1007/s12594-014-0160-9>
- Clemens, S.C., Kuhnt, W., LeVay, L.J., and the Expedition 353 Scientists, 2016. *Proceedings of the International Ocean Discovery Program* Volume 353 publications.iodp.org doi:10.14379/iodp.proc.353.104.2016. DOI 10.1038/353720a0
- Clift, P., Gaedicke, C., Edwards, R., Lee, J.I., Hildebrand, P., Amjad, S., White, R.S., Schlüter, H.-U., 2002. The stratigraphic evolution of the Indus Fan and the history of sedimentation in the Arabian Sea. *Marine geophysical researches* 23, 223-245. <https://doi.org/10.1023/A:1023627123093>
- Clift, P.D., Hodges, K.V., Heslop, D., Hannigan, R., Van Long, H., Calves, G., 2008. Correlation of Himalayan exhumation rates and Asian monsoon intensity. *Nature Geoscience* 1, 875-880. DOI: 10.1038/ngeo351
- Cochran, J.R., 1990. Himalayan uplift, sea level, and the record of Bengal Fan sedimentation at the ODP Leg 116 sites. In Cochran, J.R., Stow, D.A.V., et al., Proc. ODP, Sci. Results, 116: College Station, TX (Ocean Drilling Program), 397–414. doi:10.2973/odp.proc.sr.116.144.1990
- Curry, J.R., 1994. Sediment volume and mass beneath the Bay of Bengal. *Earth and Planetary Science Letters* 125, 371-383. [http://dx.doi.org/10.1016/0012-821X\(94\)90227-5](http://dx.doi.org/10.1016/0012-821X(94)90227-5)
- Curry, J.R., Emmel, F.J., Moore, D.G., 2003. The Bengal Fan: morphology, geometry, stratigraphy, history and processes. *Marine and Petroleum Geology* 19, 1191-1223. DOI 10.1016/s0264-8172(03)00035-7
- Delft Hydraulics and Danish Hydraulics Institute, 1996. River Survey Project, Flood Action Plan 24, Water Resour. Plann. Org., Dhaka.
- Dennielou, B., Droz, L., Babonneau, N., Jacq, C., Bonnel, C., Picot, M., Le Saout, M., Saout, Y., Bez, M., Savoye, B., 2017. Morphology, structure, composition and build-up processes of the active channel-mouth lobe complex of the Congo deep-sea fan with inputs from remotely operated underwater vehicle (ROV) multibeam and video surveys. *Deep Sea Research Part II: Topical Studies in Oceanography* 142, 25-49. <https://doi.org/10.1016/j.dsr2.2017.03.010>
- Derry, L.A., France-Lanord, C., 1996. Neogene Himalayan weathering history and river<sup>87</sup>Sr/<sup>86</sup>Sr: impact on the marine Sr record. *Earth and Planetary Science Letters* 142, 59-74. [http://dx.doi.org/10.1016/0012-821X\(96\)00091-X](http://dx.doi.org/10.1016/0012-821X(96)00091-X)

- Derry, L., France-Lanord, C., 1997. Himalayan Weathering and Erosion Fluxes: Climate and Tectonic Controls, in: Ruddiman, W. (Ed.), *Tectonic Uplift and Climate Change*. Springer US, pp. 289-312. DOI 10.1007/978-1-4615-5935-1\_12
- Droz, L., Marsset, T., Ondreas, H., Lopez, M., Savoye, B., Spy-Anderson, F.-L., 2003. Architecture of an active mud-rich turbidite system: The Zaire Fan (Congo–Angola margin southeast Atlantic) Results from ZaiAngo 1 and 2 cruises. *AAPG bulletin* 87, 1145-1168. <https://doi.org/10.1306/03070300013>
- Dupont-Nivet, G., Lippert, P.C., Van Hinsbergen, D.J., Meijers, M.J., Kapp, P., 2010. Palaeolatitude and age of the Indo–Asia collision: palaeomagnetic constraints. *Geophysical Journal International* 182, 1189-1198. <https://doi.org/10.1111/j.1365-246X.2010.04697.x>
- Einsele, G., 2013. *Sedimentary basins: evolution, facies, and sediment budget*. Springer Science & Business Media.
- Emmel, F.J., Curray, J.R., 1983. The Bengal Submarine Fan, Northeastern Indian ocean. *Geo-Marine Letters* 3, 119-124. DOI 10.1007/bf02462456
- Ezz, H., Cantelli, A., Imran, J., 2013. Experimental modeling of depositional turbidity currents in a sinuous submarine channel. *Sedimentary Geology* 290, 175-187. <http://dx.doi.org/10.1016/j.sedgeo.2013.03.017>
- Fildani, A., Normark, W.R., 2004. Late Quaternary evolution of channel and lobe complexes of Monterey Fan. *Marine Geology* 206, 199-223. <https://doi.org/10.1016/j.margeo.2004.03.001>
- Flood, R.D., Piper, D.J., 1997. Amazon Fan sedimentation: the relationship to equatorial climate change, continental denudation, and sea-level fluctuations, *Proceedings-Ocean Drilling Program Scientific Results*. National Science Foundation, pp. 653-675.
- Flood, R.D., Piper, D.J.W., Klaus, A., and Peterson, L.C. (Eds.), 1997. *Proc. ODP, Sci. Results, 155: College Station, TX (Ocean Drilling Program)*. doi:10.2973/odp.proc.sr.155.1997
- France-Lanord, C., Derry, L., Michard, A., 1993. Evolution of the Himalaya since Miocene time: isotopic and sedimentological evidence from the Bengal Fan. *Geological Society, London, Special Publications* 74, 603-621. <https://doi.org/10.1144/GSL.SP.1993.074.01.40>
- France-Lanord, C., Derry, L.A., 1994.  $\delta^{13}\text{C}$  of organic carbon in the Bengal Fan: Source evolution and transport of C3 and C4 plant carbon to marine sediments. *Geochimica et Cosmochimica Acta* 58, 4809-4814. [http://dx.doi.org/10.1016/0016-7037\(94\)90210-0](http://dx.doi.org/10.1016/0016-7037(94)90210-0)
- France-Lanord, C., Derry, L.A., 1997. Organic carbon burial forcing of the carbon cycle from Himalayan erosion. *Nature* 390, 65-67.
- France-Lanord C., Spieß, V., Molnar, P. and Curray, J.R., 2001. Neogene and late Paleogene record of Himalayan orogeny and climate: a transect across Middle Bengal Fan, IODP Proposal 552-full3.
- France-Lanord, C., Spiess, V., Schwenk, T., Klaus, A., Scientists, E., 2016. *Proceedings of the International Ocean Discovery Program, 354: College Station, TX (International Ocean Discovery Program)*. <http://dx.doi.org/10.14379/iodp.proc.354.2016>
- Gaedicke, C., Schlüter, H.-U., Roeser, H.A., Prexl, A., Schreckenberger, B., Meyer, H., Reichert, C., Clift, P., Amjad, S., 2002. Origin of the northern Indus Fan and Murray Ridge, Northern Arabian Sea: interpretation from seismic and magnetic imaging. *Tectonophysics* 355, 127-143. [https://doi.org/10.1016/S0040-1951\(02\)00137-3](https://doi.org/10.1016/S0040-1951(02)00137-3)
- Galy, A., France-Lanord, C., 2001. Higher erosion rates in the Himalaya: Geochemical constraints on riverine fluxes. *Geology* 29, 23-26. 10.1130/0091-7613(2001)029<0023:herith>2.0.co;2



- Galy, V., France-Lanord, C., Beyssac, O., Faure, P., Kudrass, H., Palhol, F., 2007. Efficient organic carbon burial in the Bengal fan sustained by the Himalayan erosional system. *Nature* 450, 407-410. [http://www.nature.com/nature/journal/v450/n7168/supinfo/nature06273\\_S1.html](http://www.nature.com/nature/journal/v450/n7168/supinfo/nature06273_S1.html)
- Galy, V., France-Lanord, C., Peucker-Ehrenbrink, B., Huyghe, P., 2010. Sr–Nd–Os evidence for a stable erosion regime in the Himalaya during the past 12 Myr. *Earth and Planetary Science Letters* 290, 474-480. <http://dx.doi.org/10.1016/j.epsl.2010.01.004>
- Garzanti, E., Andò, S., France-Lanord, C., Vezzoli, G., Censi, P., Galy, V., Najman, Y., 2010. Mineralogical and chemical variability of fluvial sediments: 1. Bedload sand (Ganga–Brahmaputra, Bangladesh). *Earth and Planetary Science Letters* 299, 368-381. <https://doi.org/10.1016/j.epsl.2010.09.017>
- Gasparotto, G., Spadafora, E., Summa, V., Tateo, F., 2000. Contribution of grain size and compositional data from the Bengal Fan sediment to the understanding of Toba volcanic event. *Marine Geology* 162, 561-572. [http://dx.doi.org/10.1016/S0025-3227\(99\)00090-0](http://dx.doi.org/10.1016/S0025-3227(99)00090-0)
- Gibbons, A.D., Zahirovic, S., Müller, R.D., Whittaker, J.M., Yatheesh, V., 2015. A tectonic model reconciling evidence for the collisions between India, Eurasia and intra-oceanic arcs of the central-eastern Tethys. *Gondwana Research* 28, 451-492. <http://dx.doi.org/10.1016/j.gr.2015.01.001>
- Goodbred Jr, S.L., Kuehl, S.A., 1998. Floodplain processes in the Bengal Basin and the storage of Ganges–Brahmaputra river sediment: an accretion study using <sup>137</sup>Cs and <sup>210</sup>Pb geochronology. *Sedimentary Geology* 121, 239-258. [https://doi.org/10.1016/S0037-0738\(98\)00082-7](https://doi.org/10.1016/S0037-0738(98)00082-7)
- Goodbred Jr, S.L., Kuehl, S.A., 1999. Holocene and modern sediment budgets for the Ganges–Brahmaputra river system: Evidence for highstand dispersal to flood-plain, shelf, and deep-sea depocenters. *Geology* 27, 559-562. [https://doi.org/10.1130/0091-7613\(1999\)027<0559:HAMSBF>2.3.CO;2](https://doi.org/10.1130/0091-7613(1999)027<0559:HAMSBF>2.3.CO;2)
- Goodbred Jr, S.L., Kuehl, S.A., 2000a. Enormous Ganges–Brahmaputra sediment discharge during strengthened early Holocene monsoon. *Geology* 28, 1083-1086. [https://doi.org/10.1130/0091-7613\(2000\)28<1083:EGSDDS>2.0.CO;2](https://doi.org/10.1130/0091-7613(2000)28<1083:EGSDDS>2.0.CO;2)
- Goodbred, S.L., Kuehl, S.A., 2000b. The significance of large sediment supply, active tectonism, and eustasy on margin sequence development: Late Quaternary stratigraphy and evolution of the Ganges–Brahmaputra delta. *Sedimentary Geology* 133, 227-248. [https://doi.org/10.1016/S0037-0738\(00\)00041-5](https://doi.org/10.1016/S0037-0738(00)00041-5)
- Goodbred Jr, S.L., 2003. Response of the Ganges dispersal system to climate change: a source-to-sink view since the last interstade. *Sedimentary Geology* 162, 83-104. [https://doi.org/10.1016/S0037-0738\(03\)00217-3](https://doi.org/10.1016/S0037-0738(03)00217-3)
- Goodbred Jr, S.L., Paolo, P.M., Ullah, M.S., Pate, R.D., Khan, S.R., Kuehl, S.A., Singh, S.K., Rahaman, W., 2014. Piecing together the Ganges–Brahmaputra–Meghna River delta: Use of sediment provenance to reconstruct the history and interaction of multiple fluvial systems during Holocene delta evolution. *Bulletin* 126, 1495-1510. <https://doi.org/10.1130/B30965.1>
- Gopala Rao, D., Krishna, K., Sar, D., 1997. Crustal evolution and sedimentation history of the Bay of Bengal since the Cretaceous. *JOURNAL OF GEOPHYSICAL RESEARCH-ALL SERIES-* 102, 17,747-717,768. <https://doi.org/10.1029/96JB01339>
- Gradstein, F.M., Ogg, J.G., Schmitz, M., Ogg, G., 2012. *The geologic time scale 2012*. Elsevier
- Grant, J., and Schreiber, R., 1990. Modern swathe sounding and sub-bottom profiling technology for research applications: the Atlas Hydrosweep and Parasound systems, *Marine Geological Surveying and Sampling*, Springer, p. 9-19

- Hansen, L., Callow, R.H.T., Kane, I.A., Gamberi, F., Rovere, M., Cronin, B.T., Kneller, B.C., 2015. Genesis and character of thin-bedded turbidites associated with submarine channels. *Marine and Petroleum Geology* 67, 852-879. <http://dx.doi.org/10.1016/j.marpetgeo.2015.06.007>
- Hein, C.J., Galy, V., Galy, A., France-Lanord, C., Kudrass, H., Schwenk, T., 2017. Post-glacial climate forcing of surface processes in the Ganges–Brahmaputra river basin and implications for carbon sequestration. *Earth and Planetary Science Letters* 478, 89-10. <https://doi.org/10.1016/j.epsl.2017.08.013>
- Hinderer, M., 2012. From gullies to mountain belts: A review of sediment budgets at various scales. *Sedimentary Geology* 280, 21-59. <https://doi.org/10.1016/j.sedgeo.2012.03.009>
- Hu, X., Garzanti, E., Wang, J., Huang, W., An, W., Webb, A., 2016. The timing of India-Asia collision onset—Facts, theories, controversies. *Earth-Science Reviews* 160, 264-299. <https://doi.org/10.1016/j.earscirev.2016.07.014>
- Huang, H., Imran, J., Pirmez, C., 2012. The depositional characteristics of turbidity currents in submarine sinuous channels. *Marine Geology* 329–331, 93-102. <http://dx.doi.org/10.1016/j.mar-geo.2012.08.003>
- Hübscher, C., Spieß, V., Breitzke, M., Weber, M.E., 1997. The youngest channel-levee system of the Bengal Fan: results from digital sediment echosounder data. *Marine Geology* 141, 125-145. [https://doi.org/10.1016/S0025-3227\(97\)00066-2](https://doi.org/10.1016/S0025-3227(97)00066-2)
- Huntington, K.W., Blythe, A.E., Hodges, K.V., 2006. Climate change and Late Pliocene acceleration of erosion in the Himalaya. *Earth and Planetary Science Letters* 252, 107-118. <https://doi.org/10.1016/j.epsl.2006.09.031>
- Imran, J., Parker, G., Katopodes, N., 1998. A numerical model of channel inception on submarine fans. *Journal of Geophysical Research: Oceans* 103, 1219-1238. DOI:10.1029/97jc01721
- Ismail, M., Krishna, K., Srinivas, K., Mishra, J., Saha, D., 2017. Internal structure of the 85° E ridge, Bay of Bengal: Evidence for multiphase volcanism. *Marine and Petroleum Geology* 80, 254-264. <https://doi.org/10.1016/j.marpetgeo.2016.11.020>
- Jegou, I., Savoye, B., Pirmez, C., Droz, L., 2008. Channel-mouth lobe complex of the recent Amazon Fan: The missing piece. *Marine Geology* 252, 62-77. <https://doi.org/10.1016/j.margeo.2008.03.004>
- Kane, I.A., McCaffrey, W.D., Peakall, J., 2008. Controls on sinuosity evolution within submarine channels. *Geology* 36, 287-290. <https://doi.org/10.1130/G24588A.1>
- Kane, I.A., McCaffrey, W.D., Peakall, J., Kneller, B.C., 2010. Submarine channel levee shape and sediment waves from physical experiments. *Sedimentary Geology* 223, 75-85. <http://dx.doi.org/10.1016/j.sedgeo.2009.11.001>
- Klaucke, I., Masson, D.G., Kenyon, N.H., Gardner, J.V., 2004. Sedimentary processes of the lower Monterey Fan channel and channel-mouth lobe. *Marine Geology* 206, 181-198. <https://doi.org/10.1016/j.margeo.2004.02.006>
- Kneller, B., 2003. The influence of flow parameters on turbidite slope channel architecture. *Marine and Petroleum Geology* 20, 901-910. <http://dx.doi.org/10.1016/j.marpetgeo.2003.03.001>
- Kolla, V., 2007. A review of sinuous channel avulsion patterns in some major deep-sea fans and factors controlling them. *Marine and Petroleum Geology* 24, 450-469. <http://dx.doi.org/10.1016/j.marpetgeo.2003.03.001>
- Komar, P.D., 1969. The channelized flow of turbidity currents with application to Monterey deep-sea fan channel. *Journal of Geophysical Research* 74, 4544-4558. <https://doi.org/10.1029/JC074i018p04544>

- Kottke, B., Schwenk, T., Breitzke, M., Wiedicke, M., Kudrass, H.R., Spiess, V., 2003. Acoustic facies and depositional processes in the upper submarine canyon Swatch of No Ground (Bay of Bengal). *Deep Sea Research Part II: Topical Studies in Oceanography* 50, 979-1001. [http://dx.doi.org/10.1016/S0967-0645\(02\)00616-1](http://dx.doi.org/10.1016/S0967-0645(02)00616-1)
- Krishna, K., Neprochnov, Y.P., Rao, D.G., Grinko, B., 2001a. Crustal structure and tectonics of the Ninetyeast Ridge from seismic and gravity studies. *Tectonics* 20, 416-433. <https://doi.org/10.1029/2001TC900004>
- Krishna, K., Bull, J., Scrutton, R., 2001b. Evidence for multiphase folding of the central Indian Ocean lithosphere. *Geology* 29, 715-718. [https://doi.org/10.1130/0091-7613\(2001\)029<0715:EFMFOT>2.0.CO;2](https://doi.org/10.1130/0091-7613(2001)029<0715:EFMFOT>2.0.CO;2)
- Krishna, K., Bull, J., Scrutton, R., 2009. Early (pre-8 Ma) fault activity and temporal strain accumulation in the central Indian Ocean. *Geology* 37, 227-230. <https://doi.org/10.1130/G25265A.1>
- Krishna, K.S., Abraham, H., Sager, W.W., Pringle, M.S., Frey, F., Gopala Rao, D., Levchenko, O.V., 2012. Tectonics of the Ninetyeast Ridge derived from spreading records in adjacent oceanic basins and age constraints of the ridge. *Journal of Geophysical Research: Solid Earth* 117. <https://doi.org/10.1029/2011JB008805>
- Krishna, K., Ismaiel, M., Srinivas, K., Rao, D.G., Mishra, J., Saha, D., 2016. Sediment pathways and emergence of Himalayan source material in the Bay of Bengal. *CURRENT SCIENCE* 110, 363.
- Kudrass, H. R. and cruise participants. 1994. SO93/1-3 Bengal Fan-Cruise report. Federal Institute for Geoscience and Natural Resources, Hannover.
- Kuehl, S.A., Hariu, T.M., Moore, W.S., 1989. Shelf sedimentation off the Ganges-Brahmaputra river system: Evidence for sediment bypassing to the Bengal fan. *Geology* 17, 1132-113. [https://doi.org/10.1130/0091-7613\(1989\)017<1132:SSOTGB>2.3.CO;2](https://doi.org/10.1130/0091-7613(1989)017<1132:SSOTGB>2.3.CO;2)
- Kuehl, S.A., Levy, B.M., Moore, W.S., Allison, M.A., 1997. Subaqueous delta of the Ganges-Brahmaputra river system. *Marine Geology* 144, 81-96. [https://doi.org/10.1016/S0025-3227\(97\)00075-3](https://doi.org/10.1016/S0025-3227(97)00075-3)
- Lambeck, K., Rouby, H., Purcell, A., Sun, Y., Sambridge, M., 2014. Sea level and global ice volumes from the Last Glacial Maximum to the Holocene. *Proceedings of the National Academy of Sciences* 111, 15296-15303. <https://doi.org/10.1073/pnas.1411762111>
- Lopez, M., 2001. Architecture and depositional pattern of the Quaternary deep-sea fan of the Amazon. *Marine and Petroleum Geology* 18, 479-486. [http://dx.doi.org/10.1016/S0264-8172\(00\)00071-4](http://dx.doi.org/10.1016/S0264-8172(00)00071-4)
- Lupker, M., France-Lanord, C., Lavé, J., Bouchez, J., Galy, V., Métivier, F., Gaillardet, J., Lartiges, B., Mugnier, J.L., 2011. A Rouse-based method to integrate the chemical composition of river sediments: Application to the Ganga basin. *Journal of Geophysical Research: Earth Surface* 116. <https://doi.org/10.1029/2010JF001947>
- Lupker, M., Blard, P.-H., Lave, J., France-Lanord, C., Leanni, L., Puchol, N., Charreau, J., Bourlès, D., 2012. <sup>10</sup>Be-derived Himalayan denudation rates and sediment budgets in the Ganga basin. *Earth and Planetary Science Letters* 333, 146-156. <https://doi.org/10.1016/j.epsl.2012.04.020>
- Lupker, M., Lavé, J., France-Lanord, C., Christl, M., Bourlès, D., Carcaillet, J., Maden, C., Wieler, R., Rahman, M., Bezbaruah, D., 2017. <sup>10</sup>Be systematics in the Tsangpo-Brahmaputra catchment: the cosmogenic nuclide legacy of the eastern Himalayan syntaxis. *Earth Surface Dynamics* 5, 429-449. <https://doi.org/10.5194/esurf-5-429-2017>

- Mark, D.F., Renne, P.R., Dymock, R., Smith, V.C., Simon, J.I., Morgan, L.E., Staff, R.A., and Ellis, B.S., 2017, High-precision  $^{40}\text{Ar}/^{39}\text{Ar}$  dating of pleistocene tuffs and temporal anchoring of the Matuyama-Brunhes boundary: *Quaternary Geochronology*, v. 39, p. 1–23, doi: 10.1016/j.quageo.2017.01.002.
- Maslin, M., Knutz, P.C., Ramsay, T., 2006. Millennial-scale sea-level control on avulsion events on the Amazon Fan. *Quaternary Science Reviews* 25, 3338-3345. <http://dx.doi.org/10.1016/j.quascirev.2006.10.012>
- McNeill, L.C., Dugan, B., Backman, J., Pickering, K.T., Pouderoux, H.F., Henstock, T.J., Petronotis, K.E., Carter, A., Chemale Jr, F., Milliken, K.L., 2017a. Understanding Himalayan erosion and the significance of the Nicobar Fan. *Earth and Planetary Science Letters* 475, 134-142. <https://doi.org/10.1016/j.epsl.2017.07.019>
- McNeill, L.C., Dugan, B., Petronotis, K.E., and the Expedition 362 Scientists, 2017b. *Sumatra Subduction Zone*. Proceedings of the International Ocean Discovery Program, 362: College Station, TX (International Ocean Discovery Program). <https://doi.org/10.14379/iodp.proc.362.2017>
- Meiburg, E., Kneller, B., 2010. Turbidity currents and their deposits. *Annual Review of Fluid Mechanics* 42, 135-156. <https://doi.org/10.1146/annurev-fluid-121108-145618>
- Michels, K.H., Kudrass, H.R., Hübscher, C., Suckow, A., Wiedicke, M., 1998. The submarine delta of the Ganges–Brahmaputra: cyclone-dominated sedimentation patterns. *Marine Geology* 149, 133-154. [http://dx.doi.org/10.1016/S0025-3227\(98\)00021-8](http://dx.doi.org/10.1016/S0025-3227(98)00021-8)
- Michels, K.H., Suckow, A., Breitzke, M., Kudrass, H.R., Kottke, B., 2003. Sediment transport in the shelf canyon “Swatch of No Ground” (Bay of Bengal). *Deep Sea Research Part II: Topical Studies in Oceanography* 50, 1003-1022. [http://dx.doi.org/10.1016/S0967-0645\(02\)00617-3](http://dx.doi.org/10.1016/S0967-0645(02)00617-3)
- Mikkelsen, N., Maslin, M., Giraudeau, J., Showers, W., 1997. Biostratigraphy and sedimentation rates of the Amazon Fan ODP Leg, Proceedings of the Ocean Drilling Program: Scientific Results, pp. 577-594.
- Milliman, J., Farnsworth, K., 2011. Runoff, erosion, and delivery to the coastal ocean. River discharge to the coastal ocean: a global synthesis, Cambridge University Press, Cambridge, UK, 13-69.
- Mitchum, R.M., Vail, P.R., Sangree, J.B., 1977. Seismic Stratigraphy and Global Changes of Sea Level, Part 6: Stratigraphic Interpretation of Seismic Reflection Patterns in Depositional Sequences, in: Payton, C.E. (Ed.), *Seismic Stratigraphy -Applications to Hydrocarbon Exploration*. AAPG Memoir, pp. 117-133.
- Mohtadi, M., Prange, M., Steinke, S., 2016. Palaeoclimatic insights into forcing and response of monsoon rainfall. *Nature* 533, 191. DOI: 10.1038/nature17450
- Molnar, P., Boos, W.R., Battisti, D.S., 2010. Orographic controls on climate and paleoclimate of Asia: thermal and mechanical roles for the Tibetan Plateau. *Annual Review of Earth and Planetary Sciences* 38, 77. <https://doi.org/10.1146/annurev-earth-040809-152456>
- Mulder, T., 2011. Chapter 2 - Gravity Processes and Deposits on Continental Slope, Rise and Abyssal Plains, in: Heiko, H., Thierry, M. (Eds.), *Developments in Sedimentology*. Elsevier, pp. 25-148. <http://dx.doi.org/10.1016/B978-0-444-53000-4.00002-0>
- Nakajima, T., Kneller, B.C., 2013. Quantitative analysis of the geometry of submarine external levées. *Sedimentology* 60, 877-910. DOI: 10.1111/j.1365-3091.2012.01366.x
- Palamenghi, L., Schwenk, T., Spiess, V., Kudrass, H.R., 2011. Seismostratigraphic analysis with centennial to decadal time resolution of the sediment sink in the Ganges–Brahmaputra subaqueous delta. *Continental Shelf Research* 31, 712-730. <http://dx.doi.org/10.1016/j.csr.2011.01.008>

- Pandey, D.K., Clift, P.D., Kulhanek, D.K., and the Expedition 355 Scientists, 2016. *Arabian Sea Monsoon*. Proceedings of the International Ocean Discovery Program, 355: College Station, TX (International Ocean Discovery Program). <http://dx.doi.org/10.14379/iodp.proc.355.2016>
- Peakall, J., McCaffrey, B., Kneller, B., 2000. A process model for the evolution, morphology, and architecture of sinuous submarine channels. *Journal of Sedimentary Research* 70, 434-448. <https://doi.org/10.1306/2DC4091C-0E47-11D7-8643000102C1865D>
- Peakall, J., Amos, K.J., Keevil, G.M., William Bradbury, P., Gupta, S., 2007. Flow processes and sedimentation in submarine channel bends. *Marine and Petroleum Geology* 24, 470-486. <http://dx.doi.org/10.1016/j.marpetgeo.2007.01.008>
- Peakall, J., Sumner, E.J., 2015. Submarine channel flow processes and deposits: A process-product perspective. *Geomorphology* 244, 95-120. <http://dx.doi.org/10.1016/j.geomorph.2015.03.005>
- Picot, M., Droz, L., Marsset, T., Dennielou, B., Bez, M., 2016. Controls on turbidite sedimentation: Insights from a quantitative approach of submarine channel and lobe architecture (Late Quaternary Congo Fan). *Marine and Petroleum Geology* 72, 423-446. <https://doi.org/10.1016/j.marpetgeo.2016.02.004>
- Piper, D.J., Normark, W.R., 1983. Turbidite depositional patterns and flow characteristics, Navy submarine fan, California Borderland. *Sedimentology* 30, 681-694. <https://doi.org/10.1111/j.1365-3091.1983.tb00702.x>
- Piper, D., Flood, R., Cisowski, S., Hall, F., Manley, P., Maslin, M., Mikkelsen, N., Showers, W., 1997. Synthesis of stratigraphic correlations of the Amazon fan, Proceedings of the Ocean Drilling Program. Scientific results. Ocean Drilling Program, pp. 595-609.
- Pirmez, C., Hiscou, R., Kronen, J., 1997. Sandy turbidite successions at the base of channel-levee systems of the Amazon Fan revealed by FMS logs and cores: Unraveling the facies architecture of large submarine fans, proceedings-ocean drilling program scientific results. National science foundation, pp. 7-34.
- Pirmez, C., Imran, J., 2003. Reconstruction of turbidity currents in Amazon Channel. *Marine and Petroleum Geology* 20, 823-849. <https://doi.org/10.1016/j.marpetgeo.2003.03.005>
- Posamentier, H.W., Kolla, V., 2003. Seismic geomorphology and stratigraphy of depositional elements in deep-water settings. *Journal of Sedimentary Research* 73, 367-388. <https://doi.org/10.1306/111302730367>
- Radhakrishna, M., Rao, S., Nayak, S., Bastia, R., Twinkle, D., 2012. Early Cretaceous fracture zones in the Bay of Bengal and their tectonic implications: Constraints from multi-channel seismic reflection and potential field data. *Tectonophysics* 522, 187-197. <https://doi.org/10.1016/j.tecto.2011.11.026>
- Reilly B., Bergmann, F., Weber, M. E., Stoner, J.S., Selkin, P., Schwenk, T., Spiess, V., France-Lanord, C., in prep. Middle to Late Pleistocene Evolution of the Bengal Fan at 8° North: Integrating Core and Seismic Observations for IODP Expedition 354 Transect Chronostratigraphic Modeling.
- Richards, M., Bowman, M., Reading, H., 1998. Submarine-fan systems i: characterization and stratigraphic prediction. *Marine and Petroleum Geology* 15, 689-717. [http://dx.doi.org/10.1016/S0264-8172\(98\)00036-1](http://dx.doi.org/10.1016/S0264-8172(98)00036-1)
- Rogers, K.G., Goodbred Jr, S.L., Khan, S.R., 2015. Shelf-to-canyon connections: Transport-related morphology and mass balance at the shallow-headed, rapidly aggrading Swatch of No Ground (Bay of Bengal). *Marine Geology* 369, 288-299. <http://dx.doi.org/10.1016/j.margeo.2015.09.011>



- Savoye, B., Babonneau, N., Dennielou, B., Bez, M., 2009. Geological overview of the Angola–Congo margin, the Congo deep-sea fan and its submarine valleys. *Deep Sea Research Part II: Topical Studies in Oceanography* 56, 2169–2182. <http://dx.doi.org/10.1016/j.dsr2.2009.04.001>
- Schwenk, T., 2003. The Bengal Fan: architecture, morphology and depositional processes at different scales revealed from high-resolution seismic and hydroacoustic data. Dissertation, Universität Bremen.
- Schwenk, T., Spieß, V., Hübscher, C., Breitzke, M., 2003. Frequent channel avulsions within the active channel–levee system of the middle Bengal Fan—an exceptional channel–levee development derived from Parasound and Hydrosweep data. *Deep Sea Research Part II: Topical Studies in Oceanography* 50, 1023–1045. [http://dx.doi.org/10.1016/S0967-0645\(02\)00618-5](http://dx.doi.org/10.1016/S0967-0645(02)00618-5)
- Schwenk, T., Spieß, V., Breitzke, M., Hübscher, C., 2005. The architecture and evolution of the Middle Bengal Fan in vicinity of the active channel–levee system imaged by high-resolution seismic data. *Marine and Petroleum Geology* 22, 637–656. <http://dx.doi.org/10.1016/j.marpetgeo.2005.01.007>
- Schwenk, T., Spieß, V., 2009. Architecture and stratigraphy of the Bengal Fan as response to tectonic and climate revealed from high-resolution seismic data. *External Controls on Deep-Water Depositional Systems. Special Publication-SEPM (Society of Sedimentary Geologists)* 92, 107–131.
- Spieß, V., 1993. Digitale Sedimentechographie – Neue Wege zu einer hochauflösenden Akustostratigraphie. *Berichte Fachbereich Geowissenschaften, Universität Bremen*, 35, Bremen, 1–199 pp.
- Spieß, V., Hübscher, C., Breitzke, M., Böke, W., Krell, A., von Larcher, T., Matschkowski, T., Schwenk, T., Wessels, A., Züsdorff, L., and Zühlsdorff, S., 1998, Report and preliminary results of R/V Sonne cruise 125, Cochín–Chittagong, 17.10.–17.11.97: Bremen, 128 p.
- Spieß, V., Schwenk, T., Bartels, T., Blanz, T., Etourneau, J., Gainusa-Bogdan, A., Gueneli, N., Huppenkothen, D., Keil, H., Palamenghi, L., Paul, M., Schmidt, K., Thomas, R., and Vog, T., 2006. Cruise Report RV Sonne cruise 188-1, Singapore-Chittagong, 06.06–04.07.2006: Bremen, 72 p.
- Spratt, R.M., Lisiecki, L.E., 2016. A Late Pleistocene sea level stack. *Climate of the Past* 12, 1079. <https://doi.org/10.5194/cp-12-1079-2016>, 2016.
- Stow, D.A.V., Amano, K., Balson, P.S., Brass, G.W., Corrigan, J., Raman, C.V., Tiercelin, J.-J., Townsend, M., and Wijayananda, N.P., 1990. Sediment facies and processes on the distal Bengal Fan, Leg 116. In Cochran, J.R., Stow, D.A.V., et al., *Proc. ODP, Sci. Results*, 116: College Station, TX (Ocean Drilling Program), 377–396. doi:10.2973/odp.proc.sr.116.110.1990
- Stow, D.A.V., Mayall, M., 2000. Deep-water sedimentary systems: New models for the 21st century. *Marine and Petroleum Geology* 17, 125–135. [http://dx.doi.org/10.1016/S0264-8172\(99\)00064-1](http://dx.doi.org/10.1016/S0264-8172(99)00064-1)
- Straub, K.M., Mohrig, D., McElroy, B., Buttles, J., Pirmez, C., 2008. Interactions between turbidity currents and topography in aggrading sinuous submarine channels: A laboratory study. *Geological Society of America Bulletin* 120, 368–385. <https://doi.org/10.1130/B25983.1>
- Straub, K.M., Mohrig, D., Buttles, J., McElroy, B., Pirmez, C., 2011. Quantifying the influence of channel sinuosity on the depositional mechanics of channelized turbidity currents: A laboratory study. *Marine and Petroleum Geology* 28, 744–760. <https://doi.org/10.1016/j.marpetgeo.2010.05.014>
- Sun, Y., Clemens, S.C., An, Z., Yu, Z., 2006. Astronomical timescale and palaeoclimatic implication of stacked 3.6-Myr monsoon records from the Chinese Loess Plateau. *Quaternary Science Reviews* 25, 33–48. <https://doi.org/10.1016/j.quascirev.2005.07.005>

- Sylvester, Z., Pirmez, C., Cantelli, A., 2011. A model of submarine channel-levee evolution based on channel trajectories: Implications for stratigraphic architecture. *Marine and Petroleum Geology* 28, 716-727. <http://dx.doi.org/10.1016/j.marpetgeo.2010.05.012>
- Tada, R., Zheng, H., Clift, P.D., 2016. Evolution and variability of the Asian monsoon and its potential linkage with uplift of the Himalaya and Tibetan Plateau. *Progress in Earth and Planetary Science* 3, 1-26. DOI: 10.1186/s40645-016-0080-y
- Twichell, D.C., Kenyon, N.H., Parson, L.M., McGregor, B.A., 1991. Depositional patterns of the Mississippi Fan surface: evidence from GLORIA II and high-resolution seismic profiles, Seismic facies and sedimentary processes of submarine fans and turbidite systems. Springer, pp. 349-363. [https://doi.org/10.1007/978-1-4684-8276-8\\_19](https://doi.org/10.1007/978-1-4684-8276-8_19)
- van Hinsbergen, D.J.J., Lippert, P.C., Dupont-Nivet, G., McQuarrie, N., Doubrovine, P.V., Spakman, W., Torsvik, T.H., 2012. Greater India Basin hypothesis and a two-stage Cenozoic collision between India and Asia. *Proceedings of the National Academy of Sciences* 109, 7659-7664. DOI: 10.1073/pnas.1117262109
- Von der Borch, C.C., Sclater, J.C., et al., 1974. Initial reports of the Deep Sea Drilling Project Leg 22. US Government Printing Office, Washington DC, 890 pp.
- Wang, P.X., Wang, B., Cheng, H., Fasullo, J., Guo, Z., Kiefer, T., Liu, Z., 2017. The global monsoon across time scales: Mechanisms and outstanding issues. *Earth-Science Reviews* 174, 84-121. <https://doi.org/10.1016/j.earscirev.2017.07.006>
- Weber, M.E., Wiedicke, M.H., Kudrass, H.R., Hübscher, C., Erlenkeuser, H., 1997. Active growth of the Bengal Fan during sea-level rise and highstand. *Geology* 25, 315-318. [https://doi.org/10.1130/0091-7613\(1997\)025<0315:AGOTBF>2.3.CO;2](https://doi.org/10.1130/0091-7613(1997)025<0315:AGOTBF>2.3.CO;2)
- Weber, M.E., Wiedicke-Hombach, M., Kudrass, H.R., Erlenkeuser, H., 2003. Bengal Fan sediment transport activity and response to climate forcing inferred from sediment physical properties. *Sedimentary Geology* 155, 361-381. [http://dx.doi.org/10.1016/S0037-0738\(02\)00187-2](http://dx.doi.org/10.1016/S0037-0738(02)00187-2)
- Weber, M.E., Lantsch, H., Dekens, P., Das, S.K., Reilly, B.T., Martos, Y.M., Meyer-Jacob, C., Agrahari, S., Ekblad, A., Titschack, J., Holmes, B., Wolfgramm, P., 2018. 200,000 years of monsoonal history recorded on the lower Bengal Fan - strong response to insolation forcing. *Global and Planetary Change*. <https://doi.org/10.1016/j.gloplacha.2018.04.003>
- Weber, M.E., Reilly, B.T., 2018. Hemipelagic and turbiditic deposits constrain lower Bengal Fan depositional history through Pleistocene climate, monsoon, and sea level transitions. *Quaternary Science Reviews* 199, 159-173. <https://doi.org/10.1016/j.quascirev.2018.09.027>
- Wynn, R.B., Cronin, B.T., Peakall, J., 2007. Sinuous deep-water channels: Genesis, geometry and architecture. *Marine and Petroleum Geology* 24, 341-387. <http://dx.doi.org/10.1016/j.marpetgeo.2007.06.001>
- Yilmaz, Ö., 2001. *Seismic Data Analysis - Processing, Inversion and Interpretation of Seismic Data*. Society of Exploration Geoph, Tulsa.
- Zhisheng, A., Kutzbach, J.E., Prell, W.L., Porter, S.C., 2001. Evolution of Asian monsoons and phased uplift of the Himalaya-Tibetan plateau since Late Miocene times. *Nature* 411, 62-66.
- Zhisheng, A., Guoxiong, W., Jianping, L., Youbin, S., Yimin, L., Weijian, Z., Yanjun, C., Anmin, D., Li, L., Jiangyu, M., 2015. Global monsoon dynamics and climate change. *Annual Review of Earth and Planetary Sciences* 43, 29-77. <https://doi.org/10.1146/annurev-earth-060313-054623>

# **Appendix 1: Middle to Late Pleistocene Evolution of the Bengal Fan at 8° North: Integrating Core and Seismic Observations for IODP Expedition 354 Transect Chronostratigraphic Modeling**

Brendan T. Reilly<sup>1</sup>, Fenna Bergmann<sup>2</sup>, Michael E. Weber<sup>3</sup>, Joseph S. Stoner<sup>1</sup>, Peter Selkin<sup>4</sup>, Tilman Schwenk<sup>2</sup>, Volkhard Spiess<sup>2</sup>, Christian France-Lanord<sup>5</sup>

<sup>1</sup> College of Earth, Ocean, and Atmospheric Sciences, Oregon State University, Corvallis, Oregon 97331, USA

<sup>2</sup> Faculty of Geosciences, University of Bremen, Bremen, Germany

<sup>3</sup> Steinmann-Institute, University of Bonn, Bonn, Germany

<sup>4</sup> School of Interdisciplinary Arts and Sciences, University of Washington, Tacoma, Washington 98402, USA

<sup>5</sup> Centre de Recherches Péetrographiques et Géochimiques, CNRS Université de Lorraine, Vandoeuvre les Nancy, France

Status: To be submitted as a joint submission with the manuscript present in *Chapter 4*

## Abstract

We investigate chronology and age uncertainty for the Middle to Late Pleistocene Lower Bengal Fan using a novel age-depth modeling approach that factors litho-, magneto-, bio-, cyclo-, and seismic stratigraphic constraints, based on results from the International Ocean Discovery Program Expedition 354 Bengal Fan and analysis of the GeoB97-020/027 seismic line. The initial chronostratigraphic framework is established using regionally extensive hemipelagic sediment units and only age-depth models of fan deposits that respect the superposition of channel-levee systems between sites are accepted. In doing so, we reconstruct signals of regional sediment accumulation rate and lithogenic sediment input that are consistent with more distal and more ambiguous Bay of Bengal and Bengal Fan records. This chronology allows us to discuss the Middle to Late Pleistocene Bengal Fan evolution within the context of sea level, climate, and tectonic controls. We hypothesize, based on the timing of accumulation rate changes, that growth and intensification of the Bengal Fan's channel-levee system at 8° N was largely driven by increases in sea level amplitude during this time. However, it is also possible changes in Pleistocene climate occurring around the same time increased Himalayan erosion rates, resulting in greater sediment flux to the fan.

## 1 Introduction

The Bengal Fan is the final sink for a huge erosional system, containing the most complete record of Himalayan erosion since the collision of India and Asia in the early Cenozoic (Curry, 1994; France-Lanord et al., 2016). However, the climate and tectonic signals recorded in these sediments are convolved during sediment transport through rivers, floodplains, deltas, the continental shelf, and ultimately the fan's channel-levee system. Understanding the complete history of the erosional system is important as the uplift of the Himalaya is thought to have a significant impact on global climate over the Cenozoic, including the development of the Asian monsoonal systems (Zhisheng et al., 2001) as well as carbon sequestration by increased silicate mineral weathering (Raymo and Ruddiman, 1992) and, more importantly, burial of organic carbon in its resulting deep-sea fan sediments (France-Lanord and Derry, 1997). Source to sink comparisons of organic carbon concentrations in river and fan sediments suggests near perfect burial efficiency—in large part related to the very high accumulation rates of the Bengal Fan depositional system (Galy et al., 2007). Yet, complexities in fan depositional processes make it difficult to reconstruct time variations in integrated sediment flux and how these fluxes translate to sediment accumulation and associated organic carbon burial on the fan. To investigate the Pleistocene history of this depositional system, International Ocean Discovery Program (IODP) drilled a transect of seven sites along 8° North (~320 km; 85.85° – 88.74° East) and captured a range of lithologic units, including low accumulation rate hemipelagic deposits and high accumulation rate channel-levee influenced deposits which span at least the last ~1.25 Ma at all sites (Figures 1-3; Table 1; France-Lanord et al., 2016).

A fundamental problem investigated by this study is that traditional age-depth modeling approaches for depositional systems like the Bengal Fan have trouble reconstructing accumulation rates that vary by orders of magnitude between interbedded lithologic units. This is especially true when age control at any one site is limited, as was the case for the seven sites in the Expedition

354 8° N transect. One cannot assign a single sedimentation rate prior (e.g. Blaauw and Christen, 2011) as an additional constraint to produce more realistic uncertainty nor should one allow for nearly every possible monotonic age-depth combination (e.g. Haslett and Parnell, 2008), as this ignores first order geologic observations that make a majority of these scenarios unreasonable. It would also be challenging to create age-depth models for each unit independently, as many of the fan units and thin calcareous clay units do not have reliable chronostratigraphic markers nor constraints on their start and end times.

To explore accumulation rate variations for the last 1.25 Ma and work towards a complete 8° N Bengal Fan chronostratigraphic framework for future studies, we employ a system specific age-depth modeling approach that is inspired by well-established methods to address uncertainty (Blaauw and Christen, 2011) but also incorporates expert knowledge about the Bengal Fan. Sediments deposited by fan or hemipelagic depositional processes are objectively identified based on physical properties and each lithology is modeled using different strategies. The law of superposition provides additional constraints in fan deposits with few, if any site based constraints, by solving for all seven sites simultaneously and only accepting solutions that respect the channel-levee stacking pattern defined by Bergmann et al. (in prep.)<sup>2</sup> (Figure 2). Our results allow for reconstruction of the time variation in integrated sediment flux at 8° North between 85.85o and 88.74o East and allow us to assess how representative a single site and/or the Expedition 354 transect is for reconstructing past dynamics of the Bengal Fan. Implications for fan evolution and associated sedimentary processes are discussed in greater detail by Bergmann et al. (in prep.), while here we focus on the timing of depositional changes in relation to Pleistocene climate and sea level.

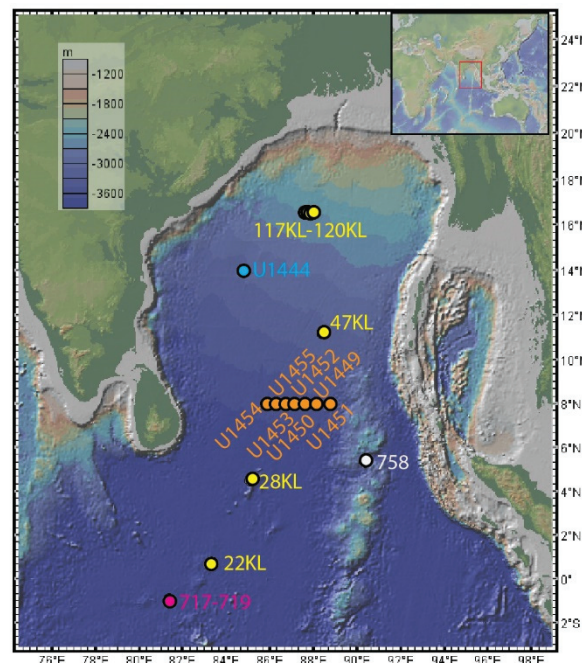


Figure 1. Locations of Bay of Bengal and Bengal Fan archives, including the IODP Expedition 354 transect (orange), IODP Expedition 353 U1444 (blue), SO93 cores (yellow), ODP Leg 116 sites (pink), and ODP Leg 121 Site 758 (white).

<sup>2</sup> The here referenced manuscript in preparation refers to Chapter 4 of this thesis.



Table 1. IODP Expedition 354 Holes used in this study

Hole	Latitude (° N)	Longitude (° E)	Water Depth (m)	Meters used in model/ cluster analysis (total penetration)
U1449A	8.01	88.11	3652.7	120 (213.5)
U1450A	8.01	87.67	3655.3	190 (687.4)
U1451A	8.01	88.74	3607.3	110 (582.1)
U1452B	8.01	87.18	3670.3	195 (217.7)
U1453A	8.01	86.79	3679.5	180 (215.7)
U1454B	8.01	85.85	3710.3	170 (161.8)
U1455C*	8.01	86.28	3732.5	110 (949.0)

\* IODP Site U1455 is the reoccupation of DSDP Site 218, drilled during Leg 22.

### 1.1 The Pleistocene Bengal Fan

Since the late Miocene, sediments have been transported by turbidity currents along channel-levee systems to 8° N (Schwenk and Spiess, 2009), that in at least recent times seem to be sourced to a single shelf canyon and extend the 2500 km length of the fan without bifurcation (Curry and Moore, 1974; Weber et al., 1997; Curry et al., 2003). On Pleistocene timescales, frequent channel avulsions have caused the migration of active deposition across the entire fan (Bergmann et al., in prep.; Curry et al., 2003; Schwenk and Spiess, 2009). Bengal Fan channels are deeply incised into underlying deposits and show vertical aggregation and lateral migration (Schwenk et al., 2003, 2005). Fan depositional processes include the overspilling and flow-stripping of channelized turbidity currents, which build channel levees, deposit inter-channel sheet-like turbidites, and/or deposit massive sands (Piper and Normark, 1983; Schwenk et al., 2005). Proximity to the channel-levee system is the primary control on sediment accumulation rate. Accordingly, no single drill site should be expected to contain a complete record of fan deposition on timescales longer than the life of a stable channel-levee system.

While it is likely that the highest fluxes of sediment were delivered to the fan during sea-level low stands (Curry et al., 2003), direct radiocarbon dating of late Pleistocene and Holocene levee turbidites (SO93 Cores 117- 120 KL, ~16.5° N) demonstrate continued sediment input through the deglacial sea-level rise and Holocene sea level high stand, with outer levee long-term accumulation rates around 70 cm/ka, but often exceeding 100 cm/ka while sea level rose, and long-term accumulation rates from a location very proximal to the active channel were around 120 cm/ka for the last 9.6 ka (Hein et al., 2017; Weber et al., 1997). Similar radiocarbon-based estimates preceding the deglacial sea level rise are not available at this time.

Previous efforts have had difficulty assigning ages and unambiguous relationships of paleo-channel-levee systems, shelf-canyons, and depocenter spatial extents. However, seismic evidence from the upper-lower fan suggests that a series of ‘subfans’, resulting from spatial restriction of the active channel-levee systems for timescales ranging from about 250-500 ka, occurred during the Pleistocene (Bergmann et al., in prep.; Curry et al., 2003; Schwenk and Spiess, 2009). During periods of local fan inactivity, when sediment routing moves the active fan depocenter elsewhere, calcareous clay sediments drape inactive channel-levee systems and other fan deposits (Bergmann et al., in prep.; Weber and Reilly, 2018). These types of sediment are well documented in the upper stratigraphy of core SO93-47KL (11.18° N), where turbiditic activity ceased ~0.3 Ma

(Weber et al., 2003) and U1452C-1H (8° N), where fan influenced sediments ceased deposition ~0.2 Ma (Weber et al., 2018). These observations provide constraints for the abandonment of local channel-levee systems on the eastern fan before the Late Pleistocene movement of the depocenter to the more western fan documented in seismic data (Subfan D of Bergmann et al., in prep.; Subfan D1 of Schwenk and Spiess, 2009).

Prior to sediments recovered during IODP Expedition 354 Bengal Fan, all older age constraints for the Pleistocene evolution of the upper-lower Bengal Fan were rooted in the stratigraphy of Deep Sea Drilling Program (DSDP) Site 218, which suffered partial coring and low recovery (59.4 m of sediment from a 773 m hole), limited biostratigraphic constraints, and ambiguity in core-seismic comparison beyond prominent continuous reflectors (Von der Borch et al., 1974). While this was sufficient to get a sense for long-term sediment accumulation rates at that site and to provide first order age estimates of Pleistocene depocenter changes within the context of seismic data (Curry et al., 2003; Schwenk and Spiess, 2009), its chronology could not constrain fan dynamics on 10-100 kyr timescales which are important for understanding fan evolution in the context of Pleistocene sea level and climate.

There are clues that major changes in fan deposition occurred during the Pleistocene. Results from Ocean Drilling Program (ODP) Leg 116 Sites 717 and 719 on the distal Bengal Fan (~10 S) show a significant increase in sediment accumulation rates between the last occurrences of small *Gephyrocapsa* spp. dominance (~1.02 Ma) and *Psuedoemiliana lacunosa* (~0.44 Ma), often reported as occurring at 0.8 Ma, with long term accumulation rates switching from values on the order of 100 cm/ka in the early and middle Pleistocene to on the order of 101 cm/ka after the switch (Gartner, 1990; ages updated according to Gradstein et al., 2012). This accumulation rate change was accompanied by sedimentological changes that could be interpreted as a change in the weathering regime of the Himalayan and flood plain– source regions, but, within the context of more recent drilling, the lithologic changes are more likely a reflection of how sediments are transported through the fan (France-Lanord et al., 2016, 1993).

Perhaps the best dated complete Pleistocene record from the region is ODP Leg 121 Site 758 on the Ninetyeast Ridge (5.38° N; recently redrilled as IODP Site U1443; Clemens et al., 2016), whose benthic  $\delta^{18}\text{O}$  record (Chen et al., 1995) was used in the construction of the LR04 Benthic  $\delta^{18}\text{O}$  stack (Lisiecki and Raymo, 2005). While no fan deposits are found in the mostly pelagic stratigraphy of Site 758, researchers have argued that changes in the concentration of lithogenic sediments, tracked by magnetic susceptibility (MS), reflect a regionally integrated signal of climate, tectonic, and/or sea level controlled inputs to the Bay of Bengal and Bengal Fan (Farrell and Janecek, 1991; Klootwijk et al., 1992; Prell and Kutzbach, 1997; Zhisheng et al., 2001). Isotopic evidence from ~3-34 ka sediments of the Ninetyeast Ridge suggests that the lithogenic fraction may be a mix of Ganges and Brahmaputra sources, the primary sources to Bengal Fan SO93 Cores 117-120KL levee sediments (Hein et al., 2017; Lupker et al., 2013), and other river systems like the Irrawaddy (Ahmad et al., 2005). While the record suggests an increase in lithogenic sediments from the Middle to Late Pleistocene, it is difficult to understand the processes that drive this signal without context from the fan itself.

IODP Expedition 354 reoccupied DSDP Site 218 (U1455) along with six other sites along 8° N (U1449-U1454; Figures 1-3; Table 1) with significantly better recovery and less disturbance than possible in 1972, thanks in part to the advent of the IODP half advanced piston corer (France-Lanord et al., 2016). Fortuitously, all seven sites recovered a regionally extensive calcareous clay unit with good reversal magnetostratigraphy—including the Matuyama-Brunhes Boundary (0.774

Ma), Jaramillo Subchron (1.071-0.990 Ma), and/or Cobb Mountain Subchron (1.208-1.187 Ma; ages according to Channell et al., 2016) and consistent physical properties (France-Lanord et al., 2016; Weber and Reilly, 2018) that also appears as a prominent reflector in seismic imaging, providing firm isochron horizons and core-seismic correlation in the Middle Pleistocene (Bergmann et al., in prep.). In the upper part of this unit, some turbidites are intercalated with calcareous clay; however, there were no turbidites recovered at any of the Expedition 354 sites for at least 300 ka, between Marine Isotope Stage (MIS) 37 and 25, about 1.244 – 0.936 Ma (MIS ages according to Lisiecki and Raymo, 2005; Unit 2a in Weber and Reilly, 2018).

Additionally, thick Late Pleistocene hemipelagic sediments were recovered in the uppermost stratigraphy at all sites except the westernmost Site U1454 located next to the most recently active channel (France-Lanord et al., 2016; Weber and Reilly, 2018). Using the Middle and Late Pleistocene hemipelagic units to establish an initial chronostratigraphic framework, we investigate age-depth relationships at all seven sites for the last ~1.25 Ma. This is an interesting period of time to study, as 1.25 Ma marks the start of increased 100 ka frequency amplitude in the benthic  $\delta^{18}O$  record driven by changes in the behavior of the major ice sheets (Clark et al., 2006), whose transition through the Middle and Late Pleistocene impacts the evolution of glacial-interglacial changes on sea level (Elderfield et al., 2012; Rohling et al., 2014) and monsoonal systems (Clemens et al., 1996; Sun et al., 2006) which have a largely unknown influence on the Bengal Fan sedimentary system.

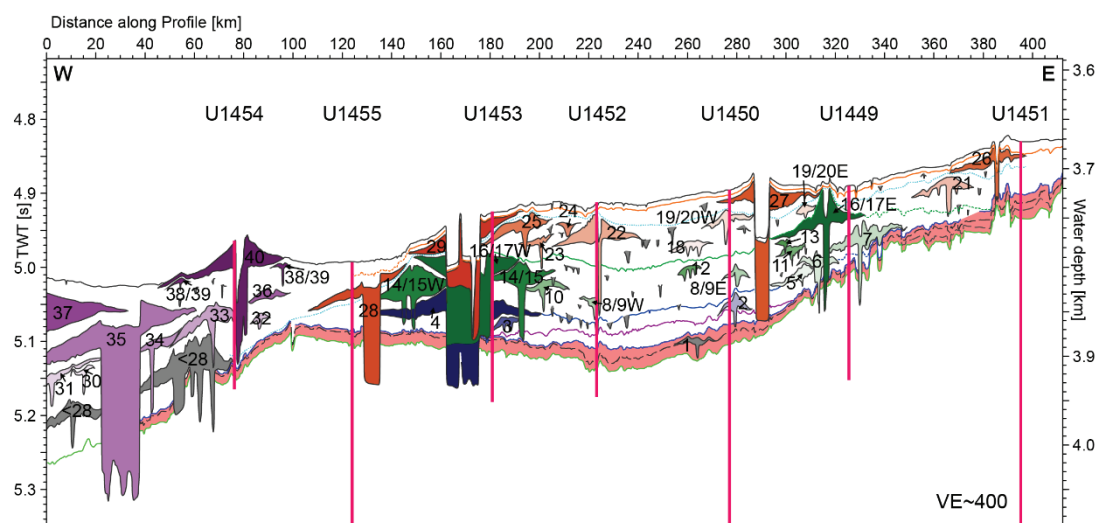


Figure 2. Seismic interpretation of line GeoB97-020/027, as interpreted by Bergmann et al. (in prep), highlighting the sediments studied here. IODP Expedition 354 Sites U1449-U1455 are indicated with vertical pink lines. Channel-levee systems are numbered after Bergmann et al. (in prep) according to their stacking pattern (1=oldest; 40=youngest). Regionally extensive reflectors are highlighted, from oldest to youngest: The Middle Pleistocene Hemipelagic Layer (red shading; lower bound is green line, upper bound is purple bound); the Brunhes Aged Reflectors BAR1 (magenta line), BAR2 (blue line), BAR3 (green line); approximate reflector for the *E. huxleyi* datums (light blue line); and the base of the Late Pleistocene Hemipelagic Layer (orange line). Vertical exaggeration (VE) is about 400 times. We refer the reader to Bergmann et al. (in prep.) for the uninterpreted seismic data.

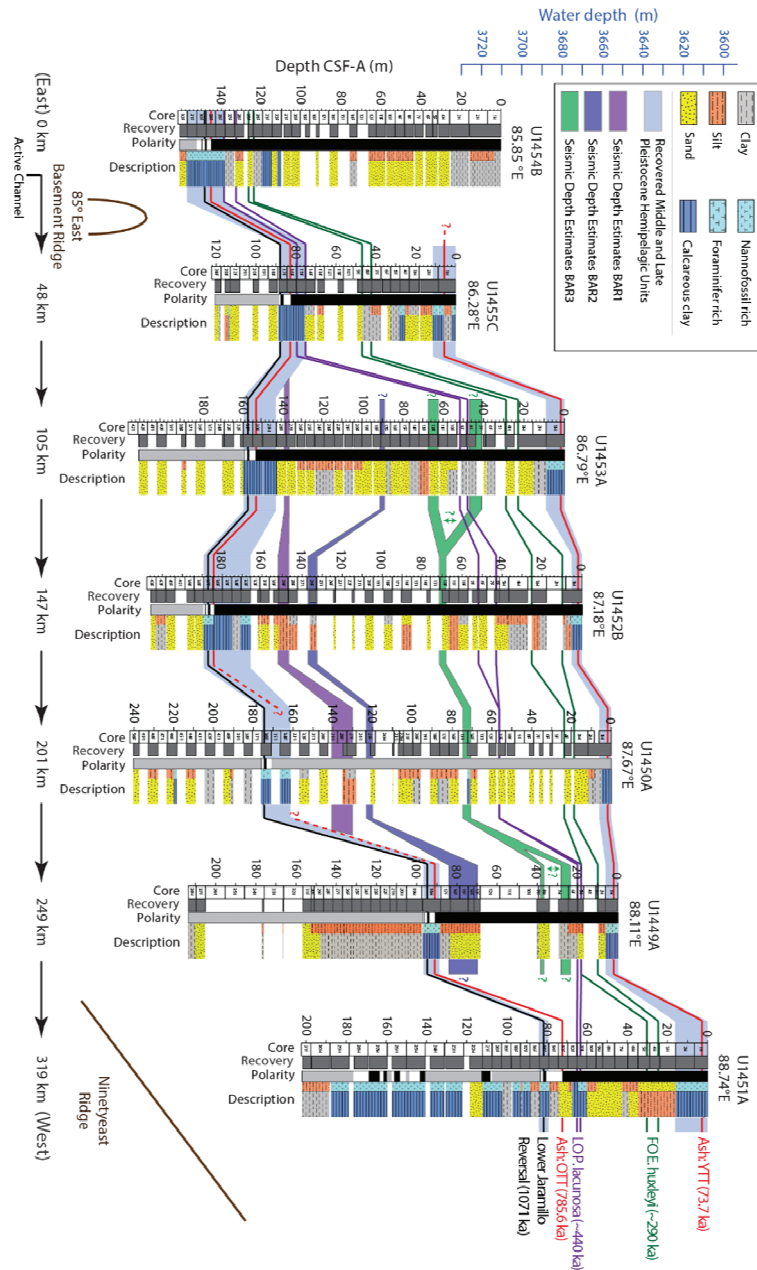


Figure 3. Stratigraphic summary of recovered sediments. Adapted from Weber and Reilly (in prep) and France-Lanord et al. (2016). Ages for important chronostratigraphic markers are noted for ash layers (Mark et al., 2017), the upper and lower range of calcareous nanofossil datums (Gradstein et al., 2012), and the lower Jaramillo magnetic reversal (Channell et al., 2016). Where recovered, the OTT is always just beneath the Matuyama-Brunhes Magnetic Reversal. Light blue shading indicates the regionally extensive thick Middle and Late Pleistocene hemipelagic units. Seismic estimates of Bergmann et al (in prep.) for the depth ranges of Brunhes Aged Reflectors (BAR) (1 = Purple; 2 = Blue; 3 = Green), which are generally associated with thin hemipelagic units where recovery is good, are also indicated. Question marks indicate uncertainty in tracing the BAR reflectors, including multiple possibilities of where BAR 3 intersects with U1453 and U1449.

## 2 Materials and Methods

Model design is discussed in Section 2.1 and inputs to the model in Section 2.2. For this study, we use the single hole at each IODP Expedition 354 site that best recovered middle to late Pleistocene aged sediments (Table 1), as most intervals were only recovered in one hole at each site. Hole recovery, lithology, and some important chronostratigraphic markers are summarized in Figure 3. A detailed discussion of all chronostratigraphic constraints is given in Weber & Reilly (in review), building on the results of France-Lanord et al. (2016), and briefly summarized in Section 2.2. Core depths in this study refer to the core depth below sea floor-B (CSF-B) scale, which applies a compression algorithm if recovery is greater than 100% to prevent overlap of recovered core with adjacent core intervals. This is necessary for this study, as uncertainty in drilling depth and core expansion led some stratigraphic markers to overlap on the primary CSF-A scale. When working with specific cores in each hole, CSF-B can be converted back to CSF-A using tables available through IODP.

X-ray Fluorescence (XRF) data were collected from the surface of u-channel samples (2 x 2 x up to 150 cm plastic tubes) over discrete intervals from Site U1452 to supplement shipboard data using the ITRAX XRF core scanner at the Oregon State University Marine and Geology Repository. Data were collected every 1 mm with 5s count time and a Mo tube.

### 2.1 System Specific Age-Depth Modeling

Our age modeling approach is inspired by well-established methods, primarily the BACON method of Blaauw & Christen (2011), and utilizes the ‘t-walk’ algorithm of Christen and Fox (2010), a Markov Chain Monte Carlo (MCMC) sampler. The algorithm is implemented in MATLAB, using the code of Colin Fox with the corrections by Andreas Nilsson ((Nilsson et al., 2018); available: [www.cimat.mx/~jac/twalk/](http://www.cimat.mx/~jac/twalk/)). While the t-walk may be less efficient than other MCMC methods, it requires little tuning and can be applied to a diverse set of MCMC problems by non-experts. We refer the reader to Blaauw and Christen (2011) for a more detailed discussion of the t-walk and how it can be applied to sediment accumulation modeling. Here, we focus on the fundamental principles and highlight the differences between this method and BACON. The fundamental concept presented here is that while we can define a prior distribution hemipelagic sediment accumulation due to good independent age constraints, fan deposits have unconstrained accumulation rates.

In our model, the Expedition 354 holes are broken into a series of sections ( $c_1, c_2, \dots, c_i$ ) between depth intervals ( $d_0, d_1, d_2, \dots, d_i$ ) with section width ( $\Delta c_i$ ). Fan deposits are nominally divided into 10 m intervals, while calcareous clay deposits are divided into 1 m intervals. As each lithostratigraphic unit is not perfectly divisible by 10 m or 1 m, section widths are allowed to be smaller when needed. Sediment accumulation ( $A$ ) in section  $i$  is modeled as:

$$A_i = (1 - w_i)\alpha_i + w_i\alpha_{i+1} \quad (\text{Equation 1})$$

where  $\alpha$  is a randomly sampled sediment accumulation value and  $w$  is a memory parameter that determines the dependence of  $\alpha$  on the preceding interval, where  $w = 0$  means  $\alpha_i$  is independent of  $\alpha_{i+1}$  and  $w = 1$  means  $\alpha_i$  is equal to  $\alpha_{i+1}$ . In our model,  $w$  is always equal to zero at the base of the section, at lithologic transitions, and in fan deposits. Because we use unevenly spaced depth



intervals, and  $w$  is dependent on interval spacing, for any interval  $w_i = w_p^{\Delta c_i}$ , where the memory has an exponential relationship with the lag (i.e.  $\Delta c_i$  in cm). In the calcareous clay sediments,  $w_p$  is the memory value randomly selected according to the prior beta distribution (Beta( $a_w$ ,  $b_w$ )) (see Blaauw and Christen, 2011). We require that all values of  $w$  be between 0 and 1 and that all  $\alpha$  values, for fan or hemipelagic deposits, are positive (i.e. monotonic accumulation). For hemipelagic sediments, we use a memory mean of 0.7 and strength of 30. Sediment age at any depth ( $t_D$ ) is calculated as:

$$t_D = \sum_{d=1}^D \Delta c_d * A_d \quad (\text{Equation 2})$$

Given that the sediment water interface is at age zero.

We provide a prior in which hemipelagic sediments  $\alpha_h$  are described by a gamma distribution (Gamma( $a_{\alpha h}$ ,  $b_{\alpha h}$ )) (after Blaauw and Christen, 2011) while fan sediments are left unconstrained. Based on observations where age control is strong (Weber and Reilly, 2018), we use accumulation mean of 3 cm/ka and 2 accumulation shape to define the distribution.

An ‘energy’ function is used as the input to the t-walk algorithm as  $U(\alpha, w | y) = -\log f(\alpha, w | y_1, y_2, \dots, y_i)$  which represents the  $-\log$  of the posterior distribution, where  $y$  are the magnetic reversal, tephra, and orbital tuning age constraints with uncertainty ( $\sigma$ ) at depth ( $D_1, D_2, \dots, D_i$ ). In this case:

$$U(\alpha, w | y) = -(1 - a_w) \log w_p - (1 - b_w) \log(1 - w_p) - \sum_{i=1}^I (1 - a_{\alpha h}) \log \alpha_{ih} + b_{\alpha h} \alpha_{ih} - \sum_{j=1}^J \log \sigma_j + \left( \frac{y_j - t_{Dj}}{\sigma_j} \right)^2 / 2 \quad (\text{Equation 3})$$

This ‘energy’ function differs with respect to BACON, as we have relatively simple probability distribution for our age constrains (i.e. we assume all normal distributions, rather than calibrated radiocarbon dates) and we set the sediment water interface to a constant value of 0 ka, thus the three lines of Equation 3, relate to fitting the memory, hemipelagic accumulation rates, and age constraint priors, respectively.

To ensure that our solutions are geologically meaningful, we implement a few additional hard constraints, where if violated, the ‘energy’ function is set to  $-\text{Inf}$  and the iteration is rejected. First, all solutions must respect the maximum limiting date provided by the first occurrence of *E. huxleyi*, where only solutions that the first occurrence is younger than 290 ka are accepted. Second, all solutions must respect the channel-levee stacking pattern of Bergmann et al. (in prep.). This is achieved by solving for all seven sites simultaneously using the t-walk algorithm and rejecting any solution by setting the ‘energy’ function to  $-\text{Inf}$  where the base of a stratigraphically higher channel-levee system is modeled as being older than the top of a channel-levee systems that is stratigraphically lower.

## 2.2 Lithostratigraphic and Chronostratigraphic Inputs for Age-Depth Modeling

Sediments recovered in the upper 200 m of each site were categorized as hemipelagic or fan (i.e. channel-levee, interlevee, and sand deposits) deposits by fitting a Gaussian mixture model cluster analysis to three physical properties measured on ship: magnetic susceptibility (MS), natural gamma radiation (NGR), and sediment lightness ( $L^*$ ). We removed measurements made within 3 cm from the edge of each section and normalized magnetic susceptibility and NGR by gamma ray attenuation (GRA) estimated wet bulk density using the method of Walczak et al. (2015) by smoothing all records to the same resolution using a Full Width at Half Maximum (FWHM) Gaussian filter of 6 cm and resampling every 5 cm. While  $L^*$  was not normalized, we also filtered and resampled to allow for direct comparison. Intervals that were not recovered by coring were categorized as hemipelagic or fan deposits based on the closest overlying or underlying sediments recovered. If both agreed, all sediments in between were classified as being the same. If both disagreed, the depth of the contact was assigned at random.

Bergmann et al. (in prep.) discuss the identification of channel-levee deposits and prominent reflectors in detail. We use their interpretation and number scheme of the channel-levee stacking pattern at 8° N (Figure 2). Their integration of cores and seismic data was conducted with constant velocities ranging from 1640-1680 m/s. Velocities were determined by the best fit of prominent reflectors with lithologic boundaries and physical properties. Velocities were also cross-checked with the shipboard measured p-wave velocities. While there are uncertainties in any time-depth conversion, broad agreement in the calculated depths of the high amplitude reflectors associated with calcareous clay and fan contacts and drilling depths lends confidence in their use in this study.

We use age constraints from Weber and Reilly, 2018 which establish an orbital resolution chronology in middle to late Pleistocene calcareous clay sediments through correlation of  $L^*$  variations to the benthic  $\delta^{18}\text{O}$  timescale of Lisiecki and Raymo (2005) within the framework of biostratigraphic and magnetostratigraphic constraints. Along the Expedition 354 transect and other sites from the lower Bengal Fan, including cores with expanded calcareous clay lithologies SO93 Cores 22KL, 28KL, and 47KL,  $L^*$  primarily reflects the relative proportion of biogenic calcareous to lithogenic sediments (Weber et al., 2003). At Site U1452, Late Pleistocene calcareous clay sediments were studied in detail and display  $L^*$  variations on orbital timescales along with planktonic  $\delta^{18}\text{O}$  and other proxies that reflect marine productivity and sediment composition (Weber et al., 2018). In our model, we assign an uncertainty of 7 ka ( $1\sigma$ ) to account for uncertainties in correlation (human uncertainty), phase (geologic uncertainty) with the benthic  $\delta^{18}\text{O}$  reference template.

We include additional constraints from magnetic reversals, using the timescale of Channell et al. (2016), which is based on direct benthic  $\delta^{18}\text{O}$  and magnetic comparison in North Atlantic IODP Site U1308 and provides stronger constraints on the timing of the Cobb Mountain Subchron with respect to the benthic  $\delta^{18}\text{O}$  timescale than the Geologic Timescale of Gradstein et al. (2012) used in the Expedition 354 Proceedings (France-Lanord et al., 2016). These tuned reversal ages are assigned uncertainty of 5 ka. Two tephra layers recovered at most sites are interpreted as the Youngest Toba Tephra and Oldest Toba Tephra (France-Lanord et al., 2016; Weber et al., 2018; Weber and Reilly, 2018). We assign the  $^{40}\text{Ar}/^{39}\text{Ar}$  dates for these events with their analytical uncertainty,  $73.7 \pm 0.3$  ka and  $785.6 \pm 0.7$  ka, of Mark et al. (2017) as additional age control points. Biostratigraphic datums are treated with caution, as the last occurrence of *P. lacunosa* (440 ka) was found in the same samples as *E. huxleyi* (first occurrence at 290 ka) in multiple

holes (Holes U1450A and U1454B), suggesting reworking of very old materials in fan deposits, and many turbiditic and sandy samples were barren, making it challenging to establish first and last occurrence depths with confidence (all nannofossil ages after Gradstein et al., 2012). While these issues likely do not impact calcareous clay sediments, until further biostratigraphic work refines shipboard estimates, the biostratigraphic markers cannot be used as tie points for establishing a  $10^5$ - $10^6$  a resolution chronology. In our model, however, we do include the first occurrence of *E. huxleyi* as a maximum limiting date, because even if the nannofossil is reworked from its actual first occurrence the interpretation doesn't change (i.e. if a sample contains *E. huxleyi*, the sample must be less than 290 ka old). When additional constraints become available, they can be incorporated to improve the age-depth model results.

### 2.3 Stacking Model Results

We build two stacks using the model results to represent the regional signals captured by the Expedition 354 8° N transect. Sediment accumulation rates were calculated for each of the age-depth combinations at each site over 1 ka intervals to capture 1 ka and greater changes in long term accumulation rates. These were used to calculate statistics for each site and for the transect as a whole. Similarly, a magnetic susceptibility stack was created by applying the median age depth relationship for each site to logarithmically transformed shipboard point magnetic susceptibility log(MS) records and resampling every 1 ka, after applying a smoothing Gaussian filter with FWHM of 2.5 ka. These smoothed and resampled log(MS) records were then stacked to extract a signal that is representative of the whole transect.

## 3 Results

### 3.1 Lithostratigraphy

Results of the Gaussian mixture model are summarized in Figures 4 and 5. We choose a three cluster solution, as it does a good job of describing the data in a geologically meaningful way without overfitting the data. In comparison to the shipboard descriptions of primary lithology, cluster 1 was mainly described as calcareous clay, cluster 2 was mainly described as sands, and cluster 3 was described as a mixture of lithogenic clays, silts, and sands. Accordingly, we interpret cluster 1 as describing hemipelagic sediments and clusters 2 and 3 as describing fan sediments, such as massive sands deposited in sand lobes and turbidites (e.g. Schwenk et al., 2005).

MS, which tracks the concentration of magnetizable material, is generally highest in sandy fan sediments (cluster 2) over muddy (clayey-sandy) turbidites (cluster 3), suggesting a particle size control on magnetic susceptibility values, consistent with previous observations for Bengal Fan sediments (Weber et al., 2003). Dilution of the relative proportion of lithogenic sediments by biogenic sediments is likely the primary control on the low magnetic susceptibility values in hemipelagic sediments (cluster 1). It is possible, but difficult to assess at this time, that there are either bedrock or weathering source controls on MS as well, as was suggested in the study of distal fan mud turbidities (Sager and Hall, 1990) and Bay of Bengal slope sediments (Phillips et al., 2014).  $L^*$  values are similar for both fan sediment clusters, but exhibit a much greater range in hemipelagic sediments, reflecting orbital timescale controls on sediment composition in the hemipelagic sediments, as documented elsewhere (Weber et al., 2003, 2018). NGR, which tracks the amount of

radioactive materials, is likely on first order related to the relative concentration of lithogenic materials and on second order related to the relative proportion of K, U, and Th bearing minerals in the lithogenic fraction. There is a strong negative correlation with  $L^*$  in hemipelagic sediments, suggesting this reflects variations in biogenic and lithogenic contributions. Conversely, there is a strong positive correlation in NGR and MS in sandy fan sediments, suggesting whatever is controlling the concentration of magnetic minerals is also controlling the concentration of K, U, and/or Th bearing minerals.

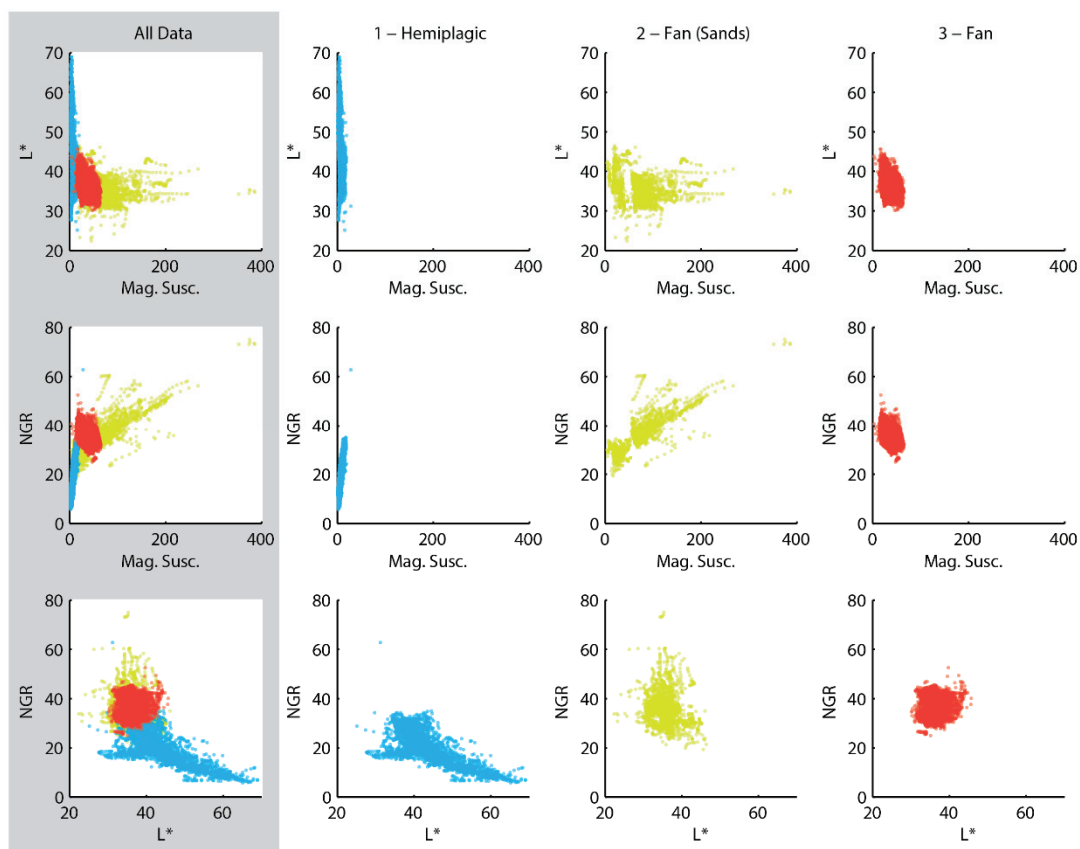


Figure 4. Comparison of physical properties and results of the cluster analysis. Natural gamma radiation (NGR) and magnetic susceptibility were normalized by gamma ray attenuation (GRA) estimates of bulk density following the method of Walczak et al. (2015).

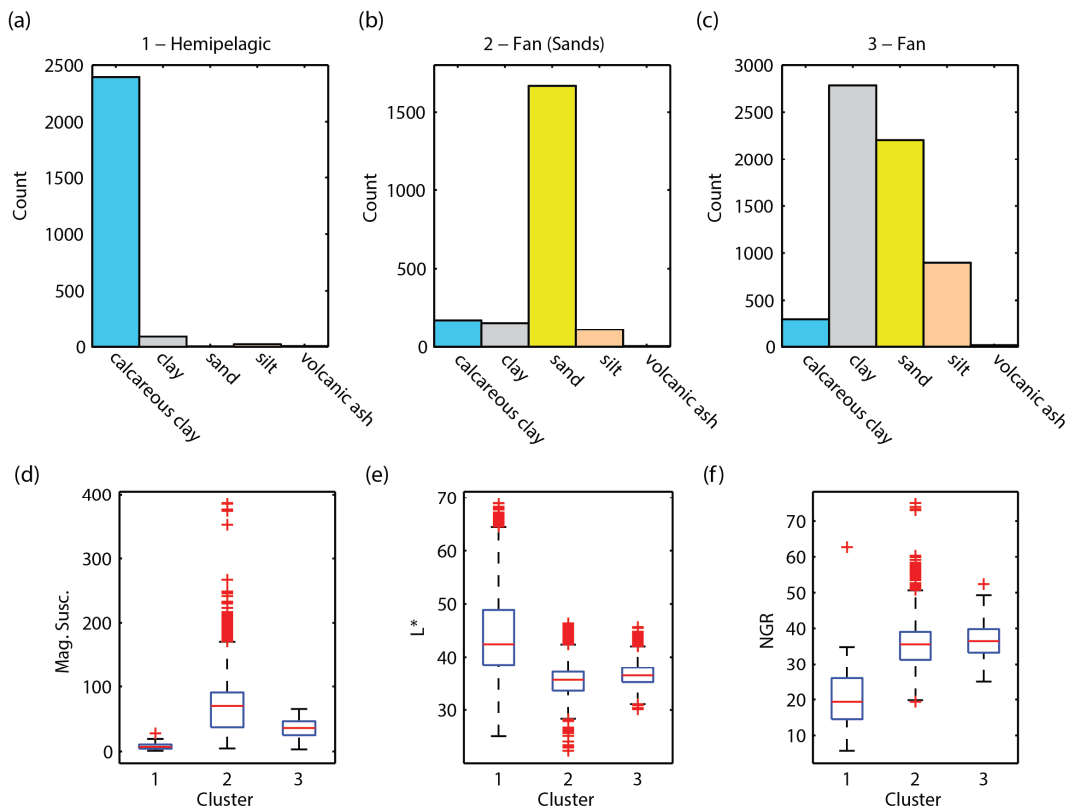


Figure 5. Comparison of cluster analysis results with shipboard visual core descriptions. Note cluster 1 (a) was primarily described as calcareous clay and can be interpreted as hemipelagic sediments while clusters 2 (b) and 3 (c) were mostly described as various mixtures of lithogenic clays, silts, and sands and can be interpreted as fan sediments. Box and whisker plots (d-e) show the median (horizontal red line), range of the 2<sup>nd</sup> and 3<sup>rd</sup> quartile (box), and 99.3% range (whiskers) for the three physical properties used in the cluster analysis.



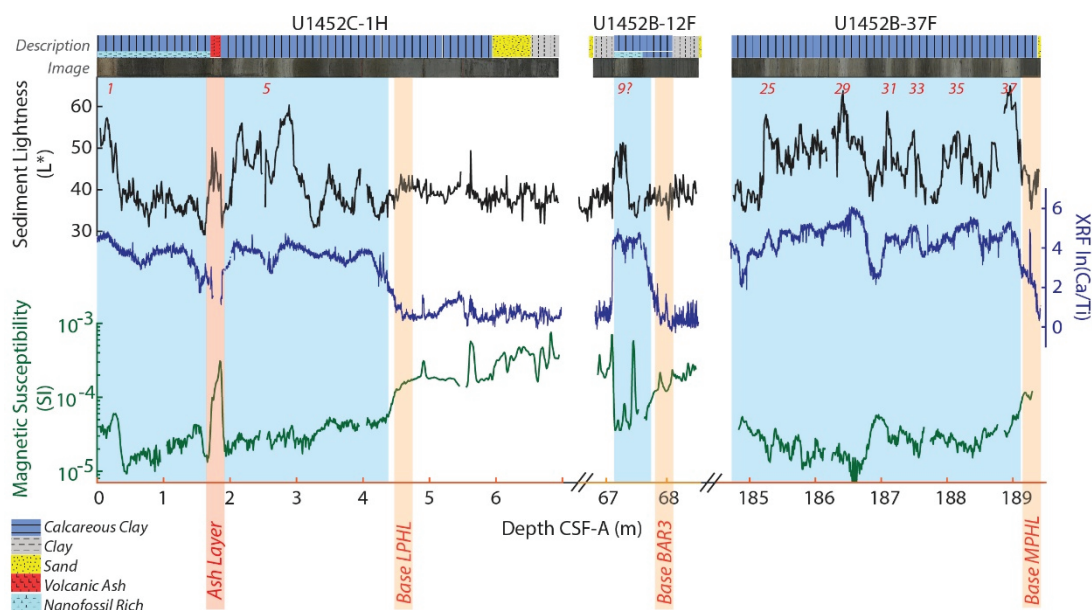


Figure 6. Shipboard measured physical properties, sediment lightness ( $L^*$ ) and magnetic susceptibility (MS), compared with the XRF ratio of Ca to Ti for hemipelagic sediments and their contacts with fan sediments at Site U1452. These contacts include the base of the Late Pleistocene hemipelagic layer (LPHL), the hemipelagic layer associated with Brunhes Aged Reflector 3 (BAR3), and the Middle Pleistocene hemipelagic layer (MPHL). Shipboard lithologic descriptions and images are included for reference. There is a stark contrast between high MS and low Ca/Ti in fan deposits and low MS and high Ca/Ti in hemipelagic sediments.  $L^*$  highs in hemipelagic deposits can be used to identify sediments deposited during interglacial times (Weber et al., 2018). Blue shading indicates the hemipelagic sediments deposited with little influence from the fan, which is different than shipboard descriptions of calcareous clay sediments.

### 3.2 Seismic Reflection Data

The multichannel seismic Profile GeoB97-020/27 crosses all seven IODP Expedition 354 sites. In addition to the seismic-stratigraphy discussed by Bergmann et al., (in prep) we identified three regionally continuous and high amplitude reflectors above the Middle Pleistocene hemipelagic layer east of U1453, which we name the Brunhes-Aged Reflectors (BAR) 1, 2, and 3 (Figure 2 and 3). BAR1 onlaps the MPHL between Site U1450 and U1449 (approximately at km 305, Figure 2). BAR2 onlaps the MPHL east of Site U1449 between approximately km 330-350 (Figure 2). BAR3 can be traced until approximately km 380-390, just west of Site U1451, where it onlaps the MPHL. The western termination of the three layers is masked by a set of channel-levee systems (Numbers 4, 16/17W, and 29 in Figure 2). Where core recovery is good, these reflectors appear to be the result of the impedance contrasts between thin calcareous clay sediments and coarse-grained fan sediments (e.g. Figure 6).

### 3.3 Age-Depth Models

Following Blaauw and Christen (2011), we only sample every 100<sup>th</sup> realization of the t-walk. Goodness of fit relative to the prior distribution is tracked by the -log of the energy function (Equation 3). Since the initial conditions poorly fit the prior distributions, a set of saved iterations need to be removed, or burned-in, as the t-walk converges on solutions with good fit. We burn-in 15,000 of the saved iterations based on where the -log of the energy function seems to stabilize, leaving 70,284 iterations, or age-depth combinations that respect stratigraphic relationship for each site of the transect, to use in our analysis (Figure 7). As expected, based on our model inputs, sediments identified as hemipelagic by the cluster analysis have low accumulation rates, while fan sediments have higher accumulation rates.

Accumulation rates are widely variable on our model outputs, reflecting a combination in the actual accumulation rate variability and uncertainty of our model itself. We calculate the distributions of accumulations rates for hemipelagic and fan deposits, based on the designation from our cluster analysis results (Figure 8). Median accumulation rates for hemipelagic deposits range from 2.1-6.0 cm/ka for the seven sites and distributions range from about  $10^0$  –  $10^1$  cm/ka. The lowest median accumulation rates are at U1454 and U1449, the latter of which is the site with best chronologic control in the Middle Pleistocene and longest recovered sequence without intercalated turbidites, due to a thick sequence recovered in Core 18H that exhibits little turbiditic influence following the Jaramillo Subchron and Matuyama-Brunhes boundary relative to other sites. High median hemipelagic accumulation rates were modeled for U1450. This is likely in part a result of drilled intervals 33I and 35I (Figure 3), which limited recovery of Middle Pleistocene hemipelagic sediments and associated age control points—notably that U1450 was the only site that didn't recover the Matuyama-Brunhes magnetic reversal or the Oldest Toba Tephra (France-Lanord et al., 2016). Other sites, like U1452, have distributions that include higher hemipelagic accumulation rates, were noted to have frequent fine grained turbidites intercalated with calcareous clay sediments near the top of the Middle Pleistocene hemipelagic layer. The differences notes in sites like U1449 versus U1452 are also observed in variations of the thickness of the Middle Pleistocene hemipelagic layer in the seismic imaging, with U1449 capturing one of the thinnest examples and U1452 capturing one of the thickest (Bergmann et al., in prep.).

Fan deposit accumulation rate distributions are much wider, ranging from about  $10^1$ - $10^4$  cm/ka. While we expect accumulation rates to be widely variable in these sediments, much of this spread is related to not using a fan accumulation rate prior in our model. Median accumulation rates range from 41.7 to 159.7 cm/ka, with the spatial pattern of median accumulation rate following the same pattern as seismic stratigraphic thickness between U1454 and U1449, with the thickest deposits found between the 85 East Basement Ridge and Ninetyeast Ridge (Schwenk and Spiess, 2009).

The spatial pattern of median modeled sediment accumulation rates, calculated over 1 ka time intervals, indicate that earliest episodes of high,  $>10^1$  cm/ka, long term accumulation rates occurred near the center of the transect following deposition of the Middle Pleistocene hemipelagic unit (Figure 8). These high accumulations are modeled earliest at U1450, which is consistent with the stratigraphically oldest channel-levee systems identified above the Middle Pleistocene hemipelagic layer in seismic imaging (Figure 2); however, as mentioned earlier, U1450 was also the only site to not recover the Matuyama-Brunhes Boundary and accordingly has worse age control than the other sites. High accumulation rates spread outwards, following

the stacking pattern defined by Bergmann et al. (in prep), and ultimately switches to the highest accumulation rates at our westernmost site, U1454, between 200 – 300 ka. Site U1455 is the only site that experiences very high accumulation rates near the base of the Middle Pleistocene hemipelagic unit, likely related to incomplete recovery of the Middle Pleistocene hemipelagic unit leading to no constraints from the Cobb Mountain Subchron (France-Lanord et al., 2016).

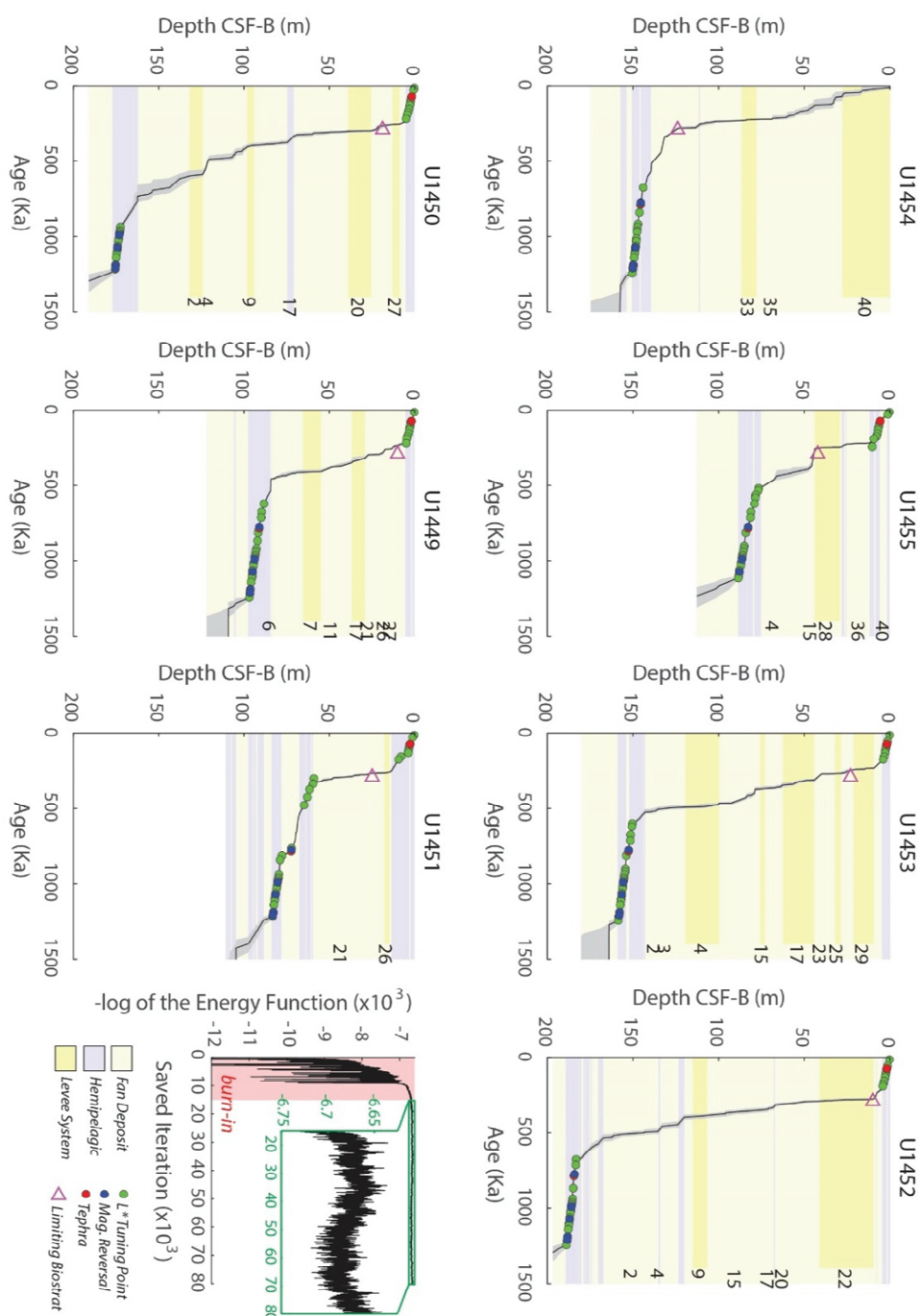


Figure 7. Age-depth models with median age (black line) and 99% confidence intervals (gray shading) for all IODP Expedition 354 sites. Representative stratigraphy for fan (yellow) and hemipelagic (blue) deposits are included for reference. Levee systems of Bergmann et al. (in prep) highlighted in darker yellow and numbered as in Figure 2. A burn-in of 15,000 model runs was used to remove early iterations that have poor fits to the prior distribution, tracked by lower values of the  $-\log$  of the energy function (Equation 3).

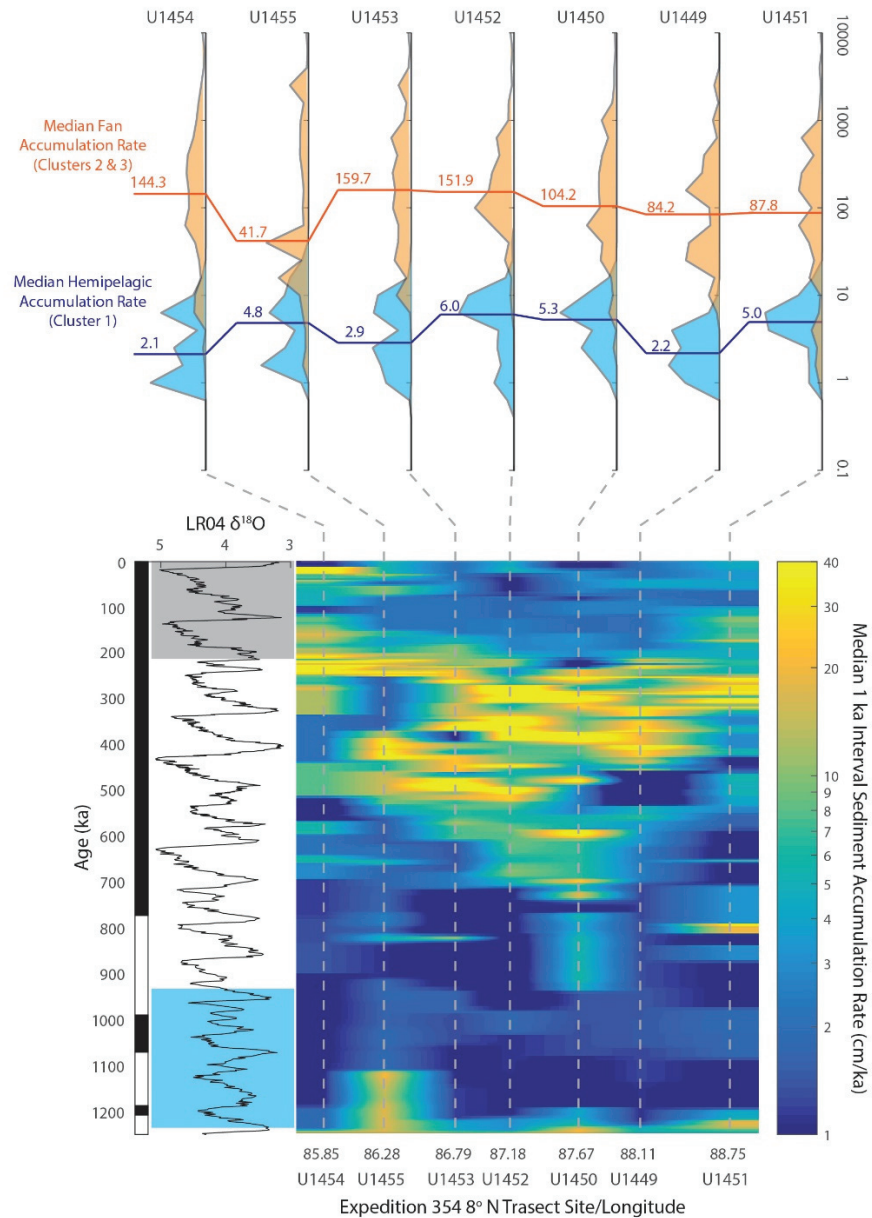


Figure 8. Resulting sedimentation accumulation rates from the age-depth models presented in Figure 7. Top: Sediment accumulation rate distributions for fan deposits (orange) and hemipelagic deposits (blue) with median values in cm/ka indicated as horizontal lines for each site. Bottom: Median modeled accumulation rates calculated in 1 ka time increments plotted as an interpolated surface against latitude and time. The LR04 Benthic  $\delta^{18}O$  stack (Lisiecki and Raymo, 2005) with the magnetic polarity timescale (Channell et al., 2016) is plotted for reference, with greater  $\delta^{18}O$  values indicating times of increased ice volume, cooler deep ocean temperatures, and lower sea level. The blue shaded interval represents the time period where no turbidites were observed along the 8° N transect and age control is best (Weber and Reilly, 2018). High accumulation rates at U1455 at the base of this unit is likely related to incomplete recovery of the Middle Pleistocene hemipelagic layer at this site (France-Lanord et al., 2016). The gray shaded interval indicates the interval where the depocenter is focused on the western fan, as recognized in seismic data (Bergmann et al., in prep.; Schwenk and Spiess, 2009).

## 4 Discussion

## 4.1 Assessing the Ages of Regionally Extensive Brunhes-Aged Reflectors (BAR)

The three regionally extensive high amplitude reflectors above the thick Middle Pleistocene hemipelagic unit, BAR 1-3 (Figure 2 and 3) often, where core recovery was good, correlate reflectors with thin calcareous clay units in the cores (e.g. Figure 6). This suggests that the impedance contrast between hemipelagic and fan deposits create these reflectors and they represent time intervals of widespread low accumulation along the 8° N transect. L\*, XRF geochemistry, and MS found in the unit that correlated with the youngest of the three reflectors, BAR-3, are consistent with a transition from glacial (Low MS, Low L\*) to interglacial sediments (Low MS, High L\*) with a sharp upper contact that could be erosional (Figure 6). It is more difficult to interpret the nature of sediments in BAR-1 and BAR-2, but this could be related core recovery or erosion of the upper hemipelagic surface. Although it is difficult to know the exact nature of these deposits, the presence of these regionally continuous reflectors suggest fan sediments deposited following deposition of the Middle Pleistocene hemipelagic unit were delivered in a series of pulses.

We investigate the ages and potential timing of each BAR so that we can discuss possible fluxes of sediment to 8° N during each of the associated fan units. To do so, we calculate the age distributions from our age models of the predicted depth range (deepest estimate to shallowest estimate), according to Bergmann et al. (in prep.), of each BAR where they are observed to cross an IODP Expedition 354 Site (Figure 9). Age distributions are often wide, illustrating the large uncertainty of ages in fan sediments between the thick regionally extensive middle and late Pleistocene hemipelagic units; however, most age distributions are within uncertainty of each other. U1450 is an exception to this with BAR1 significantly older than estimates at other sites. This may be the result of limited recovery and fewer age control points in the Middle Pleistocene as discussed in Section 4.4.2.

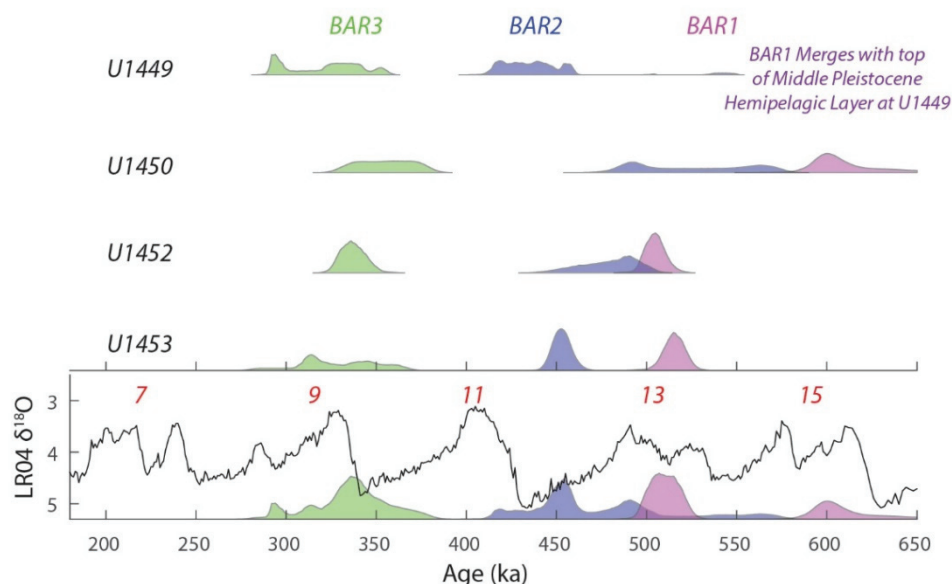


Figure 9. Age distributions of Brunhes Age Reflectors (BAR) 1-3, calculated from all ages in the interval between the uppermost and lowermost depth estimates of Bergmann et al. (in prep) based on seismic data. The bottom panel includes the sum probability distribution of all observations. The LR04 benthic isotope stack with interglacial marine isotope stage (MIS) numbers is included for comparison (Lisiecki and Raymo, 2005).



The BAR3 age distribution only spans one major glacial-interglacial transition and was likely deposited around the transition from glacial MIS 10 to interglacial MIS 9, based on sedimentological observations from U1452 (Figure 6). BAR1 at U1452 and U1453 seems to be most consistent with being deposited during MIS 13. This is consistent tracing the layer to merge with the uppermost Middle Pleistocene hemipelagic unit at U1449, which experiences little turbiditic influence and can be dated to at least MIS 15, with additional hemipelagic sediment above that marker (Weber and Reilly, 2018). Given that BAR1 and BAR3 are likely associated with interglacial sea level high stands, it is tempting to assign BAR2 to MIS 11. However, even though BAR2 maybe within uncertainty of MIS 11 in some instances of the age-depth modelling exercise presented here, there is little age control around this time and no direct support for this scenario at present.

#### 4.2 Stacking Expedition 354 Records to Establish a Regional Signal

As each Expedition 354 site has imperfect recovery, an incomplete record of fan deposition, and significant uncertainty in its age-depth model, we explore the regional signal spanning the 320 km of the transect at 8° N. To do so, we build two data stacks, one for sediment accumulation rates and one for MS, using the age models presented here. These stacks are meant to simulate an integrated signal across 8° N from the most recently active channel to the west flank of the Ninetyeast Ridge. This signal would not include sediments deposited further to the west, which has been the main depocenter of the Bengal Fan since the establishment of the most recent subfan in the Late Pleistocene (Curry et al., 2003; Schwenk and Spiess, 2009; Bergmann et al., in prep.) and potentially the depocenter while the Middle Pleistocene hemipelagic unit was deposited along our transect (Bergmann et al., in prep.). While the Nicobar Fan may have been an important depocenter for parts of the Neogene, a prominent reflector that marks the end of high accumulation rates on the Nicobar fan was dated to the Early Pleistocene (McNeill et al., 2017), meaning the Nicobar Fan was likely not a significant sink for sediments during the time period discussed here.

Our sediment accumulation rate stack median and 1  $\sigma$  intervals are plotted in Figure 10. While median values give a sense for the transect wide changes in sediment accumulation, the variance could illustrate greater uncertainty in our age-models or increased variability between sites. Successions of active channel-levee systems with limited chronostratigraphic constraints would contribute to each of these interpretations. Our magnetic susceptibility stack shows similar changes, reflecting low values in the low accumulation hemipelagic deposits and higher values as lithogenic contribution increases and particles sizes become coarser. Similar to the accumulation rate stacks, increased variance can reflect increased chronologic uncertainty or increased variability between sites (Figure 10).

We find that following the transect wide Middle Pleistocene Hemipelagic Layer, where no turbidites were recovered between MIS37 and MIS25 (1.244 – 0.936 Ma), sediment accumulation rate variance increased through about MIS17 (0.676 Ma) reflecting the onset of turbidite deposition at some sites along the transect. Accumulation rate median and variance begin to increase significantly following MIS17, reaching peak levels between 0.3 and 0.5 Ma before movement of the depocenter west of the 85 East Basement Ridge between 0.2 and 0.3 Ma.

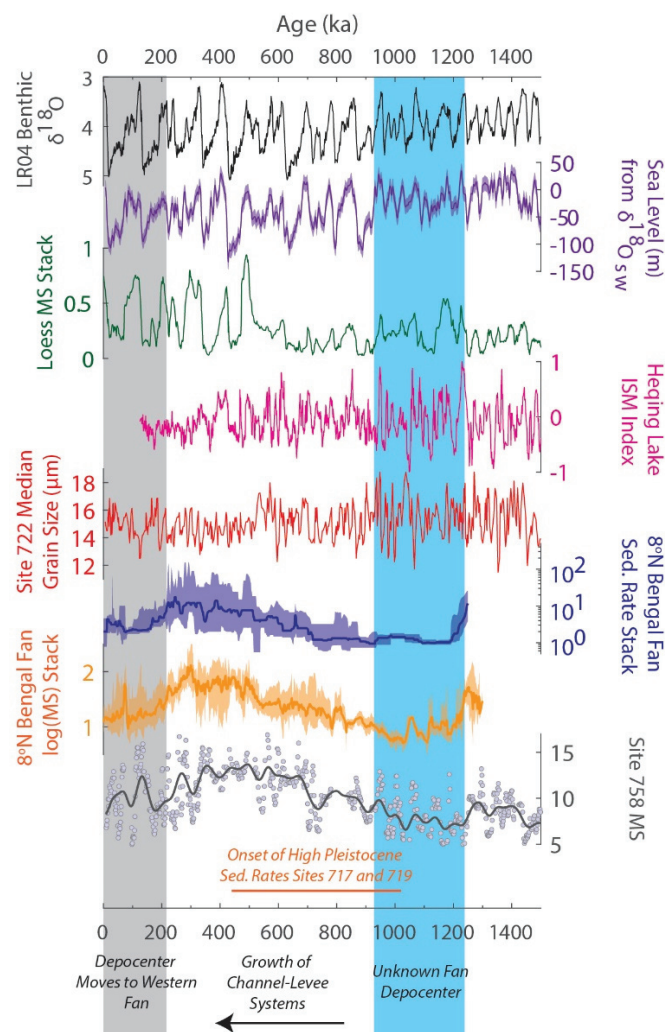


Figure 10. Stacked Bengal Fan sediment accumulation rates and magnetic susceptibility at 8° N in the context of regional and global records. From top to bottom: The LR04 benthic  $\delta^{18}\text{O}$  stack which is a signal of deep sea temperature and global ice volume (Lisiecki and Raymo, 2005); Global sea level estimates from temperature corrected benthic  $\delta^{18}\text{O}$  (Elderfield et al., 2012; Rohling et al., 2014); Magnetic susceptibility from the Chinese Loess Plateau which is a signal of East Asian summer monsoon intensity (Sun et al., 2006); Heqing Lake Indian summer monsoon (ISM) Index which used a stack of proxies sensitive to temperature, precipitation and weathering in the lake's watershed (Zhisheng et al., 2011); ODP Site 722 median grain size which tracks wind strength of the Indian summer monsoon in the Arabian Sea (Clemens et al., 1996; Clemens, 1998) Sedimentation rate stack in cm/ka median (line) and  $1\sigma$  interval (purple shading) of the seven Expedition 354 sites at 8° N on the Bengal Fan; Magnetic susceptibility stack mean (line) and  $1\sigma$  interval (orange shading) of the seven Expedition 354 sites at 8° N on the Bengal Fan; Site 758 magnetic susceptibility (Farrell and Janecek, 1991) which has been interpreted as an integrated signal of sediment flux to the Bay of Bengal and/or Bengal Fan, with tephra layers removed and smoothed using a 40 ka FWHM Gaussian filter; and range for the possible age of Pleistocene sedimentation rate increases at Sites 717/719 to the southwest of the Expedition 354 transect (Gartner, 1990). Blue highlighted box indicates the time interval where no turbidites were recovered along the Expedition 354 transect and Middle Pleistocene chronology is best resolved (Unit 2a in Weber and Reilly, 2018). Gray shading indicates when the depocenter was focused on the more western fan, as recognized in seismic data (Bergmann et al., in prep.; Schwenk and Spiess, 2009).

### 4.3 Insights to the Middle to Late Pleistocene Evolution of the Bengal Fan

We compare our 8° N stacked records with what has been argued, but not demonstrated, to be a regionally integrated record of sediment input to the Bay of Bengal and Bengal Fan (Figure 10). We use the Site 758 (5.38° N) magnetic susceptibility record after removing magnetic susceptibility highs associated with tephra layers A through I (Dehn et al., 1991; Farrell and Janecek, 1991) with chronology assigned using the benthic  $\delta^{18}\text{O}$  record of Chen et al. (1995) aligned by Lisiecki and Raymo (2005). The magnetic susceptibility is smoothed using a 40 ka FWHM Gaussian filter and resampled every 1 ka to highlight the lower frequency signal. We find broad similarity with our reconstruction, including low magnetic susceptibility values coeval with the Expedition 354 Middle Pleistocene hemipelagic layer, an increase in magnetic susceptibility coeval with a general trend of increased variance and median accumulation rates across the Expedition 354 transect, and a decrease in magnetic susceptibility coeval with movement of the Bengal Fan depocenter to the west and more distal to the Ninetyeast Ridge. While it is difficult to make direct comparisons to the ODP Leg 116 Distal Bengal Fan drill sites, we note that increases in Pleistocene sediment accumulation rates at distal Bengal Fan Sites 717 and 719 ( $\sim 10$  S) must have occurred during the development of the Middle to Late Pleistocene channel-levee systems along our transect and/or subsequent shift of the depocenter to the more western fan at 8° N.

Our observations suggest a major change in sediment routing on the fan during the Middle to Late Pleistocene that could be interpreted as the development of a more extensive channel-levee system after about 0.936 Ma. This is supported by multiple lines of evidence documenting regional changes following deposition of the regionally extensive Middle Pleistocene hemipelagic unit at 8° N and subsequent increases in magnetic susceptibility and accumulation rates. First, based on seismic observations of the BAR horizons along 8° N, fan sediments were delivered as a series of progressively larger pulses (Bergmann et al., in prep.). First, based on seismic observations of the BAR horizons along 8° N and relative changes in the thickness of each unit, fan sediments were delivered as a series of progressively larger pulses. While there are still uncertainties in the timing of these pulses, seismic unit thickness illustrates each fan building episode was larger than the last, suggesting either closer proximity to the center of the active depocenter or a longer duration of channel-levee activity. Second, sites from the very distal fan see an increase in accumulation during the time in which progressive episodes of fan building at 8° N become larger. And finally, the long-term pattern of sediment accumulation on the eastern lower fan at 8° N is remarkably similar to the long-term pattern in lithogenic concentration at the closest pelagic reference site, supporting earlier claims that this signal reflects an integrated record of sedimentation and sediment routing on the Bengal Fan, and likely, for this timeframe is influenced by processes occurring on the eastern lower Bengal Fan.

It is important to note that these observations on their own do not necessarily make the Late Pleistocene unique, as channel levee systems were present at 8°N during times since the Late Miocene (Schwenk and Spiess, 2009; France-Lanord et al., 2016) and higher accumulation rates are observed at distal fan sites during Miocene and Pliocene times (Gartner, 1990). However, the Middle to Late Pleistocene is unique in that we have better age-control and can discuss this specific change within the context of regional and global records.

In general, long term accumulation rates are controlled by changes in sediment supply, sediment transport, and accommodation space. It is always possible that the changes we observe at 8° N are entirely controlled by stochastic fan sediment transport processes. However, long term

changes in sediment supply to the Bay of Bengal is likely influenced by long term trends in climatically or tectonically driven erosion and sea level variations influence on continental shelf accommodation space and the connection between the major Himalayan river systems and the deep ocean.

While evidence from the Chinese Loess Plateau indicate strengthening of interglacial summer monsoons and associated precipitation from the Middle to Late Pleistocene (Sun et al., 2006), this change is not in sync with where we observe our initial increases in accumulation rate, with the largest intensifications of the East Asian summer monsoon around 1.25 and 0.6 Ma. It also may not be representative of the Indian summer monsoonal system (Figure 10). For example, grain size changes in the Arabian Sea that reflect the Indian summer monsoon wind strength (Clemens et al., 1996; Clemens, 1998) and precipitation and weathering proxies from Heqing Lake in Southern China (Zhisheng et al., 2011) suggest that Indian summer monsoon may have weakened during the Late Pleistocene as Northern Hemisphere glaciation intensified.

We do observe, however, that the onset of the Middle to Late Pleistocene growth of the Bengal Fan channel-levee system, as detected at 8° N following 0.936 Ma, occurs during the first very low sea level stand of the Middle to Late Pleistocene, as recognized in the ice volume signal of temperature corrected benthic foraminifera  $\delta^{18}\text{O}$  (Elderfield et al., 2012; Figure 10) and sea-level controlled hydrologic cycle signals in Mediterranean Seaplanktonic foraminifera  $\delta^{18}\text{O}$  (Rohling et al., 2014). Based on this observation, we hypothesize that the evolution of the Middle to Late Pleistocene Bengal Fan was driven by the increase in glacial-interglaciation sea level amplitude, which strengthened the connection between Himalayan Rivers and the Bengal Fan. However, changes in Pleistocene climate around the same time could have also strengthened the erosional regime in the Himalaya Mountains and increased sediment flux to the Bay of Bengal. Further work is required to investigate these hypotheses.

## 5 Conclusion

We investigate the evolution of the Middle to Late Pleistocene Bengal Fan at seven sites along the IODP Expedition 354 8° N transect using a system specific age modeling approach that assesses uncertainty and incorporates expert knowledge of the fan. By quantifying sediment accumulation rate variations from the Middle to the Late Pleistocene, we find an increasing trend in accumulation rates following a 300 ka interval (~1.244 – 0.936 Ma) where no turbidites were observed across the 320 km transect. This observation, along with seismic observations, accumulation rates on the distal fan, and lithogenic sediment concentrations at a pelagic reference site, indicate development of the Bengal Fan channel-levee system during this time to a distribution network that covers a greater extent of the fan. The onset of this change is coincident the first major sea level low of the Middle to Late Pleistocene, leading us to hypothesize that increased sea level amplitude changes associated with amplification of polar glaciation was the major driver of Pleistocene Bengal Fan changes.

## Acknowledgements

We are very grateful to the captain, crew, IODP staff, and shipboard scientists on the JOIDES Resolution that made IODP Expedition 354 and subsequent research successful. All samples and data were provided by IODP. This work was made possible by support from a United States Science Support Program post expedition award to BTR. We thank Leslie & Mark Workman and the Oregon ARCS Foundation for additional support to BTR. This study benefited greatly from a discussion with Andreas Nilsson, who recommended the use of the T-walk algorithm.

## References

- Ahmad, S.M., Anil Babu G., Padmakumari V. M., Dayal A. M., Sukhija B. S., Nagabhushanam P., 2005. Sr, Nd isotopic evidence of terrigenous flux variations in the Bay of Bengal: Implications of monsoons during the last ~34,000 years. *Geophys. Res. Lett.* 32. <https://doi.org/10.1029/2005GL024519>
- Bergmann, F., Schwenk, T., Spiess, V., France-Lanord, C., in prep. Middle to Late Pleistocene architecture and stratigraphy of the lower Bengal Fan--Integrating multichannel seismic data and IODP Expedition 354 results. *ET J.*
- Blaauw, M., Christen, J.A., 2011. Flexible paleoclimate age-depth models using an autoregressive gamma process. *Bayesian Anal.* 6, 457–474. <https://doi.org/10.1214/ba/1339616472>
- Channell, J.E.T., Hodell, D.A., Curtis, J.H., 2016. Relative paleointensity (RPI) and oxygen isotope stratigraphy at IODP Site U1308: North Atlantic RPI stack for 1.2–2.2 Ma (NARPI-2200) and age of the Olduvai Subchron. *Quat. Sci. Rev.* 131, 1–19. <https://doi.org/10.1016/j.quascirev.2015.10.011>
- Chen, J., Farrell, J., Murray, D., Prell, W., 1995. Timescale and paleoceanographic implications of a 3.6 m.y. oxygen isotope record from the northeast Indian Ocean (Ocean Drilling Program Site 758). *Paleoceanography* 10, 21–47. <https://doi.org/10.1029/94PA02290>
- Christen, J.A., Fox, C., 2010. A general purpose sampling algorithm for continuous distributions (the t-walk). *Bayesian Anal.* 5, 263–281. <https://doi.org/10.1214/10-BA60>
- Clark, P.U., Archer, D., Pollard, D., Blum, J.D., Rial, J.A., Brovkin, V., Mix, A.C., Pisias, N.G., Roy, M., 2006. The middle Pleistocene transition: characteristics, mechanisms, and implications for long-term changes in atmospheric pCO<sub>2</sub>. *Quat. Sci. Rev.* 25, 3150–3184. <https://doi.org/10.1016/j.quascirev.2006.07.008>
- Clemens, S.C., 1998. Dust response to seasonal atmospheric forcing: Proxy evaluation and calibration. *Paleoceanography* 13, 471–490. <https://doi.org/10.1029/98PA02131>
- Clemens, S.C., Kuhnt, W., LeVay, L.J., the Expedition 353 Scientists, 2016. Indian Monsoon Rainfall, in: Proceedings of the International Ocean Discovery Program. International Ocean Discovery Program, College Station, TX.
- Clemens, S.C., Murray, D.W., Prell, W.L., 1996. Nonstationary Phase of the Plio-Pleistocene Asian Monsoon. *Science* 274, 943–948.
- Curry, J.R., 1994. Sediment volume and mass beneath the Bay of Bengal. *Earth Planet. Sci. Lett.* 125, 371–383.
- Curry, J.R., Emmel, F.J., Moore, D.G., 2003. The Bengal Fan: morphology, geometry, stratigraphy, history and processes. *Mar. Pet. Geol.* 19, 1191–1223. [https://doi.org/10.1016/S0264-8172\(03\)00035-7](https://doi.org/10.1016/S0264-8172(03)00035-7)
- Curry, J.R., Moore, D.G., 1974. Sedimentary and Tectonic Processes in the Bengal Deep-Sea Fan and Geosyncline, in: Burk, C.A., Drake, C.L. (Eds.), *The Geology of Continental Margins*. Springer Berlin Heidelberg, pp. 617–627. [https://doi.org/10.1007/978-3-662-01141-6\\_45](https://doi.org/10.1007/978-3-662-01141-6_45)
- Dehn, J., Farrell, J.W., Schmincke, H.U., 1991. Neogene tephrChronology from Site 758 on northern Ninetyeast Ridge: Indonesian arc volcanism of the past 5 Ma. *Proc. Ocean Drill. Program Sci. Results* 121, 273–295.
- Elderfield, H., Ferretti, P., Greaves, M., Crowhurst, S., McCave, I.N., Hodell, D., Piotrowski, A.M., 2012. Evolution of Ocean Temperature and Ice Volume Through the Mid-Pleistocene Climate Transition. *Science* 337, 704–709. <https://doi.org/10.1126/science.1221294>
- Farrell, J.W., Janecek, T.R., 1991. 15. Late Neogene paleoceanography and paleoclimatology of the North-east Indian Ocean (Site 758), in: Proceedings of the Ocean Drilling Program, Scientific Results, Proceedings of the Ocean Drilling Program.



- France-Lanord, C., Derry, L.A., 1997. Organic carbon burial forcing of the carbon cycle from Himalayan erosion. *Nature* 390, 65–67.
- France-Lanord, C., Derry, L.A., Michard, A., 1993. Evolution of the Himalaya since Miocene time: isotopic and sedimentological evidence from the Bengal Fan, in: Treloar, P.J., Searle, M.P. (Eds.), *Himalayan Tectonics*, Geological Society Special Publication. pp. 603–621.
- France-Lanord, C., Spiess, V., Klaus, A., Schwenk, T., the Expedition 354 Scientists, 2016. Bengal Fan, in: *Proceedings of the International Ocean Discovery Program*. International Ocean Discovery Program, College Station, TX.
- Galy, V., France-Lanord, C., Beyssac, O., Faure, P., Kudrass, H., Palhol, F., 2007. Efficient organic carbon burial in the Bengal fan sustained by the Himalayan erosional system. *Nature* 450, 407–410. <https://doi.org/10.1038/nature06273>
- Gartner, S., 1990. Neogene calcareous nannofossil biostratigraphy, Leg 116 (central Indian Ocean), in: Cochran, JR, Stow, DAV, et Al., *Proc. ODP, Sci. Results*. pp. 165–187.
- Gradstein, F.M., Ogg, J., Schmitz, M., Ogg, G. (Eds.), 2012. *The Geologic Time Scale 2012*, 1st ed. ed. Elsevier.
- Haslett, J., Parnell, A., 2008. A simple monotone process with application to radiocarbon-dated depth chronologies. *J. R. Stat. Soc. Ser. C Appl. Stat.* 57, 399–418. <https://doi.org/10.1111/j.1467-9876.2008.00623.x>
- Hein, C.J., Galy, V., Galy, A., France-Lanord, C., Kudrass, H., Schwenk, T., 2017. Post-glacial climate forcing of surface processes in the Ganges–Brahmaputra river basin and implications for carbon sequestration. *Earth Planet. Sci. Lett.* 478, 89–101. <https://doi.org/10.1016/j.epsl.2017.08.013>
- Klootwijk, C.T., Gee, J.S., Peirce, J.W., Smith, G.M., 1992. Neogene evolution of the Himalayan-Tibetan region: constraints from ODP site 758, northern ninetyeast ridge; bearing on climatic change. *Palaeogeogr. Palaeoclimatol. Palaeoecol.* 95, 95–110. [https://doi.org/10.1016/0031-0182\(92\)90167-4](https://doi.org/10.1016/0031-0182(92)90167-4)
- Lisiecki, L.E., Raymo, M.E., 2005. A Pliocene-Pleistocene stack of 57 globally distributed benthic  $\delta^{18}\text{O}$  records: PLIOCENE-PLEISTOCENE BENTHIC STACK. *Paleoceanography* 20, PA1003. <https://doi.org/10.1029/2004PA001071>
- Lupker, M., France-Lanord, C., Galy, V., Lavé, J., Kudrass, H., 2013. Increasing chemical weathering in the Himalayan system since the Last Glacial Maximum. *Earth Planet. Sci. Lett.* 365, 243–252. <https://doi.org/10.1016/j.epsl.2013.01.038>
- Mark, D.F., Renne, P.R., Dymock, R., Smith, V.C., Simon, J.I., Morgan, L.E., Staff, R.A., Ellis, B.S., 2017. High-precision  $40\text{Ar}/39\text{Ar}$  dating of pleistocene tuffs and temporal anchoring of the Matuyama-Brunhes boundary. *Quat. Geochronol.* 39, 1–23. <https://doi.org/10.1016/j.quageo.2017.01.002>
- McNeill, L.C., Dugan, B., Backman, J., Pickering, K.T., Poudroux, H.F.A., Henstock, T.J., Petronotis, K.E., Carter, A., Chemale, F., Milliken, K.L., Kutterolf, S., Mukoyoshi, H., Chen, W., Kachovich, S., Mitchison, F.L., Bourlange, S., Colson, T.A., Frederik, M.C.G., Guèrin, G., Hamahashi, M., House, B.M., Hüpers, A., Jeppson, T.N., Kenigsberg, A.R., Kuranaga, M., Nair, N., Owari, S., Shan, Y., Song, I., Torres, M.E., Vannucchi, P., Vrolijk, P.J., Yang, T., Zhao, X., Thomas, E., 2017. Understanding Himalayan erosion and the significance of the Nicobar Fan. *Earth Planet. Sci. Lett.* 475, 134–142. <https://doi.org/10.1016/j.epsl.2017.07.019>
- Nilsson, A., Suttie, N., Hill, M.J., 2018. Short-Term Magnetic Field Variations From the Post-depositional Remanence of Lake Sediments. *Front. Earth Sci.* 6. <https://doi.org/10.3389/feart.2018.00039>
- Phillips, S.C., Johnson, J.E., Giosan, L., Rose, K., 2014. Monsoon-influenced variation in productivity and lithogenic sediment flux since 110 ka in the offshore Mahanadi Basin, northern Bay of Bengal. *Mar. Pet. Geol., Geologic implications of gas hydrates in the offshore of India: Results of the National Gas Hydrate Program Expedition 01* 58, 502–525. <https://doi.org/10.1016/j.marpetgeo.2014.05.007>
- Piper, D.J.W., Normark, W.R., 1983. Turbidite depositional patterns and flow characteristics, Navy Submarine Fan, California Borderland. *Sedimentology* 30, 681–694. <https://doi.org/10.1111/j.1365-3091.1983.tb00702.x>
- Prell, W.L., Kutzbach, J.E., 1997. The impact of Tibet-Himalayan elevation on the sensitivity of the monsoon climate system to changes in solar radiation, in: *Tectonic Uplift and Climate Change*. Springer, pp. 171–201.
- Raymo, M.E., Ruddiman, W.F., 1992. Tectonic forcing of late Cenozoic climate. *Nature* 359, 117–122.

- Rohling, E.J., Foster, G.L., Grant, K.M., Marino, G., Roberts, A.P., Tamisiea, M.E., Williams, F., 2014. Sea-level and deep-sea-temperature variability over the past 5.3 million years. *Nature* 508, 477–482. <https://doi.org/10.1038/nature13230>
- Sager, W.W., Hall, S., 1990. 26. Magnetic properties of black mud turbidites from ODP Leg 116, Distal Bengal Fan, Indian Ocean, in: *Proceedings of the Ocean Drilling Program, Scientific Results*.
- Schwenk, T., Spiess, V., 2009. Architecture and stratigraphy of the Bengal Fan as response to tectonic and climate revealed from high-resolution seismic data, in: Kneller, B.C., Martinsen, O.J., McCaffrey, B. (Eds.), *External Controls on Deep-Water Depositional Systems*, SEPM Special Publication. SEPM (Society for Sedimentary Geology), Tulsa, Okla.
- Schwenk, T., Spiess, V., Breitzke, M., Hübscher, C., 2005. The architecture and evolution of the Middle Bengal Fan in vicinity of the active channel–levee system imaged by high-resolution seismic data. *Mar. Pet. Geol.* 22, 637–656. <https://doi.org/10.1016/j.marpetgeo.2005.01.007>
- Schwenk, T., Spiess, V., Hübscher, C., Breitzke, M., 2003. Frequent channel avulsions within the active channel–levee system of the middle Bengal Fan—an exceptional channel–levee development derived from Parasound and Hydrosweep data. *Deep Sea Res. Part II Top. Stud. Oceanogr.* 50, 1023–1045. [https://doi.org/10.1016/S0967-0645\(02\)00618-5](https://doi.org/10.1016/S0967-0645(02)00618-5)
- Sun, Y., Clemens, S.C., An, Z., Yu, Z., 2006. Astronomical timescale and palaeoclimatic implication of stacked 3.6-Myr monsoon records from the Chinese Loess Plateau. *Quat. Sci. Rev.* 25, 33–48. <https://doi.org/10.1016/j.quascirev.2005.07.005>
- Von der Borch, C.C., Sclater, J.G., Gartner Jr, S., Hekinian, R., Johnson, D.A., McGowran, B., Pimm, A.C., Thompson, R.W., Veevers, J.J., Waterman, L.S., 1974. Initial reports of the Deep Sea Drilling Project. U.S. Government Printing Office, Washington, D. C.
- Walczak, M.H., Mix, A.C., Willse, T., Slagle, A., Stoner, J.S., Jaeger, J., Gulick, S., LeVay, L., Kioka, A., The IODP Expedition 341 Scientific Party, 2015. Correction of non-intrusive drill core physical properties data for variability in recovered sediment volume. *Geophys. J. Int.* 202, 1317–1323. <https://doi.org/10.1093/gji/ggv204>
- Weber, M.E., Lantzsck, H., Dekens, P., Das, S.K., Reilly, B.T., Martos, Y.M., Meyer-Jacob, C., Agrahari, S., Ekblad, A., Titschack, J., Holmes, B., Wolfgramm, P., 2018. 200,000 years of monsoonal history recorded on the lower Bengal Fan - strong response to insolation forcing. *Glob. Planet. Change* 166, 107–119. <https://doi.org/10.1016/j.gloplacha.2018.04.003>
- Weber, M.E., Reilly, B.T., 2018. Hemipelagic and turbiditic deposits constrain lower Bengal Fan depositional history through Pleistocene climate, monsoon, and sea level transitions. *Quaternary Science Reviews* 199, 159–173. <https://doi.org/10.1016/j.quascirev.2018.09.027>
- Weber, M.E., Wiedicke, M., Kudrass, H., Hübscher, C., Erlenkeuser, H., 1997. Active growth of the Bengal Fan during sea-level rise and highstand. *Geology* 25, 315–318.
- Weber, M.E., Wiedicke-Hombach, M., Kudrass, H.R., Erlenkeuser, H., 2003. Bengal Fan sediment transport activity and response to climate forcing inferred from sediment physical properties. *Sediment. Geol., Sedimentary Geology of the Bengal Basin, Bangladesh, in relation to the Asia-Greater India collision and the evolution of the eastern Bay of Bengal* 155, 361–381. [https://doi.org/10.1016/S0037-0738\(02\)00187-2](https://doi.org/10.1016/S0037-0738(02)00187-2)
- Zhisheng, A., Clemens, S.C., Shen, J., Qiang, X., Jin, Z., Sun, Y., Prell, W.L., Luo, J., Wang, S., Xu, H., Cai, Y., Zhou, W., Liu, X., Liu, W., Shi, Z., Yan, L., Xiao, X., Chang, H., Wu, F., Ai, L., Lu, F., 2011. Glacial-Interglacial Indian Summer Monsoon Dynamics. *Science* 333, 719–723. <https://doi.org/10.1126/science.1203752>
- Zhisheng, A., Kutzbach, J.E., Prell, W.L., Porter, S.C., 2001. Evolution of the Asian monsoons and phased uplift of the Himalaya-Tibetan plateau since Late Miocene times. *Nature* 411, 62–66.

## **Versicherung an Eides Statt / *Affirmation in lieu of an oath***

**gem. § 5 Abs. 5 der Promotionsordnung vom 15.07.2015 /  
according to § 5 (5) of the Doctoral Degree Rules and Regulations of 15 July, 2015**

Ich / I, Fenna Bergmann, Straßburger Straße 21, 28215 Bremen; Matr. Nr, 2368050  
(Vorname / First Name, Name / Name, Anschrift / Address, ggf. Matr.-Nr. / student ID no., if applicable)

versichere an Eides Statt durch meine Unterschrift, dass ich die vorliegende Dissertation selbständig und ohne fremde Hilfe angefertigt und alle Stellen, die ich wörtlich dem Sinne nach aus Veröffentlichungen entnommen habe, als solche kenntlich gemacht habe, mich auch keiner anderen als der angegebenen Literatur oder sonstiger Hilfsmittel bedient habe und die zu Prüfungszwecken beigelegte elektronische Version (PDF) der Dissertation mit der abgegebenen gedruckten Version identisch ist. / *With my signature I affirm in lieu of an oath that I prepared the submitted dissertation independently and without illicit assistance from third parties, that I appropriately referenced any text or content from other sources, that I used only literature and resources listed in the dissertation, and that the electronic (PDF) and printed versions of the dissertation are identical.*

Ich versichere an Eides Statt, dass ich die vorgenannten Angaben nach bestem Wissen und Gewissen gemacht habe und dass die Angaben der Wahrheit entsprechen und ich nichts verschwiegen habe. / *I affirm in lieu of an oath that the information provided herein to the best of my knowledge is true and complete.*

Die Strafbarkeit einer falschen eidesstattlichen Versicherung ist mir bekannt, namentlich die Strafandrohung gemäß § 156 StGB bis zu drei Jahren Freiheitsstrafe oder Geldstrafe bei vorsätzlicher Begehung der Tat bzw. gemäß § 161 Abs. 1 StGB bis zu einem Jahr Freiheitsstrafe oder Geldstrafe bei fahrlässiger Begehung. / *I am aware that a false affidavit is a criminal offence which is punishable by law in accordance with § 156 of the German Criminal Code (StGB) with up to three years imprisonment or a fine in case of intention, or in accordance with § 161 (1) of the German Criminal Code with up to one year imprisonment or a fine in case of negligence.*

\_\_\_\_\_  
Ort / Place, Datum / Date

\_\_\_\_\_  
Unterschrift / Signature